High Performance Maglev Guideway Design

by

R. Scott Phelan

Bachelor of Science in Civil Engineering
Texas Tech University (1987)

Master of Science in Civil Engineering
Carnegie Mellon University (1989)

Master of Science in Civil Engineering
Massachusetts Institute of Technology (1990)

Submitted to the Department of Civil and Environmental Engineering
in partial fulfillment of the requirements for the degree of

Doctor of Philosophy

at the

MASSACHUSETTS INSTITUTE OF TECHNOLOGY

January 1993

Author.....
Department of Civil and Environmental Engineering
January 20, 1993

Certified by.....
Professor Jerome J. Connor
Thesis Supervisor

Accepted by.....
Ole S. Madsen
Chairman, Departmental Committee on Graduate Students

High Performance Maglev Guideway Design

by

R. Scott Phelan

Submitted to the Department of Civil and Environmental Engineering
on January 20, 1993, in partial fulfillment of the requirements for the degree of
Doctor of Philosophy

Abstract

This thesis demonstrates the influence of guideway design on overall high speed maglev system performance characteristics and suggests methods for improved, high performance maglev guideway design. The research focuses on three areas:

- advanced material design and application of a hybrid fiber reinforced plastic, FRP, non-magnetic concrete reinforcing rod
- hollow-box, narrow beam reinforced concrete guideway design and analysis, using both steel and hybrid FRP reinforcement
- dynamic beam analysis showing the interactions between beam length and frequency, and vehicle velocity and loading pad configuration

Structural requirements for a maglev guideway beam, including criteria for geometry, loads, deflections, durability, toughness, fatigue, and magnetic inertness, are defined and developed. Proposed construction methods are analyzed to determine the impact that the choice of method has on both the cost and structural design of the guideway. A conceptual design follows in which candidate cross-sectional shapes and materials are compared.

An investigation is made of the potential application of advanced plastic materials in the maglev guideway design. Specifically, a hybrid FRP rod is conceptualized, manufactured, and tested for potential application as concrete reinforcement in areas where non-magnetic reinforcement is required. A description is given of the hybrid FRP rod concept along with design procedures and beam test results. Sensitivity analyses performed using the narrow beam design procedure indicate expected beam lengths, widths, heights, weights, frequencies, and costs for a number of vehicle load and deflection criteria scenarios. These sensitivity analyses indicate the importance of vehicle design on overall guideway performance.

Dynamic beam analysis is performed using both a finite element discretization and a closed form mathematical solution for simple beam spans having no assumed damping and, with uniform cross-section and stiffness properties. This closed form beam behavior solution is solved for convergent velocity cases, i.e. velocities that produce no beam residual vibrations. Sensitivity analyses performed on a variety of vehicle loading configurations demonstrate the importance of vehicle loading configuration to overall guideway performance. Dynamic analyses are confined to modeling the force of the traveling vehicle. Also, linear elastic beam behavior is assumed.

Thesis Supervisor: Jerome J. Connor, Professor of Civil and Environmental Engineering

Thesis Committee: Richard D. Thornton, Laboratory for Electromagnetic and Electronic Systems Professor
Thanasis Triantafillou, Assistant Professor of Civil and Environmental Engineering
Joseph M. Sussman, Professor of Civil and Environmental Engineering

Acknowledgments

My sincere appreciation goes to my thesis committee members, Professors: Jerome J. Connor, Richard D. Thornton, Thanasis Triantafillou, and Joseph M. Sussman.

I am indebted to Professor Sussman. He was first in the department to encourage my research interests. I am thankful for his emphasis on the overall economic viability of maglev systems and also, for being an advisor and a friend.

I thank Thanasis for really bringing excitement to my work. I'm particularly grateful for his help with conceptual designs, course direction, and especially, the hybrid FRP rod design.

Professor Thornton was instrumental in my reaching this doctoral level. He stood up for me when I needed it most. (If maglev ever comes to the U.S., more than anyone else, I believe it will be because of his efforts.) It truly has been a pleasure working with him. The sincerity, honesty, and resiliency I see in his work (and play) will be goals of mine for the rest of my life.

To Professor Connor, I am sincerely grateful for all the time he was able to devote to this research. The dynamic modeling and future maglev application discussions in his office were always instructional and inspiring. He knew when I needed to be pushed, and when I needed encouragement.

Many others deserve acknowledgment.

I thank Professor Moavenzadeh, Charlie Helliwell, and the U.S. Department of Defense, Army Research Office, for three full years of funding. Also thanks to the U.S. Department of Transportation, FRA, National Maglev Initiative, for support of this work, and to the Bechtel Group, Advanced Civil Division, San Francisco, for additional support. Material donations by Toray Industries, New York, Polygon Corporation, Walkerton, IN, and Grace Construction, Cambridge, MA, are gratefully acknowledged.

My appreciation also goes to Professors: Leung, Kausel, Wilson, Marks, Gibson, Einstein, Logcher, Sriram, and Buyukozturk. I also received much inspiration from the late James Paddock. I am indebted to Paul Taylor, Executive Director for the California-Nevada Super Speed Train Commission, for invaluable maglev and high speed rail cost data. Thanks also goes to John Harrison of Parsons Brinckerhoff for maglev cost information—and also for his encouragement. I especially thank Joe Perkowski, Gary McAlister, and Eb Lemke of Bechtel for many lively discussions (on maglev, football, etc.). I thank Joe for his early enthusiasm for my maglev doctoral work.

I am truly grateful to Ron Sanchez for his invaluable support, encouragement, and direction. Also, thanks to Len Albano for his help on just about everything, including many homework assignments. I also am indebted to the administrative staff at MIT. Especially helpful have been Pat Vargus, Terri Lehane, Claire Benoit, Georgina Teare, Vivian Mizuno, Joan McCusker, Kim Farrell, Jesse Carty, and Cynthia Stewart. Also, thanks to Michael, Mark, and the rest of the Barker Engineering Library staff.

I have enjoyed getting to know many office mates—both new and old. (I have been through several generations!) Thanks to Andy Hoffman, Feniosky Peña, David Ford, Dan Crews, Brandt Little, Tom Davies, Judah Richman, Eric Swenson, Jackie Fischer, Ashraf Hameedi, Jonathan Cherneff, Ann Brach, Antony Awaida, Tom Maglione, Shamim Ahmed, Irfan Essa, and Emmanuel Bar-Orr for all the discussions on world events,

religion, sports, etc. These discussions, along with the ski trips and basketball games are what I will remember most about MIT. Also, a special "thank you" to Jackie for her encouragement and inspiration.

I am indebted to Andy Hoffman, and Stephen and Arthur Rudolf for their assistance with the concrete beam tests. I thank Andy for the best "straight-grain Douglas fir" concrete formwork money can buy! Thanks also to Stephen and Arthur for the precision machining required for numerous testing apparatus. I also thank Tom Musson, Debbie Min, and especially, Jeroen Timmermanns for their help with testing and research.

I thank Doug Larson for the witness and friend he has been to me. Other friends and students at MIT who have been especially influential include: Kai Haas, Mike Silver, Stéphanie Roger, Fadi Selwan, Joe Saleeby, Laura Demsetz, John Everett, Mike Toole, Frank Altobelli, Hank Taylor, Ed Pendleton, Alan Brik, Paul Boyajian, Charis Gantes, Gebran Karam, Nikolaos Plevris, Nikola Deskovic, John Tom, and Dave Perreault.

Others, not at MIT who have been very supportive of my work include many friends at Newton Presbyterian Church, lifelong friends from Levelland, Texas, friends from Lubbock, Texas, the "Fab Five" from Texas Tech, and special friends from Carnegie Mellon. I am especially grateful to Professor Chris Hendrickson, my former advisor at Carnegie Mellon, for nominating me to the ASCE High Speed Ground Transportation Committee. Serving on this committee has greatly helped my work.

Special appreciation goes to Everett and Margaret Wicks, and Roy Greenland, for wiring up the "Command Center", and for making 26 Park Road "home".

I am also grateful to my in-laws Anita and John Reid, and Denise Voss for their support, encouragement, advice, and their willingness to allow their Lauralee to marry a full-time graduate student!

None of this would have been possible had it not been for the support and love given to me by my parents, Harold and Marilyn, my sister, Kim, my brother, Pat, his wife, Cara, and their son Ryan. (Mother, I can finally say, "I finished the thesis!") I thank you all for your help and encouragement. Thanks for being there. You are all the best! (Thanks also to Ryan, for always reminding me to "get a job"!)

More than any other person, I thank my beautiful wife, Lauralee. Thank you Laura for the care, support, and advice you have given to me these past few years. (I also am grateful for all the typing and proofreading—performed late into the night.) Thanks for the Bible studies, devotions, prayers, talks, walks, and bike rides. Thanks for the music... You are my best friend!

Most importantly, all praise and glory from this work goes to God. I thank Him for the beauty, order, and purpose of this world, and for His Son, Jesus Christ, my Lord. How majestic is Your Name in all the earth! I thank Him for the desire to pursue work on maglev—which I believe He gave to me over 15 years ago—and for this opportunity to fulfill the desire—which I believe He has provided. I thank Him for eternity.

PSALM 1; PROVERBS 3:5, 6
JOHN 3:1-21; JAMES 3:13-18

May we all begin to maglev!

It is the heart that experiences God, not the reason.

BLAISE PASCAL

to my parents

Harold Leon Phelan

and

Marilyn Elizabeth Phelan

your love, guidance, and inspiration
made it all possible

Table of Contents

List of Tables

List of Figures

Nomenclature

A_g : gross area of cross section

$A_{rc.h}$: area of compressive horizontal reinforcement

$A_{rc.v}$: area of compressive vertical reinforcement

$A_{r.h\max}$: maximum reinforcement allowable for web sections

$A_{r.h\min}$: minimum reinforcement allowable for web sections

$A_{r.v\max}$: maximum reinforcement allowable for flange sections

$A_{r.v\min}$: minimum reinforcement allowable for flange sections

$A_{rt.h}$: actual area of tensile horizontal reinforcement

$A_{rt.h}'$: nominal area of tensile horizontal reinforcement

$A_{rt.v}$: area of tensile vertical reinforcement

A_t : area of transverse torsional reinforcement required

$A_{t.l}$: area of longitudinal torsional reinforcement required

$A_{t.l\min}$: minimum area of longitudinal torsion reinforcement required according to ACI

$A_{t.t}$: total area of transverse reinforcement required (= $A_t + 0.5\,A_v$)

$A_{t.t\min}$: minimum total area of transverse reinforcement required according to ACI

A_v : area of transverse shear reinforcement required (one leg of stirrup)

a_h : distance from support to section where horizontal shear forces are calculated

a_s : shear aspect ratio of test beam

a_v : distance from support to section where vertical shear forces are calculated

a_y : attenuation rate *(magnetic)*

$|A|, |B|, |C|$: notation used to calculate beam deflection at $T = 0$ *(dynamic)*

$|\dot{A}|, |\dot{B}|, |\dot{C}|$: notation used to calculate beam velocity at $T = 0$ *(dynamic)*

b : beam width

b_{frp} : width of non-magnetic zone for one side of beam ($b_{frp} \leq 0.5b$)

C : total beam material cost (per meter) without FRP

C_c : concrete material cost (per meter)

$C_{c/b}$: concrete material cost (per beam)

C_{ps} : prestressing reinforcement material cost (per meter)

$C_{ps/b}$: prestressing reinforcement material cost (per beam)

C_{frp} : additional beam material cost (per meter) due to use of FRP

$C_{frp/b}$: additional beam material cost (per beam) due to use of FRP

C_r : mild reinforcement material cost (per meter) without FRP

$C_{r/b}$: mild reinforcement material cost (per beam) without FRP

C_{total} : total material cost per meter for guideway beam element

D_b : diameter of longitudinal reinforcing bar

D_{GFRP} : diameter of GFRP in pultruded hybrid FRP rod

DAF : positive dynamic amplification factor (downward deflection) *(dynamic)*

d_v : "effective" depth (top of beam to neutral axis of lower tensile reinforcement)

d_h : "effective" horizontal width

$d_{p.h}$: distance from horizontal extreme compression fiber to $0.8 \cdot b$ at section a_h

$d_{p.v}$: distance from vertical extreme compression fiber to vertical centroid of prestressing tendons at section a_v

E : beam modulus *(dynamic)*

E_c : concrete modulus

E_{hfrp} : modulus of the hybrid FRP reinforcement

E_{hs} : modulus of the pultruded high strength FRP (e.g. GFRP)

$E_{hm.fib}$: modulus of the high modulus fibers (e.g. carbon)

$E_{hs.fib}$: modulus of the high strength fibers (e.g. glass)

E_m : modulus of resin matrix in pultruded hybrid FRP rod

E_r : concrete tensile reinforcement modulus

e : midspan eccentricity of parabolic tendon profile

e_a : eccentricity of prestress at section a_v

e_h : eccentricity between the centers of gravity of the vehicle and the guideway

e_{max} : maximum amount of eccentricity available for prestressing for the given section

F_1 : force in rod just before carbon fiber rupture

F_{av} : fraction of beam depth, h, where $F_{av} \cdot h$ equals a_v

F_{ah} : fraction of beam width, b, where $F_{ah} \cdot b$ equals a_h

F_D : dead load uncertainty multiplying factor

F_h : horizontal load uncertainty multiplying factor

F_{hfrp} : ratio of hybrid FRP cost to steel on a stiffness basis

F_{lp} : long term strength loss fraction due to relaxation of prestressing tendons

$F_{nr.h}$: ratio of compressive horizontal reinforcement, $A_{rc.h}$, to required horizontal tensile reinforcement, $A_{rt.h}$

$F_{nr.v}$: ratio of compressive vertical reinforcement, $A_{rc.v}$, to required vertical tensile reinforcement, $A_{rt.v}$

F_p : force in rod just after carbon fiber rupture

F_{ra} : fraction of reinforcement allowed with respect to area of section

F_t : factor used to calculate minimum amounts of stirrup and torsion reinforcement required

F_u : ultimate load carrying capacity of rod

F_v : vertical load uncertainty multiplying factor

F_y : net magnetic force in y direction *(magnetic)*

$F_{\Delta T}$: axial force due to thermal stress

f_1 : fundamental beam frequency *(dynamic)*

$f_{c.c}^{\bullet}$: maximum compression allowable for concrete section

$f_{c.t}^{\bullet}$: maximum tension allowable for concrete section

$f_{hm.fib}$: tensile strength of the high modulus fibers

$f_{hs.fib}$: tensile strength of the high strength fibers

f_n : beam frequency of vibration mode number n *(dynamic)*

H : magnetic field *(magnetic)*

h : beam depth

h_{frp} : depth of non-magnetic zone for one side of beam ($h_{frp} \leq h$)

I : vertical beam moment of inertia *(dynamic)*

$I_{g.h}$: horizontal moment of inertia for the box section

$I_{g.v}$: vertical moment of inertia for the box section

$k_{\Delta h}$: horizontal deflection constraint

$k_{\Delta v}$: vertical deflection constraint

L : beam length

L^* : convergent beam length *(dynamic)*

L_g : actual gap length between successive loading pads *(dynamic)*

L_p : actual vehicle loading pad length *(dynamic)*

L_p^* : "convergent" vehicle loading pad length *(dynamic)*

L_v : actual vehicle length

L_v^* : "convergent" fully distributed vehicle length *(dynamic)*

$M_{cr.h}$: net horizontal cracking moment at section a_h

$M_{cr.v}$: net vertical cracking moment at section a_v

M_D : unfactored moment due to dead load

$M_{max.h}$: maximum vertical moment due to factored loads at section a_h

$M_{max.v}$: maximum vertical moment due to factored loads at section a_v

$M_{n.h}$: required horizontal bending moment

$M_{n.v}$: required vertical bending moment

m : distributed beam mass *(dynamic)*

$NDAF$: negative dynamic amplification factor (upward deflection) *(dynamic)*

n : ratio of reinforcement modulus to concrete modulus

n : vibration mode number *(dynamic)*

P : amount of prestressing force required to satisfy deflection and tension constraints

P : traveling concentrated force *(dynamic)*

P_d : conductor power dissipated *(magnetic)*

$P_{e.\min}$: minimum amount of prestressing force required to control deflection considering maximum possible eccentricity of section

P_h : concentrated horizontal midspan load

$P_{h\max}$: maximum amount of prestressing force allowed to limit compressive stress in concrete section under horizontal bending

$P_{h\min}$: minimum amount of prestressing force required to limit tensile stress in concrete section under horizontal bending

P_v : concentrated vertical midspan load

$P_{v\max}$: maximum amount of prestressing force allowed to limit compressive stress in concrete section under vertical bending

$P_{v\min}$: minimum amount of prestressing force required to limit tensile stress in concrete section under vertical bending

R : conductor radius *(magnetic)*

$RDAF$: residual dynamic amplification factor (free vibration) *(dynamic)*

S_p : actual vehicle pad spacing *(dynamic)*

S_p^* : convergent vehicle pad spacing *(dynamic)*

s : stirrup spacing

T : time during residual vibration response *(dynamic)*

T^* : time period between convergent loads *(dynamic)*

T_n : nominal (required) torsion to be resisted by beam

$T_{n,\max}$: maximum allowable torsion capacity of the beam

T_u : factored torsion

t : box beam thickness

t : time forced and residual beam vibration response *(dynamic)*

t_{CFRP} : thickness of CFRP overwrap in pultruded hybrid FRP rod

u_c : concrete unit cost

u_{hfrp} : hybrid FRP reinforcement unit cost

$u_{hm.fib}$: high modulus fibers unit cost

$u_{hs.fib}$: high strength fibers unit cost

u_m : resin matrix unit cost

u_r : unit cost of concrete tensile reinforcement (e.g. steel)

$u(x,t)$, $\dot{u}(x,t)$, $\ddot{u}(x,t)$
: beam transverse displacement, velocity, and acceleration response due to a point load at time t *(dynamic)*

$u(x,T)$, $\dot{u}(x,T)$, $\ddot{u}(x,T)$
: beam transverse displacement, velocity, and acceleration response due to a point load at time T *(dynamic)*

$V_{c/b}$: volume of concrete required per beam

$V_{ci.h}$: total nominal horizontal flexure shear cracking strength at section a_h

$V_{ci.h\min}$: minimum nominal horizontal flexure-shear strength at a_h

$V_{ci.v}$: total nominal vertical flexure-shear cracking strength at section a_v

$V_{ci.v\min}$: minimum nominal vertical flexure-shear strength at a_v

$V_{cw.h}$: horizontal web shear at section a_h

$V_{cw.v}$: vertical web shear at section a_v

V_D : dead load shear at a_v

$V_{frp/b}$: total volume of mild reinforcement required to be FRP

V_{hs} : volume fraction of high strength FRP (e.g. GFRP) in hybrid rod

$V_{hm.fib}$: volume fraction of high modulus fibers (e.g. carbon fibers) in high modulus FRP (e.g. CFRP)

$V_{hs.fib}$: volume fraction of high strength fibers (e.g. glass fibers) in high strength FRP (e.g. GFRP)

$V_{i.h}$: vertical shear due to factored load at section a_h

$V_{i.v}$: vertical shear due to factored load at section a_v

$V_{n.h}$: required horizontal shear strength

$V_{n.v}$: required vertical shear strength

V_p : vertical component of prestress

$V_{r/b}$: total volume of mild reinforcement required per beam

$V_{rc.h.frp/b}$: compression web reinforcement volume required, non-magnetic

$V_{rc.v.frp/b}$: compression flange reinforcement volume required, non-magnetic

$V_{rt.h.frp/b}$: tension web reinforcement volume required, non-magnetic

$V_{rt.v.frp/b}$: tension flange reinforcement volume required, non-magnetic

$V_{r.l/b}$: volume of longitudinal reinforcement (i.e. bars) required per beam

$V_{r.t/b}$: volume of transverse reinforcement (i.e. stirrups) required per beam

$V_{t.l.frp/b}$: torsion reinforcement volume required, non-magnetic

$V_{t.t.frp/b}$: stirrup reinforcement volume required, non-magnetic

V_u : factored shear

v : vehicle velocity

v^* : convergent vehicle velocity *(dynamic)*

v_L^*, $v_{L_p}^*$, $v_{L_v}^*$, $v_{S_p}^*$
: convergent vehicle velocities due to: beam length, pad length, fully distributed vehicle length, pad spacing *(dynamic)*

w_D : dead load

w_h : distributed horizontal load

w_m : distributed magnetic motor winding load

$w_{t.\max}$: maximum tension allowable in section

w_v : distributed vertical load

X_1 : horizontal distance between edges of stirrup confinement cage

x : distance along beam from origin of traveling force *(dynamic)*

Y_1 : vertical distance between edges of stirrup confinement cage

$y_{c.h}$: horizontal distance from side of section to mass center

$y_{c.v}$: vertical distance from top of section to mass center

$y_{t.h}$: horizontal distance from bending neutral axis to the extreme tension fiber in the cross section

$y_{t.v}$: vertical distance from the bending neutral axis to the extreme tension fiber in the cross section

α : ratio of F_1 to F_p of hybrid FRP rod

$\alpha_{\max}$: maximum value of α for hybrid FRP rod to ensure ductility

α_r : fraction of yield strain permissible during service load

α_t : torsional strength coefficient

$\alpha_{\Delta T}$: coefficient of temperature expansion

β : notation for $(\pi v/L)$ *(dynamic)*

β_1 : strength reduction factor for concrete based on the working stress block design

γ : ratio of F_u to F_1 of hybrid FRP rod

γ : notation for $(-2P/mL)$ *(dynamic)*

$\gamma_{\min}$: minimum value of γ for hybrid FRP rod to ensure reserve strength capacity

$\gamma_{ps,ps1,ps2}$: prestress factors

Δ : notation for $(\pi x/L)$ *(dynamic)*

ΔT : temperature change

Δ_T : unrestrained axial elongation or contraction due to ΔT

$\Delta_{dyn.pos}$: maximum positive (i.e. upward) dynamic beam deflection *(dynamic)*

$\Delta_{dyn.neg}$: maximum negative (i.e. upward) dynamic beam deflection *(dynamic)*

$\Delta_{dyn.res}$: maximum beam deflection during residual vibration *(dynamic)*

$\Delta_{h.\max}$: maximum horizontal beam deflection allowable

$\Delta_{stat.pos}$: maximum static beam deflection under a fully distributed load *(dynamic)*

$\Delta_{v.\max}$: maximum vertical beam deflection allowable

δ : skin depth *(magnetic)*

ε_c^* : ultimate strain of concrete in compression

ε_{hm}^* : ultimate strain of the high modulus fibers and yield strain of hybrid FRP rod

ε_{hs}^* : ultimate strain of the high strength fibers and the hybrid FRP rod

ε_r° : concrete tensile reinforcement (e.g. steel) strain during service load

ε_r' : mild (e.g. steel) reinforcement strain before yield

λ : wavelength integer multiplier *(dynamic)*

μ : conductor permeability *(magnetic)*

μ_0 : conductor free space permeability *(magnetic)*

μ_n : notation for $(n\beta)^2 - \omega_n^2$ *(dynamic)*

ρ : conductor resistivity *(magnetic)*

ρ_c : concrete density

ρ_{hfrp} : density of the hybrid FRP reinforcement

$\rho_{hm.fib}$: density of the high modulus fibers

$\rho_{hs.fib}$: density of the high strength fibers

ρ_m : density of the resin matrix

ρ_r : density of concrete tensile reinforcement (e.g. steel)

ϕ : material uncertainty reduction factor due to bending

ϕ' : material uncertainty reduction factor due to shear and torsion

ϕ_n : vibration shape for mode number n

ω_n : angular beam frequencies for vibration mode n

1.0 Introduction

1.1 Maglev background

Maglev technology refers to the magnetic levitation and propulsion of vehicles whereby, during operation, no physical contact occurs between the vehicle and guideway. Maglev vehicles are levitated on magnetic fields either by an "electromagnetic suspension", *EMS*, or an "electrodynamic suspension", *EDS*, method. An EMS, or attractive, system uses conventional electromagnets attached to the lower portion of the vehicle and, due to the need for the vehicle to "wrap around" the guideway, requires extremely small air gaps between the vehicle and guideway [Phelan 90]. In contrast, an EDS, or repulsive, maglev system operates when vehicle magnetic coils align with oppositely charged guideway magnets. The resulting repulsive magnetic forces levitate vehicles up to 20 cm (8 inches) from the guideway [Johnson, et.al. 89]. Due to their higher potential air gaps and their more efficient power consumption, EDS systems are felt to be more favorable for low cost guideway design.

German Transrapid EMS technology is the high speed maglev system that is nearing commercial implementation. Current plans for the Transrapid in the U.S. include a 21.7 km (13.5 mile) connection from the Orlando Airport to a vicinity near the Walt Disney World Resort in Florida. The Transrapid is limited to an air gap of 8-10 mm (0.3-0.4 inch), and therefore, successful operation of the system hinges on precise guideway alignment. The only EDS system near commercial operation is the Japanese MLU system. Though technically proven, the MLU concept may not be commercially feasible until advances are made in magnetic shielding technology. The unshielded MLU-002

passenger compartment currently experiences a magnetic flux density of 220 gauss[1] [Hayes 87]. Strong EDS magnet fields will limit the use of reinforcing steel in guideway structural members and are therefore likely to necessitate "magnetically inert" design and construction procedures.

Scientific feasibility studies were performed for maglev technology in the United States at the Massachusetts Institute of Technology beginning in the mid 1960's. However, primarily because the U.S. highway interstate system and the commercial airline network were predicted to supply sufficient capacity for all foreseeable national travel needs, federal funding for maglev research in the U.S. was abruptly canceled in 1975 [Johnson, et.al. 89]. Maglev research has continued abroad. Since 1975, West Germany and Japan have continued research, although along different paths, and each has produced prototypes at various stages of potential commercialization. Other countries actively pursuing maglev research include Canada, Romania, and Russia [Johnson and Giese 88].

U.S. interest in maglev research has increased dramatically in the past few years and is expected to continue with the passing of the Intermodal Surface Transportation Efficiency Act of 1991. This act allocates up to $750 million for maglev research over the next six years.

1.2 Motivation for research

Successful implementation of maglev technology in the U.S. depends greatly on the design of a high performance guideway system. High performance refers to a system

---

1 A "gauss" is a standard unit of measure for magnetic flux density. It is equal to one line of magnetic flux per square centimeter. *[1 tesla = 1 newton/(ampere•meter) = 10,000 gauss.]* Though the full extent of high magnetic field exposure on humans is not known, approximately 100 gauss is felt to be the human safety limit for extended periods of time. Current design criteria for passenger field exposure is approximately 0.5 gauss dc field and near 0.0 gauss ac field.

having a high operational characteristics to cost ratio. Thus, a high performance maglev guideway design involves not only low construction and maintenance costs, but also high performance-related attributes, such as low magnetic field interference and minimal beam residual vibrations.

Guideway construction costs are estimated to represent from 50% to 70% of all capital costs for a high speed maglev system [Phelan and Sussman 91]. Consequently, low cost guideway design is a top initial priority for a national maglev system. In addition, 1) magnetic interference between the guideway structure and the magnetic coils and 2) beam dynamic behavior effects, are important performance-related guideway design issues. The magnetic interactions between the guideway beam and the motor windings lead to significant power losses and produce stray magnetic fields—resulting in vehicle control difficulties. Significant guideway beam residual oscillations adversely affect vehicle ride quality, vehicle speed, vehicle headway scheduling, beam lifespan, and the amount of non-magnetic structural material required in the guideway.

Many maglev concepts today appear to have considered guideway design only after vehicle design was well developed, leading to expensive and potentially poorly performing guideway systems—with little possibility for either cost reduction or performance improvement by the structural engineer. The focus of this thesis is on the investigation of a high performance maglev guideway design, specifically a high performance narrow beam guideway system. A narrow beam is selected with the objective of reducing overall construction and maintenance cost of the guideway system and simplifying the task for guideway maintenance and alignment. Thus, structural optimization is desired. A narrow box beam guideway design is applicable to both EDS and EMS systems, though an EDS system is assumed in this study.

In addition to structural optimization, the civil engineering and construction industries are challenged by maglev's requirement of reliable and economical non-magnetic concrete reinforcement. Based on the conviction that EDS systems will prove to be more economical than EMS maglev suspension systems, it is expected that non-magnetic concrete reinforcement will be required for maglev guideways. Because steel girders cannot be used with EDS systems and because the use of mild steel reinforcement in concrete near high magnetic fields will be either limited or prohibited, a non-magnetic substitute for steel reinforcement is required. Currently, pultruded (i.e. extruded under tension), glass fiber reinforced plastic, FRP, is used in certain concrete applications. However, long term deterioration of glass fibers when exposed to the alkaline environment of the concrete is likely. Though carbon FRP is inert to concrete, currently it is not economical. A low cost glass and carbon hybrid FRP concrete reinforcing rod that is both inert to the concrete alkaline environment and non-magnetic, is proposed in this thesis. In addition, a design procedure for a rectangular, hollow-box, narrow guideway beam is presented.

Finally, guideway beam residual vibrations depend on the beam fundamental frequency, beam length, vehicle length, vehicle pad length, vehicle pad spacing, and vehicle speed. Designing for minimal beam residual vibration is key to long guideway lifespan, short vehicle headways, adequate passenger ride quality, and minimal non-magnetic reinforcement requirements. Currently, maglev vehicle and magnetic winding concepts are being designed by other maglev researchers—generally without regard to beam dynamic behavior. Because the dynamic behavior of the guideway beam will significantly effect the cost of the beam, the determination of satisfactory vehicle pad distributions for given beam spans is critical to high performance guideway beam design, and is therefore, an immediate research concern.

1.3 Research objectives

The ultimate objective of this research is to investigate the potential for the design of a high performance maglev guideway system. Three specific objectives of this thesis are to determine:

- if an economical and reliable non-magnetic concrete reinforcement can be produced that is acceptable to the civil and construction industry
- whether a narrow beam guideway concept can support expected operational loads, and if so, at what cost
- the dynamic response of the guideway beam under a variety of vehicle loading configurations and velocities

1.4 Thesis organization

The research is divided into three main areas;

- hybrid FRP rod conceptualization, manufacture, and testing
- narrow beam guideway design
- dynamic beam behavior analysis

Chapter 2 presents the overall maglev guideway design approach including the assumptions used. Design requirements are listed and conventional construction methods are explained. Also included is a discussion of conceptual guideway designs and material selections. Chapter 3 focuses on the design, manufacture, and testing of non-magnetic hybrid FRP concrete reinforcing rods. The theory behind the hybrid FRP rod concept is presented along with test results of concrete beams reinforced with hybrid FRP rods. Material cost factors are given and formulas for determining hybrid FRP costs, with respect to steel, are computed. A theoretical method used to determine magnetic

interference potential is included in Appendix A. Load-deflection plots for all seven concrete beams tested are shown in Appendix B.

Chapter 4 presents formulas derived for the design of a reinforced concrete, hollow-box section using both steel and hybrid FRP reinforcement. Explanations are given for equations and a step-by-step example is performed. A spreadsheet analysis program called "BoxCost" incorporates the narrow beam equations used to perform sensitivity analyses on the narrow beam design. Sensitivity analyses are performed to determine expected narrow beam: length, width, height, weight, frequency, and cost. The chapter concludes with a cost comparison of the narrow beam design with other maglev system cost projections—in particular, Transrapid cost estimates. The program, *BoxCost*, showing calculations used for the example in Chapter 4, is presented in Appendix C.

Chapter 5 focuses on the analysis of the guideway beam dynamic behavior. The analysis is performed using both a finite element method and a closed form mathematical solution for a simply-supported beam having no damping and, with uniform cross-section and stiffness. A spreadsheet analysis program called "mode3", utilizing the first three modes of the closed form beam vibration solution has been developed to analyze guideway beam behavior under a variety of vehicle velocities and loading configurations. The program, *mode3*, is shown in Appendix D along with test case examples. Close agreement between the finite element solution and the closed form solution is demonstrated.

Both the concept of convergent velocities, whereby no beam residual vibrations are present after a vehicle passes, and the mathematical derivations for these velocities, are presented in Chapter 5,. Examples are given which show the effects beam length and frequency as well as vehicle velocity, length, pad length, and pad spacing have on beam

residual vibrations. Vehicle configurations for certain beam spans are suggested. In addition, the concept of "motion based design" is discussed.

The thesis concludes in Chapter 6 with a summary and conclusions of the research. Major research contributions and suggested areas for future research also are listed in Chapter 6.

2.0 Narrow Beam Design

This chapter introduces and discusses the concept and the rationale of the narrow beam maglev guideway system. Maglev structural design requirements are discussed and identified. Conventional construction methods are presented along with construction cost comparisons. The narrow beam concept is proposed in order to significantly reduce guideway construction and maintenance costs which are subject to constraints imposed by structural design, material selection, and construction method concerns. The potential for automated guideway construction and maintenance is also discussed. The chapter concludes with a summary of design constraints assumed for the analyses of the narrow beam of this thesis.

2.1 Structural design requirements

2.1.1 Overview

A maglev structural system design must satisfy a range of functional requirements—not only traditional primary requirements, such as structural strength and stiffness, but also secondary requirements such as dynamic response, fatigue, durability, maintainability, and magnetic interference of the structure. For high speed maglev structural systems, these secondary design issues may become dominant constraints.

This section outlines various structural design requirements so that reasonable design criteria can be determined. Structural design requirements include: 1) geometry of the structure, 2) structural loads, 3) load effects, 4) durability, and 5) magnetic inertness of structural system components. Geometric structural design constraints include limits on span length, beam width, beam depth, beam wall thickness, and guideway elevation. Structural loads include beam dead weight, vehicle loads, wind loads, snow loads, and seismic loads. Load effect constraints—including deflection control, vibration limitations,

and thermal expansion and contraction criteria—influence not only material selection and cross-sectional shape, but also the initial conception and design of specific structural systems. Durability requirements are concerned primarily with corrosion, toughness, and fatigue resistance of the guideway structure. The magnetic inertness requirement for selected portions of the guideway effects both material selection and conceptual guideway shape determination. These specific maglev structural requirements are discussed in detail in the following subsections.

2.1.2 Geometry

Span length

In general, an optimal span length exists for elevated structures. Shorter spans reduce beam cost, but increase overall column, footing, and earthwork costs as more columns and footings are required for a given corridor distance. Beam costs vary approximately with the square of the span length, whereas column and foundation costs (for a given guideway elevation) are essentially proportional to the number of columns required (i.e. to the inverse of beam length). The number of columns required is determined by the length of the span. Because a typical maglev corridor traverses several hundred kilometers, it is more economical to use standard span lengths for the entire guideway system than to design site-specific structural elements of varying lengths. Significant cost savings for beam elements using off-site fabrication and automation are also possible. Thus, standardization of the beam element is desirable. Substantial cost savings resulting from automation is more difficult for column and footing designs as the design and construction of these elements are generally site-specific.

For high speed maglev design, intermediate spans (20-30m) are likely to be required.[1] For elevated sections (i.e. guideway elevations greater than 6 m), a 1985

[1] Span length also influences the choice of continuity of the structural system (e.g. continuous vs. simply supported). This is discussed in section 2.4.

Canadian Institute of Guided Ground Transportation, CIGGT, study considers a beam length of approximately 25 m as the standard span [CIGGT 89]. The Transrapid test track at Emsland, Germany has used a variety of spans concentrating primarily on 25 m spans as standard—though some spans range as high as 37 m [Hilliges and Schambeck 89].

Though a 25 m span appears desirable, it may not always be feasible. Other factors such as heavy vehicle and/or payload weight as well as the weight of the beam itself can limit the practical span length due to excessive deflections and cost. Such constraints appear to have limited the standard span length selected for the new Japanese Yamanashi maglev test track. This track, scheduled to be completed in the late 1990s, has standard span lengths of 12.6 m [Wakui, et.al. 91]. The choice of such a short span length is likely the result of the high dead load of the U-shaped channel guideway.

In general, shorter, variable span lengths are less aesthetically pleasing than longer, uniform span lengths. For the present analysis, 25 m is used as the standard span length. A sensitivity analysis is performed for spans ranging from 12.5 m to 35.0 m in Chapter 4 so as to determine a span length which best meets all the objectives.

Beam width

Beam width limits are determined primarily by the dimensions of the vehicle and the relationship between the guideway and the vehicle. For example, because the Japanese MLU-002 vehicle has a width of 3.0 m [Takeda 89] and must ride inside a U-shaped guideway, the guideway is 4.0 m in width.[2] In general, other maglev conceptual systems designed to ride within guideway walls (i.e. open channel guideway systems), will have beam widths of four to five meters. The German Transrapid T-shaped guideway system, though wrapping around the guideway, also has relatively large width

[2] The 4.0 m width is estimated from a scale drawing and is dependent on a) the vehicle width of 3.0 m, b) the airgap, c) the magnet width and d) the width of vertical beam cantilever (i.e. the wall width).

requirements as practically the entire width of the vehicle rests on the upper surface of the beam element. The MLU channel guideway has a calculated minimum mass of at least 5.0 tonnes/meter[3] while Transrapid's is reported to be 3.6 tonnes/meter for a 25m span. Thus, the mass of the 3.0 m wide Transrapid guideway beam should be significantly less than the MLU channel guideway. The other Japanese maglev guideway system, the HSST, consists of twin metal rails projected out from and attached to a concrete hollow-box beam. The width of the inner concrete beam is approximately 1.4 m without the metal rail extensions. The total width of the HSST guideway beam including the metal rail extension is 2.5 m [Hayashi and Ohishi 89].

Though current guideway designs for the high speed maglev systems nearing operational status (e.g. Transrapid, HSST, and MLU) have beam width requirements equal to or in excess of 2.5 m, it is felt that a minimum cost guideway, using a more narrow beam element, is achievable. A maglev system operating on a narrow, hollow-box beam guideway has been discussed as a method for significantly reducing overall guideway costs [Thornton 90]. Sensitivity analyses in Chapter 4 examine a range of beam widths (e.g. 1.0 m to 2.0 m) for a variety of loading patterns. Currently, it is felt that a guideway system having a beam width of 1.2 m to 1.6 m is feasible and, unless otherwise determined impractical, a maximum beam width criterion of 1.6 m should be considered for a narrow beam design.[4]

Beam depth

The guideway structure is assumed to be elevated to ensure grade separation with other structures and obstacles within its right of way (e.g. rivers, highways, railways, etc.). Therefore, beam depth standardization is not as significant as beam width and span

---

[3] Estimated from a scale drawing of a single sidewall [Wakui, et.al. 91]. Each sidewall is estimated to have an approximate mass of 1.0 tonne/m. Though the mass of the base will fluctuate with span length, a minimum 3.0 tonne/m base mass is estimated by this author.

[4] See Chapter 4.

length standardizations. In general, for heavier vehicles, the depth of the beam is increased. Due to stability concerns, however, possible depth increases for a given beam width and wall thickness are limited to an appropriate beam depth-to-thickness ratio. Also, as with any elevated structure subjected to significant wind forces, the depth is constrained as much as is practically possible in order to reduce wind exposure and to increase the torsional stability of the element. With the expectation of relatively large torsional moments and stringent wind resistant behavior requirements, it is assumed that the beam depth should not exceed approximately 1.5 times its width (e.g. an approximate 2.1 m maximum beam depth for a given 1.4 m beam width), so as to adequately resist torsion and bending. Maximizing beam depth tends to minimize the amount of mild steel required for a given stiffness criteria—and thus minimizes beam material cost.[5] Therefore, from a cost standpoint and subject to beam weight and stability constraints, maximizing beam depth is generally advantageous.

Beam wall thickness

A thin-walled box section is advantageous as both beam dead weight and overall material costs are reduced. In addition, thin-walled sections reduce adverse thermal effects.[6] Daily temperature differentials between interior and exterior beam surfaces due to prolonged solar radiation produce transverse flexural moments in the walls and top and bottom beam surfaces of the box section. These transverse flexural moments cause tensile stresses along the exterior of the cross-section [PTI 78]. Without adequate venting, thick concrete sections experience significant tensile stresses and tend to warp. Thus, it is desirable to minimize the wall thickness of the narrow beam design.

Reduction of the web section is limited however by stability, durability, and construction concerns. Traditional practice has limited minimum box beam web

---

[5] See Chapter 4.
[6] See subsection 2.1.4.

thicknesses to 0.20 m (8.0 in). A standard rule of thumb in the U.S. has been 1 inch (25 mm) of web width for every foot (300 mm) of box girder height, with 0.20 m as a minimum [Degenkolb 77]. For a 2.1 m deep section, this "one inch per foot of depth" rule-of-thumb translates into a wall thickness of 0.175 m. Primary justifications for conventional wall thickness limitations of 0.20 m are to:

- ensure sufficient section strength and stability in order to adequately resist compressive, transfer shear, and torsional shear forces
- provide adequate confinement of the stirrup reinforcement so that cracking is prevented
- provide sufficient clear cover to prevent corrosion of embedded reinforcement (i.e. ensure durability of the section)
- guarantee sufficient space for reinforcement materials (i.e. provide physical space necessary for stirrups, prestressing ducts, clear cover, etc.)

Though the majority of highway concrete box girder applications have wall thicknesses greater than 0.20 m, examples of thinner sections do exist. One recent example of a thin-walled box section is a bridge near Yverdon, Switzerland [Yverdon 90]. The box section has a wall thickness of 0.18 m with embedded pre-tensioning cables. Another, perhaps more relevant example, is the Seattle Monorail constructed for the 1962 World's Fair. Straight sections of this guideway are up to 30 m in length and approximately 1.5 m in depth. The beam wall thickness is as low as 0.11 m (4.5 in) with embedded oval-shaped prestressing ducts [Lemcke 92].

For the narrow beam concept, the wall thickness is set to the maximum value of 1) $0.10b$, where b is the beam width—in accordance with American Concrete Institute recommendations [ACI 89], and 2) 0.15 m. This 0.15 m minimum wall thickness is selected for the analyses in this thesis over the more common 0.20 m highway bridge minimum for the following reasons :

- there is more certainty of actual loading conditions with maglev than with conventional highway construction (i.e. access to the guideway and weight of vehicles are more strictly controlled)
- maglev vehicle loadings have less magnitude and greater distribution—leading to better moment distribution across the span—in comparison with highway truck, bus, and car loadings
- it is likely that higher strength concrete (e.g. 41.5 MPa) and high quality automated casting procedures will be used—therefore reducing concrete porosity and variability—which will allow for the use of thinner sections
- the expected use of fiber reinforced concrete will reduce the cracking potential of the concrete[7] and thus reduce the need for confinement—i.e., a single strand stirrup in the web can be used instead of a U-shaped stirrup [FIP 84].
- local widening of the section wall around prestressing tendons (see Figure 2.5.1) allows for the use of thinner sections

Beam wall thicknesses less than 0.10 m are not considered in the analyses of this thesis to ensure conservatism in the design. Future research regarding the minimum wall thickness acceptable is needed however, as the economic benefits of using high strength concrete are only realized with thin-walled sections.[8]

2.1.3 Loads

Dead weight

Both the weight of the beam (e.g. concrete, steel) and the weight of the structure attached to the beam (e.g. the aluminum suspension, propulsion, and guidance system) constitute the beam dead weight loading. This loading is considered to be uniformly distributed. Normally, dead loads result in an initial deflection in the beam. However, for

[7] See subsection 2.2.1.
[8] See Chapter 4.

improved ride quality and reduced cracking of the reinforced concrete beam, prestressing is used to minimize dead load deflections. Prestressed tendons are arranged to cancel any potential beam dead load deflection—to provide either zero dead load deflection or a slight upward camber. For a typical 25 m narrow box beam span, the beam dead load, including material weights of the concrete, steel, and aluminum windings of the beam, is approximately 20-30 N/m (i.e. a beam mass of 2.0-3.0 tonnes/m).[9] For the analysis in this thesis, it is assumed that all dead load deflection is canceled with prestressing.

Vehicle load

Vehicle loads can range from uniformly distributed to concentrated point loads, depending on the loading pad configuration of the vehicle. Though any vehicle loading pad arrangement can be accommodated in a beam structural design, generally, as size and strength requirements for the guideway are directly influenced by the distribution of the vehicle loading, the more distributed the load, the lower the cost of the guideway.

Examples of two loading cases are helpful. The first case is a simple concentrated (i.e. point) load applied at a beam midspan. With an equal magnitude of load as the first case, the second loading case is uniformly distributed across the beam span.[10] For a given span length, L, a concentrated midspan load of wL—where w is the uniformly distributed load (e.g. 20 kN/m)—has a midspan deflection 60% greater than that resulting from a fully distributed loading of w for a simply-supported structure (i.e. $8wL^4/384$ vs. $5wL^4/384$, respectively). In addition, the midspan bending moment for the concentrated midspan loading is 100% greater than for a fully distributed loading (i.e. $wL^2/8$ vs.

---

[9] See Chapter 4.

[10] Though this example is simple elementary beam mechanics, the point seems to be lost in number of maglev system designs as loads are concentrated. For example, the latest Japanese MLU design has switched from an essentially fully distributed loading configuration to one having two concentrated loading pads at either end of the vehicle.

$wL^2/4$, respectively). Therefore, from an economical guideway design perspective, a more uniformly distributed vehicle loading is desirable.

The expected maglev vehicle loading is 19.61 kN/m, though the extent of vehicle load distribution is not presently known. According to ACI code, live loads are multiplied by a factor of 1.7 to account for uncertainties in the actual live load [ACI 89]. The analysis performed in Chapter 4, however, incorporates a 1.4 live load uncertainty factor in its calculations, since accurate initial maglev vehicle load prediction is required for efficient motor design and operation. The expected 19.61 kN/m distributed maglev vehicle loading is structurally less demanding than typical high speed rail, HSR, loading requirements. For example, both the French TGV and the German ICE trainsets carry approximately 200 kN per axle load [Kurz 91]. Also, dynamic effects generally are less severe for more fully distributed vehicle loadings.[11]

Wind loads

Wind loads are also considered live loads, but because prediction capabilities for wind loads are less precise than they are for maglev vehicle and beam loads, estimated wind load values are multiplied by a 1.7 safety factor. Preliminary unfactored load estimations are presented in Table 2.1.1 for three maglev case scenarios [Barrows 92]. The first case is for a vehicle traveling at full speed in a 27 m/s wind. The second case is for a stationary vehicle on the guideway in a 54 m/s wind. The third case is for the guideway with no vehicle in a 90 m/s wind. Each of these three scenarios produces a different uniform horizontal pressure on the guideway. In addition, the moving vehicle produces a concentrated horizontal force on the guideway near the nose of the vehicle. The three scenarios, along with the equivalent horizontal wind loads are summarized in Table 2.1.1.

[11] See Chapter 5.

Table 2.1.1 Equivalent unfactored distributed wind load for three scenarios

wind speed (m/s)	vehicle on guideway?	vehicle moving?	deflection constraint	concentrated load (kN)	distributed load (kN/m)	equivalent distributed load (kN/m)
27	yes	yes	stringent	89.24	2.94	10.08 *
54	yes	no	moderate	0	14.71	14.71
90	no	no	relaxed	0	22.06	22.06

* *for a 25 m beam span*

Source: [Barrows 92]

The equivalent distributed load value produces an equal beam moment as the distributed load and concentrated load combined and is used for comparison between the three wind case scenarios. For the 27 m/s wind scenario, the equivalent load varies from 14.84 kN/m for a 15 m beam span to 8.04 kN/m for a 35 m beam. The 10.08 kN/m equivalent load shown in Table 2.1.1 is for a 25 m beam span. The 90 m/s wind case, having no vehicle on the guideway, is the worst case design scenario on a strength basis. However, when the vehicle is either stationary, or absent from the guideway, the stringent beam deflection criteria, necessary for acceptable maglev vehicle passenger ride quality, can be relaxed somewhat. Thus, when considering beam deflection constraints, the 27 m/s wind scenario shown in Table 2.1.1 is the determining case. For beam spans greater than 15 m, however, the equivalent distributed load for the 27 m/s wind speed case is less than that for the 54 m/s wind. Therefore, to ensure a conservative first order design, the 14.71 kN/m equivalent load for the 54 m/s wind case scenario is used along with stiffness constraints for the moving vehicle (i.e. the 27 m/s wind speed case). The analysis performed in Chapter 4 restricts maximum horizontal midspan beam deflection to as low as 2.5 millimeters.[12]

In addition to side sway, wind loads produce torsion in the guideway due to the eccentricity between the beam and vehicle centers of gravity. This eccentricity is

[12] See Chapter 4.

minimized to reduce torsion in the beam. However, as the eccentricity is reduced, aerodynamic drag and noise is increased. Currently, the eccentricity between the vehicle and beam centers of gravity is estimated at 3.0 m. As an example, the distributed 54 m/s wind, producing a 14.71 kN/m distributed horizontal load acting with a 3.00 m eccentricity between the vehicle and guideway, results in torsion of 44.13 kN distributed uniformly over the length of the guideway. These expected loadings due to wind are shown in Figure 2.1.1.

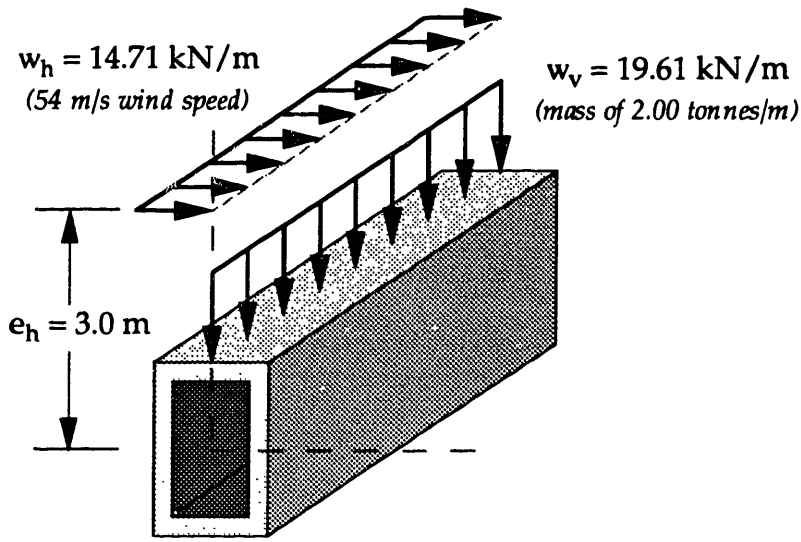

Figure 2.1.1 Expected Guideway Beam Loadings

As indicated in the figure, the 54 m/s wind speed results in a horizontal distributed force, w_h, of 14.71 kN/m acting at an eccentricity, e_h, of 3.0 m from the mass centroid of the beam. Also shown is a fully distributed vehicle load, w_v, of 19.61 kN/m, corresponding to a vehicle mass of 2.00 tonne/m. Loads shown in the Figure 2.1.1 correspond to the example presented in Chapter 4.

Additional loads

Additional potential beam loads include seismic, or earthquake, and snow loads. Potential earthquake loads on the guideway structure vary between geographic regions. Through the use of base isolation technologies, earthquake energy can be dissipated at the

top of the columns thereby removing significant earthquake induced oscillations in beam elements [Ferritto 91]. Thus, with respect to the beam element design, earthquake loads are not likely to be substantial. For guideway sections where base isolation is not used, designing the beam element to resist earthquake loads is necessary. It is likely to require a continuous structure due to difficulties in designing adequate joints for simple spans under severe lateral accelerations. This thesis neglects earthquake loads in the analyses and suggests the use of base isolation systems.

Though snow loads have not been considered specifically in this thesis, it is likely that substantial snow accumulations will be removed prior to vehicle operation. Therefore, snow loads are also neglected in the analyses of this thesis as they are unlikely to exceed vehicle design loads. Should a significant snow load be present during vehicle operation however, it is modeled as an additional live load with a 1.7 design safety factor imposed.

2.1.4 Load effects

Load effects typically refer to beam deflections resulting from static and dynamic forces and moments exerted on portions of the beam. In addition, thermal expansion and contraction tendencies of the beam can cause bowing and warping of the beam if allowances are not made for such movements. The acceptable guideway design must be capable of resisting all load effects within the constraints necessary for acceptable system operation.

Static forces and moments

Static forces induce shear, tensile, and compressive stresses in the beam. According to elementary beam theory, downward vertical bending typically produces tension forces in the lower portion of the beam and compression forces in the upper portion. These forces vary along the span and usually reach a maximum at the beam midspan. By contrast, shear stresses and torsion are typically greatest near beam supports.

midspan. By contrast, shear stresses and torsion are typically greatest near beam supports. For a conservative first order approximation, the largest forces and moments experienced along any portion of the beam are considered the design criteria for the entire beam. To resist wind loads, the member must have equal resistance to tension and compression on either side of the beam. In addition, the member must resist shear stresses and torsion resulting from both vertical and horizontal loads.

Dynamic forces and moments

Dynamic forces and moments are similar to static bending, shearing, and torsional forces and moments with the addition of "negative" conditions which result from oscillations of the element. Thus, in addition to compression during positive bending, the upper portion of the beam experiences tension during negative bending—though this tension is somewhat less than the tension found in the lower portion of the beam during positive bending. Furthermore, the lower portion of the beam is subjected to compression during negative bending conditions. Dynamic forces generally result in higher deflections than those computed using static forces. Typically, a dynamic amplification factor, DAF, is used to convert a static analysis to a dynamic one. The DAF is the ratio of the maximum positive beam deflection during dynamic loading to the maximum static deflection. In addition to the DAF, this thesis focuses on the negative dynamic amplification factor, NDAF, and the residual dynamic amplification factor, RDAF. The NDAF and the RDAF refer to the ratio of the maximum negative and residual dynamic beam deflections, respectively, to the maximum static beam deflection. These three dynamic effects (i.e. the DAF, NDAF, and RDAF) are critical to maglev guideway beam design. In general, the NDAF equals the RDAF when the loading pad configuration of the maglev vehicle is approximately fully distributed across the vehicle length.[13]

[13] See subsection 5.2.3.

Deflections

To ensure adequate ride quality, allowable beam deflections due to beam dead weight as well as to all live loads are limited. Most commonly, deflection criteria is presented as a ratio of the span length over a set numerical value, e.g. L/1000. ACI code for conventional construction, e.g. buildings, uses deflection criterion as high as L/480, with L/360 being typical [ACI 89].

Deflection criteria for maglev guideway structures are generally more stringent than for conventional construction. When considering maglev guideway roughness, and its effect on passenger ride quality, the maximum dynamic beam vertical and horizontal deflections, $\Delta_{v,max}$ and $\Delta_{h,max}$, respectively, are perhaps more appropriate deflection criteria measures. Sensitivity analyses performed in Chapter 4 have restrictions on $\Delta_{v,max}$ as low as 5 millimeters (i.e. a constraint of L/5000 for a 25 m span), and restrictions on $\Delta_{h,max}$ as low as 2.5 millimeters (i.e. a constraint of L/10,000 for a 25 m span).[14]

To enhance passenger comfort, prestressing tendons are used to eliminate beam dead load deflections. Dynamic deflections generally are larger than static deflections. However, the DAF can be limited to less than 1.2 for all expected vehicle velocities (e.g. up to 150 m/s) through proper load distribution.[15]

Dynamic deflection criteria can become secondary to beam damping for certain vehicle load distribution patterns and vehicle speeds. Damping mechanisms and material behavior must be such that the beam element either resumes a resting position before the next vehicle approaches or—if small beam vibrations remain—oscillates out of phase of approaching vehicles. The deflection criteria must consider restrictions for both short and long-term behavior. Short-term beam deflection behavior is calculated according to

---

[14] See Chapter 4.

15 The actual dynamic amplification factor depends on beam frequency, vehicle speed, and vehicle pad distribution—see Chapter 5.

elementary beam theory. Long term deflections, due to material creep, shrinkage, and/or relaxation, are estimated as a percentage increase of short term beam deflection calculations.

Thermal effects

Thermal load effects include stresses induced by strains resulting from temperature fluctuations. The coefficient of thermal expansion for steel and concrete is approximately $11\times10^{-6}/°C$, while for aluminum, it is $23\times10^{-6}/°C$. Thus, when combining aluminum with either concrete or steel, proper expansion joints must be designed to prevent thermal buckling and fatigue. When beam endpoints are constrained, changes in temperature induce thermal stresses. According to the American Association of State Highway and Transportation Officials, AASHTO, highway bridge spans must be designed to expand and contract from -34°C to +49°C [AASHTO 89].[16] For a 25 m beam, this requirement results in an allowable beam travel of approximately 2.3 cm (i.e. approximately 1 inch) as shown in the following AASHTO equation.

$$\Delta_T = \alpha_{\Delta T} L \Delta T = (11\times10^{-6}/°C)(25m)(49°C - (-34°C)) = \underline{0.023m} \qquad [2.1.1]$$

Restraining this movement within the structure requires a force equal to the unconstrained travel multiplied by the axial stiffness of the beam according to the following equation [Roeder and Moorty 91].

$$F_{\Delta T} = A_g E_c (\Delta_T / L) \qquad [2.1.2]$$

For the 25 m beam span example used in Chapter 4, this force is equal to:[17]

$$F_{\Delta T} = (0.96m^2)(28.3\times10^9\ N/m^2)(0.023m/25.0m) = \underline{\underline{24{,}800\ kN}}$$

---

[16] The temperature range shown are for metal structures in cold climates. These values are used over the less conservative rise and fall criteria for concrete structures.

[17] See Chapter 4 for values of A_g and E_c.

In general, a simply-supported beam allows free longitudinal displacement at one end of the beam which prevents thermal stress buildup in the beam. Thus, beam bowing and warping due to thermal expansion and contraction is not generally found in simply-supported structures. Elimination of beam thermal bowing and warping tendencies is one of the factors leading to the choice of a simply-supported structural suspension system for this thesis.[18]

Structural elements composed of materials having similar thermal expansion coefficients expand and contract uniformly, e.g. steel and concrete. In contrast, structural elements containing materials having significant differences in thermal expansion properties expand and contract non-uniformly. This non-uniform thermal behavior typically leads to internal thermal stresses, and potentially, to bowing of the element.

Reinforced concrete box sections have the potential for transverse beam deflections due to temperature gradients along the beam depth. These thermal gradient deflections are more pronounced for box sections when there is an overhang on the top flange of the girder which casts a shadow onto the web sections [Elbadry and Ghali 83]. Such deflections are due to uneven heating and cooling of the upper bridge deck with respect to the lower flange. For the narrow beam maglev guideway design proposed in this thesis, deflections due to thermal gradients are not expected to be significant as heat buildup during the day should quickly dissipate through the relatively thin webs of the box beam.[19] In addition, with the narrow beam design, there is a relatively small upper surface area subjected to the solar radiation.

---

[18] See Section 2.4 for a discussion of simple vs. continuous spans.
[19] See subsection 2.1.2.

2.1.5 Durability, toughness, fatigue

In addition to resisting loads and minimizing load effects, the structure must be resistant to acidic conditions—on the order of atmospheric acidity levels—as well as to vandalism and impact loads. Corrosion and other types of material deterioration must be prevented both on the exterior of the structure and in embedded materials. A number of materials deteriorate when exposed to certain environments (e.g. glass in concrete) due to chemical reactions of base material elements. Given long term durability requirements, these unfavorable chemical reactions must be prevented. The structure also must resist unexpected impact loads such as truck impacts and vandalism. Though the structure may not remain in service after certain impacts, it must be designed to ensure passenger safety for likely scenarios.

Due to the dynamic behavior of the beam from multiple vehicle passes, the structure must be designed to resist fatigue. Fatigue is a failure mode resulting from the dynamic oscillatory motion of the vibrating guideway. The fatigue failure potential of the guideway beam is evaluated based on 1) expected number of vehicle passes throughout the design life of the structure, 2) the extent of residual vibrations that occur after each vehicle pass, and 3) properties of materials used in the structure.

2.1.6 Magnetic inertness

A relatively unique design criteria for EDS maglev guideways is the requirement that significant areas of the structure be magnetically and electrically non-conducting. This is a challenge to the civil engineering design and construction industry as "magnetic inertness" is not a normal design criterion.[20] Though EMS systems do not appear to be effected substantially by structures made of magnetically conducting materials, e.g. steel, the magnetic field strengths and attenuation rates of EDS systems are likely to demand

20 An exception is magnetic resonance imaging, MRI, facilities in hospitals.

that such a criteria be imposed. Steel girders cannot be used with EDS systems, nor is steel reinforcement of concrete in areas near magnetic windings allowed [Bechtel, et.al. 92]. It is expected that the restriction of magnetic inertness can be relaxed for all but the upper portions of the guideway beam.

For the example in Chapter 4, only non-magnetic reinforcement is used in the upper two corners of the beam cross-section.[21] In Appendix A, a method developed by MIT Professor Mark Zahn to determine magnetic interactions with metals is presented. Chapter 3 of this thesis proposes an innovative application of advanced composite materials that satisfies the requirement for magnetic inertness of concrete reinforcement.

2.2 Material selection

2.2.1 Selection criteria

Strength, stiffness and damping

Of the three primary structural properties, strength, stiffness and damping, stiffness is expected to dominate any static analysis and is considered to be the primary design constraint. Dynamic loading effects increase the importance of structural damping characteristics for the overall guideway design. The tendency for damping constraints to exceed stiffness constraints depends on the particular dynamic behavior experienced by the guideway. Passive damping of two to five percent should be achievable through proper material selection. The potential amount of damping possible using active mechanisms is not known presently, but it is estimated to be between five and ten percent. For the analysis presented in this thesis, benefits from material damping are considered minimal. For the conceptual maglev guideway design, the approach is to

[21] See Figure 2.4.3.

design the guideway beam element independent of material damping properties. Subsequent innovations in beam damping mechanisms—both passive and active—can be added for additional ride quality improvements.

Corrosion resistance, magnetic inertness

Because the beam is prestressed, significant concrete cracking is prevented. As a result, water seepage through the concrete is minimized and corrosion resistance of embedded steel reinforcement is not a significant concern. The magnetic inertness criteria[22] applies to materials of the guideway structure within a specified distance of a given magnetic field.[23] Candidate substitute materials for concrete reinforcement in such restricted areas of the beam include boron, carbon, glass and aramid fibers.[24]

Glass fibers are relatively inert. However, when in direct contact with concrete, the alkaline properties of the concrete reacts with the glass causing the glass fibers to deteriorate over time. Thus, for use in concrete structures, glass fibers must be as alkaline resistant as possible and/or coated in some way to prevent contact with the concrete. Glass fibers also have somewhat uncertain long term mechanical behavior properties under long term loading conditions. Interestingly, steel actually has good long term behavior when exposed to alkaline environments. Corrosion of steel occurs when water or air is able to seep through microcracks in concrete and oxidize the embedded steel.

Durability, toughness, fatigue

Durability concerns include corrosion resistance and long term material behavior such as creep, shrinkage and relaxation. Durability of concrete sections can be increased using high strength concrete, concrete additives, and surface treatments such as sealants.

---

[22] See subsection 2.1.6.
[23] See Appendix A.
[24] See subsection 2.2.2 and Chapter 3.

Brittle materials, such as concrete, are particularly sensitive to stresses induced by extreme temperature fluctuations, dynamic loadings, and impact loadings. These stresses tend to form cracks in the concrete. Reduction of concrete cracking due to thermal expansion and contraction can be accomplished with the addition of dispersed steel and/or composite fibers to the concrete matrix. These fibers act to transfer stresses across microcracks, thus reducing the growth of microcracks. When fiber reinforced plastic, FRP, rods are used to reinforce concrete,[25] the concrete matrix is likely to experience thermal cracking due to the differences in coefficients of thermal expansion of the concrete and the FRP rods. Consequently, dispersed composite fibers can be added, along with the FRP rods, to reduce the effects of thermal cracking. Though this state-of-the-art technology represent a marginal cost increase for the concrete material, the increase is not likely to be a significant compared to overall guideway costs. Fiber volume contents of 1.5% to 2.0% are generally required for significant mechanical performance improvement [Panarese 92]. The addition of 1.5% volume of steel fibers represents a concrete mix cost increase of approximately 50%. However, due to the small impact of concrete material cost on overall system implementation cost, the total system implementation cost increase due to the addition of fibers to the concrete matrix is on the order of 1%.

Mild steel is fatigue resistant at relatively high stress levels and is therefore considered fairly fatigue insensitive. Reinforced concrete is also fairly fatigue resistant at low strains. Carbon fibers are insensitive to fatigue at low strains. Glass fibers, however, are highly sensitive to fatigue loadings at medium to high stress levels. Thus, a design requirement for the use of glass fibers in maglev guideways is a restriction to its use in low stress areas. Since glass fibers are expected to be used only in the upper portions of the narrow beam cross-section, and with stiffness requirements likely to control the beam

[25] See Chapter 3.

design, only low stress levels are expected in the glass fibers used as mild concrete reinforcement in the maglev guideway design.[26] Thus, concern over fatigue loading is not expected to significantly alter the narrow beam design concept presented in Chapter 4.

2.2.2 Candidate materials

Metals

The primary metals used in construction are steel and alloys of steel. Steel has excellent tensile and compressive behavior and is relatively inexpensive. Mild steel has a tensile strength of approximately 410 MPa and can be used alone as a structural element or combined with other materials, e.g. with concrete. Alloy, or high strength, steel, with tensile strengths up to approximately 1.9 GPa, can be used as prestressing material in concrete, but typically, it is not used as mild reinforcement due to its high cost and high failure strain. Steel has thermal expansion characteristics similar to that of concrete and therefore is an excellent reinforcing material for concrete. Major problems associated with steel structures are corrosion and magnetic interference potential.

Ceramics

Ceramic type materials are generally hard and brittle. Examples of ceramic materials are porcelain and concrete. High strength concrete is desirable for use in maglev guideways in that it has both higher strength to mass and stiffness to mass ratios than does ordinary concrete. Concrete, like other ceramics, is excellent in compression, but poor in tension. Reinforced concrete members use longitudinal bars of material having good tensile and stiffness properties, (e.g. steel bars), placed in tension zones of the member. Though tensile properties of concrete can be improved substantially through the use of embedded fibers or polymers in the matrix, these approaches generally have not been implemented due to their higher cost. For increased material toughness and

[26] See Chapters 3 and 4.

durability, however, the addition of fibers to the concrete matrix is considered economically justified.[27] Also, for maglev design where guideway tolerances are more stringent and the dynamic behavior is more pronounced than for conventional construction, the use of fibers in the concrete matrix may be justified.

Composites

Fiber reinforced plastic, FRP, is the most promising of the composite materials for use in structural applications. FRP can be produced in any number of forms including (1) pultruded shapes such as rods, I-beams and box beams, etc., (2) laminates and (3) molded shapes. Fibers typically used are boron, carbon, glass and aramid. Boron and carbon are extremely expensive. Aramid is somewhat less expensive but has low compressive strength. Glass is relatively inexpensive, has high strength, but is only one quarter as stiff as mild steel.

FRP glass rods, when properly developed to produce a mechanical bond have been used as a replacement for steel reinforcement in a number of applications including highway pavements, MRI rooms in hospitals, and chemical and marine environments. One difficulty with glass fibers is that, over time, the fibers deteriorate when exposed to the alkaline environment of concrete. In addition, glass FRP (as well as carbon, boron and aramid) fails in a brittle manner.

Table 2.2.1 shows GFRP to have roughly three times the strength of mild steel though only a quarter of the stiffness. To provide a given strength, independent of stiffness, the cost of GFRP is much less than steel. However, on a stiffness basis, GFRP is at least 2 times the cost of mild steel. For flexural design of maglev guideways, stiffness is likely to be the primary base of comparison between materials. In contrast,

[27] See subsection 2.2.1.

CFRP, especially high modulus (HM) CFRP, though roughly equal to mild steel in stiffness, has three to four times the strength. The drawback to CFRP is its estimated cost which is approximately three to eight times the cost of epoxy-coated steel on a strength basis. On a stiffness basis, CFRP is currently 10 to 25 times the cost of mild steel.

Table 2.2.1 Structural properties for selected materials

	Strength σ (MPa)	σ (ksi)	Stiffness E (GPa)	E (ksi)	ε*	ρ (kg/m^3)	Cost ($/kg)
Mild Steel (60 ksi)	415	60	200	29,000	0.002	7850	0.55
Mild Steel w/ epoxy coating	415	60	200	29,000	0.002	7850	0.75
Prestress Steel (270 ksi)	1860	270	200	29,000	0.009	7850	2.20
Glass-FRP *	1200	174	50	7,000	0.031	2000	1.50
Carbon-FRP-HS * (high strength)	1600	230	129	19,000	0.012	1500	35.00
Carbon-FRP-HM * (high modulus)	1280	186	192	28,000	0.006	1600	90.00

* Fiber reinforced plastic, FRP, consists of 0.70 fiber volume fraction, V_f, in an epoxy matrix

Sources: [Charles and Crane 89, Amoco 92, Polygon 91]

2.3 Construction methods comparison

Following a discussion on the importance of economical initial system design, in general, and conceptual maglev guideway design, in particular, this section provides a brief presentation of basic structural bridge designs as well as a discussion on current and recent innovative construction methods. The applicability of possible bridge designs and construction methods to maglev guideway systems is discussed. In addition, a cost break down of conventional prestressed concrete bridge construction is given and methods for reducing these costs—through improved initial designs—are proposed.

2.3.1 Overview

The particular construction method selected for a given project depends primarily on the type of structure being erected. Site conditions, local work force quality, equipment availability, and local cost of materials and resources are other considerations

when determining a particular construction method. Frequently, "design optimization" refers to material or weight minimization and not specifically to overall construction cost minimization. Focus on cost minimization through modification of construction procedures generally does not occur until the design process is well under way. Yet, for projects expected to have significant construction costs, efforts aimed at minimizing these costs must begin early in the design process—since once a design is relatively complete, less than 10% of the total project cost can be reduced through optimized construction methods [Albano 91]. Substantial reductions in construction costs usually are only possible when the initial overall system design is sensitive to construction costs and methods.

For an economical maglev system design, initial attention directed at reducing guideway construction costs is critical. Construction of a single lane of maglev guideway support structure (i.e. beams, columns and footings) is estimated to represent 40-45% of all system implementation costs including terminal stations, rolling stock, power substations, magnetic windings, and maintenance facilities [Phelan and Sussman 91]. Other guideway components attached to the support structure (e.g. suspension, guidance and propulsion windings) constitute another 25% of system costs resulting in a total guideway cost of 70% of total capital costs. Estimates for dual lane guideways have placed the guideway construction costs as high as 70-90% [FRA 90]. Vehicle costs are estimated to be less than 15% of capital costs [CIGGT 89].

2.3.2 Bridge designs

Bridge design is based primarily on 1) the method of support, i.e. simply-supported vs. continuous spans, and 2) the type of structure, e.g. arched, suspension, cable-stayed, girder, etc. Design is also influenced by local material quality and availability. Materials considered for structural systems generally include concrete and steel, and occasionally, wood and plastic.

It is impossible to completely separate decisions concerning the design of the structure from the method of construction. For example, in designing a reinforced concrete section using prestressed tendons, the design professional assumes prestressing materials are locally available and that local labor crews are familiar with necessary construction procedures. Also important in the design process is development of an adequate plan for transporting required materials to the construction site. Ease of transportation of both materials and work crews to the jobsite influences both the economic viability of a project and the overall quality of the completed facility. Following is a discussion of basic bridge structural systems.

Girder

The girder approach is the most basic bridge design in that it essentially connects two columns with a girder (i.e. with a beam) to form a bridge. The girder can have either a uniform or variable cross-section. Optimization based on structural requirements typically results in a variable beam cross-section—while fabrication and construction cost optimization objectives typically dictate a uniform beam cross-section. Flexural bending moments are generally high in uniform cross-section girder systems. Girder spans range from 20 to 100 m [Collins and Mitchell 91]. The narrow beam concept presented in Section 2.4 is a single beam girder system having a uniform cross-section.

Arched

An arched structure resists most forces by compression in the members. Examples include masonry and stone bridges. The arch allows the use of less expensive building materials. For smooth passage of vehicles along the bridge structure, a flat girder is either placed above or suspended below the arch structure. Cross-sectional requirements for a girder acting in conjunction with a supporting arch are much less than those for the girder system acting alone. The implications are that potential span lengths for arched systems

are much greater than that for girder systems. Efficient arch bridge spans range from 100 - 300 m.

Suspension

A suspension structure has a girder (or deck) suspended by supports connected to relatively large piers. Vertical supports transfer forces from the girder to an overhead suspension system. Typically, the geometry of the overhead suspension system is matched to offset bending moments generated in the supported girder system. A suspension bridge design allows significant reduction in cross-sectional dimensions of the suspended girder. Therefore for relatively long spans, significant cost savings are possible. Suspensions systems are used for 200-350 m spans.

Cable stayed

A derivative of the suspension system is the cable stayed system, where the girder is supported by cables directly attached to supporting piers. Cable stayed brides are considered to be state-of-the-art. They are considered aesthetically pleasing because a minimum amount of material is used. Relatively long spans are both possible and economical. Currently, spans of 150-450 m are possible with cable stayed structures.

With respect to the potential aerodynamic interference between the cables and the passing maglev vehicle, suspension and cable-stayed bridges are not expected to be applicable—except in unusual circumstances for high speed maglev guideways. The maglev guideway design is more likely to be free of extensions above the top of the beam surface (i.e. the top of the beam is flat and open). A single beam having a uniform cross-section is likely to be utilized for ease of manufacture and assembly.[28]

---

[28] Sec Section 2.4.

2.3.3 Construction methods

Cast-in-place

Cast-in-place construction offers versatility in design, but is field labor intensive. The quality of the completed structure depends on variables such as: a) site weather conditions during the construction process, b) material quality, and c) the skill level of the local work crews. Uncertainties in these variables lead to overdesigned structures. For relatively long spans, falsework is often required to support the structure during erection. Falsework and formwork are different in that falsework is placed in positions where support is needed until design strength of the structure is developed and formwork primarily provides the shape of the completed structure. Achievable tolerances for cast-in-place structures are not expected to be adequate for maglev applications.[29]

Cantilever

Cantilever construction provides cost savings by initially placing columns and allowing the beam to be "cantilevered" from the column as the span is completed. This method uses the column as support during beam construction and thereby eliminates the need for a significant amount of falsework [Collins and Mitchell 91].

Segmental

Segmental construction techniques take the cantilever method one step further by attempting to design particular beam segments to be identical from span to span, i.e. to modularize the design. This repetition allows cost savings by providing the ability for off-site fabrication. Segmental construction offers the potential for superior and more consistent material properties. Connection design becomes an important design criteria with segmental highway construction as, due to the large widths of typical highway bridge decks, a single highway beam span generally consists of a number of individual

[29] See Chapter 4.

precast segments. For the narrow beam maglev guideway system, each segment should be an entire beam. Therefore, connection design between maglev beam joints should not be as critical a concern as it is with highway beam segments.

Launching system

A fairly recent innovation is the so-called launching truss where individual girders or girder elements are both transported and placed by using a launching truss. The truss allows an assembly line type of erection. Once a beam element is placed, it becomes a platform for placing subsequent beam elements. This construction method is also referred to as "end-on", or "assembly-line" construction. A launching system is desirable for high column elevations and/or where local ground access is difficult or impossible. A launching system delivers an economy of scale for corridors of substantial lengths—approximately greater than 50 km. That is, as the number of beam segments to be placed increases, the overhead cost per beam of the launching assembly is reduced. Reduction in labor required per beam results in reduced construction cost for a launching method of assembly.

In addition, a launching system eliminates constraints on beam and material deliveries to remote construction sites since once beam elements are positioned, they become the delivery network for succeeding beams. An off-site precast plant can cast and send structural elements continually and efficiently. Thus, design and delivery of structural elements for a launching system are not limited by highway or other network constraints as the beams can be transported to the jobsite using the (just completed) guideway structure. Such a delivery scheme is possible for maglev guideways since 1) vehicle loads are only slightly less than the beam dead weight and 2) beam deflection criteria can be relaxed somewhat during beam transport. Longer spans are therefore possible using this assembly-line process.

2.3.4 Bridge construction costs

Construction cost is measured primarily by the amount of material, labor, and equipment needed for the fabrication and erection of the structure. Christian Menn breaks down the construction cost of prestressed concrete bridges into the following four main cost components [Menn 91]:

- mobilization
- structure
- accessories
- design and construction management

Mobilization costs include site preparation and provisions for access by personnel, materials, and equipment. Structure costs include 1) the substructure, e.g. piers and foundations and 2) the superstructure, e.g. columns and beams. Accessories include expansion joints, water drainage, and walkway railings. Design and construction management includes costs for project creation and execution.[30] Based on cost records for a variety of prestressed concrete bridges compiled by Menn, structure costs account for 78% of the total structure construction cost while mobilization and accessory cost 8% and 14%, respectively, of the total as shown in Table 2.3.1. A further break down shows the superstructure and substructure to represent 70% and 30%, respectively, of overall structure costs. Table 2.3.1 shows major superstructure cost components to be formwork and falsework costs. Material costs, including concrete, mild steel and prestressing steel are also considered to be major superstructure cost components. According to Menn, though a variety of bridge types and site conditions are considered in his analysis, major construction cost components do not vary significantly. Other prestressed concrete construction cost comparisons support Menn's conclusions [Collins and Mitchell 91].

[30] Though not given a specific percentage by Menn, the design professional and the construction manager each typically receive 6% of the total project cost.

Table 2.3.1 Cost break down for typical prestressed concrete bridges*

Mobilization		**8%**
Structure		**78%**
Substructure		
Foundations	18%	
Piers, abutments	5.5%	
	23.5%	
Superstructure		
Formwork, falsework	20%	
Concrete	10%	
Mild steel	13.3%	
Prestressing Steel	11.2%	
	54.5%	
Accessories		**14%**
		100%

* Percentages shown do not include design and construction management fees.

Source: [Menn 91]

Some of the costs reported by Menn—in particular formwork and falsework costs—may not be applicable for a maglev system where structural elements are manufactured in large quantities. Typically, precast concrete highway bridges are one-of-a-kind projects. Significant cost savings using repeatable elements and forms are not always possible with single highway bridge projects. As shown in Table 2.3.1, formwork and falsework costs represent the highest structural cost component. Thus, a promising objective of the conceptual maglev guideway design is to eliminate the need for all falsework and most formwork.

2.4 Narrow beam conceptual design

2.4.1 Overview

The design of an appropriate conceptual guideway system follows from an accurate and thorough analysis of structural design requirements (Section 2.1), a design criteria for the selection of materials (Section 2.2), and a comparative assessment of available construction methods (Section 2.3). The intent of this section is to develop such a conceptual design. The approach is to first investigate the potential for various cross-sectional beam shapes for expected maglev loading conditions and structural support

mechanisms, e.g. simply-supported vs. continuous spans. Prestressing techniques and FRP design-related issues are discussed. A brief overview of the effect of the switching mechanism on beam shape and design is given. This section concludes with a suggested overall beam cross-sectional shape, method of support, and structural material selection.

2.4.2 Cross-sectional shapes

The cross-sectional shape of a structural element depends both on the loads the element must resist and the structural properties of the materials used in the element. For example, to withstand vertical bending moments and shear forces using an isotropic material having high tensile, compressive, and shear strength characteristics (such as steel), an I-shaped beam is optimal due to the concentration of material in the flanges, which are distant from the neutral axis. However, for a material such as concrete having high compressive, but low tensile and shear strength, the compressive zones tend to be maximized—e.g. concrete in the compressive flange of a reinforced concrete (R/C) beam is generally maximized. When concrete is reinforced with steel bars, the steel is used to reinforce tensile areas of the section. When the section is subjected primarily to downward vertical loads, a T-shaped section is generally an optimal shape. The upper flange of an optimized R/C concrete T-shaped section maximizes the concrete area, while the web area is designed as slender and as deep as is practical. Longitudinal steel reinforcement is maximized in the lower portion of the web.

When torsion is present, an optimal section for an isotropic material such as steel is typically a hollow circular shaft. The primary design consideration for resistance to torsion is to design a closed section. A closed section has no exterior appendages such as cantilevered extensions. Closed sections significantly reduce the shear stresses resulting from torsion. Examples of closed sections include solid sections, hollow circular shafts, hollow rectangular or "box" shapes or hollow trapezoidal shapes, etc. Open sections, which are structurally inefficient in resisting torsion, include I beams, T beams, inverted

V shapes, inverted T shapes, U shapes, and semi-circular channel beams. Torsional strength for a typical open section is an order of magnitude less than that for a comparable closed section.

For concrete in bending, a circular shape usually is undesirable due, in part, to the small compressive area at the extreme compressive fiber. Considering the combination of biaxial bending, shear and torsion—and using reinforced concrete—a hollow rectangular box is an efficient, and potentially an optimal, guideway beam shape. A hollow-box maglev guideway beam has the following attributes: it 1) is a closed shape, 2) efficiently resists bending, 3) has a large compression zone in the flanges to resist vertical bending, and 4) has large compressive zones in the webs to resist horizontal bending moments. Though a rectangular box beam is the focus of this thesis, a more generalized hollow trapezoidal shape may also be desirable. The trapezoidal shape should be considered when either a) the vertical positive (downward) bending significantly exceeds vertical negative (upward) bending or b) a vehicle wrap around effect is desired to physically prevent the vehicle from completely separating from the guideway.[31]

Open channel systems, such as U shape channel sections, in general, and reinforced concrete open channel sections, in particular, are inefficient in their use of given materials and are susceptible to significant torsional warping. To resist positive vertical bending moments and torsion, the most efficient reinforced concrete open section is one where the upper portion of the cross-section maximizes the amount of concrete while the lower portion both minimizes cross-sectional area and maximizes stability—resulting in an inverted U-shaped section. A T-shaped section has similar properties in bending as the inverted U-shaped section, but it is weak in resisting torsion. A non-inverted U-shaped channel section is weak in positive vertical bending, horizontal

31 Realistically, a hollow box beam is a special case of the general hollow trapezoidal shape.

bending, and torsion resistance. These structural deficiencies are inherent with all maglev designs based on open channel guideway sections.

When negative bending moments become significant, the rectangular hollow-box beam shape is more efficient than either the T or inverted U-shaped sections. The box shape provides a relatively large negative compressive zone (i.e. the lower flange) and, due to its closed shape, has high torsional stability. Similarly, the box section provides web compressive zones for horizontal bending whereas a T-shaped section does not. By structurally connecting the lower portions of an inverted U section having webs at 90° angles to the lower slab, a closed rectangular hollow-box section is essentially formed. Such an extension to the inverted U section, which dramatically increase torsional stability, is not possible with open channel maglev guideway designs.

In addition to excess material required for a closed section, an open channel guideway section essentially dictates the width dimension of all maglev vehicles for the life of the guideway. Also, efficient snow removal, debris accumulation prevention, and water runoff strategies for open channel systems are difficult to implement. The narrow beam design is not expected to have significant snow, drainage, or debris accumulation problems due to its minimal upper surface area. Also, the upper surface of the narrow beam can be sloped somewhat to help eliminate snow, water, and debris buildup.

Some drawbacks to the box section are its: a) possibly more difficult guideway switching mechanisms, b) potentially more difficult passenger evacuation under emergency conditions and c) lack of an inherent aerodynamic noise deflection mechanism capable of shielding noise from the ground level. Switching difficulties with the narrow beam design are not prohibitive, however, as a number of switching schemes have been proposed. The only known high speed switching mechanism in operation today

is applicable to the narrow beam concept.[32] Also, though passenger egress on a narrow beam may be more difficult than on open channel beams, a number of scenarios can be envisioned including 1) using the guideway itself for passage to columns where passengers can then be transferred to the ground, or 2) providing inflatable exit ramps that extend from the vehicle for direct transfer to the ground. Finally, should aerodynamic noise deflection devices be required in certain locations, they can be added easily to the lower portion of the box beam.

Having considered a variety of cross-section shapes and vehicle operation scenarios, a hollow-box reinforced concrete section appears to be the logical choice for a high performance maglev guideway beam design. The narrow, hollow-box concept serves as the basis for the remaining analyses in this thesis.

2.4.3 Structural support mechanisms

Simply-supported vs. continuous spans

The choice of support method for the narrow beam design is basically between a simply-supported or a continuous structure. Table 2.4.1 compares the attributes for these two structural support methods with respect to maglev guideway design. Continuous spans are more effective in reducing deflection and they provide a smoother guideway surface than simple spans of equal stiffnesses. However, potential moment redistribution over columns due to foundation settlement is a greater concern with continuous spans, as modification of the fixed beam-column joint is difficult.

Continuous spans have other disadvantages—some of which may be critical for maglev design. For example, because a continuous girder cannot expand longitudinally if fixed at the column connection, thermal stresses can cause the beam to bow.[33] Thermal

---

[32] See subsection 2.4.4.
[33] See subsection 2.1.4.

stresses in continuous spans are either 1) resisted or 2) relieved by some means such as expansion joints. Thermal stress relief in continuous span highway bridges is accomplished primarily with an expansion joint and/or elastomeric pads [AASHTO 89]. The use of expansion joints, however, presents difficulties in terms of the potential for automation of the construction process, and also possibly adversely affects ride quality.

Table 2.4.1 Simple vs. continuous spans

	Simple	Continuous
Material cost	*additional stiffness required for same deflection control*	more shallow beams are possible, thereby reducing required material and beam weight ✔
Guideway roughness	*inflection points over supports affect ride comfort*	smooth transition over supports ✔
Ground Settlement	not a design difficulty—only simple adjustments necessary ✔	*adjustment difficult and expensive*
Thermal expansion	allowances for expansion can be made easily at supports ✔	*requires joints that can provide significant expansion; may handicap automation processes*
Construction	ease of transportation, less field labor required ✔	*"closure" pours, plus final post-tensioning operations are difficult and expensive*
Maintenance	single beams can be removed and replaced quickly ✔	*repairs require intensive labor as adjacent beams are affected*
Prestressing	allows prestressing to be confined to lower portion of the beam (i.e. all steel prestressing) ✔	*requires FRP prestressing of beam over supports where moment redistribution occurs*
Construction Automation Potential	automated adjustment task is simplified as possibly only one mechanism is required ✔	beam cannot be easily adjusted due to fixed connections
Aesthetics	*short, deep spans are not generally considered aesthetically pleasing*	longer, more slender spans typically are viewed as less obtrusive to the environment ✔
Resistance to seismic loading	*base isolation is likely required along with some type of lateral fix joint*	seismic response is more efficient as adjacent beams and columns work as a system ✔
Traveling Wave	none present ✔	can cause beam to oscillate prior to vehicle arrival

✔ indicates a desirable quality for maglev

Considering transportation, placement and repair of beam spans, initial attention must be given to beam length limitations. For example, if 25 m is considered a minimum maglev guideway span length, a 3 span continuous beam has a minimum length of 75 m. This length presents formidable transportation and placement problems. Though a closure

pour of three simple 25 m spans results in an effective 75 m continuous girder (and eliminates most delivery constraints), the procedure is highly labor intensive. In addition, repairs to continuous spans are difficult and expensive as embedded reinforcement from neighboring beams must be removed and regrouted. Thus, construction and maintenance costs for continuous spans are likely to be more expensive than for simple spans.

Another difficulty with continuous spans is that they require substantial amounts of mild and prestressing tensile reinforcement in the upper portion of the beam over the column due to negative moments in these areas of the beam cross-section. This prestressing tendon arrangement substantially increases the need for non-magnetic concrete reinforcement. In contrast, prestressing tendons in simple spans can be confined to the lower portion of the beam element. This allows the exclusive use of steel as a prestressing material.[34]

Should an automated alignment system be desired, a simple span offers the most promise because adjustments are less complex and they can be made at beam-column connections. It is also likely that only a single automated alignment mechanism may be required for a simple span as adjustments are identical at either end of the span. Adjustments at fixed ends of continuous spans are likely to prove either impossible or uneconomical.

The major drawback to a simply-supported beam structure is the need for greater stiffness. Thus, simple spans are 1) deeper, 2) more massive, and 3) generally considered less aesthetically pleasing than continuous spans for given lengths and stiffness criteria. Also, though easier to construct and replace, simple spans tend to have more guideway roughness due to inflection points in the deflection profile at the supports.

---

[34] See Figure 2.4.1.

In general, continuous spans are more efficient in resisting seismic loads as the number of free joints is minimized. Resisting earthquake loads with simple spans is likely to require base isolation technology to lessen accelerations at beam-column interfaces. Both continuous and simple span bridges have improved seismic resistance when using base isolation technology [Buckle 91]. The cost of base isolation technology is not known at this time, but is not expected to be a significant implementation cost.

Finally, a simply-supported system also eliminates the potential for a dynamic traveling wave effect to propagate through the beam ahead of the vehicle. This could produce undesirable beam oscillations prior to vehicle's arrival. Therefore, a simply-supported beam is stationary prior to vehicle arrival. Deflections induced by this traveling wave effect present difficulties in providing adequate vehicle ride quality when using a continuous span guideway system.

Considering the above issues and considering low cost and guideway adjustability as primary objectives, a simply-supported structure is selected as the superior structural support mechanism for the narrow beam guideway concept. Though continuous spans offer better structural efficiency and seismic response, simple spans are likely to be less expensive to construct, maintain, and repair. Thus, simple spans are assumed for the analyses performed in this thesis.

Prestressing, internal or external, pre- or post-tensioned

With expected span lengths of 25 meters and zero dead load deflection requirements, prestressing is required for the reinforced concrete narrow beam design. Post-tensioning can be administered to compensate for material creep, shrinkage, and relaxation over time. Internal post-tensioning has both the advantage of corrosion protection for the tendons and the ability to "mirror" the bending moment behavior of a distributed loading (e.g. a parabolic tendon shape). If the tendons are grouted, additional prestress cannot be added later to account for losses. External prestressing offers the

benefit of relative ease of inspection and potentially lower cost due to a reduction of the required web cross-section area. Stresses in external tendons can be monitored, and (conceptually at least) the tension adjusted.

High strength steel prestressing offers known long term material behavior at relatively low cost. FRP prestressing offers corrosion resistance (for external prestressing) and superior relaxation behavior at somewhat higher cost. Currently, it is felt that for internal prestressing, high strength steel is superior and for external applications, FRP is desirable. FRP allows a fiber optic cable to be placed inside the tendons to provide continuous monitoring of stresses in the tendon [Specht 88]. The primary difficulties in utilizing FRP tendons lies in 1) devising reliable anchorages as the tendons are weak in shear and 2) determining reliable predictions of long term material behavior.[35] Durability and fatigue are significant concerns for glass FRP.

For the narrow beam conceptual design, it is assumed that ungrouted, post-tensioned steel prestressing tendons are used. As indicated in Figure 2.4.3, the prestressing tendon arrangement is a cross between internal and external prestressing. Though tendon ducts are encased in concrete (similar to internal prestressing), only local widening of the wall near the tendons is performed (similar to external prestressing). This approach yields a relatively thin box section. The prestressing tendons have a parabolic profile as shown in Figure 2.5.2 and (theoretically) can be adjusted over time.

2.4.4 Influence of switching mechanisms

Though the box beam guideway is highly efficient structurally, it is limited in that it restricts some vehicle switching options. An optimal switching mechanism allows a vehicle to enter or exit the guideway at full speed. Either a flexible beam switch or an

35 This is not a trivial problem and though anchorage methods are being proposed, until these can be assured, steel reinforcement is likely to be the choice for prestressing tendons irrespective of the fact that FRP has superior long term relaxation properties for prestressed concrete.

alternating beam switch, (e.g. where a straight beam section and curved beam section are interchanged horizontally), is possible with the box beam design. For the flexible beam switch in an EDS system, a steel beam cannot be used due to magnetic interference. Also, since concrete beams are difficult to bend sufficiently, other beam materials must be considered for horizontal switching. A glass or carbon pultruded FRP box beam is a possible solution since both beam materials can bend sufficiently. Currently, for a reinforced concrete beam switch element, the alternative switch, where curved and straight sections are interchanged, is perhaps the only acceptable horizontal method of switching. Though horizontal switching is feasible with the narrow beam design, currently other guideway designs appear more conducive to horizontal switching (e.g. the U-shaped channel). As discussed previously, however, these other guideway shapes have major constraints of their own.[36] Other switching strategies are also possible for the narrow beam design including vertical switching.

Switching options are assumed feasible for the narrow beam conceptual design of this thesis. However, the thesis concentrates exclusively on a straight, standard guideway beam element and specific design of a beam switch is not performed.

2.4.5 Potential for automated control

The motivation for considering active control of the guideway stems from experience with other high speed ground transportation systems—namely the Japanese Shinkansen line and the French TGV system. It is speculated that over 3500 maintenance personnel are required every night for minor repair and adjustment of the Shinkansen high speed rail guideway. The newer TGV system has required significantly less maintenance labor to date, but it is likely to experience a dramatic increase in maintenance costs as the track infrastructure ages.

---

[36] See subsection 2.4.2.

Figure 2.4.1 shows the trade-off between human and automated operation as a function of required tolerance for various tasks. Precast concrete production has high quality control and dimensional tolerances on the order of 2 mm are readily achievable [Bechtel, et.al. 92]. Dimensional tolerances for field construction are much more difficult to control since the human is more involved in the operation. Achieving a tolerance of 2 mm for foundation/pier construction requires a special effort. An additional complication is the long term deformation of the soil that supports the piers. An estimate of support movement to the accuracy of a millimeter is not feasible because of the high degree of variability of the soil and the lack of an accurate prediction model.

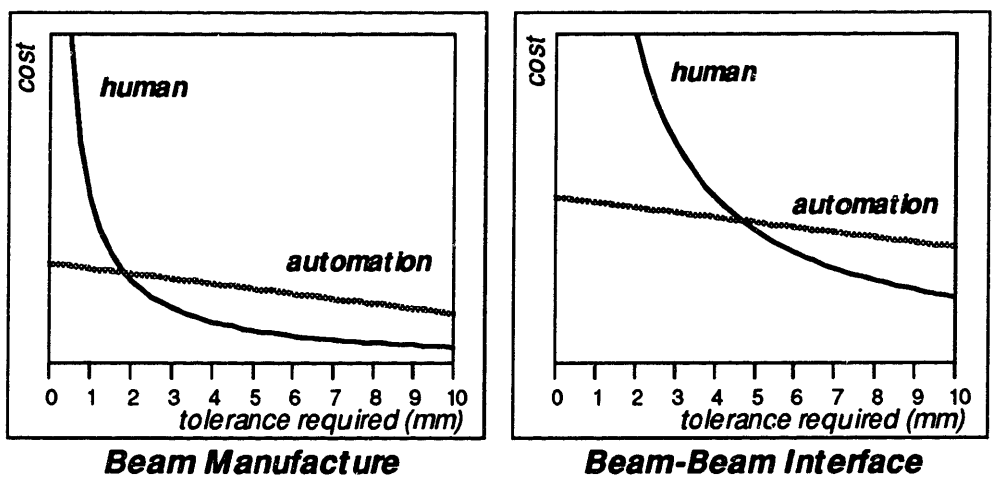

Figure 2.4.1 Interaction of Human and Automation Cost Curves

The conventional construction and maintenance approach is to initially fix the motor assembly to the guideway beam and provide for periodic adjustment at the beam-pier support. The initial positioning of the windings must compensate for construction tolerances. Adjustment at the beam-pier support is normally performed manually. A preferable strategy is to provide the capability for adjustment of the relative position of the windings with respect to the guideway beam as it displaces over time. Figure 2.4.2

illustrates a proposed method of achieving this positioning.[37] Actuators made from shape memory alloys and piezo-electric ceramics undergo a dimensional change when subjected to a voltage input. These devices have been used as "slack" adjusters to compensate for misalignment and wear in shaft/bearing systems [ASME 92]. Their role here is that of positioning elements to compensate for both the initial construction tolerance and the subsequent guideway movement due to creep and shrinkage of the guideway beam, long term foundation settlement, and other phenomena that may influence the position of the ladder. The intelligent alignment system would consist of sensors to detect differential motion of the ladder, a controller that decides how to respond, i.e. what actuators should be activated, and actuators that provide for spatial adjustment. This technology has been employed for mechanical control systems, and holds considerable promise for this application.

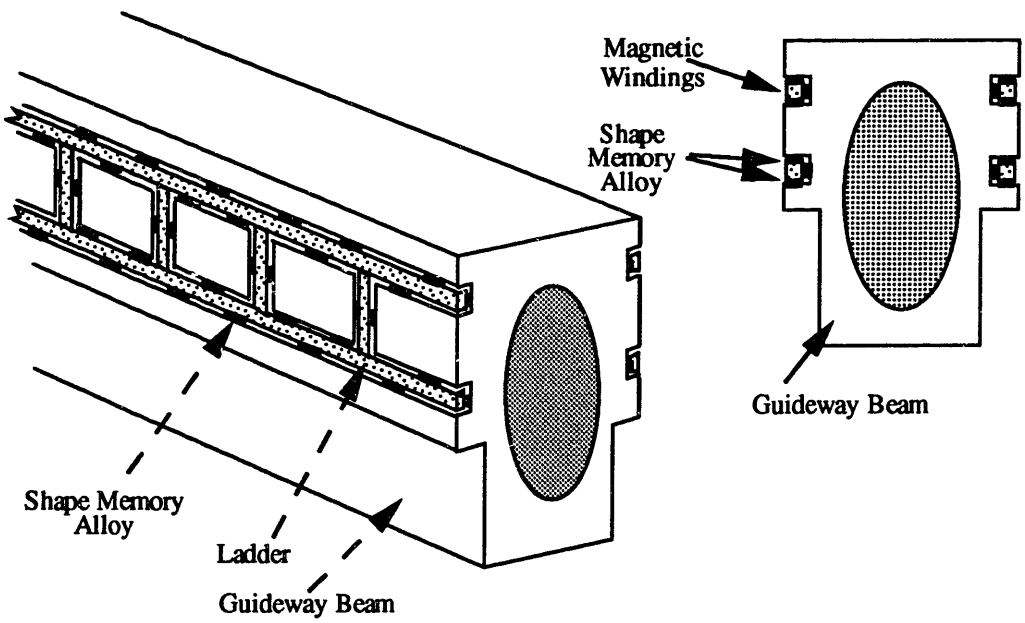

Figure 2.4.2 Shape Memory Concept

[37] The concept of using shape memory actuators and vehicle sensors for measurements and adjustments was conceived by Professor Jerome Connor, Professor Richard Thornton, and the author.

Using "best" construction practice, the initial amplitude of guideway roughness can be approximately 5 mm. The contribution due to differential motion of the supports could be at least this value, more likely greater. Combining the two effects, the system must to be able to make a vertical adjustment of about 10 mm over a distance of approximately 25 m.

The maglev vehicle acts as the sensor for the automated alignment method. The vehicle is provided with the capability of tracking its location along the guideway path and monitoring a change in the levitation force, which is interpreted to reflect a deviation in vertical position of the ladder from the desired position. The "alignment" controller receives a signal from the vehicle and activates the nearest pair of displacement positioners. An iterative correction process is employed, (i.e. a standard adjustment is made), and its adequacy is evaluated by the next vehicle passing through. No actual position measurements are made, just measurements of the change in levitation force. Iterative correction is believed to be the best approach because of the high frequency of vehicle passage [Phelan, et.al. 92]. This approach can also be applied for the construction phase. Instead of using complicated techniques to initially "fix" the guideway position, the system can be tuned by passing the vehicle over the right of way and noting the locations that need to be adjusted for excessive construction tolerance. Multiple passes are required, but the cost should be less than performing precise field measurements.

Potential benefits of an automated guideway maintenance system are:

1. **increased safety**—As the number of workers required on the guideway is reduced, the potential for worker injuries and fatalities is reduced.

2. **reduced erection tolerance requirements**—Such a system allows beam segments to be placed with approximate tolerances (e.g. 5 cm).

Once all elements are placed to course tolerances, the automated system aligns itself to precise tolerances.

3. **reduced maintenance requirements**—Once the automated system is in operation, it can continually monitor and adjust itself, thereby reducing the need for using field labor to perform minor adjustments and repairs. Field labor can be restricted to instances where necessary adjustments exceed the range of the "adjustment" controller. With proper monitoring of guideway behavior, periodic adjustments can be forecasted and planned strategically.

4. **lower construction cost**—Though the addition of such automated mechanisms increases capital costs of the guideway, less stringent placement tolerances can potentially reduce actual erection costs.

5. **lower operation and repair costs**—Reducing the amount of required personnel can significantly reduce the cost of operating and repairing the guideway. (Note that nightly repair workers typically only have 4 hours during which they can work. Thus, optimization of night worker scheduling is difficult.)

6. **increased revenue**—If nightly repair requirements can be avoided and 24 hour operation is achieved, reliability and operating revenue should increase.

2.4.6 Narrow beam concept summary

Table 2.4.2 summarizes design assumptions used in the analyses of the narrow beam concept. These assumptions have been discussed in this chapter and they serve as the basis for the analyses performed in this thesis.

Table 2.4.2 Selected design criteria summary for the narrow beam design

shape	straight guideway beam element having a uniform rectangular hollow-box cross-section
materials	concrete reinforced primarily with steel—hybrid FRP reinforcement confined to upper two corners of the beam cross-section (see Figure 2.4.2)
vehicle vertical load	19.61 kN/m (2.00 tonne/m vehicle mass)
horizontal wind load	14.71 kN/m (corresponds to a 54 m/s wind speed)
vehicle to beam eccentricity	3.0 m (see Figure 2.1.1)
seismic loads	neglected, base isolation assumed
snow loads	neglected, assumed minimal due to small upper surface area
span length	25 m
beam width	1.2 m to 1.6 m
beam depth	limited to not more than 1.5 times the beam width for decreased wind exposure and increased torsional stability
beam wall thickness	maximum value of 1) 10% of beam width or 2) 0.15 m—wall thickness assumed uniform across cross-section
beam dead weight	20-30 kN/m (see Chapter 4)—no dead load deflection, Δ, due to prestressing
deflection criteria	maximum vertical Δ limited to as low as 5.0 mm, maximum horizontal Δ limited to as low as 2.5 mm—effects of prestressing not considered for live loads
durability, toughness, fatigue	fibers in concrete matrix recommended, but not included in analysis
damping	essentially neglected as less than 2% passive damping is expected—expected increases in damping through innovative mechanisms will increase ride quality
thermal stresses and gradients	neglected—simple span eliminates thermal stresses, gradients should not be significant with relatively small upper surface area and thin wall thickness
magnetic inertness	non-magnetic glass and carbon fiber hybrid FRP reinforcement rod (see Chapter 3)
bridge design	simply-supported segmental girder system (each girder is a single segment)
beam switch design	neglected—both vertical and horizontal switching mechanisms are feasible with the narrow beam design
prestressing strategy	ungrouted post-tensioned steel tendons confined to the lower half of the beam cross-section having a parabolic profile (see Figure 2.4.2)
construction method	near-site casting, assembly-line erection, guideway itself can serve as delivery network—designed to eliminate most or all formwork and falsework costs

As indicated in the table, the narrow beam is a simply-supported, straight 25 m reinforced concrete span having a uniform hollow-box beam cross-section. Primary mild concrete reinforcement is steel. Non-magnetic hybrid FRP rods are confined to the two upper corners of the cross-section. High strength steel is used for prestressing. Due to an expected vehicle mass of 2.00 tonne/m, a fully distributed vertical load of 19.61 kN/m is assumed along with a 14.71 kN/m horizontal load resulting from an expected 54 m/s wind. The eccentricity between the vehicle and beam centers of gravity is estimated at 3.0 meters. Both seismic and snow loads are ignored in the narrow beam analysis.

The most economical beam width for the given loads varies from 1.2 m to 1.6 m, with the 1.4 m chosen as standard.[38] To increase torsional stability, beam depth is limited to 1.5 times the beam width. Wall thickness is set to the minimum of a) 0.15 m and b) 0.1 times the beam width, with local web widening for containment of prestressing tendons.

Ungrouted prestressing tendons are used to eliminate dead load deflections from the 20-30 kN/m beam dead weight. Prestressing tendons are assumed ungrouted to allow for long-term adjustments. With tendons somewhat outside the web—though not externally exposed—the conceptual arrangement is a cross between internal and external prestressing. Also, with tendons confined to the inner portion of the beam, there is no potential physical interference between the prestressing tendons and the vehicle.

Maximum live load vertical and horizontal deflections are limited to as low as 5.0 and 2.5 millimeters, respectively. Strength and stiffness effects of prestressing tendons on live loads are ignored. It is assumed beams will be precast elements—which should eliminate most formwork and falsework costs typical of conventional highway bridge construction. Each narrow beam represents a single module in a segmental construction

---

[38] See Chapter 4.

scheme. Assembly-line erection procedures are expected. Finally, the guideway structure itself can serve as the delivery network from the casting yard to the jobsite.

The cross-section of the rectangular hollow-box narrow beam concept is shown in Figure 2.4.3. As indicated in the figure, it is assumed the upper two corners of the beam cross-section require non-magnetic reinforcement. Chapter 3 introduces an innovative non-magnetic glass and carbon hybrid FRP rod that can be used in these areas, where steel reinforcement cannot be used. As illustrated in Figure 2.4.3, the two non-magnetic reinforcement areas are defined by the width, b_{frp}, and depth, h_{frp}, of a single corner.[39] Also shown in the figure is the local widening of the wall thickness near the prestressing tendons. It is assumed in the analyses of this thesis that the maximum tendon eccentricity, e_{max}, is equal to the difference between half the beam depth and twice the wall thickness (i.e. $0.5h - 2t$). This assumption for e_{max} is conservative.

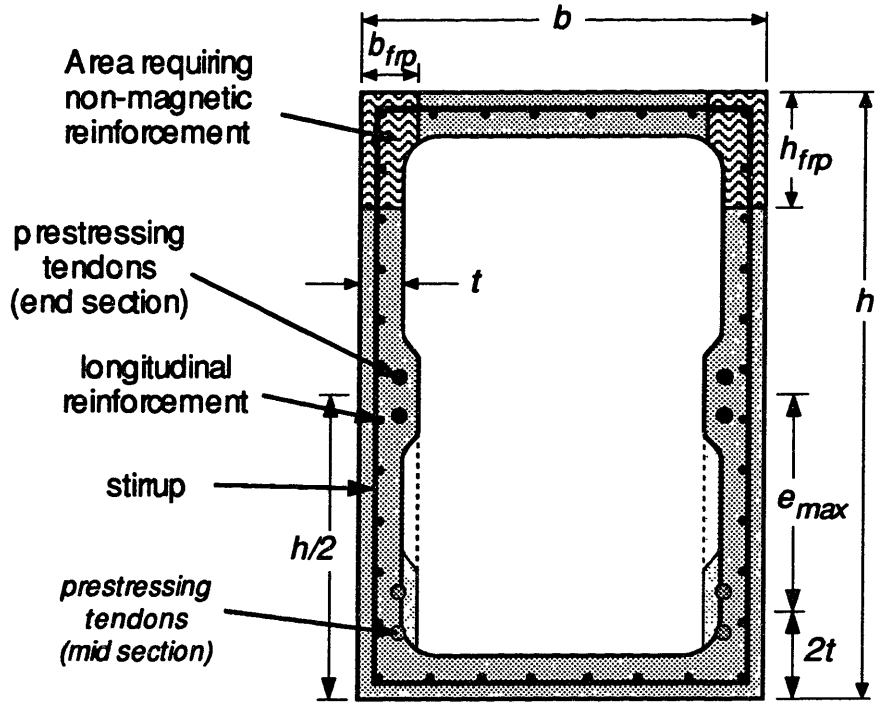

Figure 2.4.3 Narrow Beam Guideway Cross-Section (end section)

[39] See the example in Chapter 4.

Figure 2.4.4 shows the profile of the simply-supported conceptual narrow beam design. As indicated in the figure, prestressing tendons follow a parabolic profile, having a maximum eccentricity at the midspan. It also can be seen in Figure 2.4.4 that the prestressing tendons are confined to the lower half of the beam element. Thus, if magnetic fields can be confined to the upper portion of the beam element, high strength steel tendons can be used exclusively as the prestressing material.

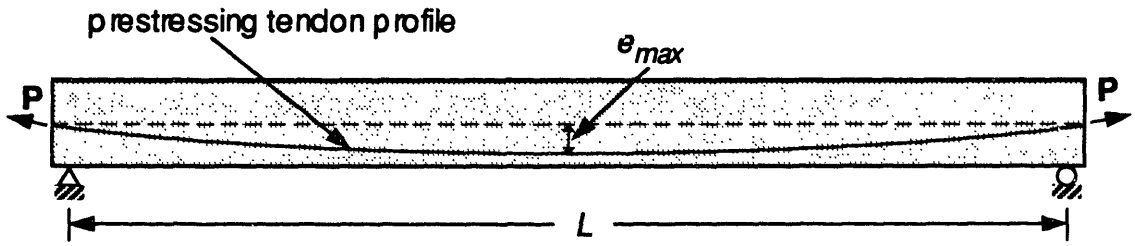

Figure 2.4.4 Narrow Beam Guideway Profile

With the narrow beam design approach and assumptions presented, Chapter 3 next focuses on the concept, design, and testing of a non-magnetic glass and carbon hybrid FRP rod. The hybrid FRP rod is designed to replace steel reinforcing bars in areas where magnetic reinforcement is restricted. Cost estimates are also provided. Additionally, information presented in Chapters 2 and 3 is used to develop the structural analysis procedure presented in Chapter 4. Sensitivity analyses presented in this thesis are based on the assumptions presented in this chapter.

3.0 Hybrid FRP Concrete Reinforcing Rod

As discussed in Chapter 2, steel reinforcement cannot be used in all portions of the reinforced concrete guideway due to magnetic field effects in areas near EDS windings. In this chapter, short-term beam flexure tests are presented which indicate that fiber reinforced plastic material, FRP, using both glass and carbon fibers, can serve as a replacement for steel reinforcement in concrete in non-magnetic areas. An innovative hybrid FRP concrete reinforcing rod design is presented along with equations for calculating appropriate hybrid FRP material properties. Equations derived and presented in this chapter are used in the example presented in Chapter 4.

To gain a better understanding of the flexural behavior of concrete reinforced with hybrid FRP rods, seven T-shaped concrete beams, each reinforced with a single glass and carbon hybrid FRP rod, were tested in 4-point bending. Results of these tests are discussed in this chapter. Cost comparisons show the hybrid FRP rod to be approximately 5.5 times the cost of steel on a stiffness basis.

3.1 FRP background

Pultruded fiber reinforced plastic, FRP, is a type of composite material which can be used as tensile reinforcement in structural applications. As discussed in Chapter 2, FRP can be produced in any number of forms such as rods, I-beams, and box beams. Pultrusion refers to the process where fibers such as boron, carbon, glass, and/or aramid, are extruded under tension, i.e. pultruded, through a thermosetting resin such as epoxy.

In general, FRP is non-magnetic, non-corrosive, and can potentially serve as tensile reinforcement in concrete guideways. Though GFRP, glass fiber reinforced plastic, is relatively inexpensive and has high strength characteristics, it suffers in that it

has: 1) low stiffness, 2) a brittle failure mode, and 3) deterioration tendencies over time in concrete due to the alkaline environment of the concrete. Carbon fiber reinforced plastic, CFRP, has high strength and stiffness properties and is inert to the concrete alkaline environment. However, CFRP is expensive and additionally, like GFRP, it fails in a brittle manner. The brittle failure mode of FRP composites is not a desirable structural material property as failure of structures composed exclusively of brittle materials is typically sudden and catastrophic.

When properly developed to produce a mechanical bond, FRP glass rods have been used as a replacement for steel reinforcement in a number of concrete construction applications including highway pavements, MRI facilities in hospitals, as well as chemical and marine environment construction. Use of FRP as reinforcement in flexural members has been limited due to the low stiffness of the material. PSI Fiberbar [PSI 90], Polystal [Specht 88, Preis and Bell 86], and Nefmac [Nakatsuji, et.al. 90] serve as examples of GFRP used as reinforcement in concrete structures. While both PSI Fiberbar and Polystal FRP rods utilize only glass fibers, some applications of the Nefmac material employ carbon fibers distributed with glass fibers to increase both stiffness and ductility properties of the glass material. With Nefmac as an exception [Nefcom 88], few applications have utilized CFRP as an embedded concrete reinforcement material.

Other composite materials, including aramid fibers, (e.g. Kevlar), and boron fibers, have properties similar in some respects to carbon. Aramid fibers are only slightly less expensive than carbon fibers, and except for increased toughness, offer no significant benefits over carbon fibers. Additionally, aramid fibers are somewhat reactive with the alkaline environment of concrete [Dolan 91]. Boron fibers, possess superior mechanical properties, but are currently much too expensive for use in large civil engineering projects. It is desirable to have a concrete reinforcing rod that 1) is relatively low cost, 2) is inert to the concrete environment, 3) fails in a ductile manner and 4) has high stiffness.

The next section presents a hybrid FRP rod that satisfies the above criteria—with the exception of high stiffness. Currently, low cost and high stiffness objectives appear to be mutually exclusive.

3.2 Hybrid FRP reinforcement design

3.2.1 Rod concept

This section presents a design approach for a "hybrid" FRP rod containing glass fibers integrated with carbon fibers in such a way that the glass is insulated from the outside environment (i.e. from concrete) by both carbon fibers and an epoxy matrix. Combining CFRP and GFRP in the form of a hybrid FRP rod serves to 1) increase the ductility of the composite material and 2) insulate the glass fibers from the alkaline concrete environment. The cross-section of such a hybrid FRP rod, conceived by this author and MIT Professor Thanasis Triantafillou, is shown in Figure 3.2.1 where t_{CFRP} is the thickness of the CFRP overwrap and D_{GFRP} is the diameter of the inner GFRP core.

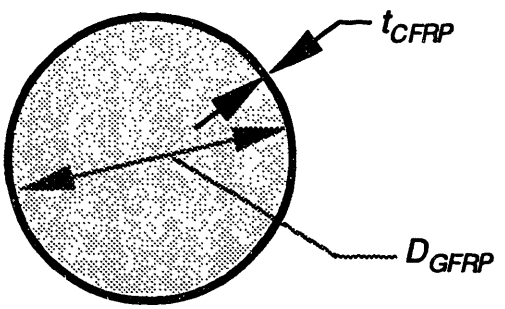

Figure 3.2.1 Cross section of Hybrid FRP Reinforcing Rod

Both fiber materials are pultruded in a resin matrix such as epoxy. The strategic control of carbon and glass fiber volumes in the hybrid rod makes possible a pseudo-ductile failure mode as shown in Figure 3.2.2. In Figure 3.2.2, F_1 and F_p represent the strength of the rod immediately before and immediately after carbon rupture,

respectively. F_u is the ultimate strength of the rod and is equal to the ultimate strength of the GFRP inner core. Also shown in the figure is a plot of high strength CFRP material alone and an idealized plot of mild steel. Note that the stiffness of the high strength CFRP is close to that of steel. The force-displacement plot of GFRP material follows a straight line from the origin to F_u.

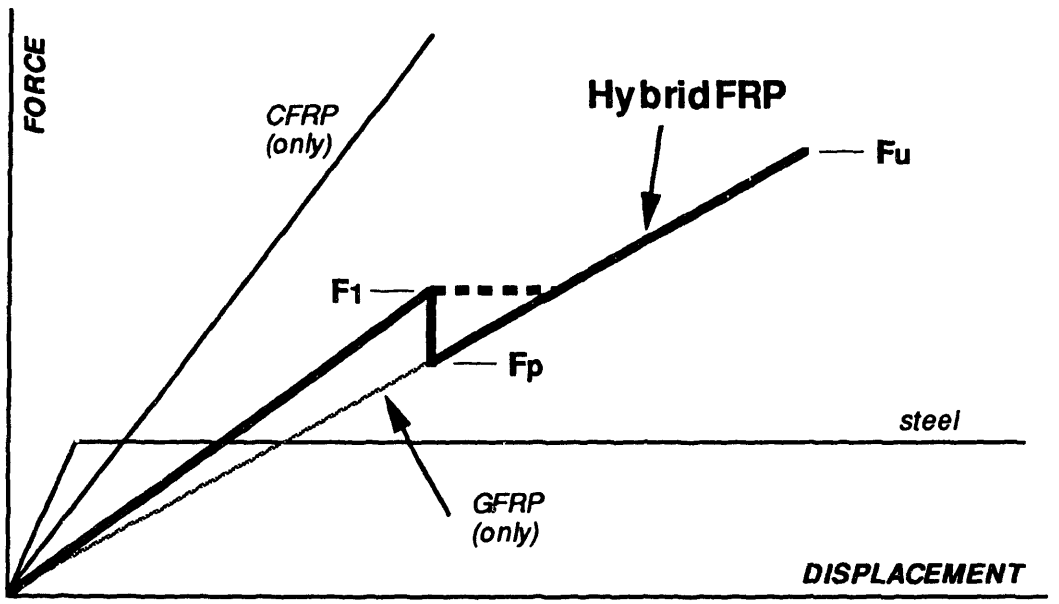

Figure 3.2.2 Pseudo-Ductility of Hybrid FRP Reinforcing Rod

Two parameters can be derived from the load-displacement points for the hybrid rod that define the pseudo-ductile failure shown in Figure 3.2.2. The first parameter, α, is a measure of the ductility during load transfer from CFRP to GFRP at carbon rupture. The parameter α must be minimized to ensure that the hybrid rod does not shear during load transfer. The second measure, γ, reflects the reserve strength in the rod after carbon rupture. These two parameters are represented by the following equations:

$$\alpha = \frac{F_1}{F_p} \qquad [3.1]$$

$$\gamma = \frac{F_u}{F_1} \qquad [3.2]$$

where

F_1: Force in rod just before the high modulus fibers rupture

F_p: Force in rod just after the high modulus fibers rupture

F_u: Ultimate load carrying capacity of rod

It can be inferred from Figure 3.2.2, that the amount of CFRP must be minimized in order to achieve a pseudo-ductile failure mode from the two brittle materials. If the amount of CFRP is not minimized to an acceptable level, γ becomes less than 1.0 and the rod does not have sufficient reserve strength.[1] There is no significant advantage in having extremely high values of γ, though it must be greater than 1.0. Before carbon rupture, both GFRP and CFRP contribute to the strength and stiffness of the rod. After carbon rupture, the rod follows the stiffness characteristics of the GFRP only. Thus, the strategic integration of two brittle FRP materials—having significant differences in stiffness characteristics—produces a hybrid FRP reinforcement material possessing a pseudo-ductile failure mode.

Mechanical properties of the hybrid rod for various cross-sectional area fractions of GFRP to CFRP are determined primarily by the properties and volume fractions of the base fibers. Figure 3.2.3 illustrates the influence of GFRP content on the properties of a glass/carbon hybrid FRP rod. The CFRP used in the hybrid rod shown in the plot is high strength. As indicated in the figure, a higher percentage of GFRP yields a lower cost hybrid FRP rod. The plot of γindicates that the higher the glass content, the higher the safety factor after carbon rupture. An increase in α results in a slight decrease in ductility and a corresponding increase in stiffness. The resulting decrease in $\gamma$is not likely to be important as long as it remains greater than unity.

---

1 Research is needed to determine how great an impact load can be transferred to the GFRP during carbon rupture without failure of the glass fibers as this will limit the value of α that can be used in the design of an acceptable hybrid FRP rod.

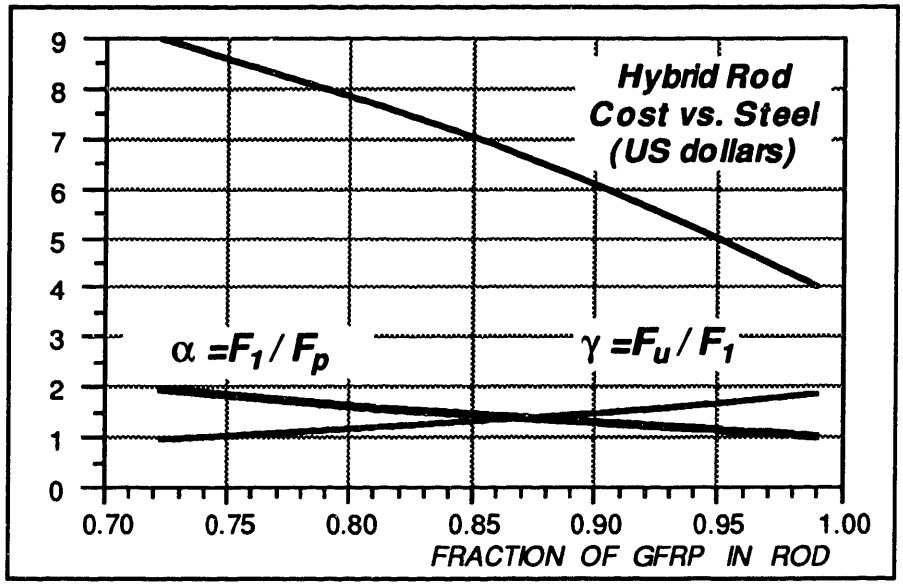

Figure 3.2.3 Cost, α, and γ for Hybrid FRP Reinforcing Rod

The thickness of the CFRP cover must be sufficient to fully insulate and ensure durability of the inner glass fibers. Durability concerns may require an increased thickness of CFRP—beyond that required for ductility—with a resulting increase in α and cost. Visual inspection of the 0.127 m (0.5 inch) diameter manufactured rods, indicates that a volume fraction of 0.92 GFRP is required to ensure full CFRP coverage of the inner core. As shown in Figure 3.2.3, a 0.92 GFRP volume fraction results in a hybrid FRP rod cost approximately 5.5 times the cost of using steel on a stiffness basis.[2]

Steel is an excellent structural material for concrete reinforcement. In contrast, GFRP is not a superior structural design material due primarily to its low modulus and its sensitivity to fatigue loadings.[3] GFRP material possesses high strength properties and is economical. Furthermore, because GFRP use in maglev guideways will be restricted to low stress levels, fatigue resistance is not considered a critical design issue. The primary

---

[2] See Section 3.3.

3 Low GFRP stiffness is beneficial for prestressing as it results in lower prestress losses. However, long term GFRP behavior under load is uncertain. GFRP is considered only for mild reinforcement in this thesis.

limitation to using GFRP as a reinforcement material within concrete is the high susceptibility of the glass fibers to the concrete alkaline environment.[4]

CFRP is an excellent structural material though it is expensive. With low cost as an objective, present carbon fiber prices exclude CFRP from being considered a viable replacement for steel in concrete. Due to its high content of GFRP, the hybrid FRP rod is relatively low cost compared to an all CFRP rod. The hybrid FRP rod is inert to the concrete matrix and it can be engineered to have a pseudo-ductile failure. Equations used to predict strength, stiffness, pseudo-ductility, and cost of the hybrid FRP are presented in the next subsection.

Table 3.2.1 Candidate material structural properties summary

	Steel	Glass (GFRP)	Carbon (CFRP)	Hybrid GFRP/ CFRP
Magnetic interference	high	inert ✔	inert ✔	inert ✔
Cost *(stiffness basis)*	low ✔	3-4 times cost of steel ✔	10-25 times cost of steel	5-8 times cost of steel ✔
Strength	high ✔	high ✔	high ✔	high ✔
Modulus	high ✔	low	high ✔	relatively low
Density	high	low ✔	low ✔	low ✔
Resistance to alkaline environments	excellent ✔	poor	excellent ✔	excellent ✔
Corrosion resistance	poor	excellent ✔	excellent ✔	excellent ✔
Long-term properties	reliable ✔	sensitive to fatigue loading	insensitive to fatigue ✔	sensitive to fatigue
Damping	poor	relatively good	excellent ✔	good ✔
Shear strength	excellent ✔	poor	poor	poor
Failure mode	ductile ✔	brittle	brittle	pseudo-ductile is possible ✔

✔ indicates a desirable quality as concrete tensile reinforcement for maglev

[4] Some manufacturers claim to have developed GFRP that is resistant to alkaline environments through the use of 1) superior glass fibers, 2) enhanced fiber treatments or 3) improved resin mixtures. Others claim to have produced alkaline free concrete. Either approach is desirable. However, long term behavior remains a significant concern and until such behavior of these advanced approaches can be substantiated, the use of an outer protective layer of CFRP is the conservative design choice.

3.2.2 Design equations

The following equations involve basic material properties and are used to determine strength and stiffness properties of the hybrid FRP rod. High modulus fibers (e.g. carbon) in conjunction with high strength fibers (e.g. glass) are pultruded in a resin matrix (e.g. epoxy) to form a hybrid FRP concrete reinforcing rod. The design procedure begins with calculating the modulus, density, and unit cost of the hybrid FRP rod. Calculation of these parameters is performed using the following equation.

$$\begin{bmatrix} E_{hfrp} \\ \rho_{hfrp} \\ u_{hfrp} \end{bmatrix} = V_{hs}\left\{ V_{hs.fib}\begin{bmatrix} E_{hs.fib} \\ \rho_{hs.fib} \\ u_{hs.fib} \end{bmatrix} + \left(1 - V_{hs.fib}\right)\begin{bmatrix} E_{m} \\ \rho_{m} \\ u_{m} \end{bmatrix} \right\} + \left(1 - V_{hs}\right)\left\{ V_{hm.fib}\begin{bmatrix} E_{hm.fib} \\ \rho_{hm.fib} \\ u_{hm.fib} \end{bmatrix} + \left(1 - V_{hm.fib}\right)\begin{bmatrix} E_{m} \\ \rho_{m} \\ u_{m} \end{bmatrix} \right\} \quad [3.3]$$

where

E_{hfrp} : modulus of the hybrid FRP reinforcement

ρ_{hfrp} : density of the hybrid FRP reinforcement

u_{hfrp} : mass unit cost of the hybrid FRP reinforcement

$E_{hs.fib}$: modulus of the high strength fibers (e.g. glass)

$\rho_{hs.fib}$: density of the high strength fibers

$u_{hs.fib}$: mass unit cost of the high strength fibers

$E_{hm.fib}$: modulus of the high modulus fibers (e.g. carbon)

$\rho_{hm.fib}$: density of the high modulus fibers

$u_{hm.fib}$: mass unit cost of the high modulus fibers

E_{m} : modulus of the resin matrix (e.g. epoxy)

ρ_{m} : density of the resin matrix

u_{m} : mass unit cost of the resin matrix

V_{hs} : volume fraction of high strength FRP (e.g. GFRP) in hybrid rod

$V_{hs.fib}$: volume fraction of high strength fibers (e.g. glass fibers) in high strength FRP (e.g. GFRP)

$V_{hm.fib}$: volume fraction of high modulus fibers (e.g. carbon fibers) in high modulus FRP (e.g. CFRP)

Yield and ultimate strains for the hybrid FRP rod are computed as follows:

$$\begin{bmatrix} \varepsilon^*_{hs} \\ \varepsilon^*_{hm} \end{bmatrix} = \begin{bmatrix} E_{hs.fib} & 0 \\ 0 & E_{hm.fib} \end{bmatrix}^{-1} \begin{bmatrix} f_{hs.fib} \\ f_{hm.fib} \end{bmatrix} \quad [3.4]$$

where

ε^*_{hs} : ultimate strain of the high strength fibers and the hybrid FRP rod

ε^*_{hm} : ultimate strain of the high modulus fibers and yield strain of hybrid FRP rod

$f_{hs.fib}$: tensile strength of the high strength fibers

$f_{hm.fib}$: tensile strength of the high modulus fibers

Properties of interest for the hybrid FRP rod include the ductility, reserve strength, and cost factor (compared to steel on a stiffness basis). The modulus of the high strength portion (i.e. the modulus of the GFRP), E_{hs}, is used to determine the amount of ductility and reserve strength in a hybrid FRP rod. This modulus is computed as follows:

$$E_{hs} = V_{hs.fib} E_{hs.fib} + \left(1 - V_{hs.fib}\right) E_m \quad [3.5]$$

where

E_{hs} : modulus of the pultruded high strength FRP (e.g. GFRP)

As discussed previously, the parameters α and γ, serve as checks to ensure ductility and reserve load capacity. The α parameter must be less than a maximum set value (e.g. 1.4) according to the following condition:

$$\alpha = \frac{F_1}{F_p} = \frac{E_{hfrp}}{E_{hs} V_{hs}} \leq \alpha_{\max} \quad [3.6]$$

where

$\alpha_{\max}$: maximum load transfer factor for the hybrid FRP rod

In addition, the γ parameter must be greater than a set value to ensure reserve load capacity (e.g. 1.0) as indicated in the following condition:

$$\gamma = \frac{F_u}{F_1} = \frac{E_{hs} V_{hs} \varepsilon^*_{hs}}{E_{hm} \varepsilon^*_{hm}} = \frac{\varepsilon^*_{hs}}{\alpha \varepsilon^*_{hm}} \geq \gamma_{min} \qquad [3.7]$$

where

γ_{min} : minimum reserve load capacity factor for the hybrid FRP rod

The cost of the hybrid rod with respect to steel reinforcement on a stiffness basis is found using the following equation.

$$F_{hfrp} = \left(\frac{E_r}{E_{hfrp}}\right)\left(\frac{\rho_{hfrp}}{\rho_r}\right)\left(\frac{u_{hfrp}}{u_r}\right) \qquad [3.8]$$

where

F_{hfrp} : ratio of hybrid FRP cost to steel on a stiffness basis

A hybrid FRP rod is deemed acceptable for use as concrete reinforcement when 1) $\alpha \leq \alpha_{max}$, 2) $\gamma \geq \gamma_{min}$, 3) there is adequate CFRP coverage to insulate the glass fibers from the concrete, and 4) there is sufficient filament-winding to ensure adequate mechanical bonding to the concrete. Several hybrid FRP rods were designed and manufactured using the above equations. Manufacture of the rods is described in the following section.

3.3 Hybrid FRP rod manufacture

Hybrid FRP rods were manufactured by the Polygon Company of Walkerton, Indiana using high strength Torayca T-300 carbons fibers which were donated by Toray Industries in New York, and PPG 700 series E glass fibers which were purchased from Polygon. Glass and carbon fibers were pultruded in an epoxy matrix to form straight, 2.4 m (8 feet) long, 1.27 cm (0.5 inch) diameter hybrid FRP rods. Figure 3.3.1 shows fibers as they are pultruded into rods. The spools of the fibers are threaded into a separation plate to maintain distribution of fiber tows. Tows are then threaded into a

confining "fixture" plate, which defines the small diameter shape of the pultruded rod. Next, fibers are extruded under tension to form smooth rods. Fiber volume fractions of 0.70 are common. Figure 3.3.1a shows fiber tows feeding into a separation plate. Figure 3.3.1b shows threaded spools of fiber tows projecting from the separation plate. The smooth, pultruded rods are filament-wound to produce surface irregularities for bonding.

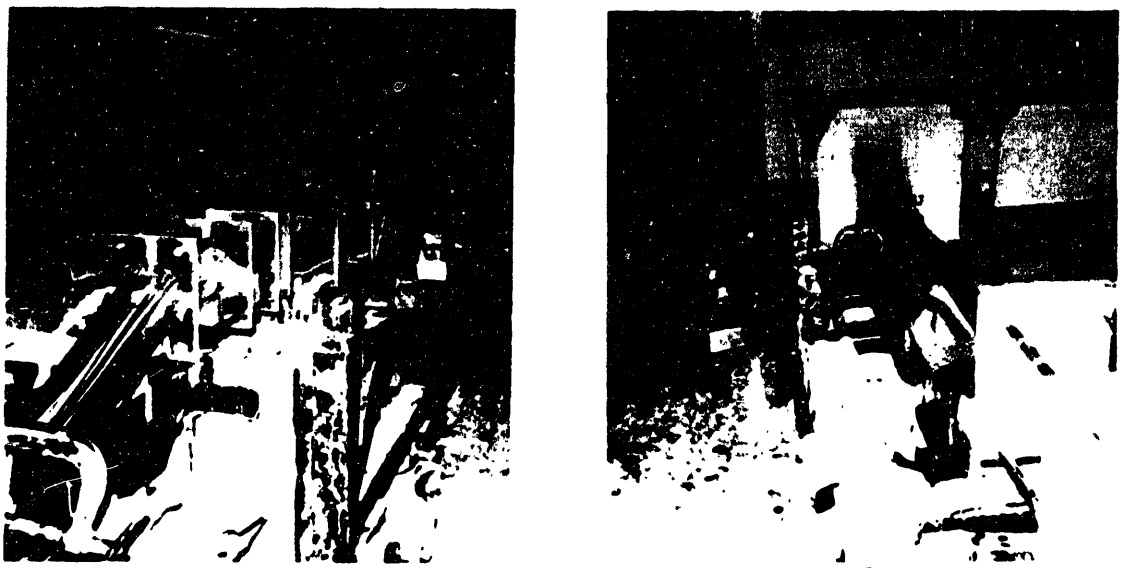

Figure 3.3.1 Pultrusion Process

Figure 3.3.2 shows the concept of the filament-wound pultruded rods. Most rods were filament-wound with PPG type 1062 E glass. Others used remaining T-300 carbon fibers. The use of glass fibers for filament-winding is only for flexural testing purposes.[5] Actual applications in concrete are expected to require carbon for filament winding.

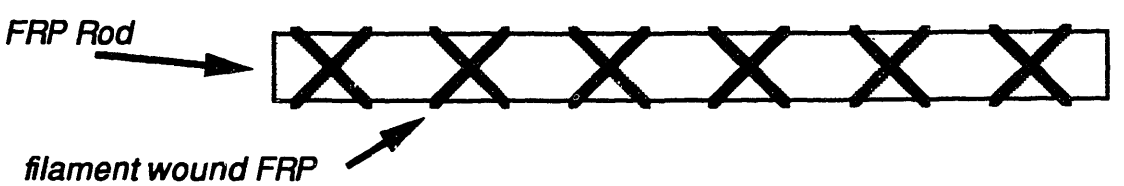

Figure 3.3.2 Hybrid FRP Rod Concept with Filament-Winding

[5] See Section 3.4.

Figure 3.3.3 shows five of the 2.4 m long manufactured rods resting one of the T-beam forms. The darker rod shown in the figure is filament-wound with carbon fibers. The other four rods shown in Figure 3.3.3 are filament-wound with glass fibers.

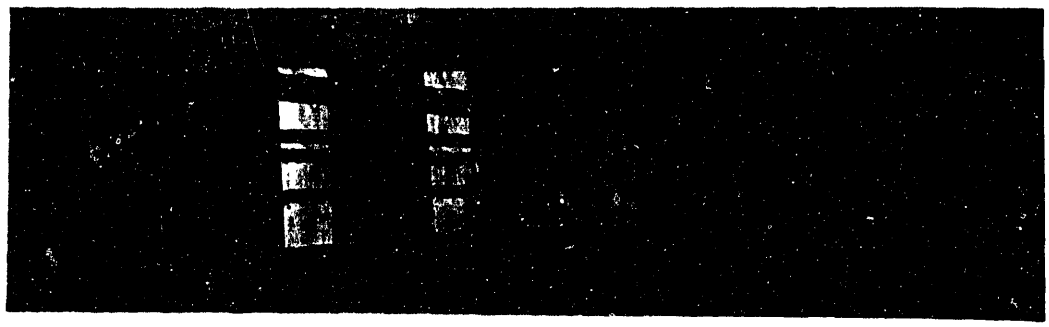

Figure 3.3.3 Manufactured Hybrid FRP Rod with Filament-Winding

Each manufactured hybrid FRP rod has with one of the three CFRP thicknesses listed in Table 3.3.1. The "hybrid3" FRP rod has a 0.040 cm thick CFRP layer, which results in a GFRP volume fraction of 0.8789. From a visual inspection, the "hybrid2" rod has the minimum number of layers of carbon fibers to ensure complete coverage of the glass fibers. Thus, for durability concerns, a GFRP volume fraction of 0.92 appears to be the largest amount of GFRP allowable for a 1.27 cm diameter hybrid FRP rod.

Table 3.3.1 Manufactured hybrid FRP rods

Rod Sample Name	number of carbon fiber layers	Thickness of CFRP	GFRP diameter	GFRP Volume Fraction	Cost WRT Steel (stiffness basis) *
hybrid1	1	0.013 cm (1/192 in)	1.244 cm (47/96 in)	0.9588	4.8
hybrid2	2	0.026 cm (1/96 in)	1.217 cm (23/48 in)	0.9184	5.5
hybrid3	3	0.040 cm (1/64 in)	1.191 cm (15/32 in)	0.8789	6.4

* See Figure 3.2.3

To process each CFRP thickness variation, a number of manual steps were required. First, the entire pultrusion process had to be shutdown. Then, outside layers of fiber tows had to be removed and re-threaded with appropriate fibers types. At least 60 m

(200 feet) of fiber were required for each setup. After the rods were pultruded and cut to appropriate lengths, each was then manually sent to a filament-winding machine for final processing.

For small hybrid FRP pultrusion orders—such as the order for test rods for this research—the number of manual procedures required for rod processing results in material costs that are rather insignificant compared to the total cost. As with most manufacturing processes, however, pultrusion processing costs for large orders become minor. Thus, in estimating the cost for a pultruded hybrid FRP rod, pultruded processing costs have not been included. Rather, the glass fibers, carbon fibers, and epoxy matrix material costs are used to estimate total hybrid FRP rod material costs.

3.4 Hybrid FRP reinforced concrete testing

3.4.1 Overview

To investigate and confirm the potential for using FRP rods as reinforcement in concrete, load-displacement tests were performed on seven 1.83 m (6.0 ft) T-shaped concrete beams, each reinforced with a single hybrid FRP rod. As discussed in section 3.2, the hybrid FRP rods consist of an inner core of pultruded glass fibers with a thin outer layer of pultruded carbon fibers (see Figure 3.2.1). Each of the hybrid FRP reinforcing rods used in the tests have a 1.27 cm (0.5 in) outside diameter with one of three different carbon thicknesses. One to three layers of carbon fiber tows were pultruded on the outside perimeter of each rod to insulate the inner glass fibers. The carbon thicknesses used and the resulting volume fractions of GFRP are shown in Table 3.4.1. As indicated in the table, one layer of carbon fiber tows is not sufficient to completely cover the inner glass fibers of the 1.27 cm diameter rod.

Table 3.4.1 Hybrid FRP rods used in tests

Rod Sample Name	number of carbon fiber layers	GFRP volume fraction	coverage sufficient (visually)	reinforced concrete T-beam tests used in *
hybrid1	1	0.9588	no	I-1, II-1a, II-1b
hybrid2	2	0.9184	yes	I-2, II-2a, II-2b
hybrid3	3	0.8789	yes	I-3

* See Table 3.4.2

3.4.2 Test setup

Two phases of tests were performed. For the first phase, one beam was cast for each of the three carbon thicknesses, (tests I-1, I-2, and I-3). The contact between the FRP reinforcing rod and the steel stirrups caused premature failure in the first test phase. These failures were attributed to the axial force from the stirrup which caused shearing on the FRP rod under severe bending. For Phase II (tests II-1a, II-1b, II-2a, and II-2b), a separation of approximately 1.9 cm (0.75 in) between the FRP rod and the stirrups was enforced—which eliminated the shearing problem.

Figure 3.4.1 shows the end of a first phase test beam. The single hybrid FRP rod is cast in the lower portion of the T-beam. Small upper steel rods are used as compression members only. Figure 3.4.2 shows the cross-section for the second phase test specimens. Stirrups and reinforcement in the concrete compression zone are approximately 0.476 cm (0.1875 in) diameter mild steel. Compressive strength for the concrete ranged from 55 to 75 MPa (8-11 ksi).

All beams were tested under 4 point bending as indicated in Figure 3.4.3. A development length of 30.5 cm (12 in) was allowed and a shear free zone (between the two loading points) of 10.2 to 20.3 cm (4-8 in) was used. A 20.3 cm shear free zone was used for the Phase I tests and a 10.2 cm zone was used for the four beams of Phase II. The 10.2 cm shear free zone gives a shear aspect ratio of:

$$a = \frac{86.36cm - 30.48cm}{14.61cm} = \underline{\underline{3.825}}$$

A shear aspect ratio of at least 2.5 is needed to ensure flexural failure of the reinforced concrete beam [Wang and Salmon 85]. In addition, stirrups were placed approximately every 5 cm (2 in) to further ensure failure in flexure.

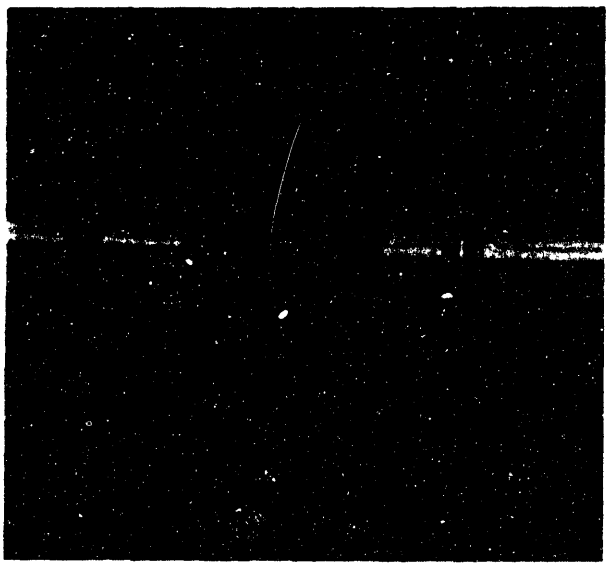

Figure 3.4.1 Hybrid FRP Test Beam Cross-Section (Phase I)

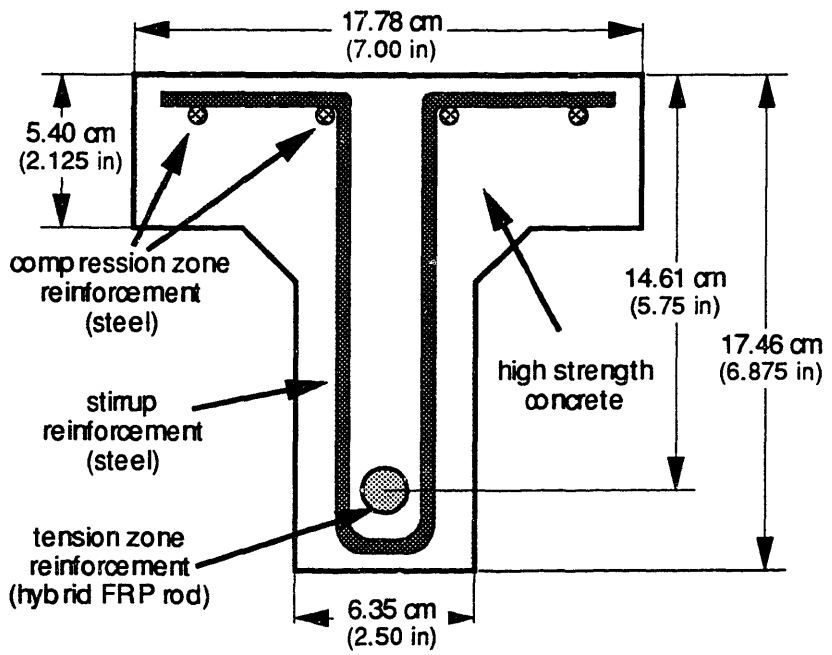

Figure 3.4.2 Hybrid FRP Test Beam Cross-Section (Phase II)

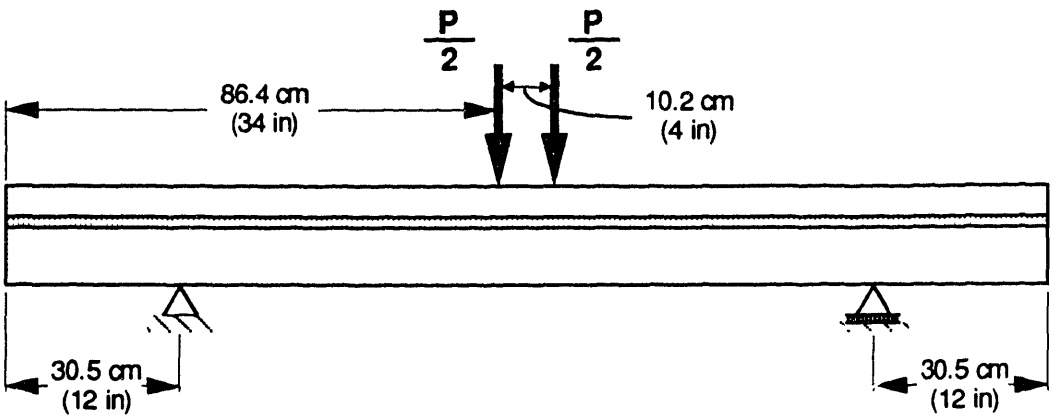

Figure 3.4.3 Hybrid FRP 4-Point Test Setup

3.4.3 Test results

Figure 3.4.4 shows the initial Phase I test setup for a hybrid FRP reinforced concrete T-beam. As shown, the beam undergoes 4-point bending. Figure 3.4.5 shows initial cracking of the beam under load. The deflection of the beam is also noticeable. Figure 3.4.6 shows the extensive cracking of the section prior to failure. Both the cracking and the small neutral axis of the section are due to the low stiffness of the hybrid FRP rod.

Figure 3.4.4 T-beam Test Setup for Phase I

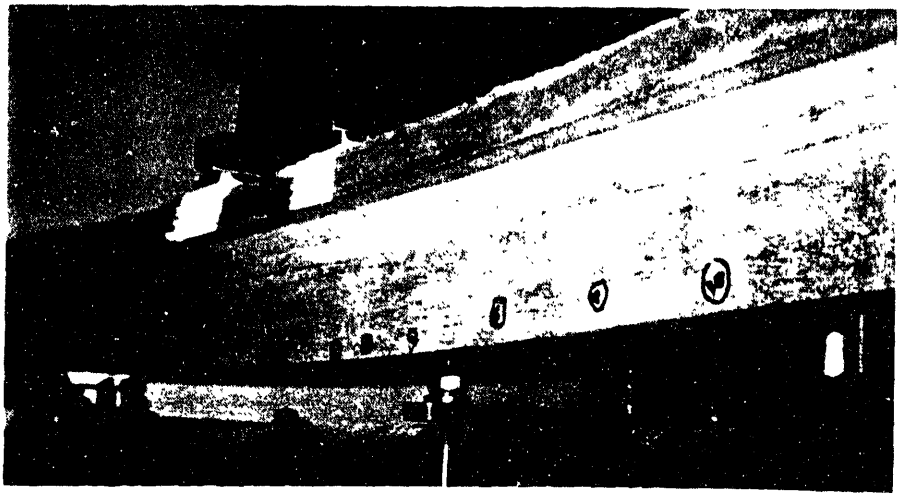

Figure 3.4.5 Initial Cracking in Phase I Test Beam

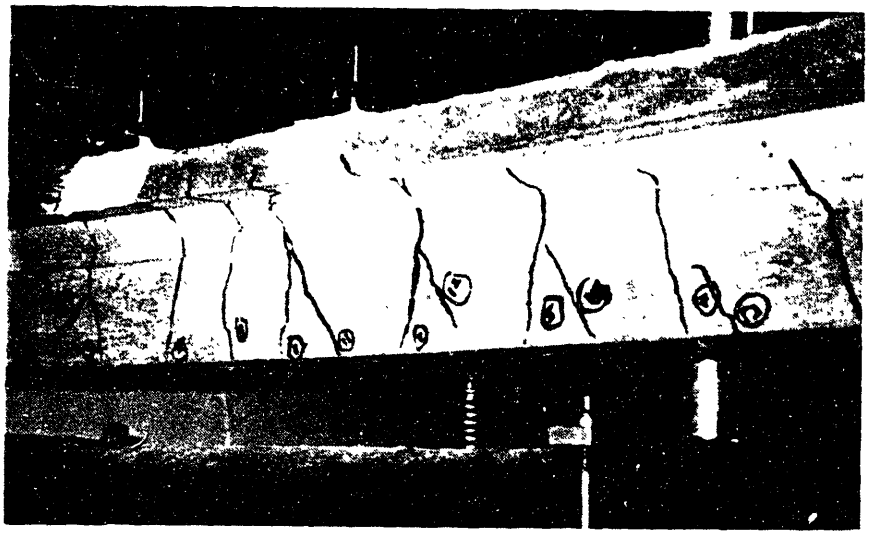

Figure 3.4.6 Extensive Cracking Before Failure of Phase I Test Beam

Because it appeared that pseudo-ductility of the hybrid FRP rod was being observed, the test beam was removed before failure. The concrete nearest to the failure plane was removed with the hope of observing carbon fiber rupture. Figure 3.4.7 shows one such area where it appears the carbon fibers did indeed rupture prior to the glass rupture. However, this could not be confirmed with the test specimen. Once a beam was reloaded, the hybrid FRP rods either failed in a brittle fashion, or could not be failed.

Figure 3.4.7 Exposed Hybrid FRP Rod Showing Carbon Failure

It became evident that the steel stirrup was causing the pultruded FRP rod to fail prematurely (see Table 3.4.2) due to the severe bending in the beam before failure. For the second test phase a physical separation between the rod and the stirrups was ensured as shown in Figure 3.4.2. In addition, the mid portion of the rod was left exposed, as shown in Figure 3.4.8, in order to visually confirm the pseudo-ductile failure.

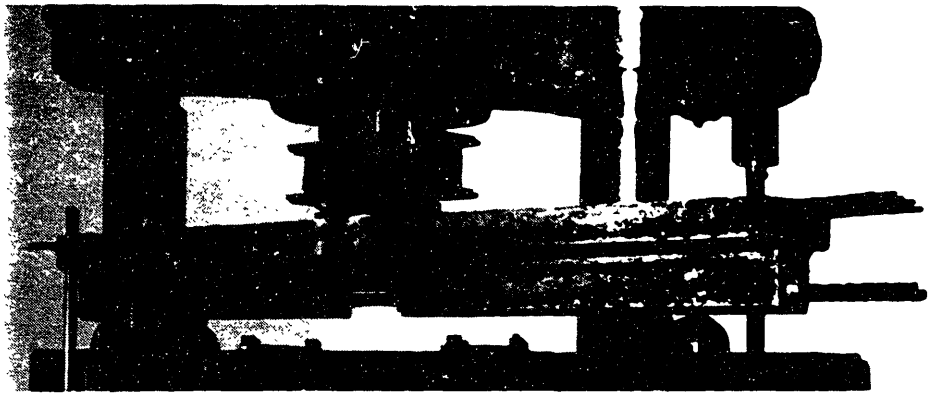

Figure 3.4.8 Test Setup for Phase II

Figure 3.4.9 shows initial cracking of a Phase II test beam. Figure 3.4.10 shows the extent of beam cracking and bowing prior to failure. Load-displacement plots for all tests are included in Appendix B.

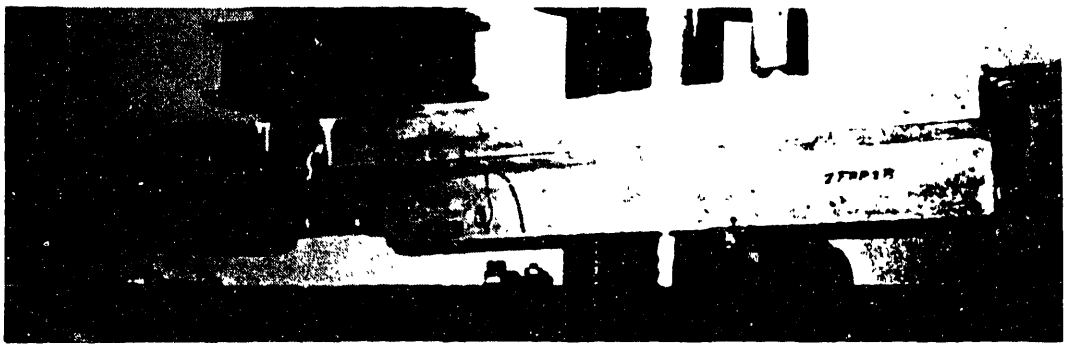

Figure 3.4.9 Initial Cracking in Phase II Test Beam

Figure 3.4.10 Extensive Cracking and Bowing of Phase II Test Beam

Figures 3.4.11 and 3.4.12 show the load-deflection curve for a Phase II hybrid reinforced concrete beam. In general, load was applied twice to test beams. The first loading was stopped prior to beam failure to check for evidence of carbon fiber rupture prior to glass fiber rupture. This would indicate ductility in the FRP rod. The second loading was an attempt to fail the beam.

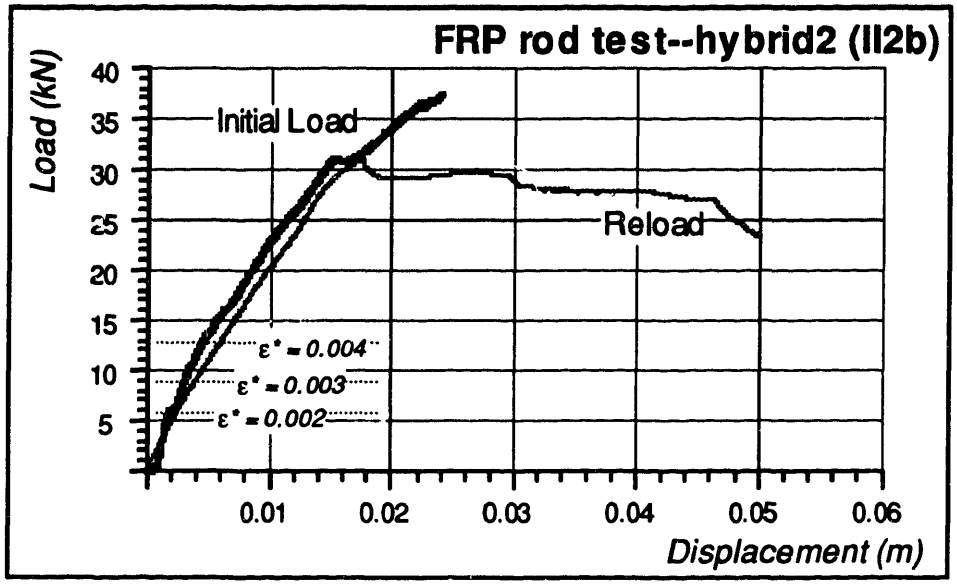

Figure 3.4.11 FRP Reinforced Concrete Force-Displacement Plot

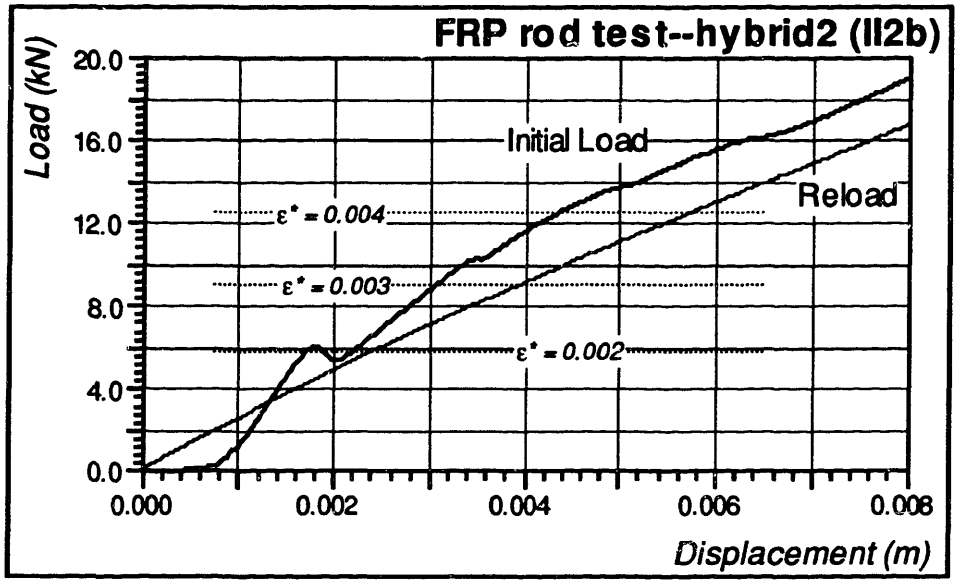

Figure 3.4.12 FRP Reinforced Concrete (magnified) Force-Displacement Plot

Test results, summarized in Table 3.4.2, indicate that the bond strength between the pultruded hybrid FRP rods with an outer filament winding, and the high strength concrete is adequate. Though one hybrid FRP rod did experience a bond failure (test I-2), it appears that the filament winding was split by the shearing action from the abutting stirrup when it was under severe beam bending. This problem was eliminated in Phase II and no bond failure occurred.

Table 3.4.2 Hybrid FRP reinforced concrete beam tests

Test Number	FRP rod used	extensive cracking before failure?	complete ductile failure?	adequate bond?	comments
Phase I tests					
I-1	**hybrid1**	yes	no	yes	stirrup sheared rod
I-2	**hybrid2**	yes	yes	no	stirrup sheared filament winding
I-3	**hybrid3**	yes	no	yes	stirrup sheared rod
Phase II tests					
II-1a	**hybrid1**	yes	yes	yes	
II-1b	**hybrid1**	yes	yes	yes	
II-2a	**hybrid2**	yes	no	yes	improper beam alignment
II-2b	**hybrid2**	yes	yes	yes	see Figures 3.4.6 and 3.4.7

There were several cases where it appeared that the carbon fibers had failed before the glass (tests I-2, II-1a, and II-2b), but this behavior was not found in all cases. Some cases appeared to have simply frayed the carbon fibers due to the interaction with either the stirrups, tie wire, or possibly even sharp aggregate. Thus, pseudo-ductility of the rod could not be confirmed in these tests though theoretically, the concept is valid. A hybrid FRP rod with a lower carbon fiber failure strain should confirm the pseudo-ductility of the material.

Ductility in the FRP rod could not be confirmed due to the high failure strains of the pultruded glass and high strength carbon fibers. However, ductility in the FRP reinforced beam was evident as significant and obvious cracking of the concrete occurred in each beam prior to failure. Only one beam failed in a brittle manner in the second phase. It was concluded the failure was due to improper alignment of the beam setup. The other three test beams demonstrated that FRP R/C beams indeed fail in a ductile manner.

3.5 FRP vs. steel cost comparison

Currently, FRP rods are not considered to be cost effective replacements for steel. They are envisioned for use only in areas where steel reinforcing rod use is restricted, e.g.

near superconducting magnets where stray magnetic fields and power losses are significant. The cost of FRP material is compared to the cost of steel on a stiffness basis in Figure 3.5.1. The cost of glass FRP is 2.2 to 4.5 times the cost of steel on a stiffness basis, while carbon FRP costs currently are 10 to 25 times the cost of steel on a stiffness basis. High strength carbon (carbon-HS) fiber costs 10 to 19 times that of steel and high modulus carbon (carbon-HM) fiber costs 13 to 25 times the cost of steel.

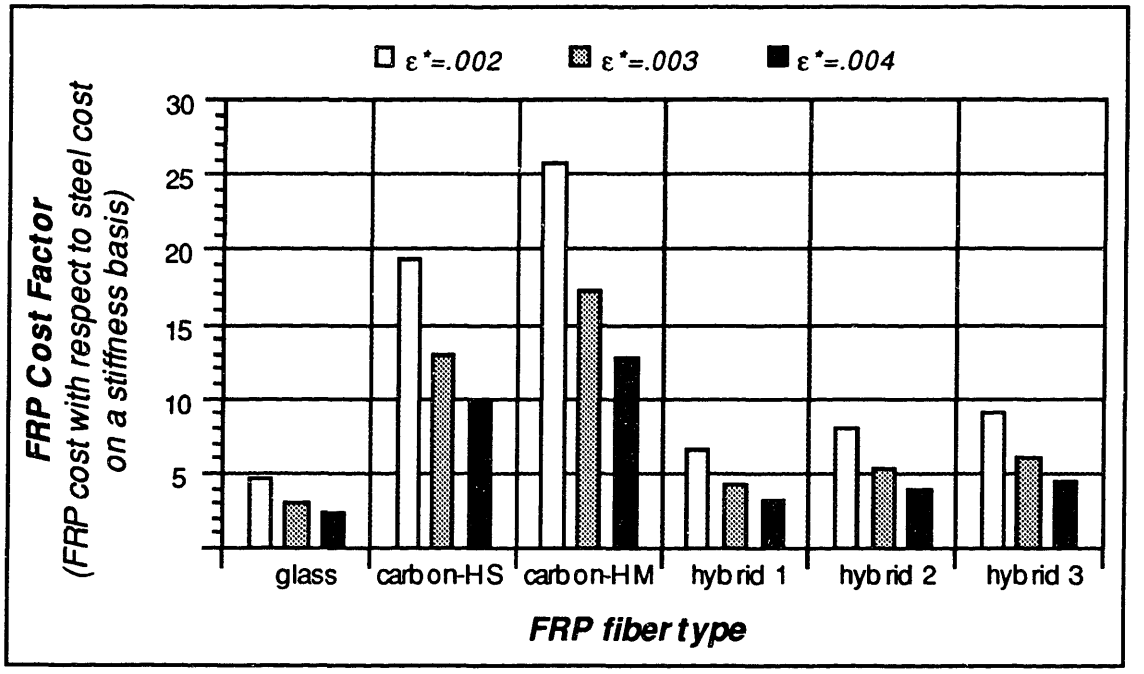

Figure 3.5.1 FRP Cost Comparison vs. Steel for Various Fiber Types

The cost of carbon-HM FRP used in the comparison is over twice the cost of carbon-HS FRP on a mass basis.[6] However, on a stiffness (or strain) basis, carbon-HM is approximately 37% greater in cost than carbon-HS due to the higher modulus and lower strain of the carbon-HM fiber. That is, because of the lower failure strain of the carbon-HM fiber, more of its fiber is utilized by the concrete. Thus, if the cost of carbon-HM fibers can be reduced substantially, it will be the superior choice for use in concrete.

6 See Table 2.2.1.

Note that costs in Figure 3.5.1 are shown for ultimate strain levels of 0.002, 0.003, and 0.004. Though glass FRP material has ultimate strains as high as 0.040, only 0.002 to 0.004 strain is utilized by a reinforced concrete member because significant cracking results when a tensile strain of 0.004 is exceeded.[7] The remaining material strength, though useful to ensure ductility in the member, represents essentially wasted FRP material for a stiffness based reinforced concrete design (see Figure 3.4.10). Also shown in Figure 3.5.1 are costs for the three hybrid FRP rods used in the tests described in the previous sections.

Current applications for carbon FRP (e.g. tennis rackets, fishing poles) are not highly cost sensitive and involve relatively small quantities. The extent to which the cost of carbon FRP can be reduced has not been determined . Cost reductions are limited by the energy costs involved in the manufacture of the carbon fibers. However, it is certainly plausible that with large volume orders—which would occur if a prototype system is built—FRP material costs will be reduced significantly.

3.6 Hybrid FRP rod summary and conclusions

A method for improving the failure mechanism, durability, and stiffness properties of a glass FRP rod has been developed and presented in this thesis in the form of a hybrid FRP rod. The concept is based on surrounding an inner GFRP core with a thin layer of CFRP to form a glass/carbon hybrid FRP rod. Because carbon fibers are inert to alkaline environments, they are extremely durable in concrete. Also, because of the higher modulus of carbon with respect to glass, the hybrid FRP rod fails in a pseudo-ductile manner.

---

[7] See Figures 3.4.11 and 3.4.12

The hybrid rod, along with all pultruded FRP rods, suffers in that it is weak in shear. This suggests that any FRP design must avoid significant axial forces perpendicular to the axis of the pultruded fibers. Thus, connection design, stirrup design, and anchorage device design will have to consider the lack of shear strength of the rods. In addition, long term FRP material behavior including creep, relaxation and fatigue must be considered. In general, the properties and the orientation of FRP fibers can be engineered for specific strength and/or stiffness requirements. However, for pultruded rods, fiber orientations other than those parallel to the rod axis are difficult to manufacture.

Though hybrid FRP rod cost reduction through mass manufacturing techniques is expected, costs for hybrid FRP rods are not expected to drop below those of steel. This suggests the need for efforts directed towards reducing areas of the guideway system that require non-magnetic reinforcement, (i.e. through modified vehicle and/or motor designs).

Because low cost is a major design objective, glass fibers and low cost carbon fibers have been used in the hybrid FRP rod presented in this thesis. Mechanical properties of this hybrid FRP rod suffer from the use of these low cost fibers. To ensure ductility and low cost, the use of GFRP must be maximized. However, by maximizing GFRP, the hybrid rod tends to behave more like GFRP alone, which has 1) a low modulus and 2) a failure strain much greater than can be effectively utilized by concrete. Currently, the hybrid rod is projected to cost 5.5 to 8.5 times the cost of steel on a stiffness comparison basis.[8] Future research focused at reducing the cost of hybrid FRP rod is needed. The hybrid FRP rod is acceptable, though improvements are possible. Specifically, mechanical properties of the hybrid FRP rod improve dramatically if only

---

[8] See Figure 3.2.3

high strength and high modulus carbon fibers are used. Currently, however, the high cost of an all carbon FRP rod restricts its viability. A mechanically superior reinforcing hybrid FRP rod is one consisting of 1) high strength, high strain carbon fibers and 2) high modulus, low strain carbon fibers, i.e. no glass fibers. However, current costs of carbon fibers prevent immediate consideration of an all carbon FRP rod. Further research into lower cost, lower strain carbon fibers is needed.

Chapter 4 applies the glass/carbon hybrid FRP rod concept presented in this chapter to the concrete reinforcement of the upper two corners of the rectangular hollow-box beam cross-section. The stirrup reinforcement in these areas is also considered to be with hybrid FRP, though no consideration for embedment length is given. In addition, the 5.5 hybrid FRP cost factor calculated in section 3.2 is used in the cost sensitivity analyses performed in Chapter 4.

4.0 Narrow Beam Analysis

This chapter introduces a design procedure as well as equations for the hollow-box reinforced concrete beam in Section 4.1. Section 4.2 presents a step-by-step example of a maglev beam design with given loading and deflection constraints. Included is a spreadsheet analysis program which uses the design procedure equations found in Section 4.1. This analysis program is used to perform a number of sensitivity analyses which are outlined and discussed in Section 4.3. Cost comparisons between the narrow beam design and the Transrapid maglev guideway are also included.

4.1 Narrow Beam Design Formulas

Formulas are derived for horizontal and vertical bending, deflection, shear, and torsion for a hollow-box reinforced concrete guideway beam. The design approach is based on American Concrete Institute (ACI) reinforced concrete design procedures [ACI 89]. Cost functions for overall beam material costs are outlined in 4.4.4. These cost functions are generalized to account for both hybrid FRP and steel reinforcement. The analysis assumes linearly elastic beam behavior. Also, horizontal and vertical bending resistance and deflections are analyzed independently. The effect of prestressing tendons on live load resistance and deflection is ignored. These assumptions are used to ensure a conservative design.

4.1.1 Bending moment resistance

The strength of a simply-supported beam element must be sufficient to withstand both bending moments and shear forces resulting from given loads. It is assumed that realistic loading patterns can be approximated by the combination of a fully distributed load and a concentrated midspan load. The beam element must have the capacity to

withstand the required vertical bending moment, $M_{n.v}$, and the horizontal bending moment, $M_{n.h}$, as computed in the following formula.

$$\begin{bmatrix} M_{n.v} \\ M_{n.h} \end{bmatrix} = \left(\frac{L}{8\phi}\right) \begin{bmatrix} F_v & 0 \\ 0 & F_h \end{bmatrix} \begin{bmatrix} w_v & P_v \\ w_h & P_h \end{bmatrix} \begin{bmatrix} L \\ 2 \end{bmatrix} \qquad [4.1]$$

where

L : beam length

F_v : vertical load uncertainty multiplying factor (1.4)

F_h : horizontal load uncertainty multiplying factor (1.7)

ϕ : material uncertainty reduction factor due to bending (0.90)

w_v, w_h : distributed vertical and horizontal loads

P_v, P_h : concentrated vertical and horizontal midspan loads

Bending constraints:

Based on the use of concrete and steel, the following constraints are imposed on the minimum cross-sectional area of steel for the primary tensile steel in the lower flange, $A_{rt.v}$, and the nominal cross-sectional area of steel in each web, $A_{rt.h}{}'$.

$$\begin{bmatrix} A_{rt.v} \\ A_{rt.h}{}' \end{bmatrix} = \left(E_r \varepsilon_r{}' \left[1 - \frac{\beta_1 \varepsilon_c^*}{2\left(\varepsilon_c^* + \varepsilon_r^\circ\right)} \right] \right)^{-1} \begin{bmatrix} d_v & 0 \\ 0 & d_h \end{bmatrix}^{-1} \begin{bmatrix} M_{n.v} \\ M_{n.h} \end{bmatrix} \qquad [4.2]$$

where

$\varepsilon_r{}'$: reinforcement strain before yield (e.g. 0.002)

α_r : fraction of yield strain permissible during service load (e.g. 0.6)

ε_r° : reinforcement strain during service load, $\varepsilon_r{}'\alpha_r$ (e.g. 0.0012)

ε_c^* : ultimate strain of concrete in compression (e.g. 0.003)

β_1 : strength reduction factor for concrete based on the working stress block design

E_r : reinforcement modulus (in Pa, N/m^2)

d_v : "effective" depth (i.e. from the top of the beam to the neutral axis of the lower tensile reinforcement)

d_h : "effective" width

Due to physical spacing requirements for reinforcing bars and stirrups, the absolute steel-to-concrete volume percentage is limited to less than 8%. Generally, however, less than 3% steel-to-concrete volume is used in reinforced concrete design. For design purposes, the absolute percentage of tensile reinforcement is used as a constraint for a given section as indicated in the following equation.

$$\begin{bmatrix} A_{r.v\max} \\ A_{r.h\max} \end{bmatrix} = F_{ra} t \begin{bmatrix} b \\ h-2t \end{bmatrix} \qquad [4.3]$$

where

F_{ra} : maximum fraction of reinforcement possible with respect to area of section (e.g. 0.08)

$A_{r.v\max}$: maximum reinforcement allowable for flange sections

$A_{r.h\max}$: maximum reinforcement allowable for web sections

t : thickness of the box beam

b : beam width

h : beam depth

Minimum reinforcement constraints result from the need to adequately distribute reinforcement in the tension zone of the concrete. Without proper distribution, 1) large cracks will develop in the section and 2) reinforcing bars will tend to pull out prematurely. According to ACI code, the following minimum constraint is placed on reinforcement distribution [ACI 89].

$$\begin{bmatrix} A_{r.v\min} \\ A_{r.h\min} \end{bmatrix} = \frac{D_b^2 \pi t^2}{8} \left(\frac{E_r \varepsilon_r^{\circ}}{w_{t.\max}} \right)^3 \begin{bmatrix} b \\ h-2t \end{bmatrix} \qquad [4.4]$$

where

$A_{r.v\min}$: minimum reinforcement allowable for flange sections

$A_{r.h\min}$: minimum reinforcement allowable for web sections

D_b : diameter of longitudinal reinforcing bar (in m)

$w_{t.\max}$: maximum tension allowable in section (e.g. 25,400,000 N/m = 145 kips/in)

The amount of reinforcement in the upper flange is dependent on the actual dynamic response of the beam.[1] The dynamic response results in beam oscillations, and thus, negative (i.e. upward) beam deflections. Therefore, as an estimate, compressive vertical reinforcement is assumed equal to a fraction, $F_{nr.v}$, of the required vertical tensile reinforcement (e.g. 0.25). The actual value of $F_{nr.v}$ used in practice will depend on the dynamic amplification factor imposed by a particular vehicle on the beam. In addition, a similar approach is followed to determine required reinforcement for the opposite web when subjected to horizontal dynamic loads. For unprotected sections, (i.e. when no other structure such as a nearby building is present that will significantly shield one side of the guideway from wind), the horizontal negative reinforcement factor, $F_{nr.h}$, equals 1.0.

$$A_{rc.v} = \max\{F_{nr.v}A_{rt.v}, A_{r.v\min}\} \qquad [4.5]$$

where

$F_{nr.v}$: fraction of compressive (negative) vertical reinforcement, $A_{rc.v}$, with respect to required vertical tensile reinforcement, $A_{rt.v}$.

$A_{rc.v}$: amount of reinforcement for the negative vertical reinforcement in upper flange

When calculating reinforcement requirements using the above formula, the amount of reinforcement required for corners of the box section is computed for both horizontal and vertical directions—and is thus redundant. Therefore, the amount of horizontal, or web, reinforcement calculated in the previous equation is reduced to the amount of reinforcement inside each web, $A_{rt.h}$. This reduction is made primarily for cost calculations. The resulting amount of reinforcement equals that required for horizontal bending resistance minus the reinforcement found in corner sections required for vertical bending moment resistance according to the Equation 4.6. Note that the horizontal

1 See Chapter 5.

reinforcement is not considered when analyzing vertical bending capacity. Similarly, vertical reinforcement is not considered when analyzing horizontal bending capacity. This approach gives a conservative first order design.

$$A_{rt.h} = \max\left\{\left[A_{rt.h}' - (A_{rt.v} + A_{rc.v})\left(\frac{t}{b}\right)\right], A_{r.h\min}\right\} \qquad [4.6]$$

and

$$A_{rc.h} = F_{nr.h} A_{rt.h} \qquad [4.7]$$

where

$F_{nr.h}$: fraction of compressive (negative) vertical reinforcement, $A_{cs.h}$, with respect to required vertical tensile reinforcement, $A_{rt.h}$.

$A_{rt.h}$: actual cross-sectional area of reinforcement in web for positive horizontal bending

$A_{rc.h}$: amounts of reinforcement in web for negative horizontal bending

4.1.2 Deflection criteria

The vertical and horizontal moments of inertia, $I_{g.v}$ and $I_{g.h}$, respectively, for the transformed box section are computed using the following equations. For simplicity in computing the section moment of inertia, it is assumed 1) that the thickness of the section, t, is uniform for each flange and web and 2) that web and flange longitudinal reinforcement is centered at a distance of $t/2$ from the exterior. These moment of inertia assumptions are valid for relatively thin-walled box sections.

section mass centroid
vertical

$$y_{c.v} = \frac{th(b-2t) + (n-1)\left[A_{rt.v} d_v + A_{rc.v}\left(\frac{t}{2}\right)\right] + th^2}{2t(b-2t) + (n-1)[A_{rt.v} + A_{rc.v}] + 2th} \qquad [4.8a]$$

horizontal

$$y_{c.h} = \frac{tb(h-2t)+(n-1)\left[A_{rt.h}d_h + A_{rc.h}\left(\frac{t}{2}\right)\right]+tb^2}{2t(h-2t)+(n-1)\left[A_{rt.h}+A_{rc.h}\right]+2tb} \qquad [4.8b]$$

section moment of inertia
vertical

$$I_{g.v} = \left(\frac{2t}{3}\right)\left[y_{c.v}{}^3 + (h-y_{c.v})^3\right] + \left(\frac{t^3}{6}\right)[b-2t] + \left(y_{c.v}-\frac{t}{2}\right)^2\left[(b-2t)t+(n-1)A_{rc.v}\right] + (d_v-y_{c.v})^2\left[(b-2t)t+(n-1)A_{rt.v}\right] \qquad [4.9a]$$

horizontal

$$I_{g.h} = \left(\frac{2t}{3}\right)\left[y_{c.h}{}^3 + (b-y_{c.h})^3\right] + \left(\frac{t^3}{6}\right)[h-2t] + \left(y_{c.h}-\frac{t}{2}\right)^2\left[(h-2t)t+(n-1)A_{rc.h}\right] + (d_h-y_{c.h})^2\left[(h-2t)t+(n-1)A_{rt.h}\right] \qquad [4.9b]$$

where

$y_{c.v}$: vertical distance from top of section to mass center $[y_{t.v} = h - y_{c.v}]$.

$y_{c.h}$: horizontal distance from side of section to mass center (should equal b/2) $[y_{t.h} = b - y_{c.h}]$.

n : ratio of reinforcement modulus to concrete modulus, E_r/E_c.

$I_{g.v}$: vertical moment of inertia.

$I_{g.h}$: horizontal moment of inertia.

To control deflection, the following minimum constraints are imposed on the vertical and horizontal moments of inertia.

$$\begin{bmatrix} I_{g.v} \\ I_{g.h} \end{bmatrix} \geq \left(\frac{L^2}{384E_c}\right)\begin{bmatrix} k_{\Delta v} & 0 \\ 0 & k_{\Delta h} \end{bmatrix}\begin{bmatrix} w_v & P_v \\ w_h & P_h \end{bmatrix}\begin{bmatrix} 5L \\ 8 \end{bmatrix} \qquad [4.10]$$

where

E_c : modulus of the concrete

$k_{\Delta v}$: vertical deflection constraint (e.g. L/1000 --> $k_{\Delta v}$ =1000)

$k_{\Delta h}$: horizontal deflection criteria (e.g. L/1000 --> $k_{\Delta h}$ =1000)

4.1.3 Prestressing

The amount of prestressing is limited by the maximum compressive and tensile stresses induced on the concrete according the following formula.

$$\begin{bmatrix} P_{v\min} \\ P_{h\min} \end{bmatrix} = \left(\frac{A_g}{1 - F_{lp}} \right) \left(\begin{bmatrix} \frac{M_{n.v} y_{t.v}}{I_{g.v}} \\ \frac{M_{n.h} y_{t.h}}{I_{g.h}} \end{bmatrix} - f^*_{c.t} \begin{bmatrix} 1 \\ 1 \end{bmatrix} \right) \qquad [4.11]$$

where

A_g : gross area of the cross-section

F_{lp} : long term strength loss due to relaxation of the prestressing tendons

$y_{t.v}$: vertical distance from the neutral axis to the extreme tension fiber in the cross-section (= h - $y_{c.v}$)

$y_{t.h}$: horizontal distance from the neutral axis to the extreme tension fiber in the cross-section (= b - $y_{c.h}$)

$f^*_{c.t}$: maximum tension allowable for concrete section (ACI code allows $500\sqrt{f'_c}$, where f'_c is in Pa)

$P_{v\min}$: amount of prestressing force required to limit tensile stress in concrete section under vertical bending

$P_{h\min}$: amount of prestressing force required to limit tensile stress in concrete section under horizontal bending

The prestressing force is calculated to be sufficient to negate dead load deflection. The dead load, w_D, is calculated using Equation 4.12. Note that the contribution due to prestressing cable weight is not included in this beam dead load equation. The weight contribution of the prestressing cables typically is not significant. When desired,

however, an estimate of the cable weight can be added to the distributed magnetic windings load, w_m.

$$w_D = A_g\rho_c + (A_{rt.v} + A_{rc.v} + A_{rt.h} + A_{rc.h})(\rho_r - \rho_c) + w_m \qquad [4.12]$$

where

ρ_c : concrete density (N/m^3)

ρ_r : reinforcement density (N/m^3)

w_m : distributed magnetic motor winding load

The minimum amount of prestressing permissible in the beam is controlled by the maximum midspan eccentricity permissible in the section and is represented in the following equation.

$$P_{e.\min} = \frac{M_D}{e_{\max}(1 - F_{lp})} \qquad [4.13]$$

where

M_D : unfactored moment due to dead weight loading (= $w_D L^2/8$)

$e_{\max}$: maximum amount of eccentricity available for prestressing for the given section (= $y_{t.v} - 2t$)

$P_{e.\min}$: amount of prestressing force required to control deflection considering maximum available eccentricity of section

Thus, the amount of prestressing required is the maximum value of $P_{v\min}$, $P_{h\min}$, and $P_{e.\min}$ as indicated below.

$$P = \max\begin{cases} P_{v\min} \\ P_{h\min} \\ P_{e.\min} \end{cases} \qquad [4.14]$$

where

P : amount of prestressing force required to satisfy deflection and tension in section constraints

To limit the amount of compressive forces in the concrete section, maximum amounts of prestressing forces are calculated by the following equation.

$$\begin{bmatrix} P_{v\max} \\ P_{h\max} \end{bmatrix} = \left(\frac{A_g}{1 - F_{lp}} \right) \left(f^*_{c.c} \begin{bmatrix} 1 \\ 1 \end{bmatrix} - \begin{bmatrix} \frac{M_{n.v} y_{c.v}}{I_{g.v}} \\ \frac{M_{n.h} y_{c.h}}{I_{g.h}} \end{bmatrix} \right) \qquad [4.15]$$

where

$f^*_{c.c}$: maximum compression allowable for concrete section (ACI code allows $0.45 f'_c$)

$P_{v\max}$: maximum amount of prestressing force allowed to limit compressive stress in concrete section under vertical bending

$P_{h\max}$: maximum amount of prestressing force allowed to limit compressive stress in concrete section under horizontal bending

Once an acceptable prestressing force is determined, a midspan eccentricity is chosen to give a zero dead load deflection. The profile of the prestressing tendons is considered parabolic for analysis. Though a draped profile may be desired for actual construction, its effect on eccentricity calculations will be minimal. The eccentricity is:

$$e = \frac{M_D}{P(1 - F_{lp})} \qquad [4.16]$$

where

e : midspan eccentricity of parabolic tendon profile

4.1.4 Torsion and shear design

The required vertical shear strength, $V_{n.v}$, horizontal shear strength, $V_{n.h}$, and torsion capacity to be resisted by the beam, T_n, are computed as follows:

$$\begin{bmatrix} V_{n.v} \\ V_{n.h} \\ T_n \end{bmatrix} = \left(\frac{0.5}{\phi'} \right) \left\{ \begin{bmatrix} F_D w_D L \\ 0 \\ 0 \end{bmatrix} + \begin{bmatrix} F_v & 0 & 0 \\ 0 & F_h & 0 \\ 0 & 0 & F_h \end{bmatrix} \begin{bmatrix} w_v & P_v \\ w_h & P_h \\ w_h e_h & P_h e_h \end{bmatrix} \begin{bmatrix} L \\ 2 \end{bmatrix} \right\} \qquad [4.17]$$

where

F_D : dead load uncertainty multiplying factor (e.g. = 1.4)

ϕ' : material uncertainty reduction factor due to shear and torsion

e_h : eccentricity between the centers of gravity of the vehicle and the guideway

$$\begin{bmatrix} V_u \\ T_u \end{bmatrix} = \begin{bmatrix} \phi' \left(\max\{V_{n.v}, V_{n.h}\} \right) \\ \phi' T_n \end{bmatrix} \qquad [4.18]$$

where

V_u : factored shear ($= \max\{V_{n.v}\phi' , V_{n.h}\phi'\}$)

T_u : factored torsion ($= T_n\phi'$)

Torsion capacity

Torsion analysis is performed using design approaches following ACI code. The ACI code provides guidelines for prestressed sections and for torsion design of unprestressed sections. However, it does not specifically address prestressed sections in torsion. ACI Committee 445 is working to include prestressed sections in torsion. The procedure outlined below is adapted from *Torsion of Reinforced Concrete*, by T. Hsu [Hsu 84]. Hsu's approach modifies current ACI code to account for torsion in prestressed sections.

prestress factors

The method uses several prestress factors to modify present ACI design criteria to be applicable for prestressed sections in torsion . Prestress factors are listed below.

$$\gamma_{ps} = \sqrt{1 + \frac{10P}{A_g f'_c}} \qquad [4.19a]$$

$$\gamma_{ps1} = 2.5\gamma_{ps} - 1.5 \qquad [4.19b]$$

$$\gamma_{ps2} = \left(1 - \frac{0.833P}{A_g f'_c}\right)\gamma_{ps} \qquad [4.19c]$$

maximum section torsion capacity

$$T_{n,\max} = \frac{635\gamma_{ps2}\sqrt{bf'_c}\,ht}{\sqrt{1+b\left(\frac{127\gamma_{ps2}hV_u}{332dT_u}\right)^2}} \qquad [4.20]$$

where

$T_{n,\max}$: maximum allowable torsion capacity of the beam

When a section is sufficient to resist the torsional moment, torsion reinforcement design proceeds. If a section is not sufficient, either the width, depth, or wall thickness must be increased and the bending calculations repeated. Once a sufficient section is determined, the amount of shear and torsion reinforcement must then be determined.

Shear strength

Both web shear and flexure shear must be considered in order to determine the shear strength of the concrete beam without reinforcement. Note that in the following approach, in order to calculate beam shear strength and torsion capacity, ACI equations have been modified by the author to account for box sections having widths significantly greater than 0.25 m—on which ACI code is based [Wang and Salmon 85, Hsu 84]. Full scale testing is desirable to confirm these modifications. Flexure-shear for the hollow-box maglev guideway beam is calculated according to the following equations.

flexure-shear cracking strength

$$\begin{bmatrix} d_{p.v} \\ d_{p.h} \end{bmatrix} = \begin{bmatrix} \max\left\{\frac{h}{2}+e_a, 0.8h\right\} \\ 0.8b \end{bmatrix} \qquad [4.21]$$

where

e_a : eccentricity of prestress at section a_v, $\left[e_a = \frac{w_D a_v(L-a_v)}{2P(1-F_{lp})}\right]$, and a_v is the distance from the support to where shear forces are calculated. ($a_v = F_{av}h$; $F_{av} = 0.5$)

$d_{p.v}$: distance from vertical extreme compression fiber to vertical centroid of prestressing tendons at section a_v

$d_{p.h}$: distance from horizontal extreme compression fiber to distance $0.8b$ at section a_h. ($a_h = F_{ah}b$; $F_{ah} = 0.5$)

$$\begin{bmatrix} V_{i.v} \\ V_{i.h} \end{bmatrix} = 0.5 \begin{bmatrix} F_v\left(w_v[L-2a_v]+P_v\right)+F_D w_D(L-2a_v) \\ F_h\left(w_h[L-2a_h]+P_h\right) \end{bmatrix} \quad [4.22]$$

where

$V_{i.v}$: vertical shear due to factored load at section a_v

$V_{i.h}$: corresponding horizontal shear due to factored load at section a_h

$$\begin{bmatrix} M_{\max.v} \\ M_{\max.h} \end{bmatrix} = 0.5 \begin{bmatrix} a_v\left\{F_v\left(w_v[L-a]+P_v\right)+F_D w_D[L-a_v]\right\} \\ a_h\left\{F_h\left(w_h[L-a_h]+P_h\right)\right\} \end{bmatrix} \quad [4.23]$$

where

$M_{\max.v}$: maximum vertical moment due to factored loads at section a_v

$M_{\max.h}$: maximum horizontal moment due to factored loads at section a_h

$$\begin{bmatrix} M_{cr.v} \\ M_{cr.h} \end{bmatrix} = \left(500\sqrt{f'_c}+\frac{P(1-F_{lp})}{A_g}\right)\begin{bmatrix} \left(\frac{I_{g.v}}{y_{t.v}}\right) \\ \left(\frac{I_{g.h}}{y_{t.h}}\right) \end{bmatrix} \quad [4.24]$$

where

$M_{cr.v}$: net vertical cracking moment at section a_v

$M_{cr.h}$: net horizontal cracking moment at section a_h

$$\begin{bmatrix} V_{ci.v} \\ V_{ci.h} \end{bmatrix} = 100\sqrt{f'_c}t\begin{bmatrix} d_{p.v} \\ d_{p.h} \end{bmatrix} + \begin{bmatrix} \left(\frac{V_{i.v}M_{cr.v}}{M_{\max.v}}+V_D\right) \\ \left(\frac{V_{i.h}M_{cr.h}}{M_{\max.h}}\right) \end{bmatrix} \quad [4.25]$$

where

$V_{ci.v}$: total nominal vertical flexure-shear cracking strength at section a_v

$V_{ci.h}$: total nominal horizontal flexure-shear cracking strength at section a_h

V_D : dead load shear at a_v, $[w_D\left(\frac{L}{2}-a_v\right)]$.

$$\begin{bmatrix} V_{ci.v\min} \\ V_{ci.h\min} \end{bmatrix} = \frac{2000}{7}\sqrt{f'_c}t\begin{bmatrix} d_{p.v} \\ d_{p.h} \end{bmatrix} \quad [4.26]$$

where

$V_{ci.v\min}$: minimum nominal vertical flexure-shear strength at a_v

$V_{ci.h\min}$: minimum nominal horizontal flexure-shear strength at a_h

web-shear cracking strength

Web shear is calculated according to the following formula.

$$\begin{bmatrix} V_{cw.v} \\ V_{cw.h} \end{bmatrix} = \left(300\sqrt{f'_c} + \frac{0.3P\left(1-F_{lp}\right)}{A_g}\right)2t\begin{bmatrix} d_{p.v} \\ d_{p.h} \end{bmatrix} + \begin{bmatrix} V_p \\ 0 \end{bmatrix} \quad [4.27]$$

where

$V_{cw.v}$: total nominal vertical web-shear cracking strength

$V_{cw.h}$: total nominal horizontal web-shear cracking strength

V_p : vertical component of prestress $= \frac{2eP\left(1-F_{lp}\right)}{L}$.

Shear and Torsion Reinforcement Design

The minimum of the computed web-shear and flexure-shear strengths equals the nominal shear strength (to be used in torsion calculations) as indicated in the following formula.

$$V_{co} = \min\{ V_{ci.v}, V_{ci.h}, V_{cw.v}, V_{cw.h} \} \quad [4.28]$$

where

V_{co} : total nominal section shear strength

The following equation is taken from Hsu and converted for general widths and IS units [Hsu 84].

$$T_{co} = 127\gamma_{ps1}\sqrt{bf'_c}ht \quad [4.29]$$

where

T_{co} : total nominal section torsion capacity

$$T_c = \frac{T_{co}}{\sqrt{1+\left(\frac{T_{co}V_u}{V_{co}T_u}\right)^2}} \qquad [4.30]$$

where

T_c : total section torsion capacity without reinforcement

$$V_c = \frac{V_{co}}{\sqrt{1+\left(\frac{V_{co}T_u}{T_{co}V_u}\right)^2}} \qquad [4.31]$$

where

V_c : total section shear strength without reinforcement

Once the shear strength and torsional capacity of the concrete section are determined, the procedure for determining adequate reinforcement is straightforward. The following equations illustrate the method.

$$\begin{bmatrix} T_s \\ V_s \end{bmatrix} = \begin{bmatrix} T_n - T_c \\ \max\{V_{n.v}, V_{n.h}\} - V_c \end{bmatrix} \qquad [4.32]$$

where

T_s : torsion to be resisted by reinforcement

V_s : shear to be resisted by reinforcement

If $T_n \le 166\phi' \gamma_{ps}\sqrt{f'_c}\, bth$, then $\frac{A_t}{s} = 0$, otherwise $\frac{A_t}{s}$ is found according to the following procedure. This procedure is used by ACI and is discussed in detail by Hsu [ACI 89, Hsu 84].

$$\begin{bmatrix} X_1 \\ Y_1 \end{bmatrix} = \begin{bmatrix} b \\ h \end{bmatrix} - (D_{stir} + 2C_c)\begin{bmatrix} 1 \\ 1 \end{bmatrix} \qquad [4.33]$$

where

X_1 : horizontal distance between edges of stirrup confinement cage

Y_1 : vertical distance between edges of stirrup confinement cage

$$\alpha_t = .66 + .33\left(\frac{Y_1}{X_1}\right) \le 1.5 \qquad [4.34]$$

where

α_t : torsional strength coefficient

$$\begin{bmatrix}\left(\frac{A_t}{s}\right)\\ \left(\frac{A_v}{s}\right)\end{bmatrix} = \begin{bmatrix}\alpha_t X_1 Y_1 E_r \varepsilon'_r & 0\\ 0 & d_v E_r \varepsilon'_r\end{bmatrix}^{-1}\begin{bmatrix}T_s\\ V_s\end{bmatrix} \qquad [4.35]$$

where

A_t : area of transverse torsional reinforcement required

A_v : area of transverse shear reinforcement required (one leg of stirrup)

transverse torsional reinforcement

$$\frac{A_{t.t}}{s} = \frac{A_t}{s} + 0.5\frac{A_v}{s} \qquad [4.36]$$

where

$A_{t.t}$: total area of transverse reinforcement required $\left(= A_t + 0.5A_v\right)$

$$F_t = \frac{190ht\sqrt{bf'_c}}{\alpha_t X_1 Y_1 E_r \varepsilon'_r} \qquad [4.37]$$

where

F_t : factor used to calculate minimum amounts of stirrup and torsion reinforcement required

$$\frac{A_{t.t\min}}{s} = F_t\left(1 + 12\frac{P}{A_g f'_c}\right) \qquad [4.38]$$

where

$A_{t.t\min}$: minimum total area of transverse reinforcement required according to ACI

$$s = \min\left\{A_{stir}\left(\frac{s}{A_{t.t}}\right), 0.30, \frac{X_1 + Y_1}{4}, \frac{d_v}{2}, \frac{d_h}{2}\right\} \qquad [4.39]$$

where

s : stirrup spacing

longitudinal torsional reinforcement

$$A_{t.l} = 2\left(\frac{A_t}{s}\right)(X_1 + Y_1) \qquad [4.40]$$

where

$A_{t.l}$: area of longitudinal torsional reinforcement required

$$A_{t.l\min} = \left[(4F_t s)\left(\frac{T_u}{\left(T_u + \frac{2bhV_u}{3d_v}\right)}\right) - \max\begin{Bmatrix} 2A_{stir} \\ 2A_{t.l\min} \end{Bmatrix}\right]\left(\frac{X_1 + Y_1}{s}\right) \qquad [4.41]$$

where

$A_{t.l\min}$: minimum area of longitudinal torsion reinforcement required according to ACI

Torsion and shear reinforcement required for FRP zones

longitudinal FRP reinforcement required (all three equations can apply)

The volume of hybrid FRP reinforcement required depends on the areas of the beam element under high magnetic flux fields. Areas of the beam cross-section required to have non-magnetic reinforcement are indicated by the parameters b_{frp} and h_{frp} (see Figure 2.4.2). These parameters are defined in the following equation which is used to determine the volume of reinforcement per beam in the top flange of the box section that must be non-magnetic. Note that all three of the following equations may apply to a given section depending upon the value of h_{frp}.

when $h_{frp} \geq 0$

$$V_{rc.v.frp/b} = \left(\frac{2b_{frp}}{b}\right) A_{rc.v} L\left(\frac{\min\{h_{frp}, t\}}{t}\right) \qquad [4.42a]$$

where

$V_{rc.v.frp/b}$: compression flange reinforcement volume required non-magnetic

b_{frp} : width of non-magnetic zone for one side of beam ($b_{frp} \leq 0.5b$)

h_{frp} : depth of non-magnetic zone for one side of beam ($h_{frp} \leq h$)

when $h - t \geq h_{frp} \geq t$

$$\begin{bmatrix} V_{rc.h.frp/b} \\ V_{rt.h.frp/b} \end{bmatrix} = \left(\frac{h_{frp} - t}{h - 2t}\right) \begin{bmatrix} A_{rc.h} \\ A_{rt.h} \end{bmatrix} L\left(\frac{\min\{b_{frp}, t\}}{t}\right) \qquad [4.42b]$$

where

$V_{rc.h.frp/b}$: compression web reinforcement volume required non-magnetic

$V_{rt.h.frp/b}$: tension web reinforcement volume required non-magnetic

when $h_{frp} \geq h - t$

$$V_{rt.v.frp/b} = \left(\frac{2b_{frp}}{b}\right) A_{rt.v} L\left(\frac{h_{frp} + t - h}{t}\right) \qquad [4.42c]$$

where

$V_{rt.v.frp/b}$: tension flange reinforcement volume required non-magnetic

lateral FRP reinforcement required (only one of three equations will apply)

The volume of stirrup and torsional reinforcement per beam that is required to be non-magnetic is determined using one of the following three equations which depend on the value of h_{frp}.

when $h_{frp} \le t$

$$\begin{bmatrix} V_{t.t.frp/b} \\ V_{t.l.frp/b} \end{bmatrix} = \left(\frac{2b_{frp}h_{frp}}{A_g} \right) \begin{bmatrix} V_{r.t/b} \\ A_{t.l}L \end{bmatrix} \qquad [4.43a]$$

where

$V_{t.t.frp/b}$: stirrup reinforcement volume required non-magnetic

$V_{t.l.frp/b}$: torsion reinforcement volume required non-magnetic

when $t \le h_{frp} \le h - t$

$$\begin{bmatrix} V_{t.t.frp/b} \\ V_{t.l.frp/b} \end{bmatrix} = \left(\frac{2b_{frp}t + (h_{frp} - t)\min\{2b_{frp}, 2t\}}{A_g} \right) \begin{bmatrix} V_{r.t/b} \\ A_{t.l}L \end{bmatrix} \qquad [4.43b]$$

when $h - t \le h_{frp}$

$$\begin{bmatrix} V_{t.t.frp/b} \\ V_{t.l.frp/b} \end{bmatrix} = \left(\frac{2b_{frp}(h_{frp} + 2t - h) + (h - 2t)\min\{2b_{frp}, 2t\}}{A_g} \right) \begin{bmatrix} V_{r.t/b} \\ A_{t.l}L \end{bmatrix} \qquad [4.43c]$$

4.1.5 Cost functions without FRP reinforcement

Once all material quantities are determined, beam costs can then be calculated. Beam material costs are computed for all steel reinforcement and for a mixture of steel and hybrid FRP reinforcement according to the following equations:

$$\begin{bmatrix} V_{r.t/b} \\ V_{r.l/b} \end{bmatrix} = \begin{bmatrix} 2A_{t.t}\left(\frac{L}{s}\right)(X_1 + Y_1) \\ (A_{rt.v} + A_{rc.v} + A_{rt.h} + A_{rc.h} + A_{t.l})L \end{bmatrix} \quad [4.44]$$

where

$V_{r.t/b}$: volume of transverse reinforcement (i.e. stirrups) required per beam

$V_{r.l/b}$: volume of longitudinal reinforcement (i.e. bars) required per beam

$$V_{r/b} = V_{r.t/b} + V_{r.l/b} \quad [4.45]$$

where

$V_{r/b}$: total volume of mild reinforcement required per beam

$$V_{c/b} = A_g L - V_{r/b} \quad [4.46]$$

where

$V_{c/b}$: volume of concrete required per beam

$$\begin{bmatrix} C_{c/b} \\ C_{r/b} \\ C_{ps/b} \end{bmatrix} = \begin{bmatrix} u_c V_{c/b} \\ u_r V_{r/b} \rho_r \\ F_{ps} u_{ps} LP \end{bmatrix} \quad [4.47]$$

where

$C_{c/b}$: concrete material cost (per beam)

$C_{r/b}$: mild reinforcement material cost (per beam) without FRP

$C_{ps/b}$: prestressing reinforcement material cost (per beam)

$$\begin{bmatrix} C_c \\ C_r \\ C_{ps} \end{bmatrix} = L^{-1} \begin{bmatrix} C_{c/b} \\ C_{r/b} \\ C_{ps/b} \end{bmatrix} \quad [4.48]$$

where

C_c : concrete material cost (per meter)

C_r : mild reinforcement material cost (per meter) without FRP

C_{ps} : prestressing reinforcement material cost (per meter)

$$\boxed{C = C_c + C_r + C_{ps}} \quad [4.49]$$

where

C : total beam material cost (per meter) without FRP

4.1.6 Cost functions with FRP and steel reinforcement

The cost of using hybrid FRP reinforcement is added to the base beam material cost as demonstrated by the following equations:

$$V_{frp/b} = V_{rt.v.frp/b} + V_{rc.v.frp/b} + V_{rt.h.frp/b} + V_{rc.h.frp/b} + V_{t.t.frp/b} + V_{t.l.frp/b} \quad [4.50]$$

where

$V_{frp/b}$: total volume of mild reinforcement required to be FRP

$$C_{frp/b} = V_{frp/b}\left(F_{hfrp} - 1\right)\rho_r u_r \quad [4.51]$$

where

$C_{frp/b}$: additional beam material cost (per beam) due to use of FRP

$$C_{frp} = C_{frp/b} L^{-1} \quad [4.52]$$

where

C_{frp} : additional beam material cost (per meter) due to use of FRP

$$\boxed{C_{total} = C + C_{frp}} \quad [4.53]$$

where

C_{total} : total material cost per meter for guideway beam element

4.2 Design Example

4.2.1 Overview

The example presented in this section is considered to be a base case for the narrow beam design. Using equations presented in Section 4.1, this section illustrates the analysis of a reinforced concrete hollow-box beam with a step-by-step example. Several sensitivity analyses are presented in Section 4.3 for a variety of span widths, depths, lengths, and deflection criteria.

4.2.2 Spreadsheet example

A complete copy of the analysis program, *BoxCost*, is shown in Appendix C. The first page of the program is shown in Figure 4.2.1. **Bold** cells in the figure indicate input values. Other cells, shown in Figures 4.2.1 and 4.2.2 (and in Appendix C) are used for either intermediate calculations or for verification of results.

User Input:							*page 1*
material data				*deflection constraints*			
Er =	200.000	(MPa)	*okay!*	k_v.min =	1000		
fconc =	41.50	(MPa)	*okay!*	k_h.min =	1000		
fr =	414.00	(MPa)	*okay!*	*load factors*			
rho.conc =	23.00	(kN/m^3)	*okay!*	F.d =	1.40		
rho.rein =	77.00	(kN/m^3)	*okay!*	F.v =	1.40		
$.conc =	$90.00	($/m^3)	*okay!*	F.h =	1.70		
$.rein =	$0.55	($/kg)	*okay!*	*negative reinforcement fractions*			
$.ps =	$2.25	($/kg)	*okay!*	F.nr.v =	0.25		
F.lp =	0.20		*okay!*	F.nr.h =	1.00		
frp data			*okay!*	*bar and clearance dimensions*			
F.frp =	5.50		*okay!*	D.stir =	0.012700	(m)	
b.frp =	0.20	(m)	*okay!*	D.b =	0.015875	(m)	
h.frp =	0.40	(m)		C.c =	0.038100	(m)	
section data			*okay!*	*concrete stress constraints*			
b =	1.40	(m)		F.c.t* =	500	(fc^.5) [Pa]	
h =	2.10	(m)	*okay!*	F.c.c* =	0.45	(*fc)	
t.min =	0.15	(m)	*okay!*	*permissible strains*			
L =	25.00	(m)		eps.conc* =	0.0030		
loadings			*okay!*	eps.r* =	0.0020		
w.v =	2.00	(tonne/m)	*okay!*	alpha.r =	0.6000		
P.v =	0.00	(tonne)	*okay!*	*material reduction factors*			
w.h =	1.50	(tonne/m)		phi =	0.90		
P.h =	0.00	(tonne)	okay!	phi' =	0.85		
e.h =	3.00	(m)		*max. shear zone check*			
w.m =	0.10	(tonne/m)		?.av =	0.50	(*h)	
				?.ah =	0.50	(*b)	

Figure 4.2.1 User Input for *BoxCost* Analysis Program *(page 1)*

As shown in Figure 4.2.1, values are entered in SI units. When necessary, the program converts to English units to correspond to ACI code equations and then reconverts final results back to SI units. For most cases, both units are shown (see Appendix C). Figure 4.2.2—page 2 of the complete analysis program—shows primary results from input given in Figure 4.2.1.

Results:					page 2
total cost w/ frp			*concrete modulus*		
C.total =	$306.87	(per m)	E.conc =	28,300	(MPa)
total cost w/o frp			*section thickness*		
C =	$242.74	(per m)	t =	0.15	(m)
mild reinforcement costs			*prestressing results*		
C.r.v =	$28.71	(per m)	P =	3,153	(kN)
C.r.h =	$42.16	(per m)	e =	0.74	(m)
C.t.t =	$22.63	(per m)	*beam dead weight*		
C.t.l =	$13.99	(per m)	w.d =	2.442	(tonne/m)
C.r =	$107.50	(per m)	*fundamental frequency*		
frp costs			f1 =	6.539	(Hz)
C.r.v.frp =	$43.32	(per m)	*deflection results*		
C.r.h.frp =	$68.52	(per m)	k .v =	4141	
C.t.t.frp =	$36.95	(per m)	k .h =	2871	
C.t.l.frp =	$22.85	(per m)	.v =	0.0060	(m)
summary of costs			.h =	0.0087	(m)
C.r.frp =	$171.64	(per m)	*resulting stiffness*		
C.ps =	$51.07	(per m)	EI.v =	1.69E+09	(kg•m^2)
C.c =	$84.16	(per m)	EI.h =	8.76E+08	(kg•m^2)
			percentage of reinforcement (w/o frp)		
			%rho.r =	2.59	%
			percentage of frp cost to total mild rein. cost		
			%rho.frp.r =	59.66	%
			percentage of frp cost to overall total cost		
			%rho.frp.tot =	26.42	%

Figure 4.2.2 *BoxCost* Spreadsheet Analysis Results *(page 2)*

A complete step-by-step example is presented below using equations presented in Section 4.1. Results, equation numbers, and notation used in the example correspond to both 1) the formulas presented and discussed in Sections 4.1 and 3.2 and 2) the analysis output shown in Figures 4.2.1 and 4.2.2 (and Appendix C). Intermediate calculations are underlined in the example. The total calculated beam material costs for cases with and without FRP reinforcement are highlighted by a surrounding border.

Bending moment resistance:

Equation 4.1

w_v = (2000 tonne/m)•(*gravity*)
w_h = (1500 tonne/m)•(*gravity*)
L = 25 meters

$F_v = 1.4$	$F_h = 1.7$
$P_v = 0$	$P_h = 0$
$\phi = 0.90$	$\phi' = 0.85$

$$\begin{bmatrix} M_{n.v} \\ M_{n.h} \end{bmatrix} = \left(\frac{25.0}{8 \times 0.9}\right)\begin{bmatrix} 1.4 & 0 \\ 0 & 1.7 \end{bmatrix}(9.807)\begin{bmatrix} 2000 & 0 \\ 1500 & 0 \end{bmatrix}\begin{bmatrix} 25 \\ 2 \end{bmatrix} = \underline{\underline{\begin{bmatrix} 2.384 \bullet 10^6 \\ 2.171 \bullet 10^6 \end{bmatrix} Nm}}$$

Equation 4.2

b = 1.4 m, t = 0.15 m h = 2.1m
E_r = 200,000 MPa

$\varepsilon_r' = 0.002$	$\varepsilon_c^* = 0.003$
$\alpha_r = 0.60$	$\varepsilon_c^\circ = 0.0012$

$$d_v = h - \frac{t}{2} = 2.025m$$

$$d_h = b - \frac{t}{2} = 1.325m$$

$\beta_1 = 0.75$ $f_c' = 41.5$ MPa

$$\begin{bmatrix} A_{rt.v} \\ A_{rt.h}{}' \end{bmatrix} = \left(2.0 \bullet 10^{11}(.002)\left[1 - \frac{0.75(0.003)}{2(0.003+0.0012)}\right]\right)^{-1}\begin{bmatrix} 2.025 & 0 \\ 0 & 1.325 \end{bmatrix}^{-1}\begin{bmatrix} M_{n.v} \\ M_{n.h} \end{bmatrix}$$

$$\underline{\underline{\begin{bmatrix} A_{rt.v} \\ A_{rt.h}{}' \end{bmatrix} = \begin{bmatrix} 4.019 \bullet 10^{-3} \\ 5.554 \bullet 10^{-3} \end{bmatrix} m^2}}$$

Equation 4.3

F_{ra} = 0.08

$$\underline{\underline{\begin{bmatrix} A_{r.v\max} \\ A_{r.h\max} \end{bmatrix} = 0.08(0.15)\begin{bmatrix} 1.4 \\ 2.1 - 2(0.15) \end{bmatrix} = \begin{bmatrix} 1.68 \bullet 10^{-2} \\ 2.16 \bullet 10^{-2} \end{bmatrix} m^2}}$$

Equation 4.4

D_B = 1.588 x 10-2 m (5/8")

$$\begin{bmatrix} A_{r.v\min} \\ A_{r.h\min} \end{bmatrix} = \frac{(1.588 \bullet 10^{-2})\pi(0.15)^2}{8}\left(\frac{2.0 \bullet 10^{11}(0.0012)}{2.54 \bullet 10^7}\right)^3\begin{bmatrix} 1.4 \\ 2.1 - 2(0.15) \end{bmatrix}$$

$$\underline{\underline{\begin{bmatrix} A_{r.v\min} \\ A_{r.h\min} \end{bmatrix} = \begin{bmatrix} 2.630 \bullet 10^{-3} \\ 3.381 \bullet 10^{-3} \end{bmatrix} m^2}}$$

Equation 4.5

$$F_{nr.v} = 0.25$$

$$A_{rc.v} = \max\left\{0.25\left(4.019 \cdot 10^{-3}\right), 2.630 \cdot 10^{-3}\right\}$$

$$\underline{\underline{A_{rc.v} = 2.630 \cdot 10^{-3}\, m^2}}$$

Equation 4.6

$$A_{rt.h} = \max\left\{A_{r.h\min}, 5.594 \cdot 10^{-3} - \left(4.019 \cdot 10^{-3} + 2.630 \cdot 10^{-3}\right)\left(\frac{0.15}{1.4}\right)\right\}$$

$$\underline{\underline{A_{rt.h} = 4.882 \cdot 10^{-3}\, m^2}}$$

Equation 4.7

$$F_{nr.h} = 1.00$$

$$A_{rc.h} = (1.00)A_{rt.h} \Rightarrow \underline{\underline{A_{rc.h} = 4.882 \cdot 10^{-3}\, m^2}}$$

Deflection criteria:

Equation 4.8a

$$E_c = 2.830 \times 10_{10}\ \text{Pa}$$

$$n = \frac{E_r}{E_c} = 7.067$$

$$y_{c.v} = \frac{(.15)(2.1)(1.4-.3) + (n-1)\left[4.019 \cdot 10^{-3}(2.025) + 2.63 \cdot 10^{-3}\left(\frac{.15}{2}\right)\right] + .15(2.1)^2}{2(.15)(1.4-.3) + (n-1)\left[4.019 \cdot 10^{-3} + 2.63 \cdot 10^{-3}\right] + 2(.15)(2.1)}$$

$$= \frac{1.059}{1.000} \Rightarrow \underline{\underline{y_{c.v} = 1.058 m}}$$

$$y_{t.v} = h - y_{c.v} \Rightarrow \underline{\underline{y_{t.v} = 1.042 m}}$$

Equation 4.8b

$$y_{c.h} = \frac{(.15)(1.4)(2.1-.3) + (n-1)\left[\left(4.882 \cdot 10^{-3}\right)\left(1.325 + \frac{.15}{2}\right)\right] + .15(1.4)^2}{2(.15)(2.1-.3) + (n-1)\left[2\left(4.882 \cdot 10^{-3}\right)\right] + 2(.15)(1.4)}$$

$$= \frac{0.713}{1.019} \Rightarrow \underline{\underline{y_{c.h} = 0.700 m}}$$

$$y_{t.v} = b - y_{c.h} \Rightarrow \underline{\underline{y_{t.v} = 0.700 m}}$$

Equation 4.9a

$$I_{g.v} = \frac{2(0.15)}{3}\left[1.058^3 + (2.1-1.058)^3\right] + \left(\frac{15^3}{6}\right)(1.4-0.3)$$
$$+\left(1.058 - \frac{0.15}{2}\right)^2\left[(1.4-0.3)0.15 + (n-1)2.630\cdot 10^{-3}\right]$$
$$+(2.025-1.058)^2\left[(1.4-0.3)0.15 + (n-1)4.109\cdot 10^{-3}\right]$$

$$\underline{I_{g.v} = 0.584\ m^4}$$

Equation 4.9b

$$I_{g.h} = \frac{2(0.15)}{3}\left[0.7^3 + 0.7^3\right] + \frac{(0.15)^3}{6}(2.1-0.3)$$
$$+\left(0.7 - \frac{0.15}{2}\right)^2\left[(2.1-0.3)0.15 + (n-1)\left(4.882\times 10^{-3}\right)\right]$$
$$+(1.325-0.7)^2\left[(2.1-0.3)0.15 + (n-1)\left(4.882\times 10^{-3}\right)\right]$$

$$\underline{I_{g.h} = 0.304\ m^4}$$

Equation 4.10

$$k_{\Delta v} = 1000$$
$$k_{\Delta h} = 1000$$

$$\begin{bmatrix} I_{g.v} \\ I_{g.h} \end{bmatrix} \geq \frac{25^2}{384\left(28.3\times 10^4\right)}\begin{bmatrix} 1000 & 0 \\ 0 & 1000 \end{bmatrix}(9.807)\begin{bmatrix} 2000 & 0 \\ 1500 & 0 \end{bmatrix}\begin{bmatrix} 5(25) \\ 8 \end{bmatrix}$$

$$\underline{\begin{bmatrix} I_{g.v} \\ I_{g.h} \end{bmatrix} \geq \begin{bmatrix} 0.141 \\ 0.106 \end{bmatrix} m^4} \quad \textit{(okay!)}$$

Prestressing:

Equation 4.11

$$F_{lp} = 0.20$$
$$f_{c.t}^{*} = 500\sqrt{f_c'}$$

$$\begin{bmatrix} P_{v\min} \\ P_{h\min} \end{bmatrix} = \frac{0.96}{(1-0.2)}\left(\begin{bmatrix} \dfrac{2.384\times 10^6(1.041)}{0.584} \\ \dfrac{2.171\times 10^6(0.7)}{0.304} \end{bmatrix} - 500\sqrt{4.150\times 10^7}\begin{bmatrix} 1 \\ 1 \end{bmatrix}\right)$$

$$\begin{bmatrix} P_{v\min} \\ P_{h\min} \end{bmatrix} = \begin{bmatrix} 1.236\times 10^6 \\ 2.139\times 10^6 \end{bmatrix} N$$

Equation 4.12

$$\rho_c = 23 \text{ kN/m3}$$
$$\rho_r = 77 \text{ kN/m3}$$
$$w_m = (0.6 \text{ tonne/m})(g)$$

$$w_D = (0.96)23000 + \left((4.019 + 2.630 + 2(4.882)) \times 10^{-3}\right)(77000 - 23000) + 100(9.807)$$
$$= 22080N/m + 886.28N/m + 980.67N/m$$

$$\underline{w_D = 2.297 \times 10^4 \ N/m}$$

$$e_{\max} = y_{t.v} - 2t$$

$$e_{\max} = 1.042 - 0.3 \Rightarrow \underline{e_{\max} = 0.742 \ m}$$

$$M_D = w_D L^2 / 8 \Rightarrow \underline{M_D = 1.795 \times 10^6 \ Nm}$$

Equation 4.13

$$P_{e.\min} = \frac{(2.395 \times 10^4)(25^2)}{8(0.742)(1 - 0.2)} \Rightarrow \underline{P_{e.\min} = 3.153 \times 10^6 \ N}$$

Equation 4.14

$$P = \max\begin{Bmatrix} 1.236 \times 10^6 \\ 2.139 \times 10^6 \\ 3.153 \times 10^6 \end{Bmatrix} \Rightarrow \underline{P = 3.153 \times 10^6 \ N}$$

Equation 4.15
(Check)

$$f^*_{c.c} = 0.45 \text{ fc'}$$

$$\begin{bmatrix} P_{v\max} \\ P_{h\max} \end{bmatrix} = \left(\frac{0.96}{0.8}\right)\left((0.45)(41.5 \times 10^6)\begin{bmatrix} 1 \\ 1 \end{bmatrix} - \begin{bmatrix} \dfrac{2.383 \times 10^6 (1.058)}{0.584} \\ \dfrac{2.171 \times 10^6 (0.7)}{0.304} \end{bmatrix}\right)$$

$$\underline{\begin{bmatrix} P_{v\max} \\ P_{h\max} \end{bmatrix} = \begin{bmatrix} 1.723 \times 10^7 \\ 1.641 \times 10^7 \end{bmatrix} N} \quad \textbf{\textit{(okay!)}}$$

Equation 4.16

$$e = \frac{M_D}{P\left(1 - F_{lp}\right)} \textit{ (for this case)}$$

$$\underline{e = 0.742}\ m$$

Hybrid FRP cost factor calculations:

Equation 3.3a

$$V_{hs.fib} = 0.68 \qquad E_{hs.fib} = 7.30 \times 10^{10}\ Pa$$
$$V_{hm.fib} = 0.68 \qquad E_{hm.fib} = 2.30 \times 10^{11}\ Pa$$
$$E_m = 3.45 \times 10^9\ Pa$$

$$E_{hfrp} = 0.92\left\{0.68\left(7.30 \bullet 10^{10}\right) + 0.32\left(3.45 \bullet 10^9\right)\right\}$$
$$0.08\left\{0.68\left(2.30 \bullet 10^{11}\right) + 0.32\left(3.45 \bullet 10^9\right)\right\} \Rightarrow \underline{E_{hfrp} = 5.929 \times 10^{10}\ Pa}$$

Equation 3.3b

$$f_m = 8.00 \times 10^7\ Pa$$
$$f_{hs.frp} = 3.450 \times 10^9\ Pa$$
$$f_{hm.frp} = 3.530 \times 10^9\ Pa$$
$$\rho_m = 1.800 \times 10^3\ kg/m^3$$
$$\rho_{hs.fib} = 2.540 \times 10^3\ kg/m^3$$
$$\rho_{hm.fib} = 1.700 \times 10^3\ kg/m^3$$
$$\mu_m = \$0.65\ /kg$$
$$\mu_{hs.fib} = \$1.50\ /kg$$
$$\mu_{hm.fib} = \$35.00\ /kg$$

$$\rho_{hfrp} = 0.92\left\{0.68\left(2.54 \times 10^3\right) + 0.32\left(1.80 \times 10^3\right)\right\}$$
$$+ 0.08\left\{0.68\left(1.70 \times 10^3\right) + 0.32\left(1.80 \times 10^3\right)\right\} \Rightarrow \underline{\rho_{hfrp} = 2.258 \times 10^3\ kg/m^3}$$

Equation 3.3c

$$V_{hs} = 0.920$$

$$\mu_{hfrp} = 0.92\left\{0.68(\$1.50) + 0.32(\$0.65)\right\} + 0.08\left\{0.68(\$35.00) + 0.32(\$0.65)\right\}$$

$$\Rightarrow \underline{\mu_{hfrp} = \$3.0504\ /kg}$$

Equation 3.4

$$\varepsilon_{ks}^{*} = \frac{3.450\times10^{9}}{7.300\times10^{10}} \Rightarrow \underline{\varepsilon_{ks}^{*} = 0.047}$$

$$\varepsilon_{km}^{*} = \frac{3.530\times10^{9}}{2.300\times10^{11}} \Rightarrow \underline{\varepsilon_{km}^{*} = 0.015}$$

Equation 3.5

$$E_{ks} = 0.68\left(7.30\times10^{11}\right) + 0.32\left(3.45\times10^{9}\right) \Rightarrow \underline{E_{ks} = 5.074\times10^{10}}\ Pa$$

Equation 3.6

$$\alpha_{max} = 1.4$$

$$\alpha = \frac{5.929}{5.074(0.92)} \Rightarrow \underline{\alpha = 1.27}\ \text{(okay!)}$$

Equation 3.7

$$\gamma_{min} = 1.0$$

$$\gamma = \frac{0.047}{0.015(1.27)} \Rightarrow \underline{\gamma = 2.432}\ \text{(okay!)}$$

Equation 3.8

$$F_{kfrp} = \left(\frac{2.0\times10^{11}}{5.929\times10^{10}}\right)\left(\frac{2.258\times10^{3}}{\left(\frac{77{,}000}{9.807}\right)\ kg/m^{3}}\right)\left(\frac{\$3.05/kg}{\$0.55/kg}\right)$$

$$= (3.373)\left(\frac{1}{3.477}\right)(5.546) = F_{kfrp} = 5.38$$

For added conservatism, use $\boxed{\Rightarrow F_{kfrp} = 5.5}$

Torsion and shear design:

Equation 4.17

$$F_D = 1.4$$
$$e_h = 3.0 \text{ meters}$$

$$\begin{bmatrix} V_{n.v} \\ V_{n.h} \\ T_n \end{bmatrix} = \frac{0.5}{0.85}\left\{\begin{bmatrix} 1.4(2.395\times10^4)25 \\ 0 \\ 0 \end{bmatrix} + \begin{bmatrix} 1.4 & 0 & 0 \\ 0 & 1.7 & 0 \\ 0 & 0 & 1.7 \end{bmatrix}(9.807)\begin{bmatrix} 2000 & 0 \\ 1500 & 0 \\ 1500(3) & 0 \end{bmatrix}\begin{bmatrix} 25 \\ 2 \end{bmatrix}\right\}$$

$$\underline{\underline{\begin{bmatrix} V_{n.v} \\ V_{n.h} \\ T_n \end{bmatrix} = \begin{bmatrix} 8.968\times10^5 N \\ 3.677\times10^5 N \\ 1.103\times10^6 Nm \end{bmatrix}}}$$

Equation 4.18

$$\underline{\underline{\begin{bmatrix} V_u \\ T_u \end{bmatrix} = \phi\begin{bmatrix} V_{n.v} \\ T_u \end{bmatrix} = \begin{bmatrix} 7.673\times10^5 N \\ 9.378\times10^5 Nm \end{bmatrix}}}$$

Equation 4.19a

$$\gamma_{ps} = \sqrt{1+\frac{(3.1526\times10^6)10}{0.96(41.5\times10^6)}} \Rightarrow \underline{\underline{\gamma_{ps} = 1.338}}$$

Equation 4.19b

$$\gamma_{ps1} = 2.5\gamma_{ps} - 1.5 \Rightarrow \underline{\underline{\gamma_{ps1} = 1.846}}$$

Equation 4.19c

$$\underline{\underline{\gamma_{ps2} = 1.250}}$$

Equation 4.20

$$T_{n.\max} = \frac{635\gamma_{ps2}\sqrt{1.4(41.5\times10^6)}(2.1)(0.15)}{\sqrt{1+1.4\left(\frac{127\gamma_{ps2}(2.1)7.623\times10^5}{332(2.025)(9.378\times10^5)}\right)^2}}$$

$$= \frac{1.906\times10^6}{1.108} \Rightarrow \underline{\underline{T_{n,\max} = 1.720\times10^6\ Nm}}$$

$$F_{av} = 0.5$$
$$F_{ah} = 0.5$$

$a_v = 0.5 \bullet h = 1.05$ m

$a_h = 0.5 \bullet b = 0.7$ m

$$e_a = \frac{(2.395 \times 10^9)(1.05)(25 - 1.05)}{2P(0.8)} \Rightarrow \underline{e_a = 1.194 \times 10^{-1}\ m}$$

Equation 4.21

$$\begin{bmatrix} d_{p.v} \\ d_{p.h} \end{bmatrix} = \max \begin{bmatrix} 1.05 + 0.119\ ,\ 0.8(2.1) \\ 0.8(1.4) \end{bmatrix} \Rightarrow \underline{\begin{bmatrix} d_{p.v} \\ d_{p.h} \end{bmatrix} = \begin{bmatrix} 1.68 \\ 1.12 \end{bmatrix} m}$$

Equation 4.22

$$\underline{\begin{bmatrix} V_{i.v} \\ V_{i.h} \end{bmatrix}} = 0.5 \begin{bmatrix} 1.4(2000g[25 - 2.1] + 0) + 1.4w_D(25 - 2.1) \\ 1.7(1500g[25 - 1.4] + 0) \end{bmatrix} = \underline{\begin{bmatrix} 6.983 \times 10^5 \\ 2.951 \times 10^5 \end{bmatrix}} N$$

Equation 4.23

$$\begin{bmatrix} M_{\max.v} \\ M_{\max.h} \end{bmatrix} = 0.5 \begin{bmatrix} \left(1.4(2000g[25 - 1.05] + 0) + 1.4w_D(25 - 1.05)1.05\right) \\ \left(1.7(1500g[25 - 0.7])0.7\right) \end{bmatrix}$$

$$\Rightarrow \underline{\begin{bmatrix} M_{\max.v} \\ M_{\max.h} \end{bmatrix} = \begin{bmatrix} 7.668 \times 10^5 \\ 2.127 \times 10^5 \end{bmatrix} Nm}$$

$$V_D = w_D\left(\frac{L}{2} - a_v\right) = w_D(12.5 - 1.05) \Rightarrow \underline{V_D = 2.742 \times 10^5\ N}$$

$$V_p = \frac{2(0.742)P(0.8)}{25} \Rightarrow \underline{V_p = 1.497 \times 10^5\ N}$$

Equation 4.24

$$\begin{bmatrix} M_{cr.v} \\ M_{cr.h} \end{bmatrix} = \left(500\sqrt{41.5 \times 10^6} + \frac{P(0.8)}{0.96}\right) \begin{bmatrix} \left(\frac{0.584}{1.042}\right) \\ \left(\frac{0.304}{0.7}\right) \end{bmatrix} \Rightarrow \underline{\begin{bmatrix} M_{cr.v} \\ M_{cr.h} \end{bmatrix} = \begin{bmatrix} 3.279 \times 10^6 \\ 2.537 \times 10^6 \end{bmatrix} Nm}$$

Equation 4.25

$$\begin{bmatrix} V_{ci.v} \\ V_{ci.h} \end{bmatrix} = 100\sqrt{41.5\times10^6}(0.15)\begin{bmatrix} 1.68 \\ 1.12 \end{bmatrix} + \begin{bmatrix} \dfrac{(6.983\times10^5)(3.279\times10^6)}{7.668\times10^5} + 2.742\times10^5 \\ \dfrac{(2.951\times10^5)(2.537\times10^6)}{2.127\times10^5} \end{bmatrix}$$

$$\Rightarrow \underline{\underline{\begin{bmatrix} V_{ci.v} \\ V_{ci.h} \end{bmatrix} = \begin{bmatrix} 3.423\times10^6 \\ 3.628\times10^6 \end{bmatrix} N}}$$

Equation 4.26

(Check)

$$\begin{bmatrix} V_{ci.v\min} \\ V_{ci.h\min} \end{bmatrix} = \frac{2000}{7}\sqrt{41.5\times10^6}(0.15)\begin{bmatrix} 1.68 \\ 1.12 \end{bmatrix} \Rightarrow \underline{\underline{\begin{bmatrix} V_{ci.v\min} \\ V_{ci.h\min} \end{bmatrix} = \begin{bmatrix} 4.638\times10^5 \\ 3.092\times10^5 \end{bmatrix} N}}$$

Equation 4.27

$$\begin{bmatrix} V_{cw.v} \\ V_{cw.h} \end{bmatrix} = \left(300\sqrt{41.5\times10^6} + \frac{0.3P(0.8)}{0.96}\right)2(0.15)\begin{bmatrix} 1.68 \\ 1.12 \end{bmatrix} + \begin{bmatrix} 1.497\times10^5 \\ 0 \end{bmatrix}$$

$$\underline{\underline{\begin{bmatrix} V_{cw.v} \\ V_{cw.h} \end{bmatrix} = \begin{bmatrix} 1.521\times10^6 \\ 9.142\times10^5 \end{bmatrix} N}} \quad (okay!)$$

Equation 4.28

$$V_{co} = \min\begin{Bmatrix} 3.423\times10^6 \\ 3.628\times10^6 \\ 1.521\times10^6 \\ 9.142\times10^5 \end{Bmatrix} \Rightarrow \underline{\underline{V_{co} = 9.142\times10^5 N}}$$

Equation 4.29

$$T_{co} = 127(\gamma_{ps1})\sqrt{1.4\left(41.5\times10^6\right)}(2.1)(0.15) \Rightarrow \underline{\underline{T_{co} = 5.629\times10^5 Nm}}$$

Equation 4.30

$$T_c = \frac{T_{co}}{\sqrt{1+\left(\dfrac{T_{co}\left(7.623\times10^5\right)}{V_{co}\left(9.377\times10^5\right)}\right)^2}} \Rightarrow \underline{\underline{T_c = 5.034\times10^5 Nm}} < T_n$$

Equation 4.31

$$V_c = \frac{V_{co}}{\sqrt{1+\left(\frac{V_{co}\left(9.377\times10^5\right)}{T_{co}\left(7.623\times10^5\right)}\right)^2}} \Rightarrow \underline{V_c = 4.092\times10^5\,N} \;<\; V_n$$

Equation 4.32

$$\begin{bmatrix}T_s\\V_s\end{bmatrix} = \begin{bmatrix}T_n - T_c\\ \max\{V_{n.v}, V_{n.h}\} - V_c\end{bmatrix} = \begin{bmatrix}1.103\times10^6 - 5.034\times10^5\\ 8.968\times10^5 - 4.092\times10^5\end{bmatrix} \Rightarrow \underline{\underline{\begin{bmatrix}T_s\\V_s\end{bmatrix} = \begin{bmatrix}5.999\times10^5\,Nm\\ 4.876\times10^5\,N\end{bmatrix}}}$$

$$166(0.85)\gamma_{ps}\sqrt{41.5\times10^6}(1.4)(2.1)(0.15) = 5.365\times10^5 \leq T_n$$

therefore must find A_t/s

steel reinforcement requirements

Equation 4.33

$$D_{stir} = 0.0127\text{m (0.5")}$$
$$C_c = 0.0381\text{m (1.5")}$$

$$\begin{bmatrix}X_1\\Y_1\end{bmatrix} = \begin{bmatrix}1.4\\2.1\end{bmatrix} - (0.0127 - 2(0.0381))\begin{bmatrix}1\\1\end{bmatrix} \Rightarrow \underline{\underline{\begin{bmatrix}X_1\\Y_1\end{bmatrix} = \begin{bmatrix}1.311\\2.011\end{bmatrix} m}}$$

Equation 4.34

$$\alpha_t = 0.66 + 0.33\left(\frac{Y_1}{X_1}\right) = 0.66 + 0.33\left(\frac{2.011}{1.311}\right) \Rightarrow \underline{\underline{\alpha_t = 1.166}}$$

Equation 4.35

$$\begin{bmatrix}\frac{A_t}{s}\\ \frac{A_v}{s}\end{bmatrix} = \begin{bmatrix}1.166(2.011)(1.311)\left(2\times10^{11}\right)(0.002) & 0\\ 0 & (2.025)\left(2\times10^{11}\right)(0.002)\end{bmatrix}^{-1}\begin{bmatrix}5.998\times10^6\\4.876\times10^5\end{bmatrix}$$

$$\Rightarrow \underline{\underline{\begin{bmatrix}\frac{A_t}{s}\\ \frac{A_v}{s}\end{bmatrix} = \begin{bmatrix}4.877\times10^{-4}\\6.020\times10^{-4}\end{bmatrix}\left(\frac{m^2}{m}\right)}}$$

$$if\left(166\phi'\gamma_{ps}\sqrt{f_c'}bth < T_n\right), then\left(\frac{A_t}{s}\right) is\ set\ to\ zero$$

Equation 4.36

$$\frac{A_{t.t}}{s} = 4.877\times10^{-4} + (0.5)\left(6.020\times10^{-4}\right) \Rightarrow \underline{\underline{\frac{A_{t.t}}{s} = 7.887\times10^{-4}}}\ \left(\frac{m^2}{m}\right)$$

Equation 4.37

$$F_t = \frac{2.1(0.15)\sqrt{1.4\left(41.5\times10^6\right)}}{(1.166)(1.311)(2.011)\left(2\times10^{11}\right)(0.002)} \Rightarrow \underline{\underline{F_t = 1.952\times10^{-6}}}$$

Equation 4.38

$$\frac{A_{t.t\min}}{s} = 190\left(1.952\times10^{-6}\right)\left(1+\frac{12P}{(0.96)\left(41.5\times10^6\right)}\right)$$

$$\Rightarrow \underline{\underline{\frac{A_{t.t\min}}{s} = 7.231\times10^{-4}}}\left(\frac{m^2}{m}\right) < \frac{A_{t.t}}{s}\ \textbf{(okay!)}$$

Equation 4.39

$$s = \min\left\{\begin{array}{c}\dfrac{\pi(0.0127)^2}{4\left(7.887\times10^{-4}\right)} = 0.161m \\ 0.3 = 0.3m \\ \dfrac{1.311+2.011}{4} = 0.831m \\ \dfrac{2.025}{2} = 1.013m \\ \dfrac{1.325}{2} = 0.663m\end{array}\right\} \Rightarrow \underline{s = 0.161m}$$

$$A_{t.t} = \left(\frac{A_{t.t}}{s}\right)s = \left(7.887\times10^{-4}\right)(0.161) \Rightarrow \underline{\underline{A_{t.t} = 1.267\times10^{-4}}}\ m^2$$

$$m = 0.1104in^2 \Rightarrow \underline{\underline{A_{t.t\min} = 0.713\times10^{-4}}}\ m^2$$

$$V_{stir} = \frac{\pi}{4}(D_{stir})^2(X_1+Y_1)\frac{L}{s} \Rightarrow \frac{2L\pi}{4s}(D_{stir})^2(X_1+Y_1)$$

$$V_{stir} = \frac{2A_{stir}L}{s}(X_1+Y_1)$$

$$V_t = A_tL = V_{stir} = \frac{2A_{stir}L}{s}(X_1+Y_1)$$

Equation 4.40

$$A_{t.l} = 2\left(\frac{A_t}{s}\right)(X_1 + Y_1)$$

$$A_{t.l} = 2\left(4.877\times10^{-4}\right)(1.311+2.011) \Rightarrow \underline{\underline{A_{t.l} = 3.241\times10^{-3}\ m^2}}$$

Equation 4.41

$$A_{t.l\min} = 4\left(1.952\times10^{-6}\right)(0.161)\left(\frac{9.377\times10^5}{9.377\times10^5 + \frac{2(1.4)(2.1)\left(7.623\times10^5\right)}{3(2.025)}}\right)$$

$$-\max\left\{\begin{matrix}0.5\pi(0.127)^2 \\ 2\left(7.231\times10^{-4}\right)(0.161)\end{matrix}\right\}\left(\frac{1.311+2.011}{0.161}\right)$$

$$\Rightarrow \underline{\underline{A_{t.l\min} = -5.226\times10^{-3}\ m^2}} < 0 < A_{t.l}\ \textbf{(okay!)}$$

FRP reinforcement requirements

Equation 4.42a

$$V_{rc.v.frp/b} = \left(\frac{2b_{frp}}{b}\right)A_{rc.v}L = \frac{2(0.2)}{1.4}\left(2.630\times10^{-3}\right)(25) \Rightarrow \underline{\underline{V_{rc.v.frp/b} = 1.878\times10^{-2}}}\ m^3$$

Equation 4.42b

$$\begin{bmatrix}V_{rc.h.frp/b}\\ V_{rt.h.frp/b}\end{bmatrix} = \left(\frac{0.4-0.15}{2.1-0.3}\right)\begin{bmatrix}4.882\times10^{-3}\\ 4.882\times10^{-3}\end{bmatrix}(25) \Rightarrow \underline{\underline{\begin{bmatrix}V_{rc.h.frp/b}\\ V_{rt.h.frp/b}\end{bmatrix} = \begin{bmatrix}1.695\times10^{-2}\\ 1.695\times10^{-2}\end{bmatrix}}}\ m^3$$

Equation 4.42c

$$V_{rt.v.frp/b} = 0$$

Equation 4.43c

Note:
Equation 4.43a is not applicable in this example
Equation 4.43c is not applicable in this example

$$\begin{bmatrix}V_{t.t.frp/b}\\ V_{t.l.frp/b}\end{bmatrix} = \left(\frac{2(0.2)(0.15)+(0.4-0.15)(2)(0.15)}{0.96}\right)\begin{bmatrix}1.310\times10^{-1}\\ 3.241\times10^{-3}(25)\end{bmatrix}$$

$$\Rightarrow \underline{\underline{\begin{bmatrix}V_{rc.h.frp/b}\\ V_{rt.h.frp/b}\end{bmatrix} = \begin{bmatrix}1.695\times10^{-2}\\ 1.695\times10^{-2}\end{bmatrix}}}\ m^3$$

Cost functions without FRP reinforcement:

Equation 4.44a

$$V_{r.t/b} = 2\left(1.267\times10^{-4}\right)\left(\frac{25}{0.161}\right)(1.311+2.011) \Rightarrow \underline{V_{r.t/b} = 1.310\times10^{-1}\ m^3}$$

Equation 4.44b

$$V_{r.l/b} = \left(4.019\times10^{-3} + 2.630\times10^{-3} + 2\left(4.882\times10^{-3}\right) + 3.241\times10^{-3}\right)(25)$$

$$\Rightarrow \underline{V_{r.l/b} = 4.913\times10^{-1}\ m^3}$$

Equation 4.45

$$\underline{V_{r/b} = 6.223\times10^{-1}\ m^3}$$

Equation 4.46

$$V_{c/b} = (0.96)25 - V_{r/b} \Rightarrow \underline{V_{c/b} = 2.338\times10^{1}\ m^3}$$

Equation 4.47a

$$u_c = \$90/\text{m3}$$

$$C_{c/b} = (\$90)V_{c/b} \Rightarrow \underline{C_{c/b} = \$2103.99}\ per\ beam$$

Equation 4.47b

$$u_r = \$0.55/\text{kg}$$

$$C_{r/b} = (\$0.55/kg)V_{r/b}\left(\frac{77000N/m^3}{9.807N/kg}\right) \Rightarrow \underline{C_{r/b} = \$2687.60}\ per\ beam$$

Equation 4.47c

$$F_{ps} = 7.2\text{x}10\text{-}6$$
$$u_{ps} = \$2.25/\text{kg}$$

$$C_{ps/b} = \left(7.2\times10^{-6}\right)(\$2.25)(25)\left(3.153\times10^{6}\right) \Rightarrow \underline{C_{ps/b} = \$1276.81}\ per\ beam$$

Equation 4.48

$$\begin{bmatrix} C_c \\ C_r \\ C_{ps} \end{bmatrix} = (25)^{-1}\begin{bmatrix} \$2103.989 \\ \$2687.602 \\ \$1276.815 \end{bmatrix} \Rightarrow \underline{\begin{bmatrix} C_c \\ C_r \\ C_{ps} \end{bmatrix} = \begin{bmatrix} \$84.16 \\ \$107.50 \\ \$51.07 \end{bmatrix} m^{-1}}$$

Equation 4.49

$$C = C_c + C_r + C_{ps} \Rightarrow \underline{C = \$242.74\ m^{-1}}$$

Cost functions with FRP and steel reinforcement:

Equation 4.50

$$V_{frp/b} = 1.878 \times 10^{-2} + 2\left(1.695 \times 10^{-2}\right) + 1.842 \times 10^{-2} + 1.139 \times 10^{-2}$$

$$\underline{V_{frp/b} = 8.250 \times 10^{-2}\ \ m^3\ per\ beam}$$

Equation 4.51

$$C_{frp/b} = 8.250 \times 10^{-2}(5.5 - 1.0)\left(\frac{77{,}000}{9.807}\right)(\$0.55) \Rightarrow \underline{C_{frp/b} = \$1603}\ per\ beam$$

Equation 4.52

$$C_{frp} = \frac{\$1603}{25m} \Rightarrow \underline{C_{frp} = \$64.13\ m^{-1}}$$

Equation 4.53

$$C_{total} = \$242.74 + \$64.13 \Rightarrow \underline{C_{total} = \$306.87\ m^{-1}}$$

4.3 Sensitivity analyses

Using the spreadsheet analysis program *BoxCost*, a number of sensitivity analyses are performed. Specifically, sensitivity analyses are performed on the narrow beam design based on 1) beam width, 2) beam depth, 3) beam length, 4) vehicle mass, 5) vehicle eccentricity with respect to the beam, 6) beam deflection criteria, 7) beam wall thickness, and 8) required FRP zones. For each parameter analyzed, plots of changes in the beam a) material costs, b) midspan deflections, c) fundamental frequency, and d) mass are presented and discussed in the following subsections. Costs are given in 1992 US dollars per meter for a single lane of maglev guideway. A cost factor of 5.5 (over steel) has been used for the required hybrid FRP concrete reinforcement. All figures referred to in the following subsections are included at the end of this section.

4.3.1 Beam width

Beam widths are varied to determine the effects various widths have on overall guideway performance. For the sensitivity analysis, the beam width, b, is varied from 1.10 m to 3.00 m. The depth of the beam, h, is set equal to 1.5 times the beam width (i.e. $1.5 \cdot b$) for each case. The 25 m beam span length, L, and all other values of loadings and material properties, are consistent with a) the example presented in Section 4.2 and b) the loadings shown in Figure 2.1.1.

Figure 4.3.1a shows costs for concrete sections reinforced with a) steel and hybrid FRP rods and b) steel reinforcement only. As indicated in the figure, for the given beam loadings and material properties and costs, minimum overall cost of the beam is achieved when the beam cross-sectional width is approximately 1.4-1.6 m. For the given loads, beam widths less than 1.2 m are too narrow for the section to adequately resist horizontal bending moments and torsion. Therefore, these smaller sections require more tension reinforcement (i.e. more steel and FRP), which drives up material costs. Sections with

widths greater than 1.8 m are overdesigned for the given loads. For such sections, additional vertical and prestressing reinforcement is required to compensate for the additional weight of the oversized beam. As indicated in Figure 4.3.1a, the marginal cost for using hybrid FRP rods is higher for more narrow width beams. This higher cost results from the need for additional torsional and horizontal reinforcement.

A specific standard beam width can be determined with certainty only when more exact vehicle loadings and structural design requirements are determined. The actual optimal beam width is likely to be less than the absolute minimum value shown in Figure 4.3.1a due to the conservative design assumptions used in this analysis. Thus, a standard beam width of 1.4 m is selected for the 25 m span.

Figure 4.3.1b shows the change in maximum vertical and horizontal midspan deflection, Δ_v and Δ_h respectively. For the analysis, the maximum deflection allowed for both parameters is set at $L/1000$, or 25 mm. However, when the cost of a section is minimized (typically by an increase in section depth, h) the resulting maximum deflection is less. As indicated in Figure 4.3.1b, for beam widths between approximately 1.4 m and 1.9 m, Δ_v is approximately 5 mm, or $L/5000$. In contrast, Δ_h ranges from 9 mm for a beam width of 1.4 m to 4 mm for a beam width of 1.9 m. The abrupt changes in Δ_v at beam widths between 1.5 m and 1.8 m shown in Figure 4.3.1b are due to the increase in beam mass when beam wall thickness increases from 0.15 m to 10% of the beam width.

Figure 4.3.1c shows changes in beam mass and frequency for given beam widths. For the 1.4 m wide beam, a fundamental frequency of 6.54 Hz, with a corresponding beam mass of 2.44 tonne/m, is shown. In comparison, a 2.5 m wide box beam is shown to have a frequency of 7.45 Hz and a mass of 5.34 tonne/m.

4.3.2 Beam depth

Though a standard beam depth is not as critical to the overall narrow beam guideway design as is a standard beam width, beam depth does play a major role in determining the stiffness, frequency, and cost of the beam. The more shallow the beam depth, the more reinforcement required to achieve a given stiffness. Additional reinforcement results in a higher cost for the section. Conversely, the deeper the section, typically the lower the cost. Because torsion is expected to be significant for the maglev narrow beam, a limitation of $1.5 \cdot b$ is placed on section depth. As shown in Figure 4.3.2a, the maximum depth constraint of $1.5 \cdot b$ is exercised with 2.1 m as the lowest cost depth for the 1.4 m wide beam cross-section. For the 2.1 m depth, the cost of the beam is calculated to be $ 243 per meter with all steel reinforcement and $ 307 per meter with hybrid FRP reinforcement in the top corners of the cross-section (see Figure 2.4.2). Thus, the use of FRP in this example (see Figure 4.3.8, Case 2) increases the total beam material cost by $ 64 per meter, or 26 %.

Figure 4.3.2b shows the influence beam depth has on Δ_v. As beam depth increases from 1.2 m to 2.1 m, Δ_v decreases from 23 mm to 6 mm. As shown in Figure 4.3.2b, though Δ_h also decreases with an increase in section depth, the effect is minimal. Figure 4.3.2c shows the effect that increases in section depth have on beam mass and on fundamental frequency. The beam mass increases from 1.82 tonne/m at a section depth of 1.2 m to 2.44 tonne/m at a depth of 2.1 m. Similarly, the fundamental beam frequency increases from 3.85 Hz to 6.54 Hz for the depth range.

4.3.3 Beam length

For the narrow beam cross-section having a 1.4 m width, a 2.1 m depth, and a 0.15 m wall thickness, Figure 4.3.3a shows the effect guideway beam span length, L, has

on overall beam material cost. As the span is reduced, so is beam material cost. However, as the span length decreases, column and foundation costs increase[2]. Since in general, longer spans are more aesthetically pleasing, it is common practice to choose a slightly longer standard span over one the that is most economical [Menn 91].

Selecting an optimal beam span length is not possible without additional information regarding guideway column and foundation costs. Other studies have used 25 m as a standard beam span [Harrison, et.al. 92, CIGGT 89]. Also, the Transrapid test track in Emsland, Germany, uses 25 m as its standard span [Hilliges and Schambeck 89]. Though this beam length sensitivity analysis does not confirm that a 25 m span length is optimal, Figure 4.3.3a does show that a 25 m span, at approximately $ 307 per meter, is not prohibitively expensive. For assumptions used in this analysis, beam spans up to 35 m at $ 460 per meter, appear to be economically viable. They are only 55% more expensive in terms of material cost than the 25 m span.[3] Increased acceptance of longer spans by the public may justify their additional cost.

Figure 4.3.3b shows the increase in Δ_v and Δ_h for increases in span length. As shown in the figure, for the 25 m span, Δ_v is 6 m and Δ_h is approximately 9 mm. In Figure 4.3.3c, the fundamental beam frequency decreases by L^{-2} with increases in beam length. Concerns over beam dynamic effects may lead to a standard beam length longer than what is considered economically optimal. Because beam length is relatively simple to alter for a given application, it may be advantageous to tailor design beam lengths to meet certain beam dynamic behavior criteria.[4] Based on the given beam cross-sectional geometry, a 25 m span length is considered standard.

---

[2] See Section 2.1.

[3] For very long spans (i.e. greater than 40 m), a special support structure for the beam will be required. Such cases are not considered in determining a standard beam length.

[4] See Section 5.4.

4.3.4 Vehicle mass

Figure 4.3.4 shows the effect increased vehicle mass has on beam behavior. In this analysis, no additional restrictions are placed on Δ_v (i.e. only the $L/1000$ constraint given in the example in Section 4.2 is used).[5] Because Δ_v is allowed to fluctuate, only a minimal cost increase occurs as the distributed vehicle mass, w_v, ranges from 1.0 to 4.0 tonne/m. For the 3.0 tonne/m vehicle mass case, Figure 4.3.4a shows the cost of the concrete beam with steel and hybrid FRP reinforcement to be $322 per meter. As shown in Figure 4.3.4b, Δ_v for the 3.0 tonne/m vehicle mass is 9 mm. Because beam geometrical parameters are constant, the beam mass and fundamental beam frequency are essentially constant. This is illustrated in Figure 4.3.4c. There is an increase in vertical reinforcement because of increased vehicle mass. Due to the high cost of this reinforcement, the increases in required reinforcement are reflected in Figure 4.3.4a. However, because of the relatively small amount and mass of reinforcement used, the increase in reinforcement has virtually no effect on the beam mass or fundamental frequency (see Figure 4.3.4c).

4.3.5 Vehicle eccentricity

An important system design-related issue is the extent of vehicle eccentricity with respect to the beam. As indicated in Figure 2.1.1, the assumed standard eccentricity is 3.0 m. Aerodynamic concerns tend to increase the vehicle eccentricity in order to reduce surface drag. That is, the lower the vehicle rests on the narrow beam, the more surface area interaction there is between the vehicle and the beam. This increase in surface area increases aerodynamic drag.

Figure 4.3.5a shows that an increase in vehicle eccentricity has only a moderate effect on beam cost for the given beam cross-section (see Figure 2.4.2). Figure 4.3.5b

---

[5] See subsection 4.3.6 for an analysis where stringent tolerances are placed on Δ_h and Δ_v.

shows that an increase in vehicle eccentricity has no effect on Δ_v and Δ_h. Also, because only reinforcement changes are made to the beam cross-section, the beam mass and frequency are constant as indicated in Figure 4.3.5c.

This analysis demonstrates that the narrow box beam is robust against changes in vehicle eccentricities for expected loadings. Twisting and warping of the section is not modeled. To reduce beam dead weight, it is expected that beam wall thickness less than 0.15 m may be used.[6] For such thin-walled cross-sections, there will be more sensitivity to changes in vehicle eccentricity as the torsional resistance of the section is reduced. More refined analysis is required for these thin-walled sections.

4.3.6 Deflection criteria

Figure 4.3.6 reflects changes in beam behavior under stringent beam deflection criteria. For this analysis, $\Delta_{v.max}$ is set equal to $2 \bullet \Delta_{h.max}$. As indicated in Figure 4.3.6a, beam material costs begin to increase substantially as $\Delta_{v.max}$ becomes less than 13 mm. For maximum vertical midspan deflection constraints greater than 13 mm, overall beam material costs remain relatively constant at approximately $280 per meter. A beam material cost for $\Delta_{v.max}$ of 5 mm (and a corresponding $\Delta_{h.max}$ of 2.5 mm) is shown to be $473 per meter. This cost is significantly higher than the $307 per meter cost of the 1.4 m wide by 2.1 m deep standard beam for similar Δ_v constraints. The increased cost for beams in this sensitivity analysis is due to the more stringent Δ_h limitations. Such restrictions on Δ_h result in minimum beam width requirements. Figure 4.3.6b shows beam widths less than 1.5 m for $\Delta_{v.max}$ values greater than 13 mm. In contrast, when $\Delta_{h.max}$ is 2.5 mm, (i.e. $\Delta_{v.max} = 5.0$ mm), the minimum acceptable beam width is 2.12 m. Figure 4.3.6b indicates that the $\Delta_{h.max}$ constraint is exercised for all given deflection criteria, while the $\Delta_{v.max}$ constraint is not exercised in any of the cases.

---

[6] See subsection 4.3.7.

The beam mass increases with increases in beam widths for these more restrictive $\Delta_{v,max}$ and $\Delta_{h,max}$ criteria. However, the fundamental beam frequency, remains relatively constant between 6 and 7 Hz for the given cases. This is shown in Figure 4.3.6c. The increased beam mass is offset by a corresponding increase in bending stiffness, resulting in the relatively constant beam frequencies.

4.3.7 Beam wall thickness

Analysis of the wall thickness to less than 14 cm for the 1.4 m wide narrow beam section is outside the scope of both the ACI code and Hsu's method for torsion design of reinforced concrete box sections [ACI 89, Hsu 84]. Stability is a major concern for such thin-walled sections as the slenderness ratio becomes excessive.[7] Nonetheless, it is instructive to perform sensitivity analyses on such sections in order to determine the potential effect reduction in beam mass may have on material costs of the beam. The dashed lines in Figures 4.3.7a and 4.3.7b indicate that the analysis is outside the scope of ACI code and Hsu's recommendations. Figure 4.3.7c shows that the beam mass is reduced from 2.42 to 1.70 tonne/m as the wall thickness is reduced from 15 cm to 10 cm. Because the decrease in mass is matched with a decrease in stiffness, the frequency remains constant at 11.5 Hz for this wall thickness range. Though the cost of concrete and vertical reinforcement decreases dramatically with a decrease in beam wall thickness, the cost of torsional reinforcement increases substantially. Thus, overall material cost savings are minimal. For more stringent deflection criteria, decreases in wall thickness should result in more dramatic cost savings.

4.3.8 FRP zone influence

Areas of the beam cross-section requiring FRP reinforcement are dictated by the maglev motor design. Where high magnetic fields and low attenuation rates are present,

---

[7] See subsection 2.1.2.

non-magnetic concrete reinforcement is required. Where magnetic fields are low and attenuation rates are high, steel reinforcement can be used. Thus, strategic vehicle and motor design can help reduce the need for FRP reinforcement in the guideway structure. Six conceptual cases are analyzed to reflect the influence of hybrid FRP reinforcement on overall beam material costs. Cross-sectional representations of the six cases are shown in Figure 4.3.8.

Case 1 of Figure 4.3.8 represents a cross-sectional beam design requiring no hybrid FRP reinforcement. That is, Case 1 represents a concrete section reinforced with steel only. Though for an EDS system, an all steel reinforcement scenario currently is not considered viable, it serves as a basis for comparison. Case 2 represents the ideal situation for an EDS system where the areas requiring FRP reinforcement are confined to the top corners of the guideway beam cross-section. All reinforcement not in the top corners of the beam cross-section is steel. For a design such as Case 2 to be feasible, no magnetic coils can be placed along the center of the top portion of the beam, (i.e. magnetic windings must be confined to the upper sides and/or the extreme corners of the top of the beam cross-section).[8] Case 3 allows windings to be placed at any location along the top portion of the guideway. Case 4 allows windings to be placed along the top of the beam and as far down as half the depth of the beam. Case 5 limits steel reinforcement to the bottom flange of the box beam. The all hybrid FRP reinforced section is represented by Case 6.

Figure 4.3.9 shows overall guideway beam material costs for the six cases described above and shown in Figure 4.3.8. Accurate and reliable cost and performance data for FRP ***prestressing*** is not currently available. Therefore, costs shown in Figure

[8] Note Case 2 is used in the example in Section 4.2.

4.3.9 do not consider replacing steel prestressing with FRP prestressing, though for Cases 5 and 6 (and possibly Case 4) such replacement is necessary.

Figure 4.3.9 shows the all steel case to cost $ 243 per meter. Case 2 represents a 26% increase in cost at $ 307 per meter. The all hybrid FRP reinforced section, (i.e. Case 6), at $ 727 per meter, represents a 200% increase from the all steel reinforced section, (Case 1), and a 135% increase from the assumed standard narrow beam section, (Case 2).

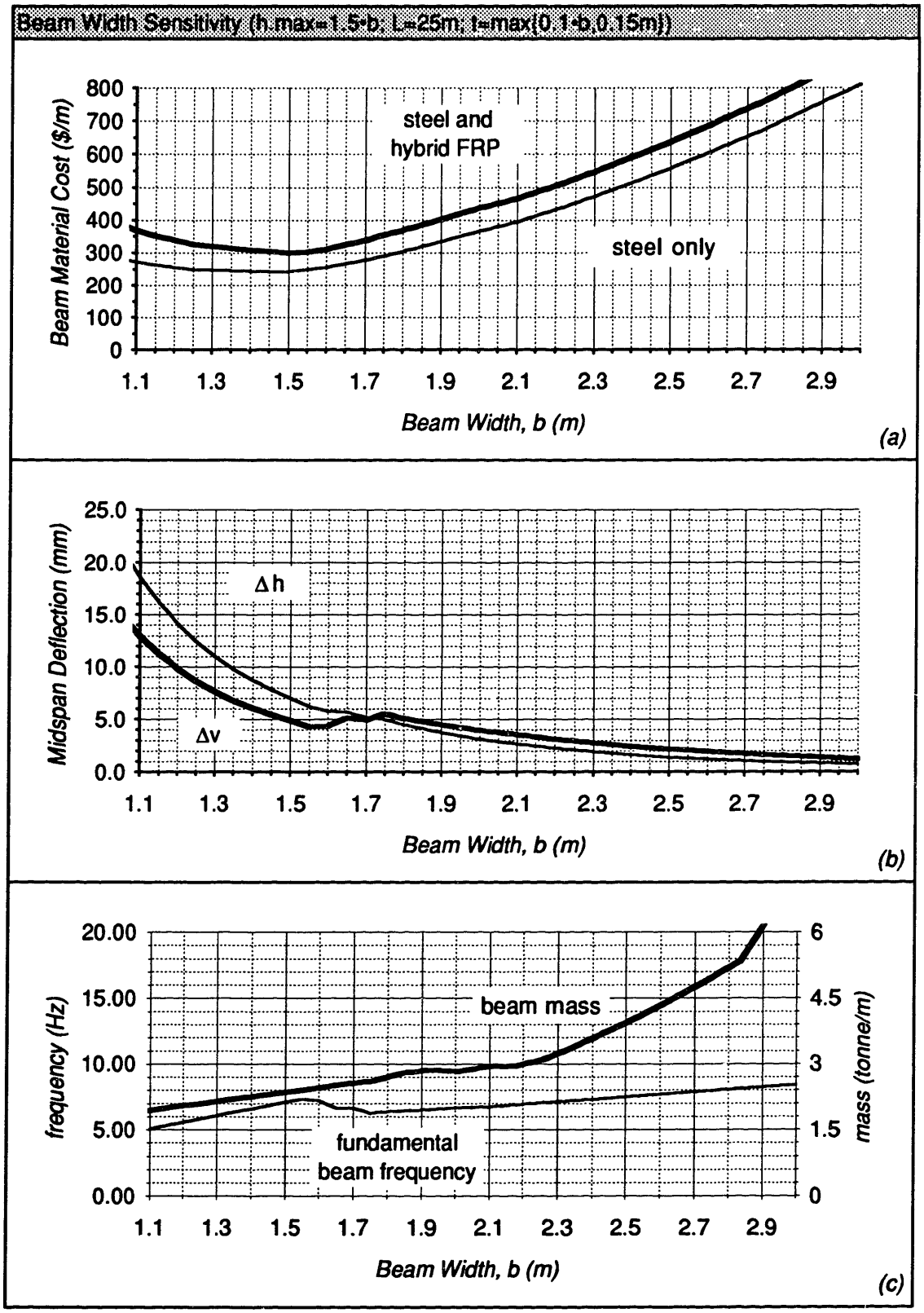

Figure 4.3.1 Beam Width Sensitivity Analysis

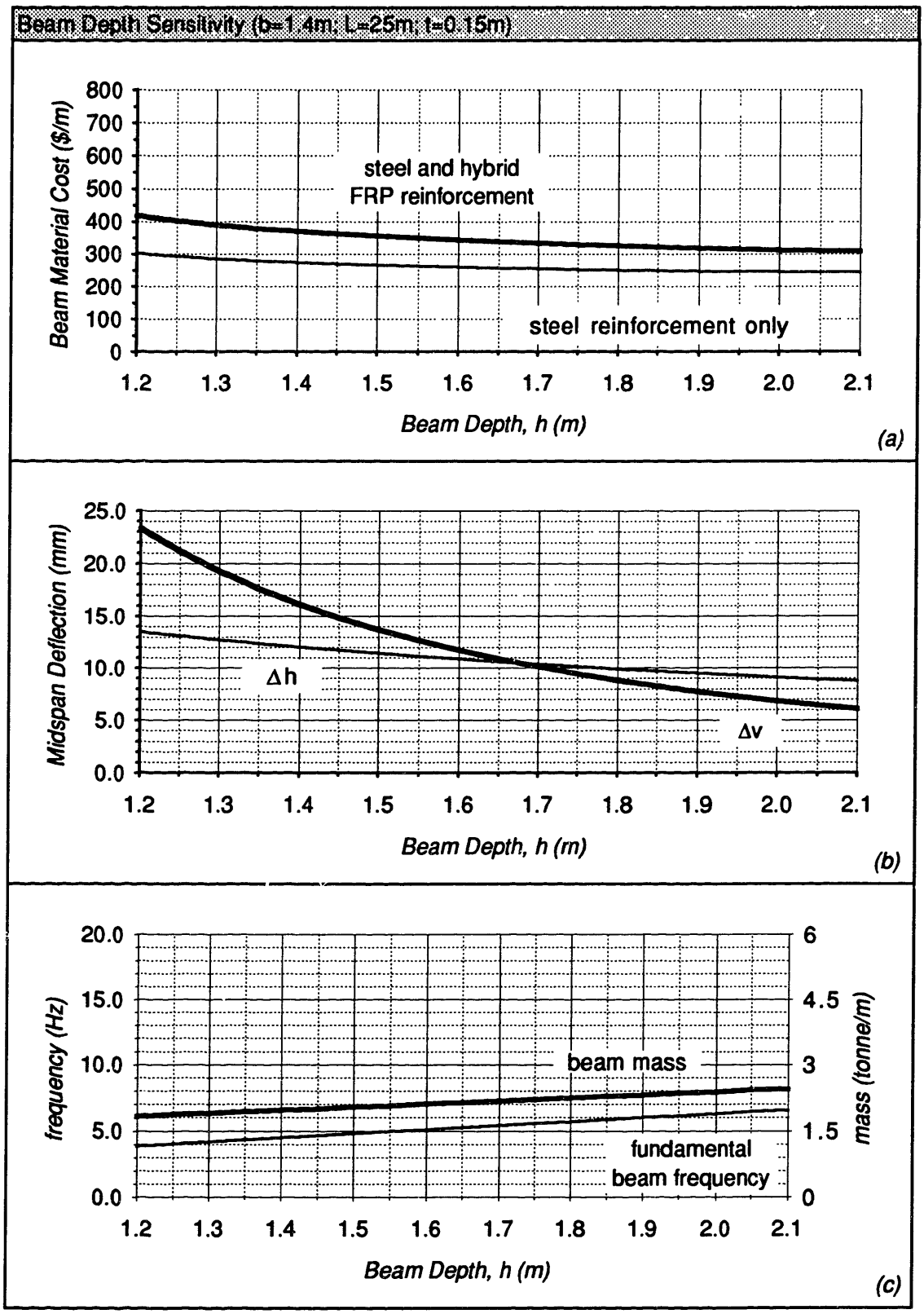

Figure 4.3.2 Beam Depth Sensitivity Analysis

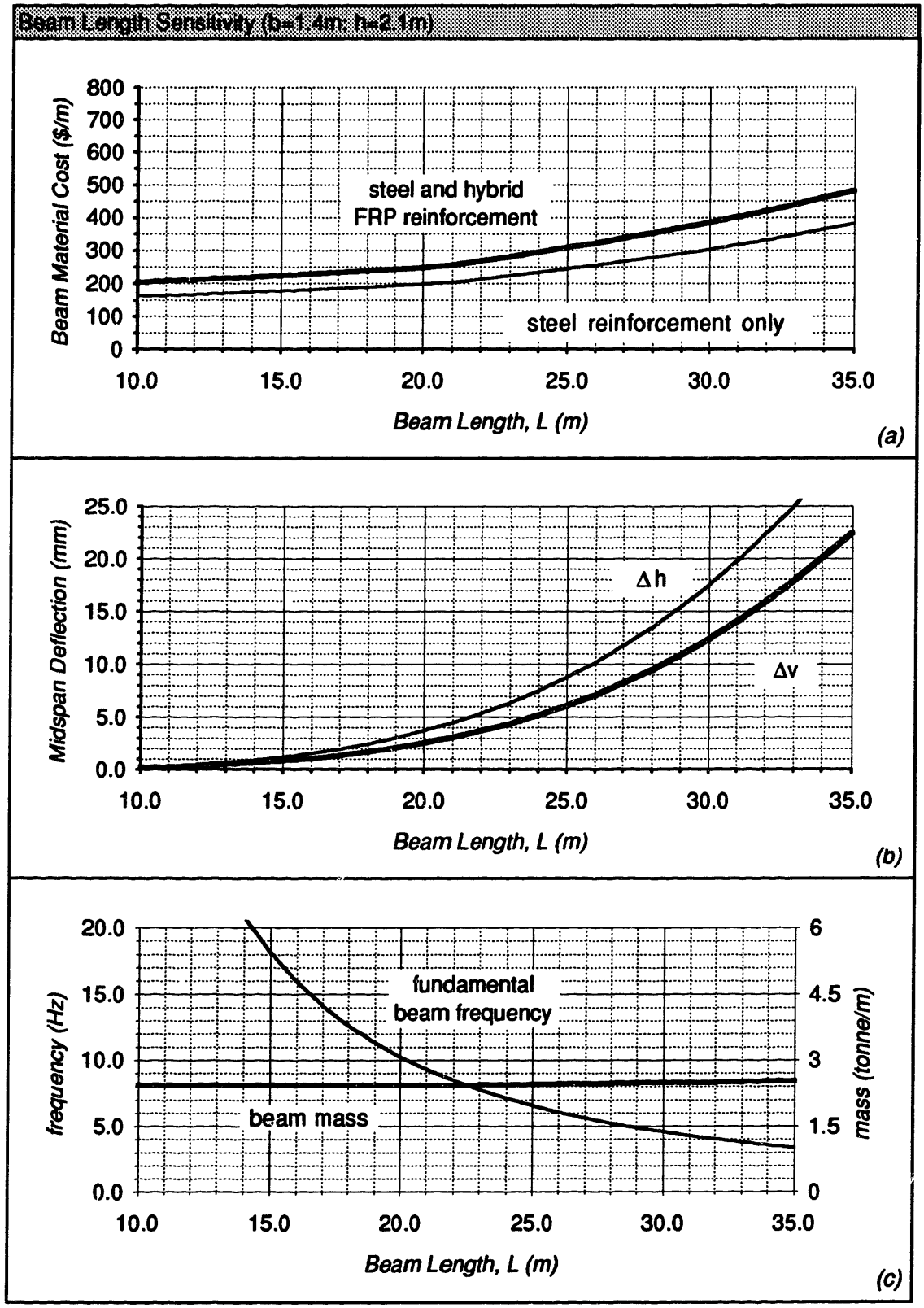

Figure 4.3.3 Beam Length Sensitivity Analysis

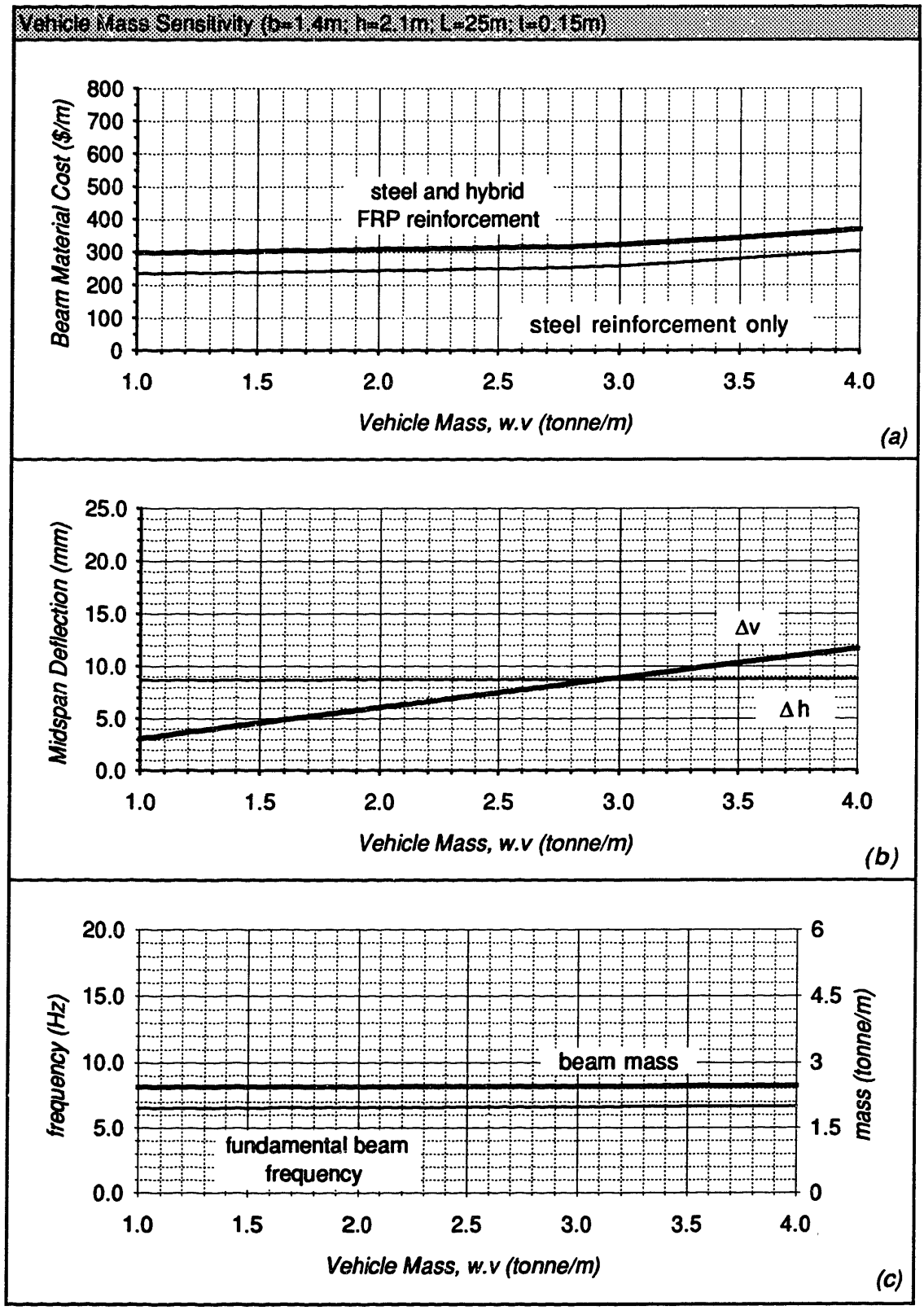

Figure 4.3.4 Vehicle Mass Sensitivity Analysis

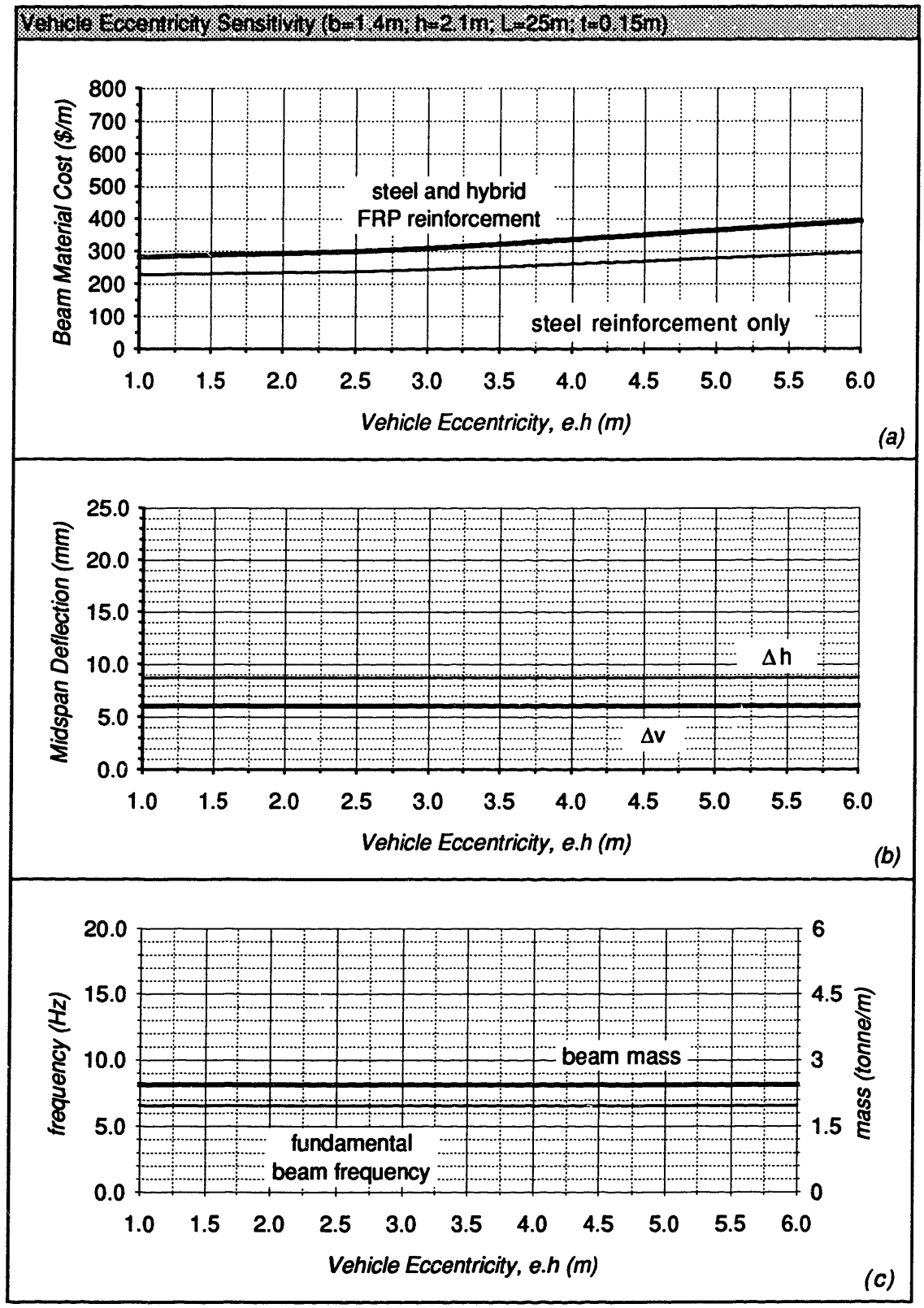

Figure 4.3.5 Vehicle Eccentricity Sensitivity Analysis

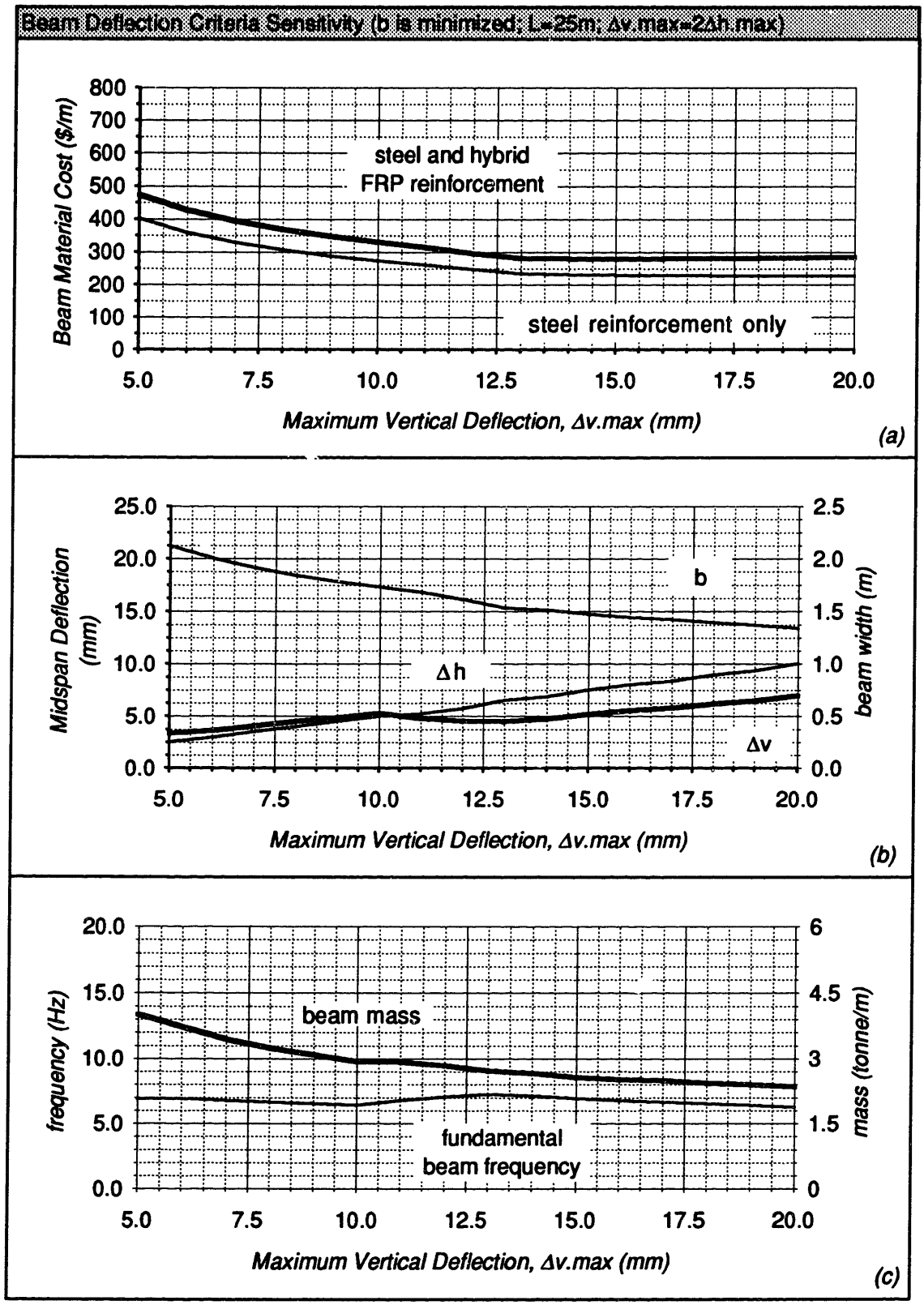

Figure 4.3.6 Beam Deflection Criteria Sensitivity Analysis

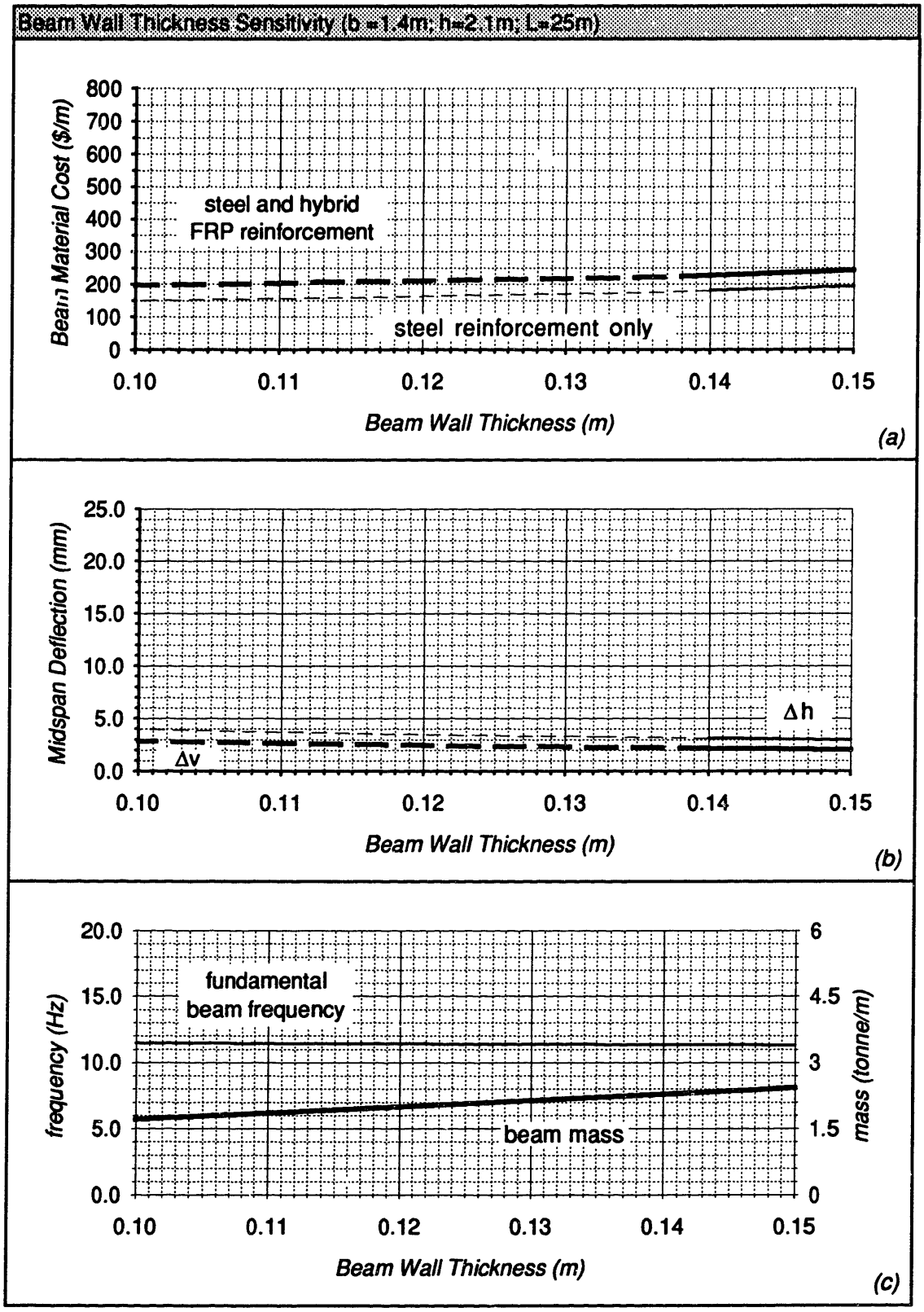

Figure 4.3.7 Beam Wall Thickness Sensitivity Analysis

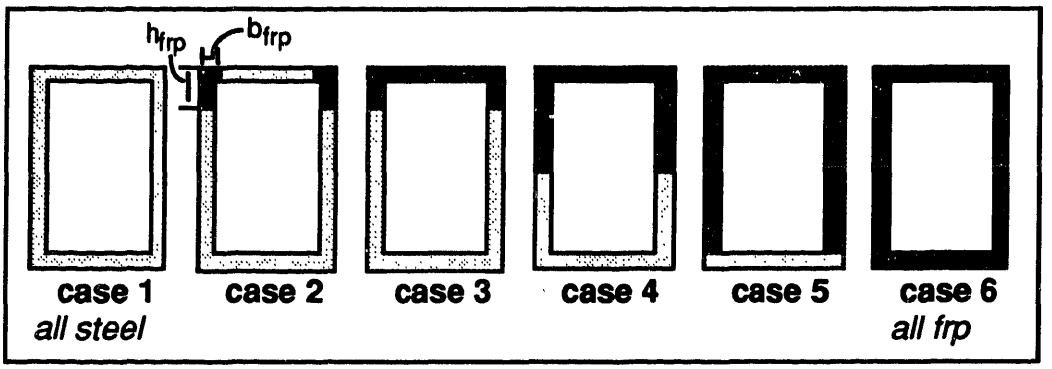

Figure 4.3.8 Hybrid FRP Cross-Section Zones (6 cases)

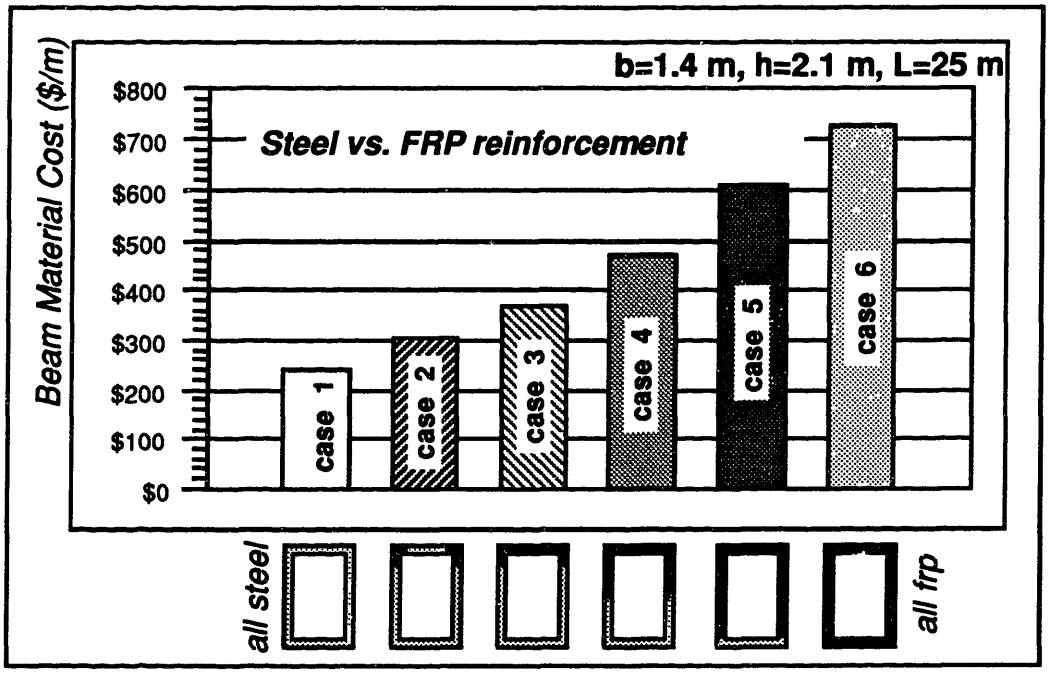

Figure 4.3.9 FRP Zone vs. Cost Sensitivity Analyses

4.4 Beam cost comparison

This section compares narrow beam guideway cost projections with Transrapid guideway cost estimates. Using Transrapid cost data, beam material cost data calculated in Section 4.2 can be translated to a projected total per meter cost for an installed dual elevated maglev guideway system. The Transrapid guideway is chosen as a base comparison primarily because 1) it is nearing commercial implementation and 2) cost data for the system is available. Currently, cost comparisons with other maglev guideway systems are difficult because actual cost data generally is not available.

4.4.1 Transrapid guideway costs

Calculated costs for the narrow beam design are compared with estimations presented in *The Maglev Estimation: Capital Cost Elements Interim Report*, prepared by Parsons Brinckerhoff Quade & Douglas, Inc. and the Volpe National Transportation Systems Center, henceforth referred to as the **"P/B Report"** [Harrison, et.al. 92]. The P/B Report allows projections to be made based on material cost calculations for given beam sections. In particular, for the reinforced concrete Transrapid beam element, the P/B Report considers:[9]

- material cost
- beam casting facility cost
- cost of each cast
- quality control
- contingencies

[9] Actually, the P/B Report combines these cost items into a single general category of guideway beam fabrication cost. The more detailed cost breakdown shown here was obtained via telephone from the principal author of the report, John Harrison of Parsons Brinckerhoff, on 5/11/92.

The P/B Report estimates the beam fabrication costs: a) $315 per meter for beam material costs, b) $187 per meter for beam casting facility costs, considering a casting yard approximately every eight kilometers, c) $581 per meter for each cast, which includes labor and equipment costs, and d) $49 per meter for quality control, which includes costs for recesses in the concrete for motor attachments and other costs imposed due to high precision cost requirements. An additional 20% of the subtotal of these four cost categories used to account for contingencies, yields a total beam fabrication cost of $1358 per meter for the Transrapid beam. These costs are converted to costs factors based on the beam material cost in Table 4.3.1 in order to compare component costs against beam material costs alone.

Table 4.3.1 Transrapid beam fabrication cost (based on P/B report)

Beam cost item	Cost ($ per meter of single guideway)	Cost Factor (based on beam material cost)
material	315	1.00
casting facility	187	0.59
each cast	581	1.84
quality control	49	0.16
subtotal	⇒ *1132*	⇒ *3.59*
20% contingencies	226	0.72
Total	⇒ **1358**	⇒ **4.31**

As indicated in Table 4.3.1, the total Transrapid guideway beam fabrication cost is 4.31 times its beam material cost. The P/B Report forecasts the total installation cost for the entire elevated double track Transrapid guideway structural system—which includes foundation, column, power station, and guideway beam costs—to be approximately $10,500 per meter, of which approximately $630 per meter is beam material cost. Total beam fabrication cost for the dual Transrapid guideway is estimated to be approximately $2700 per meter, or 25% of the total installation cost.[10] Thus, the

[10] Actually, the cost estimate for elevated double track sections ranges from $9295 per meter ($14,960,000/mile) to $12,888 per meter ($20,741,000/mile). The $10,500 per meter estimate used for comparison specifically is based on "rural undulating" terrain, which is considered average terrain.

total installation cost for the Transrapid guideway installation is estimated at 16.7 times the cost of its beam material.

4.4.2 Transrapid costs vs. narrow beam guideway

Direct comparisons between the Transrapid system and the narrow beam guideway concept is restricted to beam material and fabrication costs. Other costs—column, foundation, motor, and transportation costs—are not considered in this thesis. Exact dimensions for the narrow beam section presented in this report, (i.e. the 1.4 m width, 2.1 m depth, 25.0 m length, and 0.15 m uniform wall thickness), are subject to change given the uncertainties of actual a) vehicle loads, b) ride quality constraints, and c) column and foundation costs. However, they can be used for preliminary cost comparison. The calculated mass of the 25 m narrow beam is 61,050 kg. Reportedly, a 25 m Transrapid reinforced concrete beam has a mass of approximately 90,000 kg [Hilligies and Schambeck 89] or approximately 50% greater mass than the narrow beam. Comparisons of beam masses between systems are important as greater mass typically results in higher structural costs.

Projected narrow beam material cost for a single lane of guideway as calculated in Section 4.2, is $243 per meter using only steel reinforcement and $307 per meter using both steel and FRP reinforcement. These narrow beam cost projections appear conservative against Transrapid estimates of $315 per meter. Normally, material cost is strictly a function of the amount of material required. Ideally, with the narrow beam containing only two-thirds the mass of the Transrapid beam, the narrow beam material cost is expected to be approximately two-thirds that of the Transrapid beam, or approximately $210 per meter.

The narrow beam cost estimate presented in this thesis may be high due to the conservative design approaches taken. However, based on differences in beam mass

between the two systems, either: a) material cost projections for the narrow beam are excessive, or b) material cost projections for the Transrapid system are overly optimistic.

In addition to lower material cost, manufacture, transportation, and fabrication costs should also be less with the narrow beam design. For the narrow beam, the cost of each cast and of the casting facility should be less than that projected for the Transrapid design shown in Table 4.3.1, since the hollow-box design can essentially be pultruded in an automated manufacturing process. A design goal for the hollow-box beam is to limit total casting costs to less than beam material cost. It is expected that total guideway cost savings of 50% are possible with the narrow beam design compared with the Transrapid guideway.

Cost comparisons of the narrow beam guideway with other maglev guideway designs—especially channel guideway designs—should be even more dramatic.[11] Channel guideway beam designs, such as the Japanese MLU system, are substantially more expensive than the narrow beam concept in that 1) the amount of material required for the channel beam to surround the vehicle is many times greater than that required for the narrow beam design and 2) channel beam designs require extensive amounts of reinforcing steel and hybrid FRP material due to the low torsion capacity of the cross-section.

4.5 Narrow beam summary and conclusions

A conservative design procedure is developed and presented for a rectangular, hollow-box concrete maglev guideway beam. The design procedure is conservative in that it considers only first order linearly elastic beam behavior. The approach is general,

[11] See subsection 2.4.2.

however, in that it allows analysis of both steel and non-magnetic hybrid FRP concrete reinforcement. A spreadsheet analysis program, *BoxCost*, is developed based on the equations presented in Sections 4.1 and 3.2. A design example presented in Section 4.2 illustrates the overall design approach.

In Section 4.3, a number of sensitivity analyses are performed using the *BoxCost* program. The analyses show that a 25 m span reinforced concrete beam cross-section with a a) width of 1.4 m, b) depth of 2.1 m, and c) wall thickness of 0.15 m is economical. The cross-section is shown to be adequate for moderate beam deflection. Beam depth increases result in less beam deflection, and typically, in lower overall beam cost. For moderate deflection requirements, changes in beam span lengths dramatically affect guideway beam frequency. Provided only moderate beam deflection constraints are imposed, increases in vehicle mass have only a minimal impact on total cost for the assumed standard beam cross-section. Also, for loadings given in Section 4.2, changes in vehicle eccentricity have little effect on beam behavior of the standard beam design. Increases in vehicle eccentricity, however, are likely to have a significant impact on more narrow beam widths and wall thicknesses.

For stringent deflection constraints—especially more stringent horizontal deflection requirements—an increase in beam width is required and results in a higher overall beam cost. The standard beam design is more sensitive to horizontal load changes and deflection constraints than to vertical influences. Additionally, though a decrease in wall thickness reduces beam mass. Its impact on overall beam cost is minimal.

Due to the high cost of the hybrid FRP non-magnetic reinforcement, it is suggested that magnetic suspension, guidance, and propulsion windings be restricted to the upper two corners of the beam cross-section. The narrow beam is shown to be at least

1/3 less massive than the Transrapid guideway beam and as a result, significant cost savings are expected.

This chapter has considered the effects vehicle loadings and magnetic winding positioning have on overall beam material costs through a number of sensitivity analyses. Chapter 5 explores the influence of vehicle loading pad configuration on guideway beam dynamic behavior.

5.0 Dynamic Analysis

5.1 Overview

This chapter focuses on the dynamic analysis of guideway beam behavior during high speed vertical maglev vehicle loading. Analysis is performed using both 1) finite element discretization and 2) a closed form mathematical solution of dynamic beam behavior. Dynamic analyses consider the first three modes of beam vibration. Only the force of the traveling vehicle (i.e. not the mass), on a simply-supported straight guideway beam is modeled in this thesis.[1] Governing equations and modeling approaches used for the analysis of an undamped, simply-supported straight maglev guideway beam, are presented in Section 5.2. Additionally, a brief discussion of beam damping behavior and material damping properties is given. Effects due to beam damping are not considered specifically in either the equation derivations or in the majority of sensitivity analyses performed. It is demonstrated that for the small percentages of damping expected in elevated maglev guideway beams, beam damping effects are not expected to be significant.[2] A dynamic sensitivity analysis is performed in Section 5.3 to demonstrate the effects of distributed versus concentrated vehicle loadings on beam response.

In addition to peak dynamic *positive* (i.e. downward) beam deflection, dynamic analyses in this chapter focus on peak *negative* (i.e. upward), and *residual* (i.e. free) beam vibration response. The formulas derived in Section 5.4 predict exact speeds at which a vehicle—having a certain loading configuration—can travel over a given beam and yet produce no residual vibration in the beam! These *convergent* vehicle velocities are shown to be determined by both beam properties and vehicle loading configurations. The beam

---

1 Future research focused on modeling the effect of vehicle mass under a variety of vehicle pad distributions and beam structural support mechanisms is recommended in Chapter 6.

2 See subsection 5.2.4.

properties which determine convergent velocities are 1) fundamental frequency, f_1, and 2) length, L. For vehicles having a fully distributed loading configuration, the vehicle length, L_v, determines additional convergent velocities. Similarly, for vehicles having discretely spaced loading pads, additional convergent velocities are determined based on a) the number of pads, n_p, b) the pad length, L_p, and c) the spacing between loading pad centroids, S_p. Section 5.4 presents mathematical proofs for the solution of convergent velocities as well as sensitivity analyses to illustrate interrelationships between vehicle loading arrangements and beam dynamic behavior.. Finally, based on the results of these analyses, the concept of *motion based design* is presented in Section 5.5. It is suggested that individual beam segments can be designed specific for an expected vehicle speed and loading configuration so as to provide superior beam behavior and longer guideway lifespan.

5.2 Fundamental guideway beam dynamic behavior

5.2.1 Governing equations

Governing equations are presented for undamped, simply-supported beam behavior. Beams are considered to have uniform mass and bending stiffness across the span length. Equations are presented for beam frequencies and mode shapes. In addition, closed form solutions that describe forced and residual (i.e. free) beam vibration response to a traveling load are derived. Forced beam response formulas are solved in closed form for a traveling single point load. Extensions to these point load equations are made to model distributed and multiple vehicle pad loadings.

Equations presented in this subsection, are incorporated into a spreadsheet analysis program entitled "mode 3". The *mode3* program, along with finite element verification plots for several vehicle speeds and loading configurations, are shown in Appendix D.

Beam frequency

For a simply supported beam with uniform cross section, mode shapes and frequencies are [Humar 90]:

$$\Phi_n(x) = \sqrt{\frac{2}{mL}} \sin\left(\frac{n\pi x}{L}\right) \qquad n = 1, 2, 3, \ldots \quad [5.1]$$

$$\omega_n = 2\pi f_n = n^2\pi^2 \sqrt{\frac{EI}{mL^4}} \qquad n = 1, 2, 3, \ldots \quad [5.2]$$

where

$\Phi_n(x)$	: nth mode shape
ω_n	: nth mode beam angular frequency (rad/sec)
f_n	: nth mode beam frequency (cycles/sec)
x	: distance along the beam
m	: uniform beam unit mass
n	: mode number

The number of theoretical vibration modes and frequencies for the beam indicated in the above equations is infinite. Typically, however, only a few modes are required to perform adequate guideway beam dynamic analysis. The required number of modes to properly model beam behavior depends not only on beam properties, but also on vehicle speeds and frequencies contained in the vehicle forcing function. Only the first three beam vibration modes are considered for the analyses performed in this thesis. As both indicated in Equation 5.2 and shown in Figure 4.3.3c, the fundamental beam frequency, f_1, decreases by L^{-2} as the beam length, L, is increased. As beam depth, h, is increased, beam bending stiffness, EI, also increases. The result is a linear increase in beam frequency, as indicated in Figure 4.3.2c. Thus, to a certain extent, it is possible to design a beam frequency to a specific value. Analyses in this chapter focus on a 25 m beam length having a 6⅔ Hz fundamental frequency.

Forced Beam Deflection

Transverse deflection response for an undamped beam having uniform mass and stiffness when subjected to a traveling point load is given by the following formula [Humar 90]:

$$u(x,t)=\frac{-2P}{mL}\sum_{n=1}^{\infty}\frac{1}{(n\pi v/L)^2-\omega_n^2}\left\{\frac{n\pi v}{L\omega_n}\sin\omega_n t-\sin\frac{n\pi v t}{L}\right\}\sin\frac{n\pi x}{L} \qquad [5.3]$$

$$n=1,2,3,\ldots,\infty;\ 0\le t\le L/v$$

where

$u(x,t)$: transverse displacement at a distance x along the beam at time t (downward deflection is considered positive)

P : force of the load

v : velocity of the traveling load

Equation 5.3 considers all beam vibration modes. It is valid when $n\pi v/L \neq \omega_n$ and for the time period that the single concentrated load is on the beam, i.e. when $0 \le t \le L/v$. The following notation is helpful in representing the beam response for the first three vibration modes:

$$\Delta=\frac{\pi x}{L};\quad \partial=\frac{-2P}{mL};\quad \beta=\frac{\pi v}{L} \qquad [5.4]$$

$$\mu_1=(\beta)^2-\omega_1^2;\quad \mu_2=(2\beta)^2-\omega_2^2;\quad \mu_3=(3\beta)^2-\omega_3^2 \qquad [5.5]$$

$$A(t)=\frac{\partial}{\mu_1}\left\{\frac{\beta}{\omega_1}\sin\omega_1 t-\sin\beta t\right\}$$

$$B(t)=\frac{\partial}{\mu_2}\left\{\frac{2\beta}{\omega_2}\sin\omega_2 t-\sin 2\beta t\right\} \qquad [5.6]$$

$$C(t)=\frac{\partial}{\mu_3}\left\{\frac{3\beta}{\omega_3}\sin\omega_3 t-\sin 3\beta t\right\}$$

Using the given notation, the transverse *deflection*, u, due to a single point load, considering the first three vibration modes, at time t and distance x along the beam is:

$$\boxed{u(x,t) = A(t)\sin\Delta + B(t)\sin 2\Delta + C(t)\sin 3\Delta} \qquad [5.7]$$

Because linearly elastic beam behavior is assumed, a distributed load can be modeled as a series of closely spaced point loads. Equation 5.7 represents forced vibration response only. To completely model a distributed load, the beam free vibration response is needed. Free vibration response is dependent on the deflection and velocity of the beam at the time the forcing function leaves the beam. These parameters are initial conditions for free vibration response. Velocity and acceleration equations for the traveling point load forcing function are obtained in a similar fashion as those for the single point forced deflection response equation (i.e. for Equation 5.7).

Forced Beam Velocity and Acceleration

To remain consistent with the forced beam deflection notation (Equations 5.4 through 5.7), the following notation is used to describe forced beam velocity and acceleration behavior:

$$\begin{aligned}
\dot{A}(t) &= \frac{\partial}{\mu_1}\{\beta\cos\omega_1 t - \beta\cos\beta t\} \\
\dot{B}(t) &= \frac{\partial}{\mu_2}\{2\beta\cos\omega_2 t - 2\beta\cos 2\beta t\} \\
\dot{C}(t) &= \frac{\partial}{\mu_3}\{3\beta\cos\omega_3 t - 3\beta\cos 3\beta t\}
\end{aligned} \qquad [5.8]$$

$$\begin{aligned}
\ddot{A}(t) &= \frac{\partial}{\mu_1}\{-\beta\omega_1\sin\omega_1 t + \beta^2\sin\beta t\} \\
\ddot{B}(t) &= \frac{\partial}{\mu_2}\{-2\beta\omega_2\sin\omega_2 t + (2\beta)^2\sin 2\beta t\} \\
\ddot{C}(t) &= \frac{\partial}{\mu_3}\{-3\beta\omega_3\sin\omega_3 t + (3\beta)^2\sin 3\beta t\}
\end{aligned} \qquad [5.9]$$

Using the notation given in Equations 5.8 and 5.9, the following equations are derived which describe beam *velocity*, and *acceleration* response, respectively, to a traveling point load in the first three modes of vibration.

$$\boxed{\dot{u}(x,t) = \dot{A}(t)\sin\Delta + \dot{B}(t)\sin 2\Delta + \dot{C}(t)\sin 3\Delta} \qquad [5.10]$$

$$\boxed{\ddot{u}(x,t) = \ddot{A}(t)\sin\Delta + \ddot{B}(t)\sin 2\Delta + \ddot{C}(t)\sin 3\Delta} \qquad [5.11]$$

Free Vibration Initial Conditions

Free (i.e. residual) vibration initial conditions due to a single point load traveling across the beam, are equal to the beam deflection and velocity at the time the load leaves the guideway, (i.e. when $t = L/v$). The following notation is used to describe these free vibration initial conditions:

$$|A| = A(L/v); \quad |B| = B(L/v); \quad |C| = C(L/v) \qquad [5.12]$$

$$|\dot{A}| = \dot{A}(L/v); \quad |\dot{B}| = \dot{B}(L/v); \quad |\dot{C}| = \dot{C}(L/v) \qquad [5.13]$$

Time during beam residual vibration response is denoted by T, where $T = t - L/v$. By definition, T is zero when $t = L/v$. Also, by definition, residual vibration equations for a single given point load are valid only when T is greater than zero for the given point load.

Residual Vibration Deflection

Beam residual vibration response equations are presented without derivation. They have been solved in closed form using general continuous beam response equations as presented by J.L. Humar for undamped free transverse vibrations of a simply-supported beam, with uniform mass and stiffness [Humar 90]. The equations are based on a modal beam analysis.

For an undamped simply-supported beam having uniform mass and stiffness, the free (or residual) vibration deflection response in the first three modes is given by Equation 5.14.

$$\begin{aligned} u(x,T) = &\left[|A|\cos\omega_1 T + \left(\frac{|\dot{A}|}{\omega_1}\right)\sin\omega_1 T\right]\sin\Delta \\ &+\left[|B|\cos\omega_2 T + \left(\frac{|\dot{B}|}{\omega_2}\right)\sin\omega_2 T\right]\sin 2\Delta \\ &+\left[|C|\cos\omega_3 T + \left(\frac{|\dot{C}|}{\omega_3}\right)\sin\omega_3 T\right]\sin 3\Delta \end{aligned} \qquad [5.14]$$

From Equation 5.14, residual beam velocity and acceleration response formulas are derived and presented as Equations 5.15 and 5.16, respectively.

$$\begin{aligned} \dot{u}(x,T) = &\left[-|A|\omega_1\sin\omega_1 T + |\dot{A}|\cos\omega_1 T\right]\sin\Delta \\ &+\left[-|B|\omega_2\sin\omega_2 T + |\dot{B}|\cos\omega_2 T\right]\sin 2\Delta \\ &+\left[-|C|\omega_3\cos\omega_3 T + |\dot{C}|\cos\omega_3 T\right]\sin 3\Delta \end{aligned} \qquad [5.15]$$

$$\begin{aligned} \ddot{u}(x,T) = &\left[-|A|\omega_1^2\cos\omega_1 T - |\dot{A}|\omega_1\sin\omega_1 T\right]\sin\Delta \\ &+\left[-|B|\omega_2^2\cos\omega_2 T - |\dot{B}|\omega_2\sin\omega_2 T\right]\sin 2\Delta \\ &+\left[-|C|\omega_3^2\cos\omega_3 T - |\dot{C}|\omega_3\sin\omega_3 T\right]\sin 3\Delta \end{aligned} \qquad [5.16]$$

Beam Vibration Response under Multiple Point Loads

The preceding beam response equations apply to a single point load traveling across a simply-supported beam. Because linear elastic beam behavior is assumed, these same equations can also be used to model distributed and discrete vehicle pad loading configurations. The modeling approach for beam response under multiple loads is to divide the vehicle loading configuration into a series of closely spaced point loads. The preceding equations, with the addition of an appropriate time offset, are used for each

given point load. Linear elastic beam behavior assumptions allow superposition of beam deflections, velocities, and accelerations for each successive point load. Thus, beam behavior due to any given vehicle loading configuration can be modeled using the equations derived for a single traveling point load.

This superposition approach has been used in a spreadsheet analysis program, developed by the author, entitled "mode3" to model the first three vibration modes of an undamped simply-supported beam for any given maglev vehicle loading configuration. The *mode3* analysis program is used to perform a variety of dynamic beam sensitivity analyses in this thesis. In addition to *mode3* simulations, analyses have been performed using the ADINA dynamic finite element analysis program [ADINA 89]. The finite element ADINA analyses serve as verification of *mode3* results . The *mode3* program and dynamic beam response examples are shown in Appendix D.

5.2.2 Dynamic beam behavior under a two-point vehicle load

An example application of *mode3* to guideway beam behavior is useful. Figure 5.2.1 represents a 30 m maglev vehicle traveling at 125 m/s. The mass of the vehicle is 2.0 tonne/m and is transferred to the guideway by two 294.2 kN point loads located at each end of the vehicle. For this example, the vehicle travels over a beam 25 m in length with a fundamental frequency, f_1 of 6.67 Hz, and a vertical bending stiffness, EI, of 1.9952×10^{10} N•m^2.

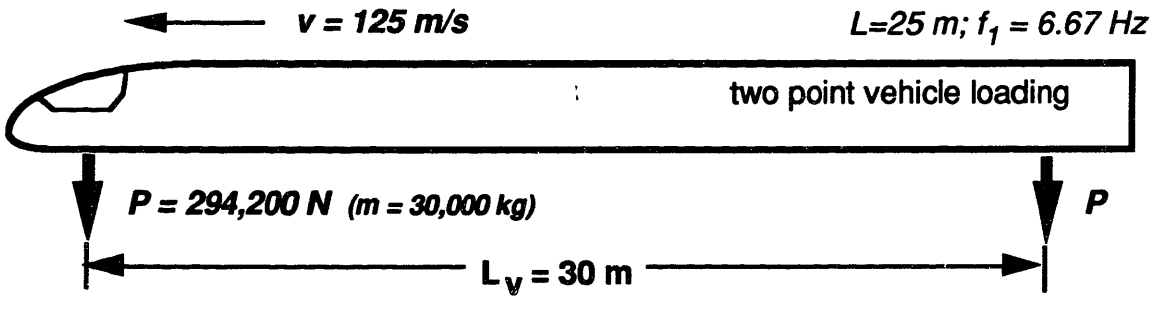

Figure 5.2.1 Two Point Vehicle Loading

Figure 5.2.2 shows the dynamic response of the beam midspan when it is subjected to the moving two-point concentrated vehicle load shown in Figure 5.2.1. The plot shown in Figure 5.2.2 is obtained using the *mode3* analysis program. Due to the discretization of the beam element, the point loads are actually modeled as two 1.25 m, 235.3 kN/m pressure loads, separated by a 27.5 m gap.[3]

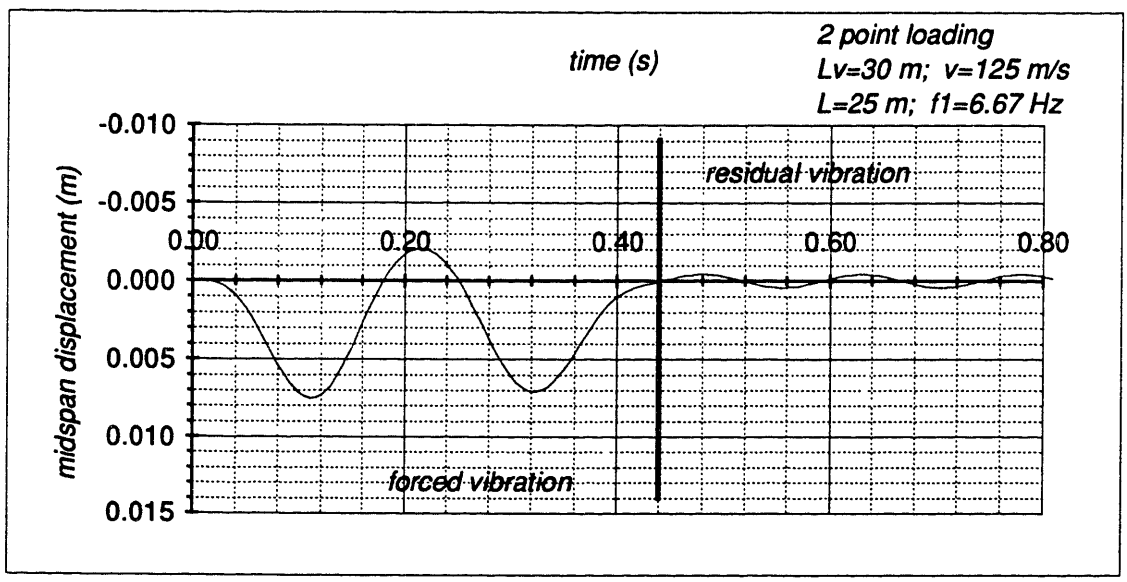

Figure 5.2.2 Beam Dynamic Response (Two Point Loading, v=125m/s)

As indicated in Figure 5.2.2, the beam has a peak positive (i.e. downward) midspan deflection of 7.53 mm at $t = 0.110$ s during forced vibration response. The peak negative (i.e. upward) deflection during forced response occurs at $t = 0.215$ s, and is equal to 2.06 mm. When $t > 0.440$ s, the beam is in residual, or free, vibration. In Figure 5.2.2, the bold vertical line shown at $t = 0.440$ s represents the time at which the trailing edge of the vehicle leaves the guideway beam. At this time, the beam changes from forced to residual vibration response. The maximum residual deflection of the beam in this example is 0.44 mm.

---

[3] This results in a pad centroid spacing, S_p , of 28.75 m. (See Section 5.4.)

5.2.3 Dynamic amplification factors

Positive Dynamic Amplification Factor

The positive dynamic amplification factor, *DAF*, is the ratio of the maximum positive beam deflection under dynamic loading to the maximum static beam deflection under a fully distributed load, as indicated in the following formula.

$$DAF = \frac{\Delta_{dyn.pos}}{\Delta_{stat.pos}} \qquad [5.17]$$

where

$\Delta_{dyn.pos}$: maximum positive (i.e. upward) dynamic beam deflection

$\Delta_{stat.pos}$: maximum static beam deflection under a fully distributed load

For the 60 tonne, 30 m maglev vehicle shown in Figure 5.2.1, an equivalent fully distributed load, w_v, is 19.6 kN/m (see Figure 5.3.1). Thus, for this example, $\Delta_{stat.pos}$ is equal to 5.00 mm (i.e. $5w_vL^4/384EI$), and the DAF is equal to 1.51.

Both the time it takes for a vehicle to cross a beam span and the fundamental beam frequency, play significant roles in determining the DAF for a beam subjected to a passing vehicle. For concentrated vehicle loads, the "crossing frequency", V_c, relates the period of the first beam vibration mode, $1/f_1$, to the time required for the front of the vehicle to cross the beam span [Richardson and Wormley 74]. The crossing frequency is given by the following equation:

$$V_c = \frac{v}{f_1 L}. \qquad [5.18]$$

where v is the velocity of the vehicle and L is the span length. A plot of DAF versus crossing frequency is shown in Figure 5.2.3. For the analyses in this chapter, f_1 is assumed to be equal to 6⅔ Hz and L equal to 25 m. With these beam properties, a vehicle speed of 125 m/s gives a crossing frequency of 0.75 according to Equation 5.18.

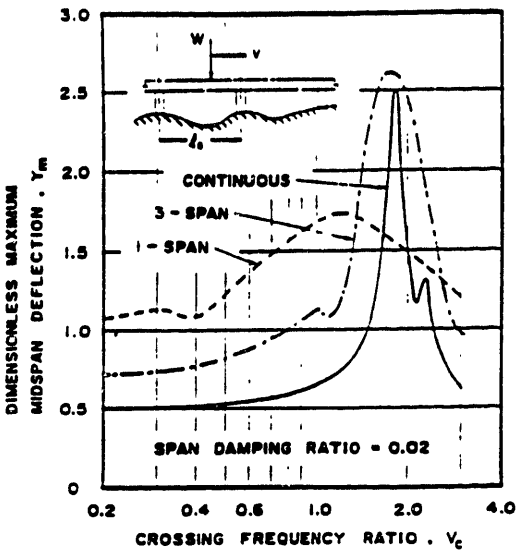

Source: [Richardson and Wormley 74]

Figure 5.2.3 Dynamic Amplification Factor vs. Crossing Frequency

As shown in Figure 5.2.3, a V_c of 0.75 on a simple span (i.e. "1-span" shown in the figure), has a DAF of approximately 1.52. Thus, the 1.51 DAF factor obtained from the *mode3* spreadsheet analysis program for the concentrated vehicle loading, shown in Figure 5.2.1, corresponds with the Richardson and Wormley plot shown in Figure 5.2.3.

Figure 5.2.3 indicates that the DAF's for continuous and semi-continuous spans are significantly less than for simply-supported spans at crossing frequencies less than 1.00.[4] In addition, Figure 5.2.3 indicates that a crossing frequency of 0.40 for a single span beam results in a minimum dynamic amplification factor. For speeds of approximately 125 m/s, however, a crossing frequency of 0.40 is likely to be impossible to achieve with an elevated maglev guideway system having spans greater than 20 m.[5] A desirable design goal is simply to minimize V_c as much as is practical (e.g. to less than 0.80) in order to minimize positive dynamic amplification effects.

---

[4] A number of additional factors have led to the choice of a simple span for the analyses in this thesis (see subsection 2.4.2).

5 For "at-grade" elevations (i.e. <= 2 m elevations), beam spans less than 20 m are likely to be used. Thus, higher frequencies for these shorter "at-grade" spans are possible (see Figure 4.3.3c).

Negative and Residual Dynamic Amplification Factor

Also important for maglev guideway design are two additional dynamic amplification measures obtained from the dynamic beam analysis. The maximum negative dynamic amplification factor, *NDAF*, is the ratio of the maximum upward, or "springback", beam deflection to maximum static deflection. Similarly, the maximum residual vibration factor, *RDAF*, is the ratio of maximum beam deflection occurring during residual, or free, vibration to the static deflection. These two amplification factors are represented in the following equations.

$$NDAF = \frac{\Delta_{dyn.neg}}{\Delta_{stat.pos}} \qquad [5.19]$$

$$RDAF = \frac{\Delta_{dyn.res}}{\Delta_{stat.pos}} \qquad [5.20]$$

where

$\Delta_{dyn.neg}$: maximum negative (i.e. upward) dynamic beam deflection

$\Delta_{dyn.res}$: maximum beam deflection during residual vibration

The higher the NDAF, the more compressive concrete reinforcement that is required—including non-magnetic FRP reinforcement. In addition to increased requirements for reinforcement, higher RDAF values lead to greater guideway fatigue, and thus, to shorter guideway lifespans. For the two point loading case shown in Figures 5.2.1 and 5.2.2, the NDAF and RDAF are equal to 0.41 and 0.09, respectively.

5.2.4 Damping effects

Should any distortion remain once a vehicle passes a beam, the beam will experience residual vibration. Residual vibration must be minimized for the sake of vehicle ride quality and beam fatigue loading constraints. Damping mechanisms in the beam are one means of reducing residual vibrations. However, only a small amount of

passive damping can be expected in an elevated guideway beam element. Typical absolute damping percentages—i.e. the percentage decrease of maximum deflection amplitude in one beam oscillation—for such structures range from 1% to 2%.

Exact damping properties for structural materials are somewhat difficult to determine. In general, steel is not a good material for damping. Concrete, though considered better than steel, achieves a great deal of its damping only when it is allowed to crack. Due to durability concerns, the maglev guideway beam element is not allowed to crack. Therefore, the damping potential of concrete is not likely to be high for maglev guideway applications. Glass alone is poor in damping. In addition, glass is highly susceptible to fatigue loadings resulting from residual vibrations. However, when glass fibers are pultruded in an epoxy matrix to form a composite, the resulting GFRP material has fairly good damping properties.[6] Carbon, either alone as a fiber, or pultruded to form CFRP, is an excellent damping material. In addition, carbon is virtually insensitive to fatigue loadings. The limiting factor with carbon is its high cost.

Figure 5.2.4 shows beam midspan dynamic behavior for the same two point vehicle loads shown in Figure 5.2.1 traveling at 150 m/s over the 25 m beam. The figure shows the effects of 0%, 1%, 2%, and 5% beam damping. The plots have been generated using the ADINA dynamic finite element analysis program [ADINA 89]. Rayleigh damping is assumed [Bathe 82].

The beam deflection response shown in Figure 5.2.4 is somewhat of an extreme case. Damping effects typically are less critical for more distributed vehicle loads and other vehicle speeds. Even for this relatively extreme vehicle loading case, the effect of beam damping on midspan deflection is minor for beam damping of less than 2%.

---

6 Long term properties of GFRP reinforcement in concrete under cyclic loadings presently are not well documented. Currently, GFRP use is restricted to low stress levels. (See Section 3.2.).

Because beam damping of greater than 2% is not expected for the maglev guideway, the remaining analyses in this chapter neglect beam damping effects.

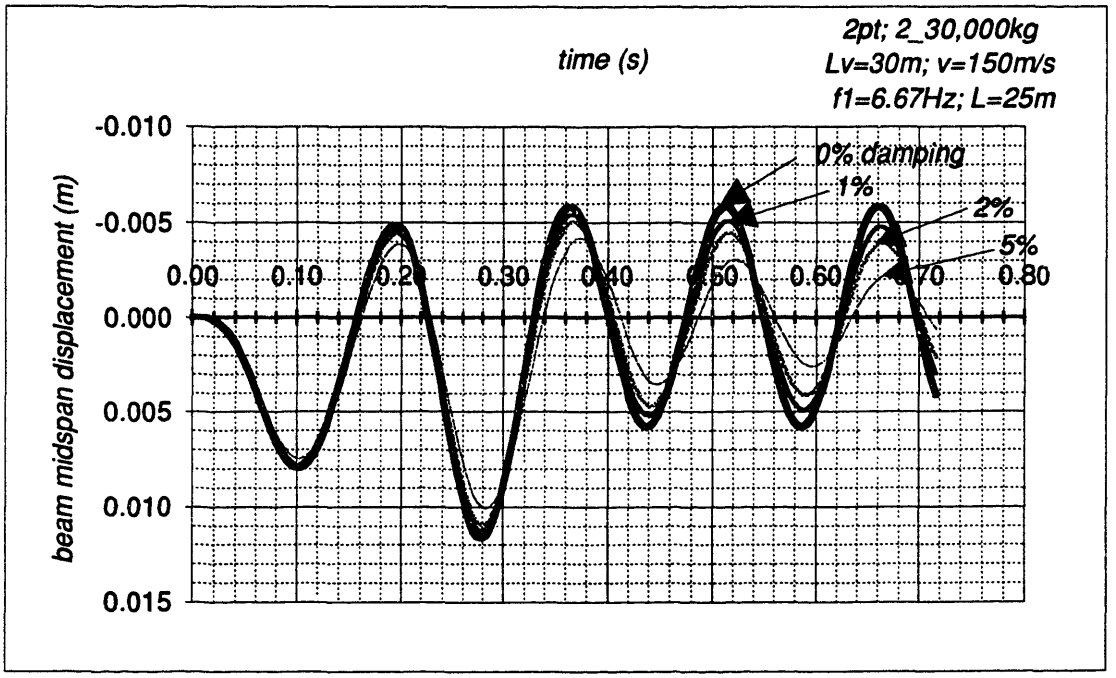

Figure 5.2.4 Damping Effects on Guideway Beam Behavior

5.3 Concentrated vs. distributed vehicle loading

The positive dynamic amplification factor, DAF, values shown in Figure 5.2.3 are based on concentrated (i.e. point) loads. This section demonstrates that both the positive and negative dynamic amplification factors, DAF and NDAF, respectively, can be reduced considerably when a fully distributed vehicle loading arrangement is employed.

Figure 5.3.1 shows a fully distributed vehicle loading, where the 2 tonne/m vehicle mass produces a 19,613 N/m fully distributed force traveling across a 25 m, 6⅔ Hz beam.[7] Figure 5.3.2 shows the dynamic beam response when it is subjected to this fully distributed vehicle load at 125 m/s. The maximum dynamic midspan deflection of

7 Note that only the force of the vehicle is modeled in the analyses of this thesis.

5.40 mm occurs at $t = 0.175$ s. Thus, according to Equation 5.17, the maximum positive dynamic amplification factor for the fully distributed load case is 1.08. In this case, the maximum negative beam deflection of 0.78 mm is equal to the maximum residual vibration. Using Equations 5.19 and 5.20, the NDAF and the RDAF for this example are both equal to 0.16.

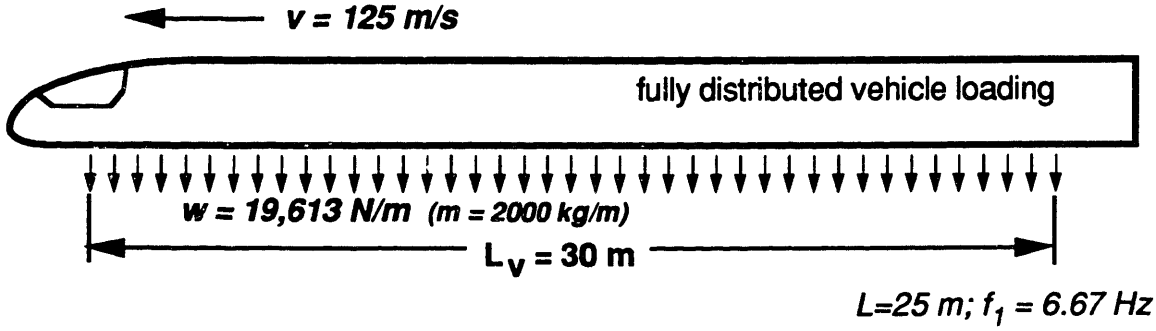

Figure 5.3.1 Fully Distributed Vehicle Loading

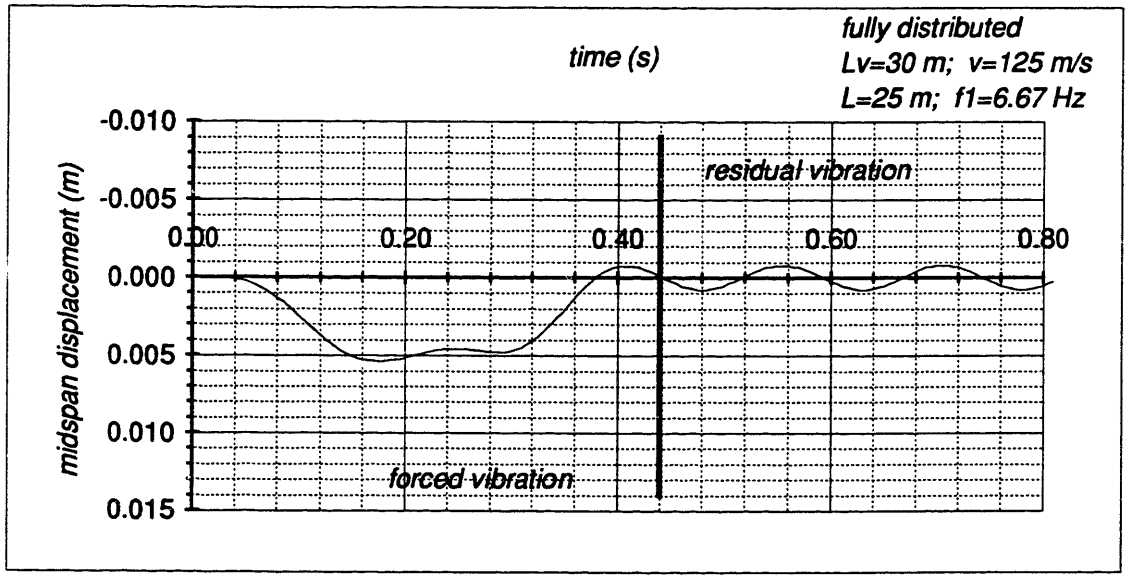

Figure 5.3.2 Beam Dynamic Response (Fully Distributed Loading)

Thus, by fully distributing the vehicle load, the DAF is reduced by 28% (i.e. from 1.51 to 1.08) and the NDAF is reduced 61% (i.e. from 0.41 to 0.16). For this example, the RDAF is actually increased by the fully distributed vehicle load. The next section shows

that residual vibrations are determined not only by the distribution of vehicle loads, but also by the spacing between loading pads.

Figure 5.3.3 presents the dynamic amplification factor for the 25 m simply-supported span used in the previous two examples. The figure shows that as the loading pad configuration for the 30 m vehicle ranges from two concentrated loads[8] to a fully distributed vehicle load, the DAF decreases from 1.51 to 1.08. The highest DAF that occurs in this example is at a vehicle load distribution factor of 0.375 (i.e. a pad length, L_p, of 5.625 m). The DAF for this vehicle configuration is 1.73. Also shown in Figure 5.3.3 is the effect vehicle load distribution has on both the NDAF and the RDAF for this example. The figure indicates that the NDAF is significant for vehicles having large gaps between loading pads. As the gap between loading pads decreases, the maximum negative beam deflection occurs during residual vibration. Thus, for closely spaced vehicle loading pads, NDAF is equal to RDAF.

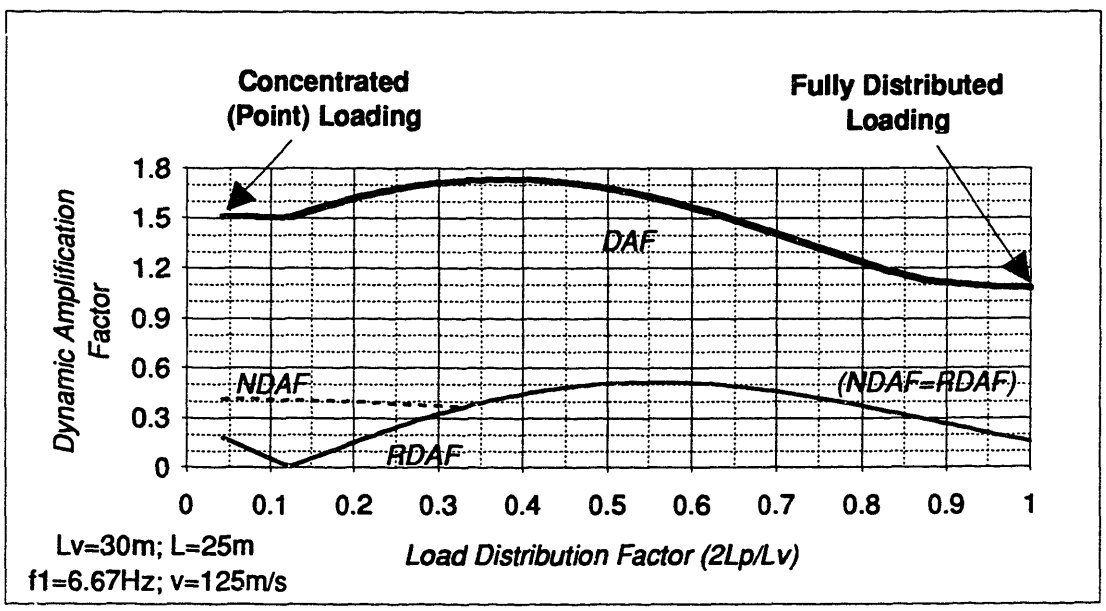

Figure 5.3.3 Dynamic Amplification Factor: Point vs. Distributed Loadings

[8] Actually, each concentrated load is modeled with an L_p of 1.25 (see Section 5.2).

5.4 Convergent velocities

In order to reduce guideway fatigue and the amount of non-magnetic reinforcement required, it is helpful to cancel both negative and residual vibrations when possible. As indicated in Figures 5.2.2 and 5.3.2, negative beam deflections can occur during both forced and residual vibration response. Adequate vehicle load distribution can eliminate negative deflections during forced vibration response. However, elimination of residual oscillations is more complicated.

This section demonstrates that residual vibrations are dependent on 1) beam frequency, 2) beam length, 3) vehicle loading configuration, and 4) vehicle speed. Vehicle speeds at which beam residual vibrations are completely canceled are termed *convergent* velocities, v^*. In this section, closed form solutions are derived in order to predict when convergent velocities occur. Examples are presented and sensitivity analyses are performed to demonstrate the usefulness of the derived equations in predicting convergent beam behavior. Based on these analyses, the concept of motion-based design—where individual beam segments are designed for specific vehicle speed and loading configurations—is presented in Section 5.5.

5.4.1 Beam length influence

For conditions where a single point load exits a given beam and where no beam deflection, velocity, or acceleration occurs, no residual beam vibration will result. In order to determine when such a condition occurs, an evaluation of zero deflection conditions for the first three modes of beam vibration is performed.

Beam deflection, $u(x,t)$ in Equation 5.7 is zero when $A(t)$, $B(t)$, and $C(t)$ are all equal to zero. At $t = \frac{L}{v}$, $\beta t = \pi$, and $\omega_1 t = \frac{\pi^2}{Lv}\sqrt{\frac{EI}{m}}$. Thus, assuming velocity is positive, $A(t)$ is zero when $\sin\omega_1 t$ is zero. Since $\sin\omega_1 t$ is zero when $\omega_1 t = \lambda\pi(\lambda = 1,2,3,...)$,

$\sin \omega_1 t$ is zero when $v = \frac{\pi}{\lambda L}\sqrt{\frac{EI}{m}} = (\lambda = 1,2,3,...)$. Thus, the set of convergent deflection velocities for the first mode of vibration due to beam length is:

$$v^*_{L-\Delta 1} = \frac{2Lf_1}{\lambda} \quad (\lambda = 1,2,3,...) \qquad [5.21]$$

Similarly, the sets of convergent deflection velocities due to beam length for the second and third modes of vibration are found to be:

$$v^*_{L-\Delta 2} = \frac{8Lf_1}{\lambda} \quad (\lambda = 1,2,3,...)$$
$$v^*_{L-\Delta 3} = \frac{18Lf_1}{\lambda} \quad (\lambda = 1,2,3,...) \qquad [5.22]$$

The set of first mode velocities (i.e. Equation 5.21) is a subset of the second, third, and all higher frequency mode sets. Thus, convergent deflection velocities can be represented by the fundamental mode case (Equation 5.21).

For zero beam velocity due to beam length, the following convergent vehicle velocity conditions are found:

$$v^*_{L-v1} = \frac{2Lf_1}{2\lambda + 1} \quad (\lambda = 1,2,3...)$$
$$v^*_{L-v2} = \frac{8Lf_1}{2\lambda + 2} \quad (\lambda = 1,2,3...) \qquad [5.23]$$
$$v^*_{L-v3} = \frac{18Lf_1}{2\lambda + 3} \quad (\lambda = 1,2,3...)$$

Though the fundamental set of velocities for zero beam velocity conditions is a subset of the higher frequency mode sets, $v^*_{L-\Delta 1}$ is not equal to v^*_{L-v1}. The interaction of these two sets is $\frac{2Lf_1}{2\lambda + 1} \quad (\lambda = 1,2,3,...)$.

Finally, beam convergent accelerations due to beam length, v^*_{L-an}, occur when beam convergent deflections due to beam length occur (Equations 5.21 and 5.22). These relationships are represented by Equation 5.24.

$$v^*_{L-a1} = v^*_{L-\Delta 1}$$
$$v^*_{L-a2} = v^*_{L-\Delta 2} \qquad [5.24]$$
$$v^*_{L-a3} = v^*_{L-\Delta 3}$$

Thus, the set of convergent vehicle velocities due to beam length and frequency is found by the following equation.

$$\boxed{v^*_L = \frac{2Lf_1}{2\lambda + 1} \quad (\lambda = 1,2,3,...)} \qquad [5.25]$$

5.4.2 Vehicle length influence (for fully distributed vehicle loads)

The mathematical derivation of convergent velocities due to the vehicle length contribution of a fully distributed vehicle is performed in this subsection. Figure 5.4.1 illustrates the solution approach. The fully distributed load is represented by a time series of individual point loads. The time separation between loads is $\frac{a}{v}$, and the total vehicle length, L_v, is equal to $n_{pt}a$, where a is the distance between successive point loads, and n_{pt} is the total number of point loads used to represent the fully distributed load.

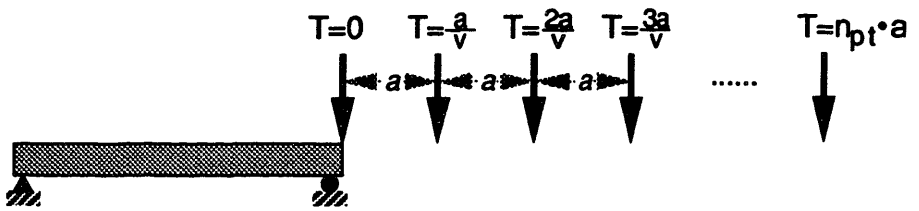

Figure 5.4.1 Time Series of Distributed Vehicle Loads

To determine conditions at which stationary beam conditions occur, it is helpful to represent the beam deflection in terms of f_1. This is performed in the following equation which represents free beam deflection in the first mode of vibration.

$$u_1(x,T) = \frac{-Pv}{m\pi^2 L^2 f_1}\left[\frac{1}{\left(\frac{v}{L}\right)^2 - 4f_1^2}\right]\left\{\left(\sin\frac{2\pi f_1 L}{v}\right)\cos 2\pi f_1 T + \left(\cos\frac{2\pi f_1 L}{v} + 1\right)\sin 2\pi f_1 T\right\}\sin\frac{\pi x}{L}$$

[5.26]

To determine the convergent time, T^*, at which $u(x,T)=0$ for a successive number of equally spaced point loads, the following equation must be satisfied:

$$\begin{aligned}
0 = &\left(\sin\frac{2\pi f_1 L}{v}\right)\cos 2\pi f_1(0) \quad + \left(\cos\frac{2\pi f_1 L}{v}+1\right)\sin 2\pi f_1(0) \\
&+(\quad '' \quad)\cos 2\pi f_1\left(\frac{a}{v}\right) \quad +(\quad '' \quad)\sin 2\pi f_1\left(\frac{a}{v}\right) \\
&+(\quad '' \quad)\cos 2\pi f_1\left(\frac{2a}{v}\right) +(\quad '' \quad)\sin 2\pi f_1\left(\frac{2a}{v}\right) \\
&+(\quad '' \quad)\cos 2\pi f_1\left(\frac{3a}{v}\right) +(\quad '' \quad)\sin 2\pi f_1\left(\frac{3a}{v}\right) \\
&\vdots \qquad\qquad\qquad\qquad \vdots \\
&+(\quad '' \quad)\cos 2\pi f_1\left(\frac{n_{pt}a}{v}\right)+(\quad '' \quad)\sin 2\pi f_1\left(\frac{n_{pt}a}{v}\right)
\end{aligned} \qquad [5.27]$$

For Equation 5.27 to be satisfied, both $\sum_{i=0}^{n_{pt}}\cos 2\pi f_1\frac{ia}{v}$ and $\sum_{i=0}^{n_{pt}}\sin 2\pi f_1\frac{ia}{v}$ must equal zero. These two summations equal zero when $f_1 n_{pt}a/v=\lambda \quad (\lambda=1,2,3,...)$. Thus, T_1^* occurs when $L_v=\frac{\lambda v}{f_1}$ $(\lambda=1,2,3,...)$. The convergent deflection velocities for the first mode of vibration due to the fully distributed vehicle length are:

$$v^*_{L_v-\Delta 1}=\frac{L_v f_1}{\lambda} \quad (\lambda=1,2,3,...) \qquad [5.28]$$

In a similar manner, convergent deflection velocities for the second and third modes are found to be:

$$\begin{aligned}
v^*_{L_v-\Delta 2}&=\frac{4L_v f_1}{\lambda} \quad (\lambda=1,2,3,...) \\
v^*_{L_v-\Delta 3}&=\frac{9L_v f_1}{\lambda} \quad (\lambda=1,2,3,...)
\end{aligned} \qquad [5.29]$$

Thus, the set of first mode deflection convergent velocities due to distributed vehicle length, given by Equation 5.28, is a subset of all higher first mode deflection velocity sets.

In a similar manner, it can be shown that Equation 5.28 is a subset of beam velocity and acceleration convergent velocities due to distributed vehicle length. Thus, the set of convergent velocities determined by distributed vehicle length is given by the following equation.

$$v^*_{L_v} = \frac{L_v f_1}{\lambda} \quad (\lambda = 1,2,3,...) \qquad [5.30]$$

5.4.3 Vehicle loading pad influence

Two sets of convergent velocities result from vehicles having evenly spaced loading pads of equal lengths. The first set is due to the length of a single distributed loading pad, L_p. Convergent velocity derivation for vehicle pad length is identical to that for fully distributed vehicle length, L_v. Thus, the equation representing the set of convergent velocities due to pad length is:

$$v^*_{L_p} = \frac{L_p f_1}{\lambda} \quad (\lambda = 1,2,3,...) \qquad [5.31]$$

For expected maglev speeds and guideway fundamental frequencies, the convergent velocities given by Equation 5.31 are useful only when the distributed pad length, L_p, is relatively long. A second set of convergent velocities results as the gap length, L_g, between vehicle loading pads is varied. Specifically, convergent velocities are dependent on the distance between the centroids of the pads, S_p. Figure 5.4.2 illustrates the method used to derive the closed form solution for convergent velocities based on S_p.

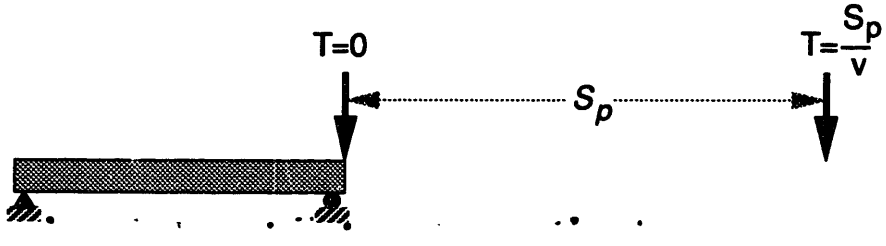

Figure 5.4.2 Time Series of Discrete Vehicle Loading Pads

Figure 5.4.2 shows a two-point, vehicle load with a separation between loads of S_p. Similar to the approach for a fully distributed vehicle load, convergent deflection velocities due to pad spacing, S_p, are found when the following equation is satisfied.

$$0=\left(\sin\frac{2\pi f_1 L}{v}\right)\cos 2\pi f_1(0) \quad +\left(\cos\frac{2\pi f_1 L}{v}+1\right)\sin 2\pi f_1(0)$$
$$+(\quad '' \quad)\cos 2\pi f_1\left(\frac{S_p}{v}\right) \quad +(\quad '' \quad)\sin 2\pi f_1\left(\frac{S_p}{v}\right) \qquad [5.32]$$

Equation 5.32 is satisfied when $\cos 2\pi f_1\left(\frac{S_p}{v}\right)=-1$ and $\sin 2\pi f_1\left(\frac{S_p}{v}\right)=0$. Both conditions are satisfied when $S_p=\frac{(2\lambda-1)v}{2f_1}$ $(\lambda=1,2,3,...)$. Thus, for a two point vehicle load, deflection residual vibrations in the first mode are canceled when the following equation is satisfied.

$$v^*_{S_p.2pt-\Delta 1}=\frac{2S_p f_1}{2\lambda-1} \quad (\lambda=1,2,3,...) \qquad [5.33]$$

Deflection convergent velocities for the two point load in the second and third beam vibration modes can be similarly shown to be:

$$v^*_{S_p.2pt-\Delta 2}=\frac{8S_p f_1}{2\lambda-1} \quad (\lambda=1,2,3,...)$$
$$v^*_{S_p.2pt-\Delta 3}=\frac{18S_p f_1}{2\lambda-1} \quad (\lambda=1,2,3,...) \qquad [5.34]$$

Though the first mode set of convergent velocities is a subset of the third mode set, it is not a subset of the second mode set. Thus, an exact equation representing absolute cancellation of beam vibration for all beam vibration modes due to pad spacing is not possible. However, the second mode of vibration principally effects the quarter points (i.e. $x=L/4,3L/4$) of the beam. Because the first beam vibration mode dominates beam behavior, Equation 5.33 can be assumed to represent near-zero deflection vibration conditions for the entire beam under two-point vehicle loading.

In a similar fashion, velocities and accelerations can be shown mathematically to be canceled when these same velocity sets are present. Thus, for a two point load, near-zero beam residual vibration conditions occur during the following set of vehicle vibrations.

$$v^{*}_{S_p,2pt} = \frac{2S_p f_1}{2\lambda - 1} \quad (\lambda = 1,2,3,...) \qquad [5.35]$$

It is clear from the preceding derivation that the convergent velocities are independent of pad length, L_p, for the two loading pads—provided this length is the same for both pads. Thus, the only vehicle load arrangement contribution to this set of vehicle convergent velocities is the centroid spacing of the pads, S_p. If n_p is taken as the number of equally spaced vehicle loading pads, a similar approach shows that when pad centroids are spaced in such a way that $\sum_{i=0}^{n_p} \cos 2\pi f_1 \left(\frac{iS_p}{v}\right) = -1$ and $\sum_{i=0}^{n_p} \sin 2\pi f_1 \left(\frac{iS_p}{v}\right) = 0$, near convergence is reached in the beam. These two conditions are satisfied when $S_p = \frac{\lambda v}{n_p f_1}$ $\left(\lambda = 1,2,3,... \text{ and } \lambda \neq in_p;\ i = 1,2,3,...\right)$. The generalized formula for convergent velocities due to the spacing of loading pads—for any number of pads—is:

$$\boxed{v^{*}_{S_p} = \frac{n_p S_p f_1}{\lambda} \quad \left(\lambda = 1,2,3,... \text{ and } \lambda \neq in_p;\ i = 1,2,3,...\right)} \qquad [5.36]$$

Velocities represented by Equation 5.36 are considered to be near convergence, as not all beam vibration modes are completely canceled when the equation is satisfied. A vibration mode, n, is canceled when the following condition is satisfied.

$$n^2 \neq in_p \quad (i = 1,2,3,...) \qquad [5.37]$$

Thus, for a two pad vehicle, every odd numbered vibration mode is canceled. The same is true of four pad vehicles. For three pad vehicles, every third vibration mode remains in effect at convergent velocities obtained form Equation 5.36. Similarly, for five and six pad vehicles, every fifth and sixth mode, respectively, remains in effect for

convergent velocities given by Equation 5.36. Equation 5.37 shows that all first mode beam vibration response is canceled at convergent velocities obtained from Equation 5.36—independent of the number of loading pads used. Table 5.4.1 lists particular vibration modes canceled at convergent velocities determined by Equation 5.36.

Table 5.4.1 Vibration modes canceled at S_p convergent velocities

✔ *vibration mode is canceled when* $n^2 \neq in_p$ $(i = 1,2,3,\ldots)$											
						n_p = number of loading pads; n = mode number					
n \ n_p	**2**	**3**	**4**	**5**	**6**	**7**	**8**	**9**	**10**	**11**	**12**
1	✔	✔	✔	✔	✔	✔	✔	✔	✔	✔	✔
2		✔		✔	✔	✔	✔	✔	✔	✔	✔
3	✔		✔	✔	✔	✔	✔		✔	✔	✔
4		✔		✔	✔	✔		✔	✔	✔	✔
5	✔	✔	✔		✔	✔	✔	✔	✔	✔	✔
6				✔		✔	✔		✔	✔	
7	✔	✔	✔	✔	✔		✔	✔	✔	✔	✔
8		✔		✔	✔	✔		✔	✔	✔	✔
9	✔		✔	✔	✔	✔	✔		✔	✔	✔
10		✔			✔	✔	✔	✔		✔	✔
11	✔	✔	✔	✔	✔	✔	✔	✔	✔		✔
12				✔		✔			✔	✔	

In general, as indicated in Table 5.4.1, the more number of pads, n_p, the more beam vibration modes that are canceled. However, the first mode of vibration is by far the dominant mode for guideway structures. Vibration modes higher than three are typically inconsequential in beam design. Also, the greater the number of pads used, the longer the vehicle must be to obtain convergent velocities due to the pad length, L_p (see Equation 5.31).

5.4.4 Equation derivations summary

Summarizing the proofs of the above subsections, the convergent vehicle velocities are found in the following situations. Complete cancellation of beam residual vibrations occur according to the following equations:

Beam Length

$$v_L^* = \frac{2Lf_1}{2\lambda + 1} \quad (\lambda = 1,2,3,\ldots) \qquad \textit{(all vehicles) [5.25]}$$

Vehicle Length

$$v_{L_v}^* = \frac{L_v f_1}{\lambda} \quad (\lambda = 1,2,3,\ldots) \qquad \textit{(fully distributed vehicle loads) [5.30]}$$

Pad Length

$$v_{L_p}^* = \frac{L_p f_1}{\lambda} \quad (\lambda = 1,2,3,\ldots) \qquad \textit{(vehicle pads) [5.31]}$$

Near-zero cancellation occurs at velocities according to the following equation for vehicles having equally spaced loading pads of equal length. Complete beam residual vibration cancellation occurs at mode, n, when $n^2 \neq in_p$ $(i = 1,2,3,\ldots)$.

Pad Spacing

$$v_{S_p}^* = \frac{n_p S_p f_1}{\lambda} \quad \left(\lambda = 1,2,3,\ldots \text{ and } \lambda \neq in_p;\ i = 1,2,3,\ldots\right) \qquad \textit{(vehicle pads) [5.36]}$$

5.4.5 Pad distribution example cases

Figure 5.4.3 shows a vehicle with three 5 m loading pads each separated by 7.5 m. The distance between pad centroids, S_p, is 12.5 m. The fundamental frequency of the beam is 6.67 Hz. According to Equation 5.36, the set of convergent vehicle spacings for the 90 m/s vehicle speed, is: $S_p^* = \lambda(4.5\text{m})$, where $\lambda = 1,2,4,5,7,\ldots$, or 4.5 m, 9.0 m, 18.0 m, 22.50 m, 31.50 m, etc. Any of these pad spacings can be expected to result in near-zero beam residual vibrations. The vehicle pad spacing, S_p, of 12.5 m for the vehicle

in Figure 5.4.3, however, does not match any of these 90 m/s convergent pad spacings and therefore convergence is not expected. This is confirmed in Figure 5.4.4 where the maximum midspan deflection in residual vibration is shown to be over 50% of the maximum midspan positive deflection during forced vibration.

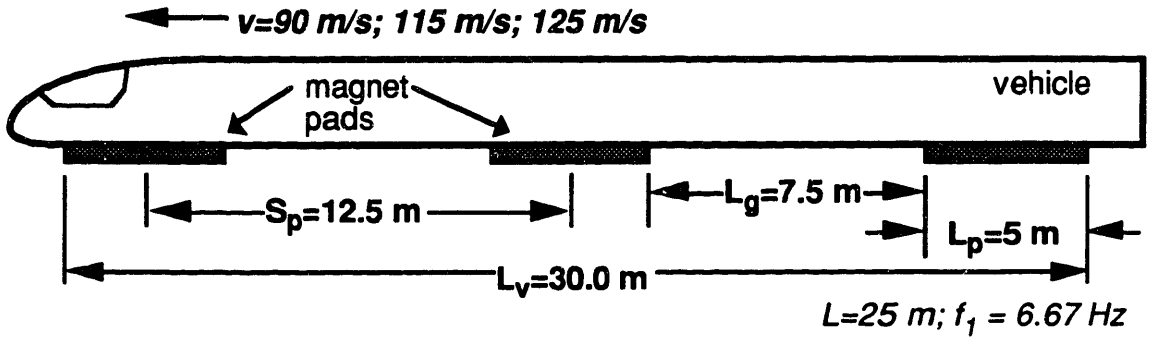

Figure 5.4.3 Three Pad Vehicle, Sp = 12.5 m (Lv= 30 m)

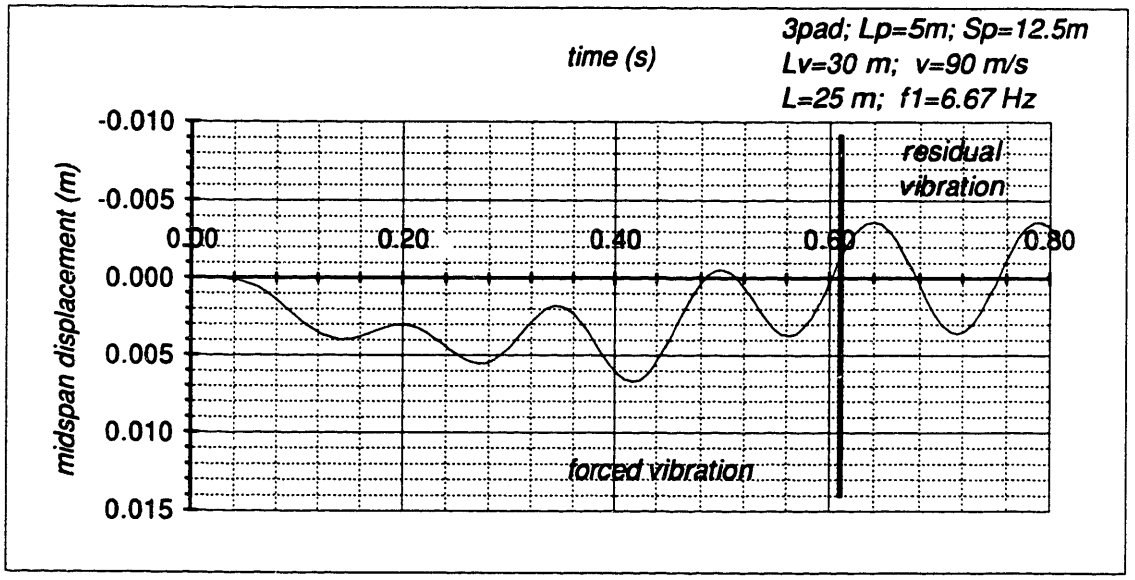

Figure 5.4.4 Beam Dynamic Response for Sp =12.5 m (v=90 m/s)

Figure 5.4.5 shows the beam midspan dynamic response for the same vehicle traveling at 115 m/s. At this speed, the convergent pad spacings of: $S_p^* = n(5.75\,\mathrm{m})$, where $n = 1,2,4,5,7,\ldots$, or 5.75 m, 11.5 m, 23.0 m, 28.75 m, 40.25 m, etc., can be expected to result in near-zero beam residual vibrations.

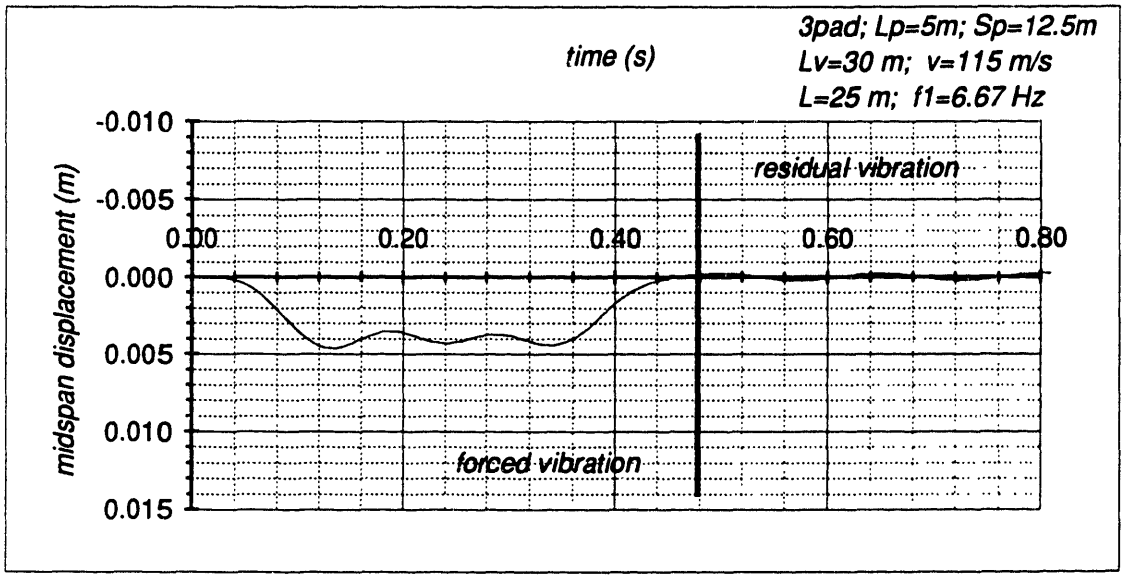

Figure 5.4.5 Beam Dynamic Response for Sp =12.5 m (v=115 m/s)

Because the vehicle pad spacing, S_p, of 12.5 m is approximately equal to the 11.5 m convergent pad spacing, it is expected that residual vibrations at this speed will be minimal. Figure 5.4.5 confirms this expectation as the maximum beam midspan deflection during residual vibration is less than 0.5 mm. This small beam midspan deflection is insignificant.

When the vehicle travels at 125 m/s on the same beam, convergent pad spacings of: $S_p^* = n(6.25\text{m})$, where $n = 1,2,4,5,7,\ldots$, or 6.25 m, 12.5 m, 25.0 m, 31.25 m, 43.75 m, etc., are expected to result in near-zero beam residual vibrations. Since the S_p of the vehicle is equal to one of these convergent spacings, no beam residual vibration is expected at this speed. This expectation is confirmed in Figure 5.4.6, where the beam residual deflection response to the given vehicle load traveling at 125 m/s is shown to be completely canceled!

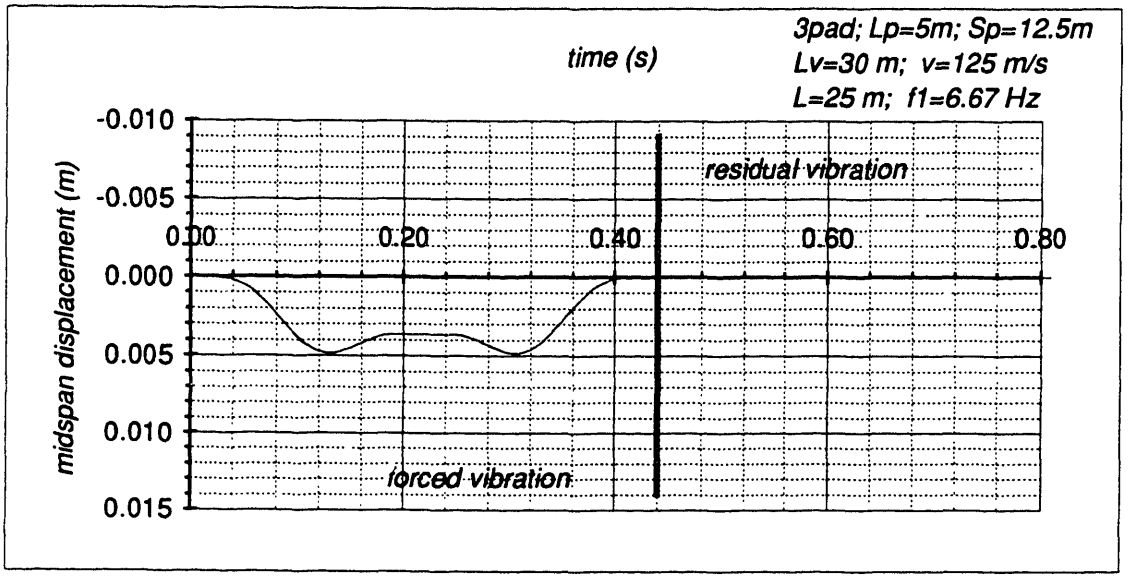

Figure 5.4.6 Beam Dynamic Response for Sp =12.5 m (v=125 m/s)

Figures 5.4.7 and 5.4.8 demonstrate that convergence criteria is indeed dependent on the vehicle pad spacing, S_p, and not simply on vehicle velocity, v. Figure 5.4.7 shows a 35 m long vehicle with three 5 m pads separated by 10 m producing a pad spacing, S_p, of 15.0 m. The response of the 25 m, 6⅔ beam to the vehicle shown in Figure 5.4.7 traveling at 125 m/s, is shown in Figure 5.4.8. When compared with Figure 5.4.6, Figure 5.4.8 shows that a slightly different loading pad arrangement can produce a drastically different dynamic beam response.

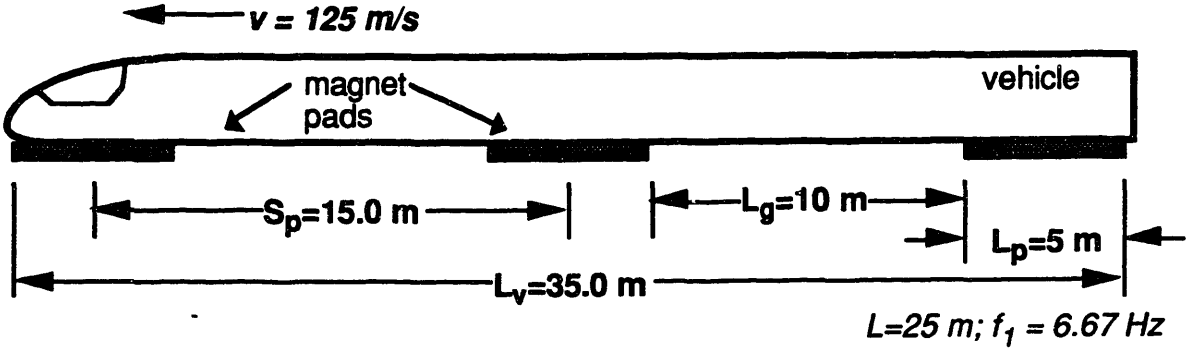

Figure 5.4.7 Three Pad Vehicle , Sp = 15.0 m (Lv= 35 m)

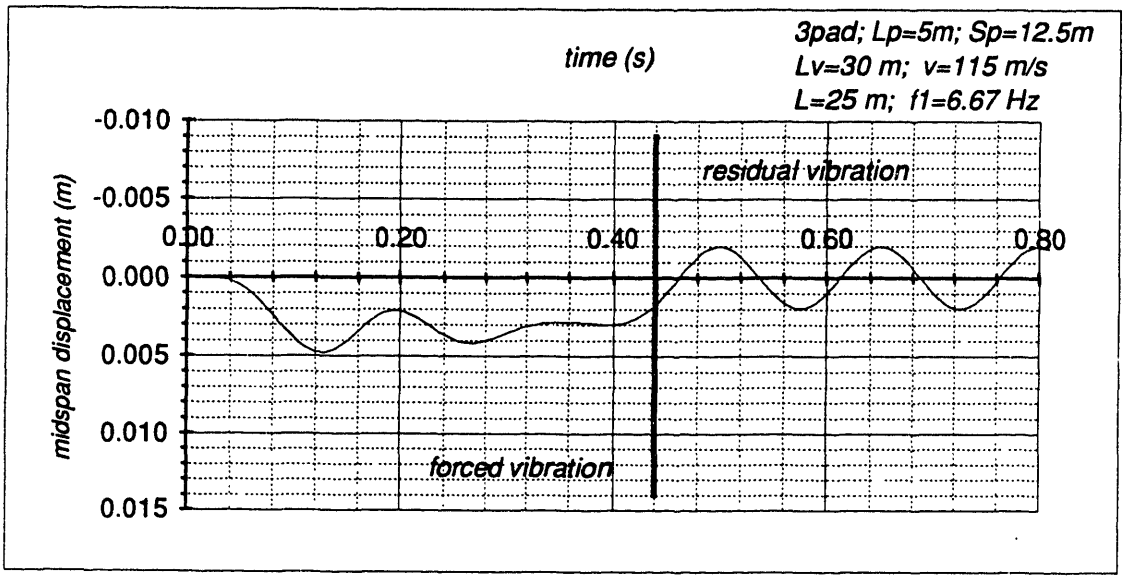

Figure 5.4.8 Beam Dynamic Response for Sp =15.0 m (v=125 m/s)

5.4.6 Convergent velocity sensitivity analyses

Table 5.4.2 lists convergent vehicle velocities between 30 and 150 m/s for the a) two point, b) fully distributed, and c) three pad vehicles shown in Figures 5.2.1, 5.3.1, and 5.4.3, respectively. These convergent velocities result from equations 5.25, 5.30, 5.31, and 5.36 for a beam span of 25 m and a beam fundamental frequency of 6⅔ Hz. Each vehicle listed is 30 m in length. Because each point load modeled for the two-point vehicle has an effective 1.25 m length due to discretization of the beam, the effective pad spacing is 28.75 m.[9] Velocities listed in the table are identified by the parameter with which they were calculated. These parameters are 1) the beam length, L, 2) the fully distributed vehicle length, L_v, 3) the distributed pad length, L_p, and 4) the pad spacing, S_p. At these velocities, no beam residual vibration will occur.

As seen in Table 5.4.2, it is possible for the convergent velocity to be obtained from more than one parameter. For example, the 66.67 m/s convergent speed obtained for

[9] See Section 5.2.

the fully distributed vehicle load results both from the beam and the vehicle length parameters. In general, it is not beneficial to have multiple parameters determine the same convergent velocity, as this reduces the set of unique vehicle velocities at which convergence occurs. Convergent velocities for the 3 pad vehicle case shown in Table 5.4.2, are relatively well distributed across the given velocity range (i.e. from 30 m/s to 150 m/s). However, the 5 m pads are too short to contribute to high vehicle speed convergent beam behavior. The only convergent velocity resulting from the 5 m pad length is 33.33 m/s. Rigorous dynamic analysis for these three vehicle cases has been performed. Appendix D contains full beam midspan response, including deflection, velocity, and acceleration plots for each of the three vehicle loading configurations, traveling at speeds of a) 90 m/s, b) 115 m/s, c) 125 m/s, and d) 150 m/s. The plots in the appendix give results obtained both from the *mode3* analysis program and the ADINA finite element analysis program.

Table 5.4.2 Convergent velocities for the three, 30 m vehicle cases

2 point Vehicle S_p=28.75m (Figure 5.2.1)		**Full Vehicle** L_v=30.00m (Figure 5.3.1)		**3 pad Vehicle** S_p=12.50 m (Figure 5.4.3)	
v^* (m/s)	*(due to)*	v^* (m/s)	*(due to)*	v^* (m/s)	*(due to)*
127.78	S_p	**111.11**	L	**125.00**	S_p
111.11	L	**100.00**	L_v	**111.11**	L
76.67	S_p	**66.67**	L and L_v	**66.67**	L
66.67	L	**50.00**	L_v	**62.50**	S_p
54.76	S_p	**47.62**	L	**50.00**	S_p
47.62	L	**40.00**	L_v	**47.62**	L
42.59	S_p	**37.04**	L	**37.04**	L
37.04	L	**33.33**	L_v	**35.71**	S_p
34.85	S_p	**30.30**	L	**33.33**	L_p
30.30	L	—		**31.25**	S_p
—		—		**30.30**	L

$L = 25\ m;\ f_1 = 6.67\ Hz$

In addition to analyzing beam response at any given vehicle velocity, it is instructive to determine beam response for a particular vehicle at all expected vehicle velocities. Such a sensitivity analysis has been performed using the *mode3* program. This analysis considers the beam to be subjected to the three vehicle loading configuration for all speeds up to 160 m/s. Results from these analyses are summarized in the three plots shown in Figure 5.4.9. The figure indicates the positive, negative, and residual dynamic amplification factors (i.e. the DAF, NDAF, and RDAF, respectively) for the given speed range. Velocities for which zero RDAF values occur, correspond to the predicted convergent velocities found in Table 5.4.2.

Beam behavior due to the two-point vehicle loading is shown in Figure 5.4.9a. For the majority of speeds in Figure 5.4.9a, (e.g. 100 m/s), NDAF is equal to RDAF. This indicates that the maximum negative deflection during forced vibration is either equal to or less than the maximum residual deflection. For velocities where NDAF is greater than RDAF, the beam experiences higher negative deflection during forced response than during residual response. Figure 5.2.2 is an example of this type of beam behavior. In such situations, though the beam experiences less fatigue loading, sufficient compressive reinforcement is required to resist peak negative bending moments. In general, reduction of the spacing between loading pads eliminates this effect.

Figure 5.4.9b shows the beam response to the fully distributed vehicle loading at all speeds less than 160 m/s. When compared with Figure 5.4.9a, Figure 5.4.9b shows that the beam behavior under the fully distributed vehicle is much more stable across the speed range than it is when subjected to the two-point vehicle loading. For the fully distributed vehicle load, the DAF remains less than 1.30 for all speeds shown. Similarly, both the NDAF and RDAF remain less than 0.45 for the speed range given.

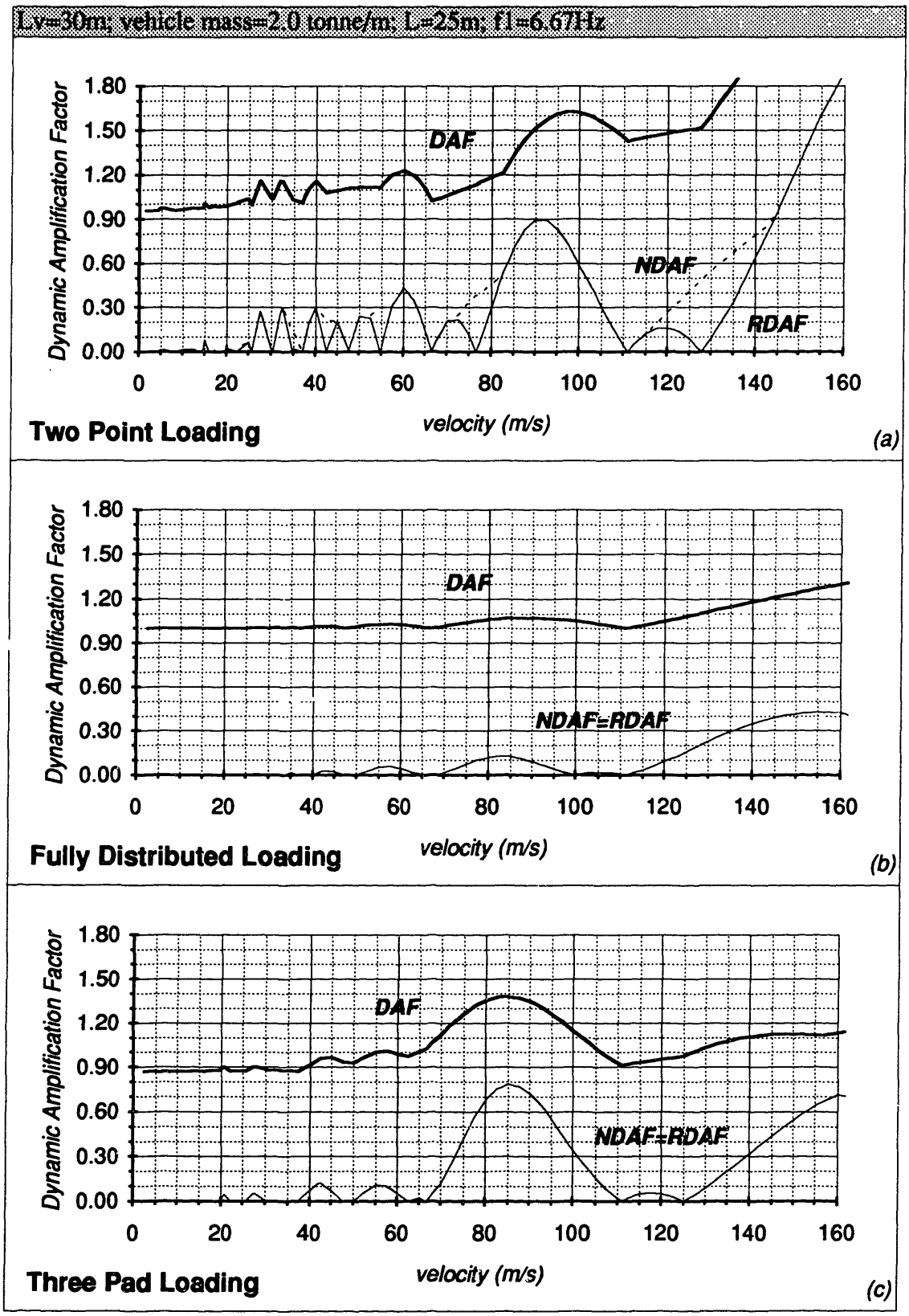

Figure 5.4.9 Beam Dynamic Response and Convergent Velocities (3 cases)

Figure 5.4.9c shows the beam dynamic behavior when subjected to the three pad vehicle of Figure 5.4.3 for all speeds up to 160 m/s. The DAF behavior for the beam, when subjected to this three pad vehicle, is actually superior to that observed for the fully distributed vehicle case shown in Figure 5.4.9b for speeds greater than 110 m/s. Additionally, the high speed range at which zero and/or near-zero residual vibrations occur shifts from the 100 to 111 m/s range in the fully distributed vehicle load case, to the 111 to 125 m/s range in the three pad vehicle case. However, the "cost" of this high speed beam response improvement for the three pad vehicle case is the resonant beam behavior that occurs in the 67 to 111 m/s speed range, as shown in Figure 5.4.9c.

The analyses shown in Figure 5.4.9 illustrate that it is possible to modify beam behavior through changes in vehicle loading configurations. The following section proposes the concept of motion based design whereby the vehicle loading configuration and the beam deflection behavior are designed for specific expected vehicle velocities.

5.5 Motion based design

As demonstrated in the previous section, the ability to cancel all beam residual vibration, is remarkable and potentially has a number of important design implications including benefits such as a) increased guideway lifespan and b) shorter allowable headways for vehicles. Motion based design analyses for maglev guideway design are performed in this section. Three sensitivity analyses are presented to illustrate potential benefits of matching vehicle loads with guideway dynamic beam response.

Though only two and three pad vehicle distributions are analyzed in section 5.4, any number of vehicle loading pads can be used, with a resulting number of specific convergent velocities (see Equation 5.36). As the number of vehicle loading pads increases, the spacing between the pads decreases for a given vehicle length. A greater

number of vehicle pads, n_p, results in a greater probability that convergent vehicle velocities based on the pad spacing, S_p, will be found. In contrast, for a given vehicle length, the more loading pads, the less influence of pad length, L_p, on convergent velocities. For the three pad vehicle shown in Figure 5.4.3, the maximum pad length possible with the given S_p of 12.5 m is 12.5 m. Such a "three-pad" loading configuration is essentially a fully distributed, 37.5 m vehicle. For the 25 m, 6⅔ Hz beam, the highest convergent velocity for a 12.5 m pad is 83.33 m/s according to Equation 5.36. With normal maglev cruising speeds expected to be between 100 and 135 m/s, this maximum convergent velocity of 83.33 m/s from the 12.5 m pad does not contribute significantly to improved beam behavior for the 25 m, 6⅔ Hz beam.

To determine efficient vehicle loading configurations for maglev guideway beam structures, several sensitivity analyses are performed. Specifically, distributed vehicle lengths, L_v, from 37.5 m to 62.5 m are modeled for all speeds up to 160 m/s for the 25 m, 6⅔ Hz beam used in previous examples. In addition, analysis is performed using various vehicle loading pad gap lengths, L_g, for a two-pad, 52.5 m maglev vehicle. The third and final sensitivity analysis presented in this section uses a six pad, 29 m vehicle and models beam behavior for a variety of beam spans and frequencies. The results of these analyses are discussed in this section. Figures referred to in the following discussions are found at the end of this section.

5.5.1 Fully distributed vehicle

Figure 5.5.1 shows the effect that changes in fully distributed vehicle length have on the positive dynamic amplification factor, DAF, for expected maglev vehicle velocities. The fully distributed vehicle length, L_v, varies from 37.5 m to 62.5 m. The surface curve in Figure 5.5.1 shows essentially no change in DAF for the beam as the length of the vehicle varies. This plot agrees with results presented by Richardson and

Wormley in Figure 5.2.3 [Richardson and Wormley 74]. In contrast to the stability of the DAF to changes in vehicle length, Figure 5.5.2 shows the dramatic effect these changes in length have on the beam residual dynamic amplification factor, RDAF for the same speed range.

As shown in Figure 5.5.2, each vehicle length produces a different set of convergent and resonant velocities. All convergent velocities in Figure 5.5.2 are predicted by Equations 5.23 and 5.30. The vehicle length cases shown in Figure 5.5.2 produce neither zero nor near-zero residual vibrations in the beam for all speeds within the 0 to 160 m/s range. However, with maglev vehicle speeds expected to range from 0 to 150 m/s, the 45.0 m vehicle appears to offer the best compromise of the vehicle lengths for all speeds in this range. For speeds less than 150 m/s, the RDAF for the 45.0 m vehicle remains less than 0.20. Since the NDAF is equal to the RDAF in each distributed vehicle load case, from a practical perspective, if the 45.0 m vehicle is selected, an NDAF of less than 0.20 can be used when designing for negative beam deflection. (Other vehicle lengths will require a higher NDAF.) Thus, by limiting the NDAF and RDAF in a given beam, a particular vehicle loading configuration can reduce the need for negative concrete reinforcement, and therefore, reduce a) the demand for non-magnetic hybrid FRP concrete reinforcement and b) the cost of the beam.[10] Additionally, by limiting the RDAF for all expected vehicle velocities, overall beam fatigue loadings are reduced.

5.5.2 Two pad vehicle

To evaluate the influence of vehicle pad length and spacing on dynamic guideway beam behavior, sensitivity analyses were performed for a variety of vehicle pad loading configurations. Figure 5.5.3 illustrates a two pad, 52.5 m vehicle analysis. The two

[10] See Figure 2.4.3 and Chapter 4.

vehicle loading pads are positioned at each end of the vehicle, with a gap length, L_g, between the two pads. Spacing between the centroids of the pads, S_p, is equal to $L_p + L_g$. In Figure 5.5.3, the 0.00 m L_g represents a fully distributed 52.5 m vehicle. The DAF remains below 1.50 in the speed range for gap lengths less than 5 m. In contrast to changes in fully distributed vehicle lengths, Figure 5.5.3 shows that changes in loading pad configurations influence the DAF of the beam.

Figure 5.5.4 shows beam RDAF for the 52.5 m, two pad vehicles. None of the gap length cases result in a beam RDAF less than 0.20 for all speeds in the range. Superior high speed beam behavior results from the 5 m gap vehicle, as shown in Figure 5.5.4. However, the beam behavior at mid-range speeds for this vehicle is not desirable. Since maglev operation is expected to occur at the higher vehicle velocities, this loading configuration could be desirable. If this vehicle loading is chosen, operation at mid-range speeds should be minimized.

5.5.3 Six pad vehicle

The third and final dynamic beam behavior sensitivity analysis performed in this section is shown in Figures 5.5.5 and 5.5.6. The vehicle is modeled to represent the six pad, 29 m vehicle proposed by the Bechtel/MIT maglev team for the U.S. National Maglev Initiative's system concept definition study [Bechtel, et.al. 92].[11] The Bechtel/MIT vehiclehas six 4 m pads, each separated by a 1 m gap. Beam behavior caused by the traveling vehicle for a variety of beam lengths and frequencies is analyzed. Table 5.5.1 shows the beam lengths and assumed frequencies used in this analysis.

As shown in Figure 5.5.5, the DAF is less than 1.20 for speeds less than approximately 150 m/s when beam length is 25 m and less. However, Figure 5.5.6 shows

[11] Research performed by the Bechtel/MIT team is independent of the research presented in this thesis.

that the RDAF behavior for the 25 m beam is extreme at high speeds. In contrast, the RDAF for a 20 m beam is less than 0.20 for all speeds in the given range. Thus, this 29 m vehicle appears well suited for the 20 m beam span, but not for the other spans.

Table 5.5.1 Beam lengths and frequencies used for six pad vehicle analysis

Beam Length, L	Beam Fundamental Frequency, f_1
15	18.00
20	10.00
25	6.67
30	4.00
35	3.00
40	2.50

The three analyses performed and discussed in this section demonstrate that the guideway beam dynamic behavior is highly sensitive to vehicle loading configuration and to vehicle speed. All three analyses have particular design implications. The first example shows that though various distributed vehicle lengths have little effect on the DAF of a beam, the RDAF is highly sensitive to these changes. One difficult design issue is that no single vehicle length performs satisfactorily on the given beam at all expected maglev vehicle speeds. The second example shows that though the DAF increases with increased vehicle gap length and with the use of discrete loading pads, the RDAF of the beam becomes more controllable. Figure 5.5.4 indicates that specific vehicle loading configurations can be designed to complement beam dynamic behavior at particular operating speed ranges. Conversely, the third example shows that individual beam segments can be designed to match a particular vehicle loading configuration and an expected speed at specific locations along the guideway corridor.

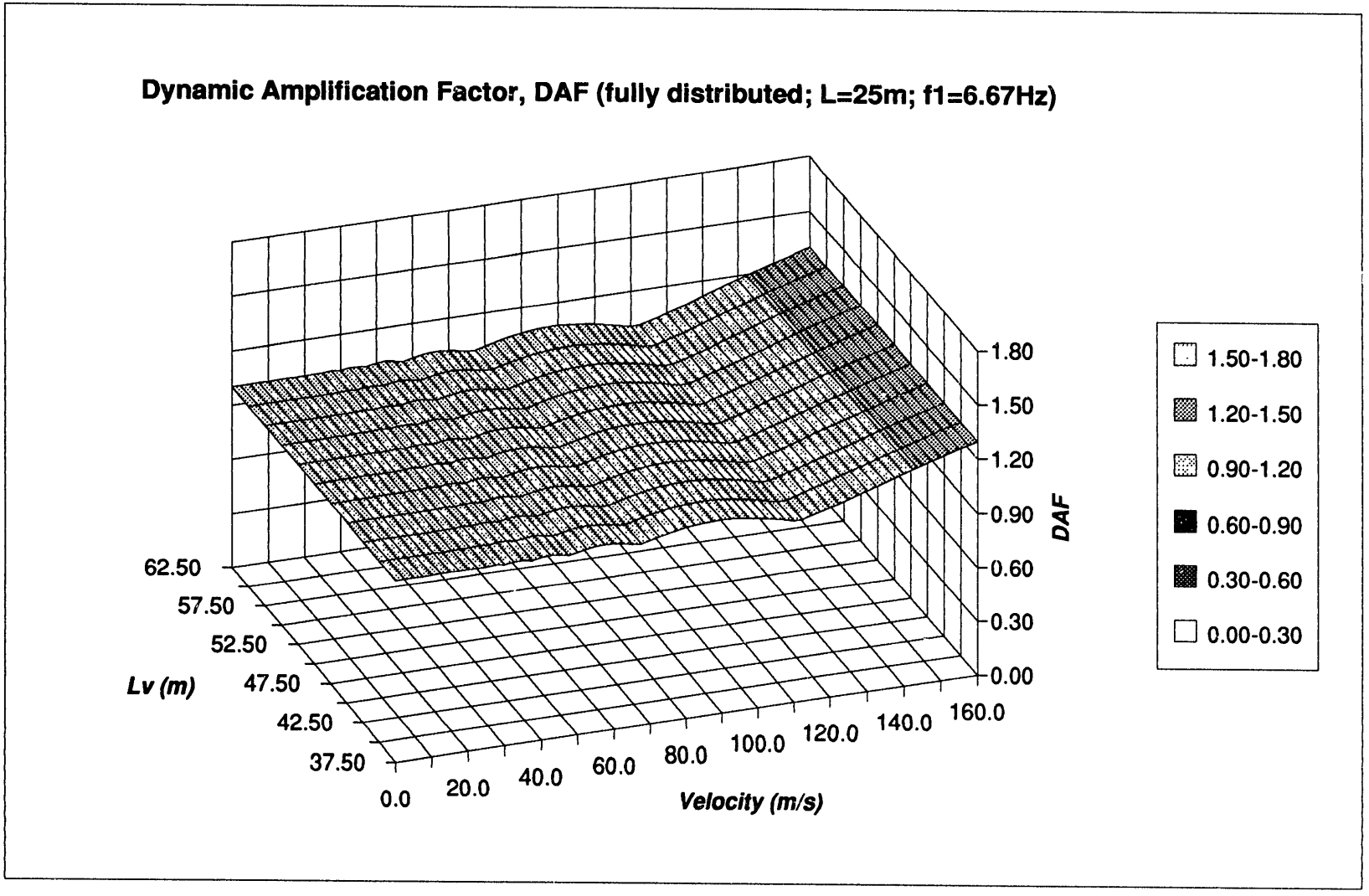

Figure 5.5.1 Fully Distributed Vehicle Length Sensitivity Analysis (DAF)

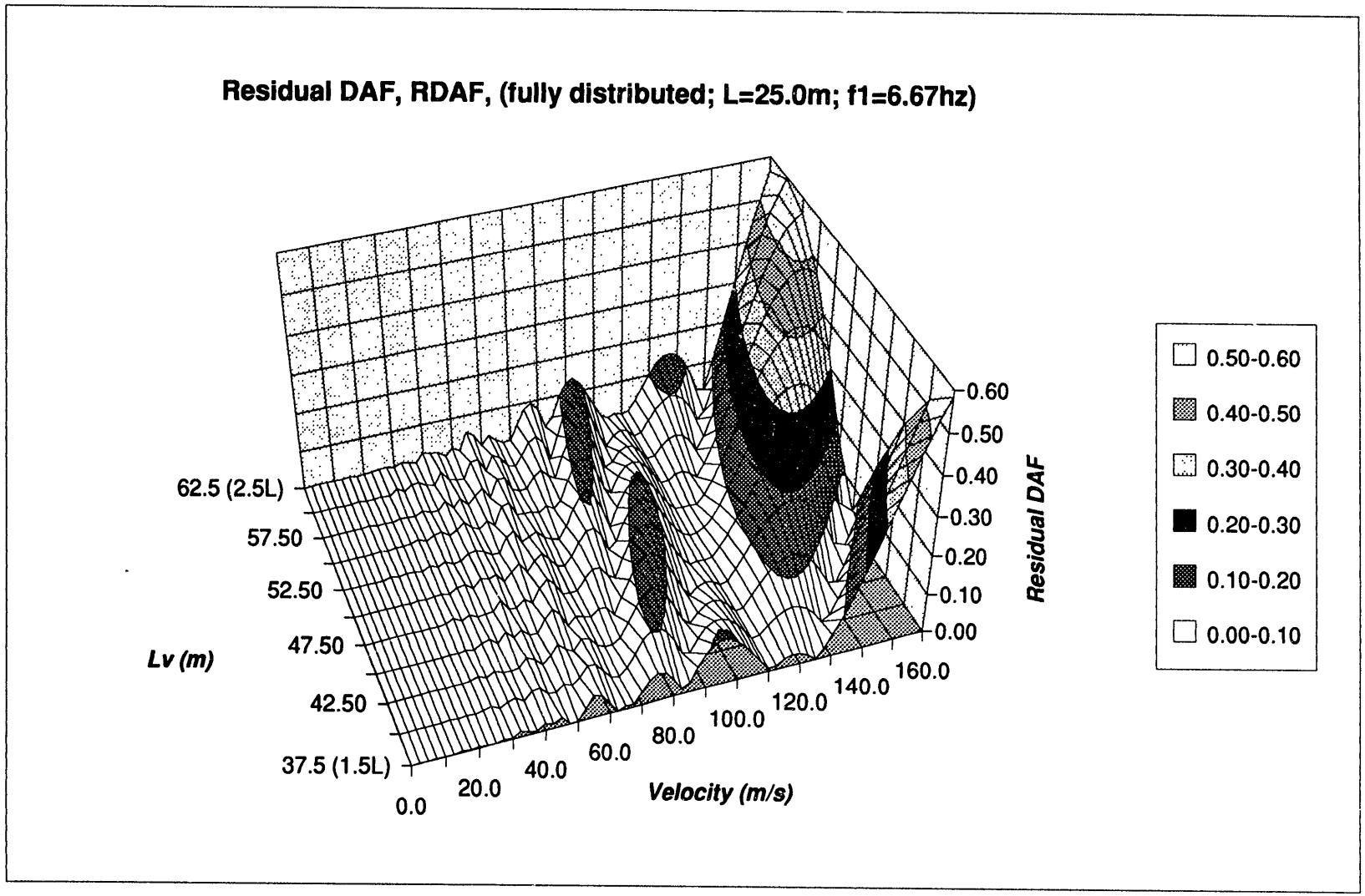

Figure 5.5.2 Fully Distributed Vehicle Length Sensitivity Analysis (RDAF)

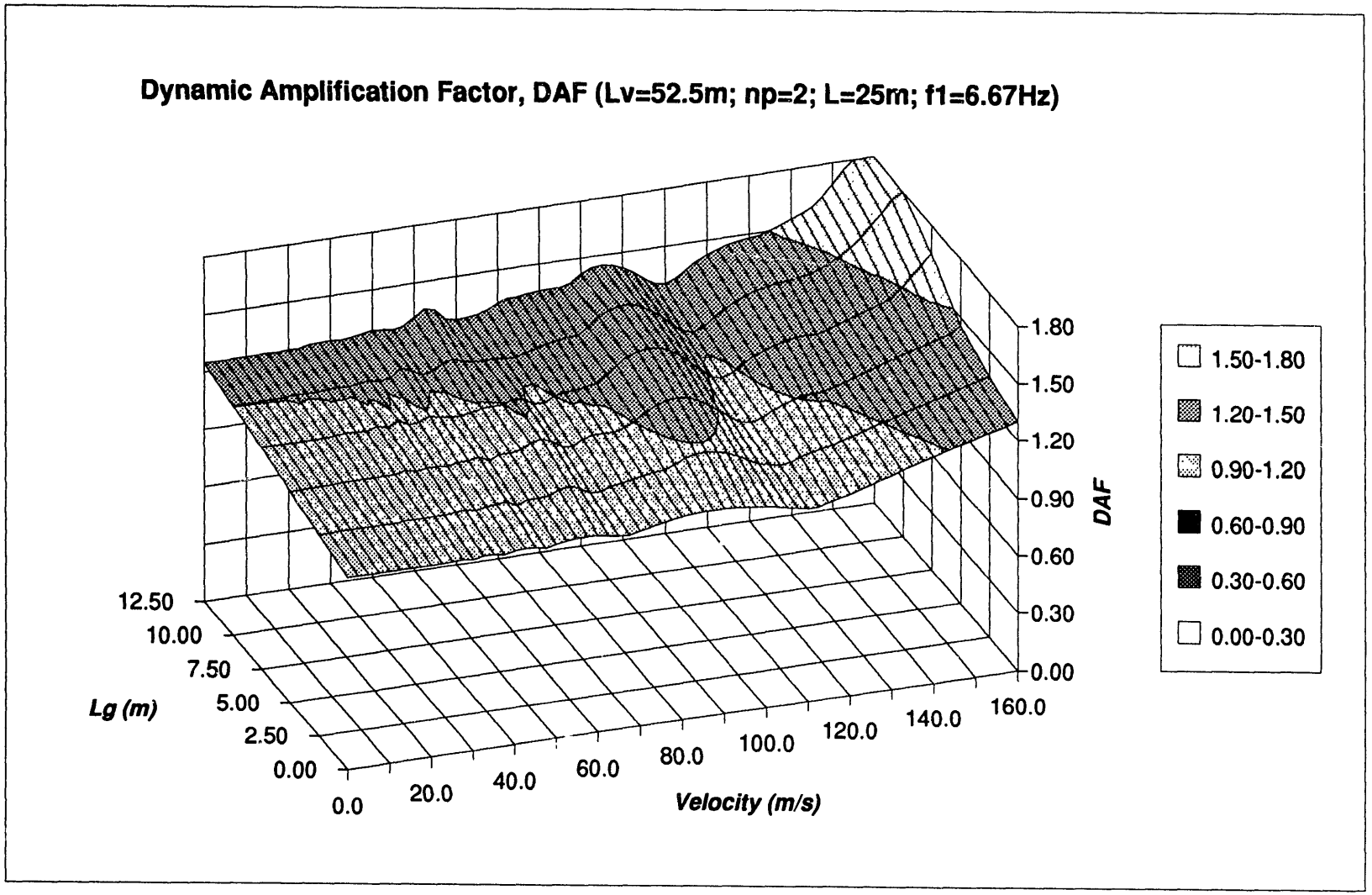

Figure 5.5.3 Vehicle Loading Pad Length Sensitivity Analysis (DAF)

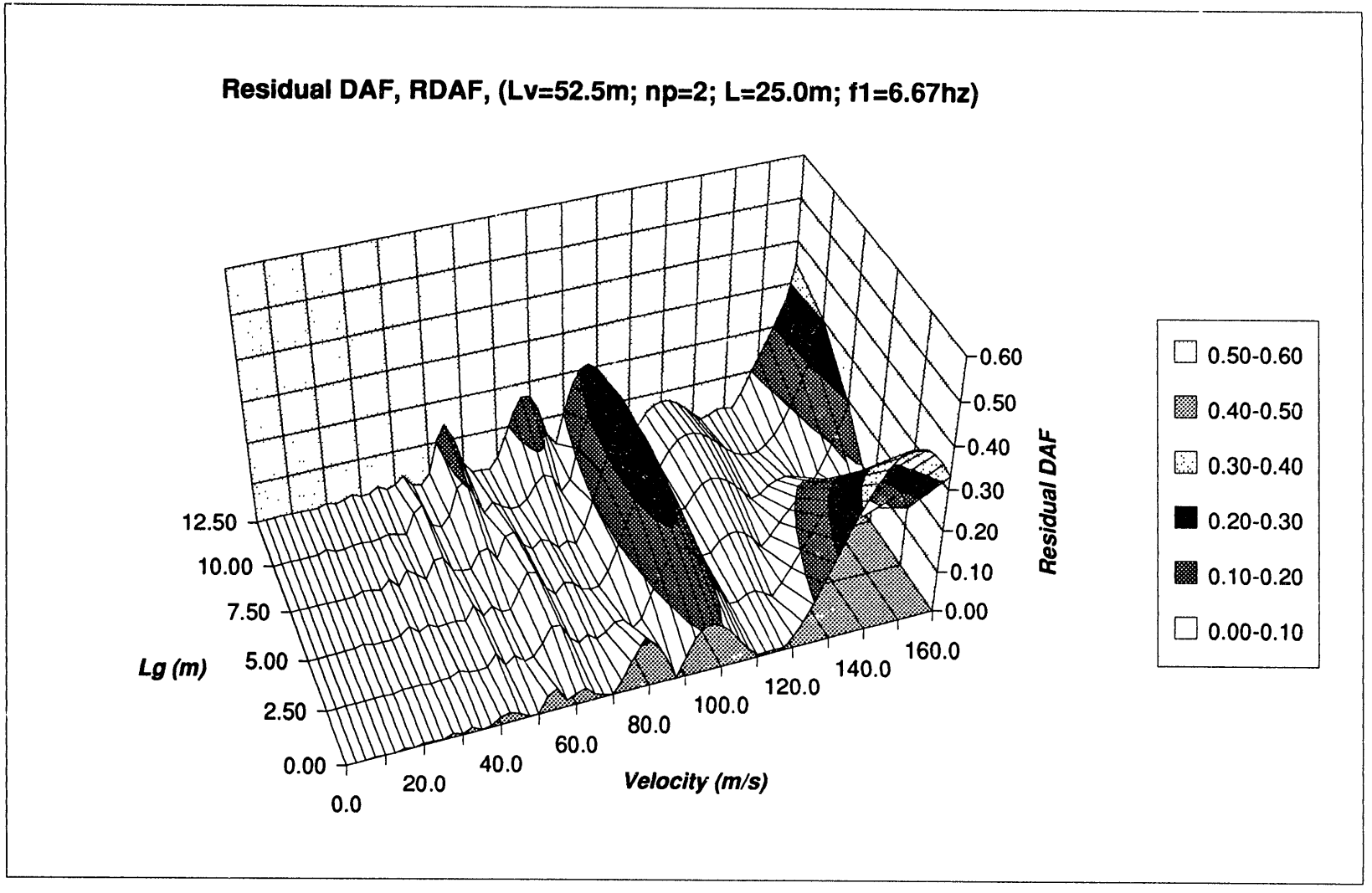

Figure 5.5.4 Vehicle Loading Pad Length Sensitivity Analysis (RDAF)

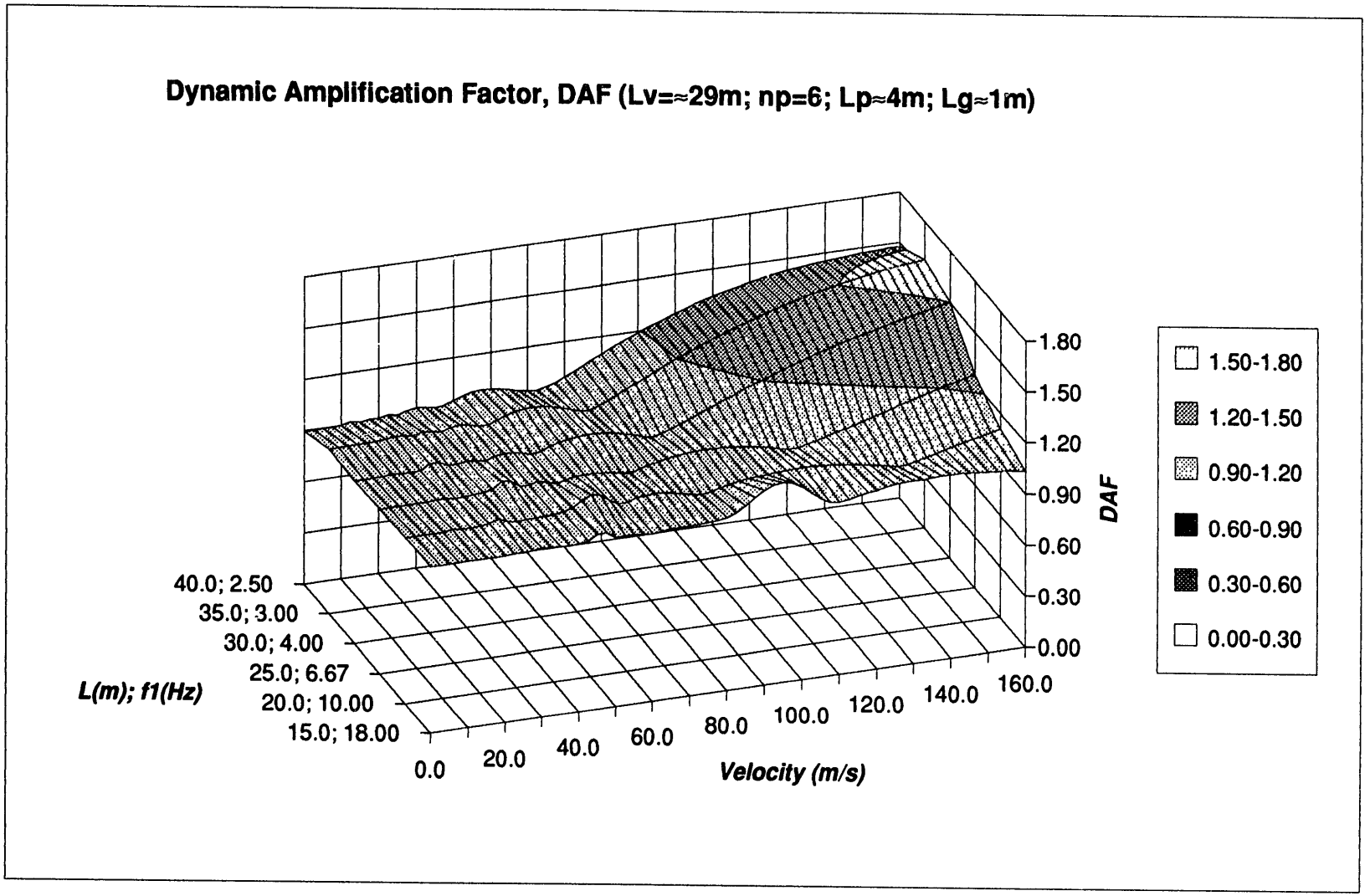

Figure 5.5.5 Beam Length and Frequency Sensitivity Analysis (DAF)

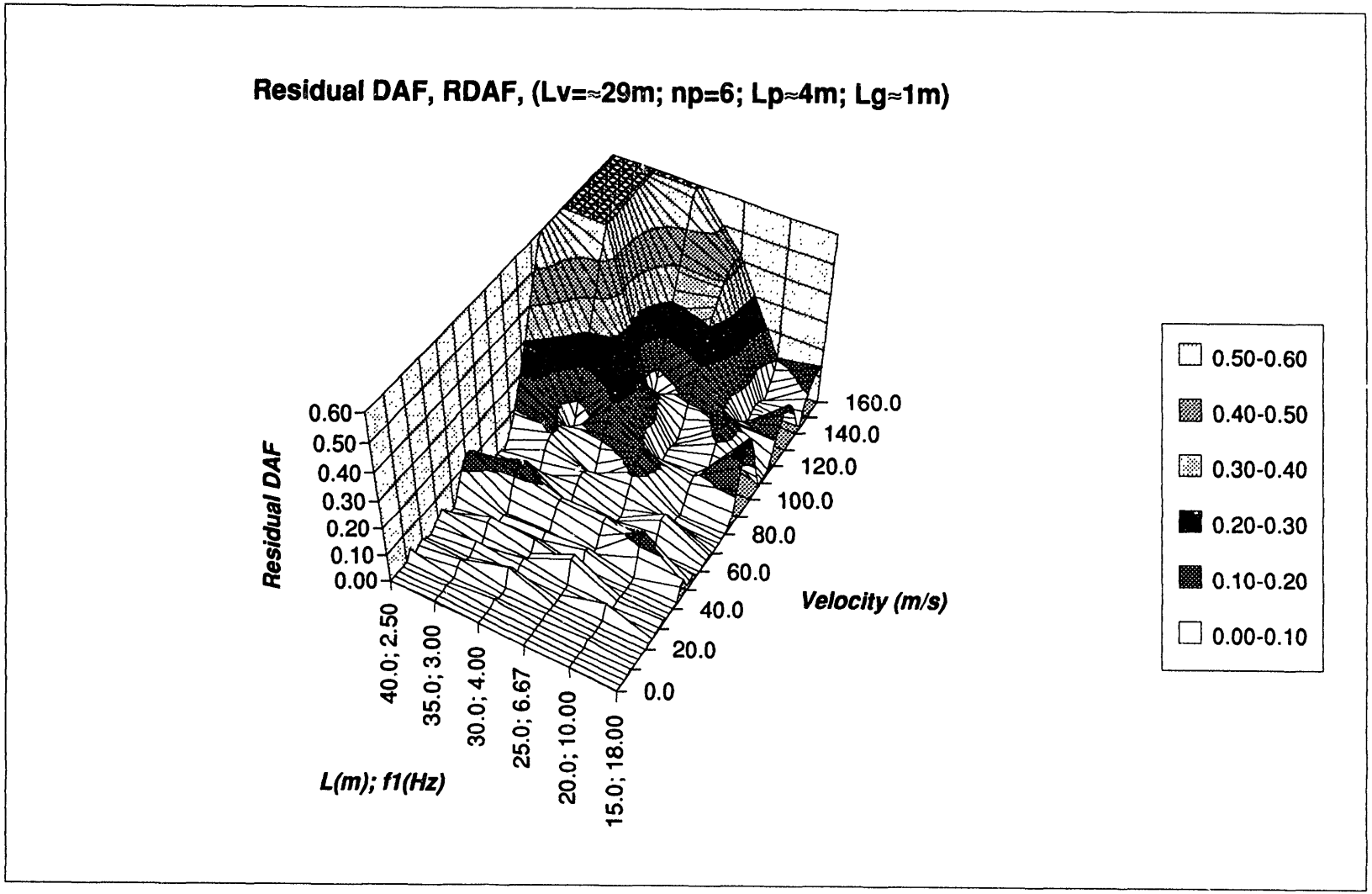

Figure 5.5.6 Beam Length and Frequency Sensitivity Analysis (RDAF)

6.0 Summary and Conclusions

The following summary, conclusions, and research contribution sections are divided according to the three main research areas performed in this thesis: 1) hybrid FRP concrete reinforcing rod design and manufacture, 2) narrow beam guideway design, and 3) dynamic beam response analysis. The chapter concludes with a discussion of suggested future research directions.

6.1 Summary

Maglev guideway costs are expected to represent over 70% of maglev implementation costs—making low cost high performance guideway design a high priority. A maglev design employing a superconducting electro-dynamic suspension, EDS, system is expected to prove more economical than competing electro-mechanical suspension, EMS, systems. Since steel girders, and even steel reinforcing bars for concrete, cannot be used near EDS windings, an economical and reliable non-magnetic structural material is needed. This thesis presents the concept for such a material for use as concrete reinforcement.

Based on expected loads, structural support mechanisms, low cost, and ease of assembly, a rectangular hollow-box narrow beam guideway design is proposed and analyzed. The analysis shows that a relatively narrow beam is sufficient to resist expected maglev vehicle loads. The narrow beam is reinforced with both magnetic and non-magnetic materials. Included in Appendix A is a method for determining magnetic forces on metallic components of guideways, written by Professor Mark Zahn of MIT.

Beam dynamic analysis is performed which demonstrates the importance of vehicle speed and loading configuration on guideway beam response. The concept of

convergent vehicle velocities is presented and a closed form mathematical solution for determining such velocities is given.

Hybrid FRP rods

A conceptual design is presented for a non-magnetic hybrid glass and carbon fiber reinforced plastic, (i.e. hybrid FRP), concrete reinforcing rod. Currently available glass FRP rods are not desirable for maglev because glass fibers are susceptible both to deterioration from the alkaline environment of the concrete and to fatigue loadings. Glass FRP is low in cost, yet also low in stiffness. Though carbon fibers are inert to the alkaline concrete environment and are excellent in fatigue resistance and in stiffness, currently, they are too expensive to be considered for use in an all-carbon FRP rod. Both glass FRP and carbon FRP rods fail in a brittle manner.

In order to 1) insulate glass fibers from the concrete environment, 2) increase the stiffness of the rod, and 3) provide a pseudo-ductile failure mechanism, an innovative hybrid FRP rod is proposed in this thesis. The hybrid FRP rod consists of an inner core of glass fibers surrounded by a thin layer of carbon fibers. These fibers are pultruded (i.e. extruded under tension), in an epoxy resin. The resulting straight, smooth pultruded rod is then filament-wound in such a way as to produce physical bumps on its surface. These bumps provide mechanical bonding to the concrete. Such hybrid FRP rods have been designed, manufactured, and tested. Short-term flexure test results, included in this thesis, show that 1) the rods have adequate bond with high strength concrete and 2) a ductile failure of concrete beams reinforced with the rods occurs. The pseudo-ductility of the hybrid rod is not confirmed by the tests. Load-deflection plots of all seven tests are included in Appendix B.

The glass and carbon hybrid FRP rod is superior to currently available all-glass FRP rods in that it should be inert to the alkaline concrete environment. It also has increased stiffness compared with an all-glass rod. The cost of the hybrid glass and

increased stiffness compared with an all-glass rod. The cost of the hybrid glass and carbon FRP rod is expected to be 5.5 times the cost of steel on a stiffness basis. An all-carbon FRP rod currently is projected to cost 25 to 30 times the cost of steel on a stiffness basis. An all-glass FRP rod is projected to cost 3.0 times that of steel.

Narrow beam guideway design

The narrow beam structural analysis focuses on a straight guideway section with horizontal wind loads of up to 75% of vehicle vertical loads. Maximum beam midspan deflection criteria is modeled as low as 5 mm. Also, non-magnetic reinforcement is assumed to be required in areas near magnetic windings. Expected maglev vehicle mass is two tonnes per meter. The vehicle load distribution is modeled as uniformly distributed.

For a narrow beam using both steel and hybrid FRP reinforcement, design equations are derived and a design procedure based on American Concrete Institute (ACI) Code 38 [ACI 89] is presented. A spreadsheet analysis program called "BoxCost" is developed. It incorporates the design procedure and equations and calculates total beam material cost. *BoxCost* allows sensitivity analyses to be performed on a variety of beam loading conditions, span lengths, cross-sectional geometries, deflection criteria, and material costs. This spreadsheet program is shown in Appendix C. Using *BoxCost*, it is determined that a beam width range of 1.2 m to 1.6 m is sufficient and economical for expected vehicle loads. It is also determined that an all hybrid FRP reinforced guideway beam is approximately three times the cost of an all steel reinforced beam. When areas requiring non-magnetic reinforcement can be constrained to the upper two corners of the beam cross-section, the cost of the hybrid FRP and steel reinforced guideway beam is approximately 30% higher than the cost of all steel reinforcement. A cross-section of the beam design is shown in Figure 2.4.3 and a summary of the design assumptions is given in Table 2.4.2.

Dynamic guideway beam analysis

Dynamic response of the guideway beam under high speed vehicle loads has been analyzed using both a finite element method and a closed form mathematical solution. The importance of vehicle load distribution to guideway beam dynamic behavior is demonstrated. The dynamic amplification factor, DAF, for positive bending (i.e. downward deflection) can be reduced substantially using a fully distributed vehicle load. Also, the smaller the gap lengths between vehicle loading pads, the less the negative dynamic amplification factor, NDAF, (i.e. upward or "spring-back" deflection) that is produced in the beam. Residual vibration of the beam due to a passing maglev vehicle is a significant guideway design concern since little damping can be expected in the beam. The maximum NDAF and the maximum residual vibration dynamic amplification factor, RDAF, under all expected vehicle velocities (e.g. up to 150 m/s), determine the amount of negative concrete reinforcement—and thus the amount of hybrid FRP reinforcement—required in a guideway beam design.

The concept of convergent velocities is introduced whereby a beam experiences no residual vibration after the passing of a vehicle. Also presented, is a closed form mathematical solution for the convergent velocities for simply-supported beam spans with a uniform cross-section and stiffness and with no assumed beam damping. Convergent velocities are found for the following four cases:

all cases:

$$v_L^* = \frac{2Lf_1}{2\lambda + 1} \quad (\lambda = 1,2,3,...) \qquad [5.25]$$

fully distributed vehicle loadings:

$$v_{L_v}^* = \frac{L_v f_1}{\lambda} \quad (\lambda = 1,2,3,...) \qquad [5.30]$$

discrete pad loadings:

$$v^*_{L_p} = \frac{L_p f_1}{\lambda} \quad (\lambda = 1,2,3,...) \qquad [5.31]$$

and

$$v^*_{S_p} = \frac{n_p S_p f_1}{\lambda} \quad \left(\lambda = 1,2,3,... \text{ and } \lambda \neq i n_p;\ i = 1,2,3,...\right) \qquad [5.36]$$

Equations 5.25, 5.30, and 5.31 are valid for all beam vibration modes. In contrast, Equation 5.36 is valid only for vibration mode numbers, n, when $n^2 \neq i n_p$ $(i = 1,2,3,...)$. However, since the first mode dominates all other modes, the speeds given by Equation 5.36 are considered to be essentially convergent.

A spreadsheet analysis program called "mode3" is developed which allows sensitivity analyses of a number of vehicle speeds and pad loading configurations. Sensitivity analyses performed using *mode3* demonstrate the influence of beam length and frequency, as well as vehicle length, speed, and loading configuration on the dynamic behavior of the beam. Motion based design, whereby a beam is designed specifically to match a given vehicle loading pad configuration and an expected speed, is proposed and discussed. Analyses performed with the *mode3* program demonstrate the potential of motion based design strategies. The *mode3* program and example beam response analyses are included in Appendix D.

6.2 Conclusions

Hybrid FRP rods

Hybrid FRP concrete reinforcing rods are a viable replacement for steel in areas of the maglev guideway structure requiring non-magnetic mild reinforcement. Fatigue of the glass fibers should not be a problem as the beam design is based on stiffness. Thus, due to the low stiffness of the glass, the hybrid FRP rods will be designed for low stress

levels. Care must be taken when installing the hybrid FRP rods as they are weak in shear. Specifically, if steel stirrups are to surround the rod, sufficient space must be allowed between the two embedments to prevent premature failure of the hybrid FRP rod due to shearing action from the steel stirrup. This minimum spacing concern is not as significant if the stirrup is also made of FRP, since it will then be more flexible under extreme bending. Additional concerns with using hybrid FRP rods for concrete reinforcement include providing adequate lap splices and anchorage devices as well as monitoring long term behavior under load.

The high failure strains of both glass fibers and high strength carbon fibers does not allow the pseudo-ductility—inherent in the hybrid FRP rod—to take effect in the concrete. Though the hybrid FRP reinforced concrete beam fails in a ductile manner, this is due to the low stiffness of the hybrid FRP rod. A structurally superior solution is to have a hybrid FRP rod where the inner glass fibers are replaced with high strength carbon fibers and the outer high strength carbon fibers are replaced with high modulus carbon fibers. Such an arrangement provides stiffness comparable with steel, and pseudo-ductility at strain levels compatible with concrete. However, carbon fiber costs, currently restrict the viability of this all-carbon FRP rod option.

The proposed hybrid FRP rod containing both glass and carbon fibers, suffers in that it 1) is low in stiffness, 2) does not exhibit pseudo-ductility in concrete, and 3) is possibly susceptible to fatigue loadings. However, it is a viable replacement for mild steel in selected maglev guideway areas in that a) it is inert to the concrete alkaline environment, b) it is relatively inexpensive, c) the hybrid FRP reinforced concrete beam fails in a ductile manner (due to the low stiffness and high strain of the rod), and d) it is likely to be used only at low stress levels—and thus less likely to fail by fatigue.

Narrow beam guideway design

A narrow beam, hollow-box concrete section is structurally sufficient to resist expected maglev vehicle and wind loads within proposed deflection constraints. Glass and carbon hybrid FRP rods can be used in place of steel in areas where non-magnetic reinforcement is required, such as the upper sections of the cross-section (see Figure 2.4.2). Proper magnetic suspension, propulsion, and guidance winding design can reduce the amount of non-magnetic reinforcement required and significantly reduce the cost of the guideway structure. Also, because the narrow beam concept is approximately 1/2 to 2/3 the mass of an EMS guideway and 1/4 to 1/2 the mass of a channel guideway system, innovative vehicle design will allow substantial savings in overall guideway costs.

Dynamic guideway beam analysis

Guideway beam dynamic behavior depends on beam characteristics, vehicle load configurations, and vehicle operating speeds. Convergent vehicle velocities, (i.e. velocities where all beam residual vibrations are completely canceled), are determined by 1) beam length, 2) beam fundamental frequency, 3) vehicle length, 4) loading pad configuration, and 5) vehicle speed. Convergent velocities are desirable as the need for less negative concrete reinforcement can substantially reduce the cost of the structure. In addition, less residual vibration allows longer guideway lifespan, shorter vehicle headways, and improved ride quality.

It is possible to design the vehicle length, pad length, and pad spacing in a manner that will substantially reduce the amount of beam negative deflection and residual vibration. It is also possible to design particular beam segments at given locations of the guideway corridor for a particular set of speeds at which a vehicle is expected to travel. Such beams would be designed specifically to have zero upward deflection and zero residual vibration at certain speeds. Though these beams would be designed to withstand resonant speeds, when convergent speeds occur, a much longer guideway lifespan is

ensured. Such motion based design is practical along sections near terminal stations where speeds can be more easily predicted.

6.3 Research contributions

Non-magnetic hybrid FRP concrete reinforcement

This research presents short-term beam flexure tests which indicate that hybrid fiber reinforced plastic, FRP, rods can be used as a replacement to steel reinforcement in concrete. The added cost due to this option is forcasted. Carbon fiber covering of an inner glass fiber core of a pultruded FRP rod is an innovative method that 1) ensures protection of the glass fibers from the alkaline environment of the concrete, 2) increases stiffness of the hybrid FRP rod, and 3) allows a pseudo-ductile rod failure.

Design of a minimum cost girder

A design procedure for a reinforced concrete, rectangular hollow-box, narrow beam girder is developed which incorporates both steel and hybrid FRP concrete mild reinforcement. This design is likely to have the lowest possible cost consistent with required strength, stiffness, and longevity constraints. A spreadsheet program is developed which allows a user to optimize beam dimensions and predict the cost for any given set of load and stiffness requirements. With the beam design-cost tradeoffs presented in this thesis, maglev vehicle and motor designs can proceed with a better knowledge of the beam cost implications of other system-related choices—ultimately yielding a more efficient overall design.

Dynamics of vehicle guideway interaction

Analysis of the dynamic interaction of a vehicle moving over a guideway is performed and a relatively simple means for predicting the transient behavior of the girder is presented. This analysis is performed for vehicle alternatives ranging from

highly concentrated loads, such as would be expected with wheeled vehicles, to fully distributed vehicles, such as is found in many maglev designs. In general, the more distributed the vehicle load, the less the dynamic amplification factor. Therefore, there is a definite advantage to using multiple vehicle loading pads.

It is shown that a guideway can have substantial resonant behavior. A means for determining critical speeds that should be avoided in the interest of improved ride quality and longer girder life is also given. Residual vibration is influenced by the centroid spacing of the vehicle pads and by the extent of vehicle load distribution. Convergent speeds for a variety of vehicle pad distributions and beam frequencies are identified.

6.4 Future research

Future research is needed in a number of areas including 1) advanced material research, 2) guideway beam dynamic analysis, 3) opportunities for improved guideways, and 4) large scale manufacturing processes. These specific research areas are discussed below.

Advanced material research

Research into the applications of new materials is needed for a number of new and existing materials. Though research into many basic materials types and derivatives such as mild steels, prestressing steels, stainless steels, polymer modified concrete, polymer impregnated concrete, fiber reinforced concrete, high strength concrete, fiber reinforced plastic material, low cost carbon fibers, high modulus aluminum, high strength aluminum, etc., is beneficial, only advanced FRP research is discussed in this section.

Though fiber reinforced plastic, FRP, is in use today, it is generally not considered economical. Its use in construction is primarily required when structures are exposed to corrosive or high magnetic field environments. Research to reduce the cost of using FRP should be performed in the following three areas: 1) connection design, 2) lower cost, lower strain carbon fibers, and 3) long term durability. Connection design is

lower cost, lower strain carbon fibers, and 3) long term durability. Connection design is important since pultruded FRP material, due to its orthotropic nature, cannot be as easily spliced or "welded" together as isotropic materials (e.g. steel) can. There is plenty of connection design experience in the aerospace and automobile industries and this experience can be applied directly to most construction FRP applications. However, in general the construction industry is unfamiliar with the assemblage of FRP elements. Research into more cost effective and easily used connection designs is suggested.

Lower cost, lower strain fibers result in improved utilization of the FRP material in concrete. Higher strength fibers are not critical, nor is reduced weight necessarily beneficial in FRP reinforcement. Rather, for use in maglev concrete beams, high modulus and low strain fibers are beneficial. Though this proposed research runs counter to current emphasis in the composite industry on higher strength to weight ratio fibers (due primarily to aerospace and automobile industry needs), it should have a moderate to high chance of success. Any reduction in fiber cost will have a significant impact on making FRP a more practical alternative to steel. Finally, though much durability and fatigue testing has been performed on composites, additional testing focused on FRP material behavior under long term load and concrete alkaline attack is suggested.

Guideway beam dynamic analysis

Another important future research area is in determining the direct implications that vehicle loading configuration and speed have on long term guideway life. As demonstrated in this thesis, certain speeds can be identified for particular vehicle configurations and beam stiffnesses which allow residual vibrations of the beam to be completely canceled without damping. Worst case scenarios must be designed for however, with appropriate amounts of damping mechanisms used. Therefore, it is important to continue studying the influences that the number of pads, the length of pads, and the spacing of pads have on guideway beam behavior. Once convergent speed

relationships are determined, constant monitoring of vehicles passing particular beams will allow time-history profiles to be derived for each beam segment. These profiles will allow improved prediction of long term life for each particular beam.

In addition, future dynamic analysis which models vehicle mass and a variety of support structures is suggested. Additional dynamic analysis is proposed that will consider 1) non-linear effects, 2) three dimensional effects, 3) curved beam sections, 4) lateral vehicle accelerations, 5) beams having non-uniform mass and stiffness, 6) multiple spans, and 7) multiple vehicles.

Opportunities for improved guideways

Finally, in order to achieve satisfactory ride quality, a maglev guideway with very tight tolerances—probably a factor of 2 to 5 tighter tolerance than is possible with normal construction procedures—must be designed. High speed railroads have found it necessary to maintain rail alignment to a 1 or 2 millimeter tolerance. This entails relatively expensive track maintenance. The French TGV estimates maintenance cost to be comparable to energy cost. The Japanese Shinkansen requires several men per kilometer of guideway for continuous maintenance. The Transrapid design requires precise field installation and adjustment and there is concern that the maintenance cost could be high. This thesis has explored this problem in a qualitative way and has recommended alternatives worthy of further study. These alternatives should be pursued.

Large scale manufacturing processes

Construction of the guideway is the single largest cost for a maglev system. There appears to be substantial potential for developing automation methods that lower the cost of a long distance guideway. Such automation may entail the use of new materials that allow more flexibility in adapting to varied terrain and/or methods to achieve precision alignment with minimum labor.

Concrete guideways appear to be the most appropriate choice for EDS maglev. However, there is very little cost reduction experience in the construction of long distance guideway segments over several years. Formwork is very expensive for highway bridge construction. Also, for the long distances involved with potential maglev corridors, multiple concrete cast sites will be necessary. Research is needed to 1) develop two or three approaches to automated manufacturing, 2) simulate the operation of each approach to see which is more effective and 3) determine how much cost reduction can be expected from automated procedures.

Bibliography

[AASHTO 89] *Standard Specifications for Highway Bridges*, 14th Edition, American Association of State Highway and Transportation Officials, 1989.

[ACI 89] *Building Code Requirements for Reinforced Concrete* (ACI 318-89) *and Commentary*—ACI 318R-89, American Concrete Institute, 1989.

[ADINA 89] *ADINA-IN: User's Manual, ADINA-PLOT: User's Manual, ADINA Theory and Modeling Guide, ADINA Verification Manual-Linear Problems*, Watertown, Massachusetts, September 1989.

[ASME 92] *Mechanical Engineering*, ASME, April 1992, p. 114.

[Albano 91] Albano, L.D., *An Axiomatic Approach to Performance-Based Design*, MIT Doctoral Dissertation, Department of Civil Engineering, February 1992, pp. 2-10.

[Amoco 92] *New Dimensions in Design Freedom: Thornel® Carbon Fibers and Composites*, promotional literature and price lists from Amoco Performance Products, Inc., Atlanta, Georgia, 1992.

[Barrows 92] "Aerodynamic Forces", private memo from Tim Barrows, The Charles Stark Draper Laboratory, Cambridge, MA, Oct. 1991.

[Bathe 82] Bathe, K.J., *Finite Element Procedures in Engineering Analysis*, Prentice-Hall, 1982.

[Bechtel, et.al. 92] *Maglev System Concept Definition*, Final Report—Volume 1, prepared by Bechtel Corp., Huges Aircraft, General Motors Electromotive, Massachusetts Institute of Technology, and Draper Laboratories for the U.S. Department of Transportation Federal Railroad Administration, September 30, 1992.

[Buckle 91] Buckle, I.G., "Seismic Design Criteria for Highway Bridges", *Third Bridge Engineering Conference*, Transportation Research Record N1290 V, 1991, pp. 80-94.

[CIGGT 89] *Maglev Technology Assessment, Task 9.2: Review, Validation and Revision of the Capital and Operating Costs for a Transrapid TR-06 Maglev System and for a TGV System in the Las Vegas-Southern California Corridor*, Super-Speed Ground Transportation System Las Vegas/Southern California Corridor Phase II, The Canadian Institute of Guided Ground Transport, July 28, 1989.

[Charles and Crane 89] Charles, J.A. and F.A.A. Crane, *Selection and use of Engineering Materials*, Second Edition, 1989.

[Collins and Mitchell 91] Collins, M.P. and D. Mitchell, *Prestressed Concrete Structures*, 1991, p. 613. (Numbers used by Collins and Mitchell for construction costs were adapted from Schlaich, J. and H. Scheef, "Concrete Box Girder Bridges", Structural Engineering Documents, International Association for Bridge and Structural Engineering, Zurich, 1982, p.108.)

[Degenkolb 77] Degenkolb, Oris H., *Concrete Box Girder Bridges,* ACI Monograph No. 10, 1977, p. 19.

[Dolan 91] Dolan, C.W., "Kevlar Reinforced Prestressing for Bridge Decks", *Third Bridge Engineering Conference*, Transportation Research Board N1290 V1, 1991, pp. 68-75.

[Elbadry and Ghali 83] Elbadry, M.M., and A. Ghali, "Temperature Variations in Concrete Bridges", *ASCE Journal of Structural Engineering*, V109 N10, Oct. 1983, pp. 2355-2374.

[FIP 84] *Prefabricated thin-walled concrete units*, FIP State of the art report, 1984.

[FRA 90] *Assessment of the Potential for Magnetic Levitation Transportation Systems in the United States--A Report to Congress*, Federal Railroad Administration, U.S. Department of Transportation, June 1990.

[Ferritto 91] Ferritto, J.M., "Studies on Seismic Isolation of Buildings", *Journal of Structural Engineering*, Vol 117, No 11, September 1991, pp. 3293-3314

[Harrison, et.al. 92] Harrison, J.A., J.B. Gilmore, S. Mahgerefteh, W.H. McDonald, and K.B. Ullman, *Maglev Cost Estimation: Capital Cost Elements*, Parsons Brinckerhoff Quade & Douglas, Inc., under contract to the Volpe National Transportation Systems Center, Cambridge, MA, Interim Report, January 1992.

[Hayashi and Ohishi 89] Hayashi, A., and Ohishi, A., "HSST Maglev Train at Yokohama Expo '89", *Magnetic Levitation Technology for Advanced Transit Systems*, 1989, SAE Publication SP-792, pp.23-32.

[Hayes 87] Hayes, W.F., "Magnetic Field Shielding for Electrodynamic Maglev Vehicles", *International Conference on Maglev and Linear Drives '87*, Las Vegas, Nevada, May 19-21, 1987, p. 54.

[Hilliges and Schambeck 89] Hilliges, D., and H. Schambeck, "The Concrete Guideway", I.K. Heinrich and I.R. Kretzschmar, editors, *Transrapid Maglev System*, p. 21-44, HESTRA-VERLAG Darmstadt, 1989.

[Hsu 84] Hsu, T.T.C., *Torsion of Reinforced Concrete*, Van Nostrand Reinhold, 1984, pp. 171-204.

[Humar 90] Humar, J.L., *Dynamics of Structures*, Prentice Hall, 1990, pp. 668-671.

[Johnson and Giese 88] Johnson, L.R., and Giese, R.F., "Maglev: The Double Benefits of High-Tc Superconductors and Its Development as an Aerospace Technology", *Superconductivity and Its Applications*, Hoi S. Kwok and David T. Shaw, Editors, Elsevier Science Publishing, 1988, pp. 306-317.

[Johnson, et.al. 89] Johnson, L.R., et. al., "Maglev Vehicles and Superconductor Technology: Integration of High-Speed Ground Transportation into the Air Travel System", *Energy and Environmental Systems Division, Center for Transportation Research, Argonne National Laboratory*, Argonne, Illinois, April 1989, pp. 10-12.

[Kurz 91] Kurz, D.E., "Beyond the IC-Express", *Railway Gazette International*, May 1991, pp. 299-303.

[Lemcke 92] Private telephone conversation with Eberhard Lemcke, Project Manager for Bechtel Civil, Transportation Division, San Francisco, CA, on 12/29/92.

[Menn 91] Menn, Christian, *Prestressed Concrete Bridges*, 1991, pp. 49-64.

[Nakatsuji, et.al. 90] Nakatsuji, T., M. Sugita and F. Toshiaki, "FRP Grid Reinforcement for Concrete and Soil", *Transportation Research Board, 69th Annual Meeting*, Washington, D.C., 1990.

[Nefcom 88] Nefcom Corporation "Nefmac--Technical Leaflet 1: New Fiber Composite Material for Reinforcing Concrete", Tokyo, Japan, 1988.

[Nefmac 90] *Nefmac®*, promotional literature from NEFCOM Corporation, Tokyo, Japan, 1990.

[PSI 90] *PSI Fiberbar: Composite Reinforcing Bar*, promotion literature and specifications sheet for PSI Fiberbar, Polystructures, Inc., Little Rock, AR, 1990.

[PTI 78] *Precast Segmental Box Girder Bridge Manual*, Published by the Post-Tensioning Institute and the Prestressed Concrete Institute, USA, 1978, p. 59.

[Panarese 92] Panarese, W.C., "Fiber: Good for the Concrete Diet?", *Civil Engineering*, V62 N5, May 1992, pp. 44-47.

[Phelan, et.al. 92] Phelan, R.S., R.D. Thornton, J.J. Connor, T. Triantafillou, Low Cost Guideways for Maglev, National Maglev Initiative Final Report, October 1992, DOT/FRA/NMI-92/16.

[Phelan and Sussman 91] Phelan, R.S. and J.M. Sussman, "Maglev Technology: A Look at Guideway and Maintenance Concerns", *Applications of Advanced Technologies in Transportation Engineering*, Proceedings of the Second International Conference, American Society of Civil Engineers, 1991, pp. 193-197

[Phelan 90] Phelan, R.S., "Construction and Maintenance Concerns for High Speed Maglev Transportation Systems", Masters Thesis, *MIT Department of Civil Engineering*, September 1990, Chapters 2 and 3.

[Polygon 91] *Pultrusions*, mechanical properties and price lists for glass fibers and GFRP, Polygon Company, Walkerton, Indiana, 1991.

[Preis and Bell 86] Preis, L. and T. Bell, "Fiberglass Tendons for Post-tensioning Concrete Bridges", *Transportation Research Record 1118*, 1986, pp. 77-82.

[Richardson and Wormley 74] Richardson, H.H. and D.N. Wormley, "Transportation Vehicle/Beam-Elevated Guideway Dynamic Interactions: A State-of-the-Art Review", *Journal of Dynamic Systems, Measurement, and Control*, 74-Aut-P, ASME, pp. 1-11., 1974.

[Roeder and Moorty 91] Roeder, C.W., and S. Moorty, "Thermal Movements in Bridges", *Third Bridge Engineering Conference*, Transportation Research Record N1290 V, 1991, pp. 135-143.

[Specht 88] Specht, I.M., "The Pedestrian Bridge to Marienfelde Leisure Park--Adof-Kiepert Bridge", summary report on research bridge in Berlin, Germany using partially prestressed glass tendons, 1988.

[Takeda 89] Takeda, H., "Japanese Superconducting Maglev: Present State and Future Perspective", *Magnetic Levitation Technology for Advanced Transit Systems*, 1989, SAE Publication SP-792, pp. 57-62.

[Thornton 90] Thornton, R.D., "Monorail Maglev", *Magnetic Levitation and Transportation Strategies*, Future Transportation Technology Conference and Display, San Diego, CA August 13-16, 1990, SAE Publication SP-834, Paper #90479, pp. 61-67.

[Toray 91] *Torayca*, mechanical properties and price lists for carbon fibers, Toray Industries America Inc., New York, NY, 1991.

[Wang and Salmon 85] Wang, C. and C.G. Salmon, *Reinforced Concrete Design*, Fourth Edition, 1985, pp. 125-130.

[Wakui, et.al. 91] Wakui, H., S. Tottori, N. Matsumoto, H. Okuda, and T. Watanabe, "Structure of Side-wall Levitated MAGLEV Guideway System and its Dynamic

Property", *Quarterly Journal of Railway Technical Research Institute* (Japan), V 32 N 4, December 1991, pp. 234-243.

[Yverdon 90] "Bridge near Yverdon, Switzerland: single-span beam for multispan continuous road bridge", *FIP handbook on practical design: Examples of the design of concrete structures*, Thomas Telford Limited, London, 1990, pp. 21-30.

Appendix A Magnetic Aspects of Maglev Guideways

by

Prof. Richard D. Thornton, MIT

with equations derived by

Prof. Mark Zahn, MIT

Appendix A Magnetic aspects of maglev guideways

Maglev vehicles with electrodynamic suspensions (EDS) produce magnetic fields that extend significant distances from the vehicle. With proper design, the fields can be made to attenuate rapidly enough with distance so that they do not interfere with people and equipment. However, there does not appear to a cost effective way to avoid having the fields interact with guideway beams. Steel girders cannot be used at all, except as a part of a more complex structure. Even concrete girders must be carefully designed to avoid unacceptable interaction with steel reinforcing. One design uses steel reinforcement wherever it is possible, but uses FRP or other magnetically inert materials where exposure to high fields is not avoidable. This section explains the nature of the problem, analyzes suitable models that can give quantitative predictions, and describes typical applications.

A.1 Overview

At normal operating speeds the magnetic fields of a moving vehicle induce currents in electrical conductors on the guideway, and these currents produce power dissipation and forces on the guideway. There are three distinct situations:

1 The magnetic field of a rapidly moving vehicle will induce currents in any nearby electrical conductor. These currents may cause substantial power losses local heating which could lead to catastrophic results.

2 Induced currents will produce forces that act on the vehicle in various ways. The normal suspension and guidance structures are carefully designed to use these forces to advantage, but unwanted induced currents will produce excess drag and could interfere with the normal suspension and guidance forces. In analyzing these forces the primary concern is the time average force, although the effect of peak instantaneous forces can be significant even if the time average force is small.

3 When a vehicle is moving slowly or is stopped, there can be forces on steel reinforcement used in concrete girders. These forces could provide useful lift or guidance, but a theorem of physics (Earnshaw's Theorem) states that the sum total of these forces can not produce stable lift and guidance. These destabilizing forces occur at the low speeds where normal EDS guidance is least effective. For example, a vehicle simply sitting on the guideway could have very strong forces attracting the vehicle magnets towards a concrete girder containing reinforcing steel. These forces would be symmetric with no net force if the vehicle was centered on the guideway. Any deviation from symmetry, however, would cause destabilizing forces, and the vehicle could then lurch to one side and latch onto the guideway.

A.2 Modeling the interaction

The objective of this appendix is to describe relatively simple models that allow a designer to know what types of materials can be used in the guideway and its mounting structures, and where it is possible to use conventional steel reinforcing. The models should give good first order analysis approximations for a wide range of situations.

Transverse *H* fields and cylindrical conductors

One important case is transverse magnetic fields which produce longitudinal currents in a conducting cylinder, as shown in Figure A.1. There is no net longitudinal current, but the resulting currents can produce a force. The currents are calculated with the assumption that the magnetic field is constant over the cross section of the conductor, but in order to develop any net force there must be a gradient of **H** in the *y* direction as indicated in Figure A.1. The net force is in the *y* direction is designated F_y.

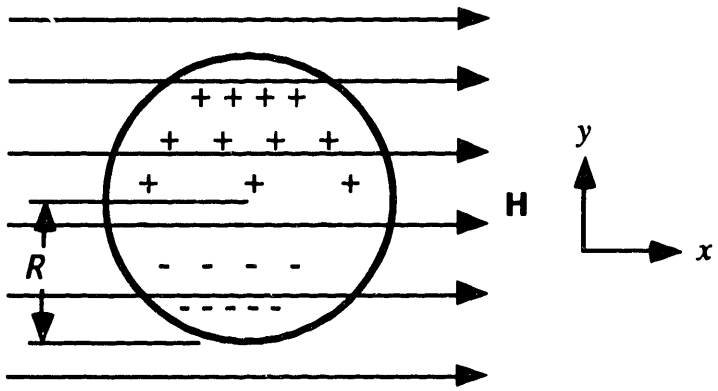

Figure A.1 Transverse magnetic field in cylindrical conductors

Axial magnetic fields and cylindrical conductors

A second important case is axial magnetic fields which produce circulating currents as shown in Figure A.2. In this case the **H** field is assumed to be *z* directed and if **H** has a *y* directed gradient then there will be a net *y* directed force.

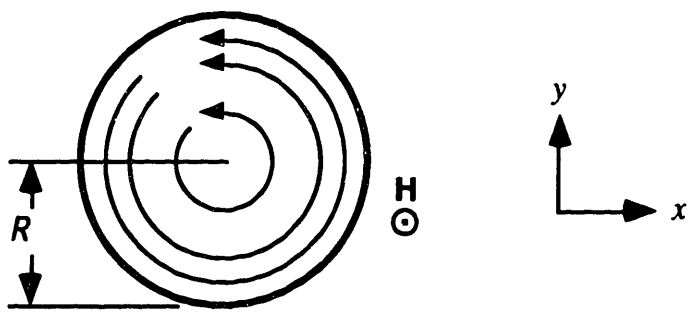

Figure A.2 Axial magnetic field in cylindrical conductors

Notation

To simplify calculations we use complex notation with the understanding that the quantity of interest is the real part. The radius of the conductor is assumed to be R, and force and power are assumed to be per unit volume of conductor. With reference to Figures A.1 we define the following quantities:

$\mathbf{H}(t) = \mathrm{Re}\left[H_0 e^{j\omega t}\mathbf{i}_x\right]$ is the **x** directed **H** field

$\langle P_d \rangle$ is the time average power dissipated per unit volume of conductor

$\langle F_y \rangle$ is the time average force in the y direction unit length of conductor

ρ is the resistivity of the conductor

μ is the permeability of the conductor

$\delta = \sqrt{\frac{2\rho}{\omega\mu}}$ is the skin depth

$a_y = \left(\frac{1}{H_0}\frac{dH_0}{dy}\right)$ is a measure of the rate of field attenuation with distance

Similar notation applies to Figure A.2. Following is a discussion of the parameters used in these definitions.

Skin depth

For any good conductor there is a skin effect wherein time varying magnetic fields create induced currents which, in turn, create a reaction magnetic field that prevents currents from penetrating very far into the conductors. The skin effect causes the magnetic field density and electric current density to both attenuate exponentially with distance into the conductor. The distance required to attenuate by a factor of $e = 2.718$ is called the skin depth. A precise field solution that considers the skin effect often involves complex calculations, (e.g., using Bessel Functions), but there is usually a sharp dividing line so that one can either assume that the skin depth is small or large in comparison with key dimensions.

Rate of field attenuation

The parameter a_y has dimensions of m^{-1}, and is a measure of how fast the field is attenuates in the direction of y. For example, if the field is decreasing exponentially with y, then a_y^{-1} is the increase in y required for the field to decrease by a factor of e.

In many practical cases the magnetic field source can be approximated as a multipole with a field that decreases as an inverse power of distance from the source. As a specific example:

$$\text{if } H \approx \frac{kI}{y^n}$$

$$\text{then } a_y = \frac{1}{H}\frac{dH}{dy} \approx -\frac{n}{y}$$

If a reinforcing rod is 0.2 m from the center of a two dimensional dipole field, then $n = 2$ and a_y is on the order of 10 m^{-1}. Consideration of typical reinforcing material examples suggests that a_y will be in the range 5 to 25 m^{-1} for most practical cases.

Types of materials

There are two important types of materials, those that have high magnetic permeability, such as most steels, and those that have the permeability of free space, μ_0, such as copper, aluminum and some types of stainless steel; the analysis is substantially different for these two cases. If a material has high permeability there can be large static forces. The high permeability will also produce a major reduction in skin depth. The permeability, resistivity, and skin depth for some important materials are given in Table A.1. This data indicates that normal size concrete reinforcing rods, with radii on the order of 5 to 10 mm, will not exhibit skin depth phenomena if $\mu = \mu_0$, but ferromagnetic materials with $\mu > 1000\mu_0$ will have currents and forces dominated by skin depth phenomena.

Table A.1 Electrical properties of various metals at 20° C

Material	μ/μ_0	ρ, *μohm-m*	δ *at 60 Hz, mm*
Copper	1	0.01724	8.5
Aluminum	1	0.0283	10.9
Steel: mild	5000	0.118	0.316
stainless	1	0.910	62.0

A.3 Analysis

The following equations were derived by Prof. Mark Zahn, MIT. They were derived from Maxwell's equations, using the approximations described above.

Transverse field

1. $R << \delta$

$$\langle P_d \rangle = \frac{\rho R^2}{2\delta^4}\left(\frac{2\mu_0}{\mu+\mu_0}\right)^2 |H_0|^2$$

$$\langle F_y \rangle = \left(\frac{(\mu-\mu_0)(3\mu_0+\mu)\mu_0}{2(\mu+\mu_0)^2} - \frac{6\mu R^4}{5\delta^4}\right) a_y |H_0|^2$$

2. $R >> \delta$

$$\langle P_d \rangle = \frac{2\rho}{R\delta}|H_0|^2$$

$$\langle F_y \rangle = -\frac{3\mu_0}{2} a_y |H_0|^2$$

Axial field

1. $R << \delta$

$$\langle P_d \rangle = \frac{\rho R^2}{4\delta^4}|H_0|^2$$

$$\langle F_y \rangle = \left(\frac{\mu-\mu_0}{2} - \frac{\mu R^4}{10\delta^4}\right) a_y |H_0|^2$$

2. $R >> \delta$

$$\langle P_d \rangle = \frac{\rho}{R\delta}|H_0|^2$$

$$\langle F_y \rangle = -\frac{\mu_0}{2} a_y |H_0|^2$$

A.4 Application examples

Situations to be analyzed

The following three effects are analyzed for the models in Figures A.1 and A.2:

- Time average losses and forces produced by vehicles moving at normal cruise speeds near non-magnetic materials with skin depth greater than the key dimensions.

- Time average losses and forces produced by vehicles moving at normal cruise speeds near ferromagnetic materials with skin depth less than critical dimensions.
- Instantaneous forces on stationary or slowly moving vehicles near ferromagnetic materials with large skin depth.

General observations

- A given ac field interacting with a non-magnetic cylinder will produce more loss when it is transverse than when it is axial, but the loss varies as the same powers of R and δ.
- For all cases studied, if the resistivity is held constant and the permeability is increased then the power loss will increase.
- Assuming the total volume of reinforcing rods is constant, when currents are limited by skin depth, it is preferable to use a few large reinforcing rods. When currents are not skin depth limited, then it is preferable to use a larger number of smaller rods.
- There is no force unless there is a gradient in the magnetic field, and the force is in the direction of the gradient.
- For ferromagnetic materials there can be large static forces.

Typical numerical values

The normal speed regime of the vehicle is assumed to cause induced electrical currents with frequencies in the range 30 to 120 Hz. Numerical examples for a frequency of 60 Hz are presented in Table A.2. Simple scaling laws allow one to extrapolate the results to all normal frequencies.

Table A.2 Typical power loss and force due to transverse field on reinforcing rods
Assumptions: $f = 60$ Hz, $a_y = 10\ m^{-1}$, $R = 0.01$ m. Note that there are forces on the non-magnetic materials, but they are not significant compared to other forces. P_d and F_y are time average except for the static case.

Field and Material	$\mu_0 H_0$, *Tesla*	P_d, *MW/m³*	F_y, *kN/m³*
Transverse field			
Mild steel, static	1	0	7,960
	0.1	0	79.6
	0.01	0	0.80
Mild steel, δ<R	1	47,300	11,900
	0.1	473	119
	0.01	4.7	-1.2
Stainless steel, δ>R	1	1.95	-1.62
	0.1	0.02	-0.16
	0.01	nil	nil
Aluminum, δ>R	1	63.5	-1,690
	0.1	0.63	-16.9
	0.01	0.01	-0.17
Axial field			
Mild steel, static	1	0	39,800,000
	0.1	0	398,000
	0.01	0	3,980
Mild steel, δ<R	1	23,600	3,980
	0.1	236	39.8
	0.01	2.3	0.4
Stainless steel, δ>R	1	0.97	-0.54
	0.1	0.01	-0.01
	0.01	nil	nil
Aluminum, δ>R	1	31.7	-564
	0.1	0.32	-5.64
	0.01	nil	-0.06

A.5 Conclusions

Materials for mounting

The least expensive materials for reinforcing is mild steel, but its use leads to strong ferromagnetic forces. Guideway conductors are only exposed to high fields for a small fraction of the time. If 30-meter-long vehicles are spaced at least 3 km apart, then the duty cycle is less than 1 percent. Considering only the heating caused by power dissipation, losses as high as 100 MW/m^3 = 100 W/cm^3 are probably acceptable if there is adequate cooling limits temperature rises to between 20° and 40° C. Hence, small amounts of stainless steel mounting materials can be exposed to fields as high as 1 Tesla, but mild steel must not be exposed to fields over about 0.05 Tesla. Somewhat higher fields would be acceptable if the steel resistivity could be increased by alloying. Aluminum has a cost advantage over stainless steel and could be used at fields up to 1 Telsa, but the losses and forces will be larger than for stainless steel. A more detailed calculation is needed to ascertain the acceptability of aluminum fastening devices, and where they are used the diameter should be limited to the smallest possible value.

Materials for reinforcing

In a typical example, concrete with all metallic reinforcing rods might have 0.01 m^3 of reinforcing rods exposed to the fields of a single vehicle at any time. If we limit the loss to 1 MW/m^3, then the total dissipation will only be about 100 kW, and this is probably acceptable. Using this criteria, mild steel should not be used where the fields exceed 100 gauss. Stainless steel reinforcing could be exposed to axial fields of over 1 Tesla, but should not be exposed to transverse fields of more than 0.7 Tesla. However, if the radius of the reinforcing rod is decreased by a factor of 2 then stainless steel could be used at twice as high a field. Aluminum is never used for reinforcing because of problems with thermal expansion, and clearly it is not a good material to use when time varying

magnetic materials are present. If it is used, it should be fabricated into insulated strands in a "Litz wire" fashion.

Magnetic forces

Loss considerations virtually preclude the use of ferromagnetic steel in regions where these materials could create significant forces. If heating were not a criterion, then one would have to determine the impact of the very large forces. There will be forces on non-magnetic material, but if the mounting and reinforcing materials are of relatively small size, then these forces are not significant except in so far as they create magnetic drag. Stainless steel does not appear to create significant undesirable forces.

Recommendations

Thick rods of ordinary ferromagnetic steel should not be used where there are time varying fields of more than a few hundred gauss. High resistivity, non-magnetic steels can be used almost anywhere if care is used in matching the steel properties, rod diameter, and orientation. Aluminum is usable if fabricated into insulated strands, with the diameter of individual wires limited to 1 or 2 mm. These rough guidelines are intended only for conceptual design, and in a final design a detailed calculation should be done using the methodology described above.

Appendix B Hybrid FRP Reinforced Concrete Beam Tests

Appendix B Hybrid FRP Reinforced Concrete Beam Tests

This appendix contains test results from seven hybrid FRP reinforced concrete (R/C) beams tested in bending. Tests were conducted in two phases. The first phase included three beams each having a hybrid rod of a different carbon thickness—hybrid1, hybrid2, and hybrid3. The second phase tested four beams, two with hybrid1 rods and two with hybrid2 rods. Four of the test beams (I-1, I-2, II-1a, and II-2b) were loaded until it appeared the hybrid rod had yielded. The beam was removed from the test machine and concrete cleared to reveal the hybrid rod. Only the rod in test I-1 appeared to have carbon failure before glass failure.

Though several of the plots appear to indicate a brittle failure (I-1, I-3, and II-2a), extensive beam section cracking was evident long before any failure. Also, since the area under each plot can be taken to indicate ductility in the beam, it is clear that each beam failed in a ductile manner. For a stiffness based, the design service load for the given test beams is constrained to less than 6000 kN (as indicated in plots II-1a and II-2b). At approximately 6000 kN, the hybrid rod experiences a strain of approximately 0.002. This strain level corresponds approximately with the yield strain of 414 MPa (60 ksi) mild steel. Since concrete crushes at approximately a strain of 0.003, the hybrid rod is constrained to perform at or below the 0.002-0.003 strain range.

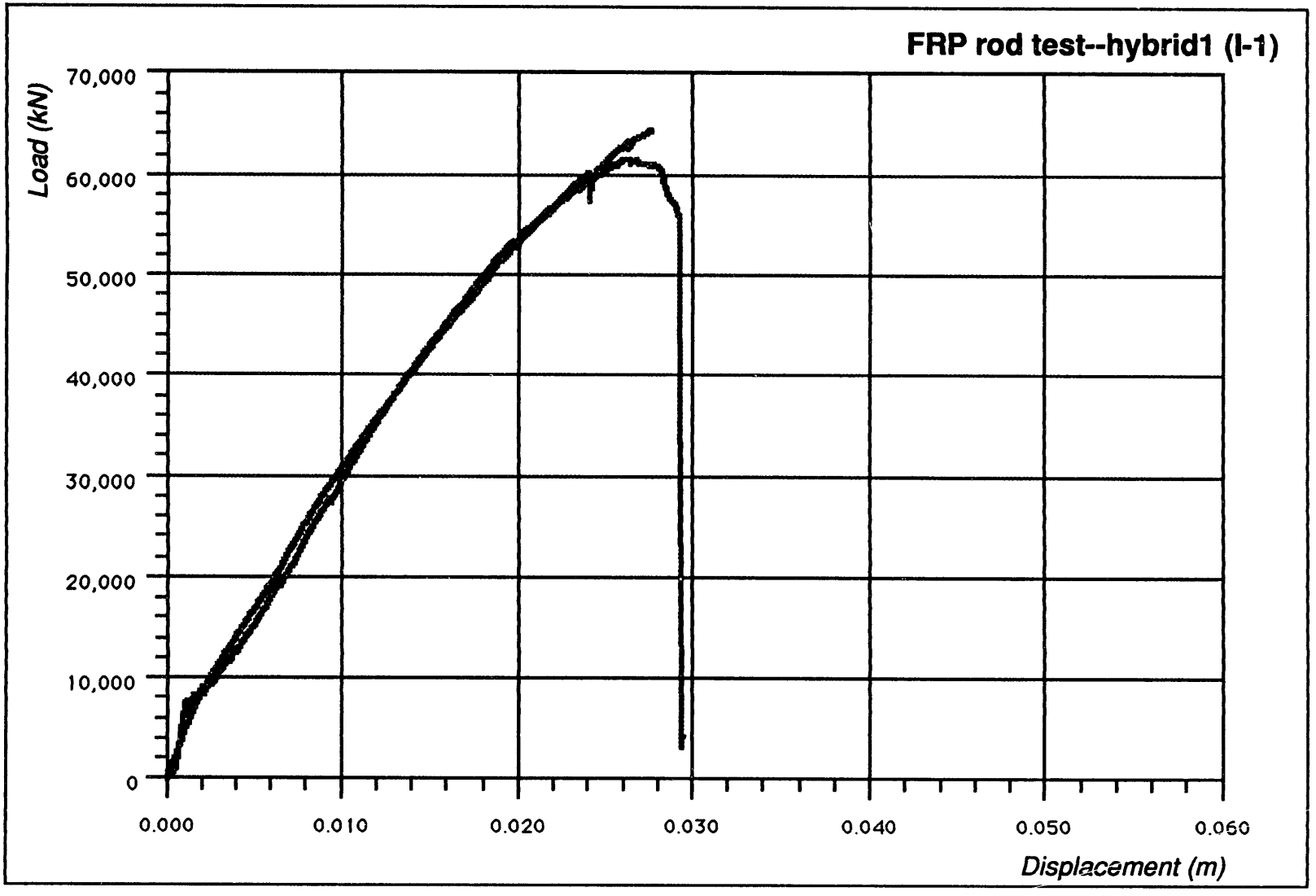

Figure B.1 Hybrid FRP Reinforced Concrete T-Beam Phase I, Test 1 (hybrid1)

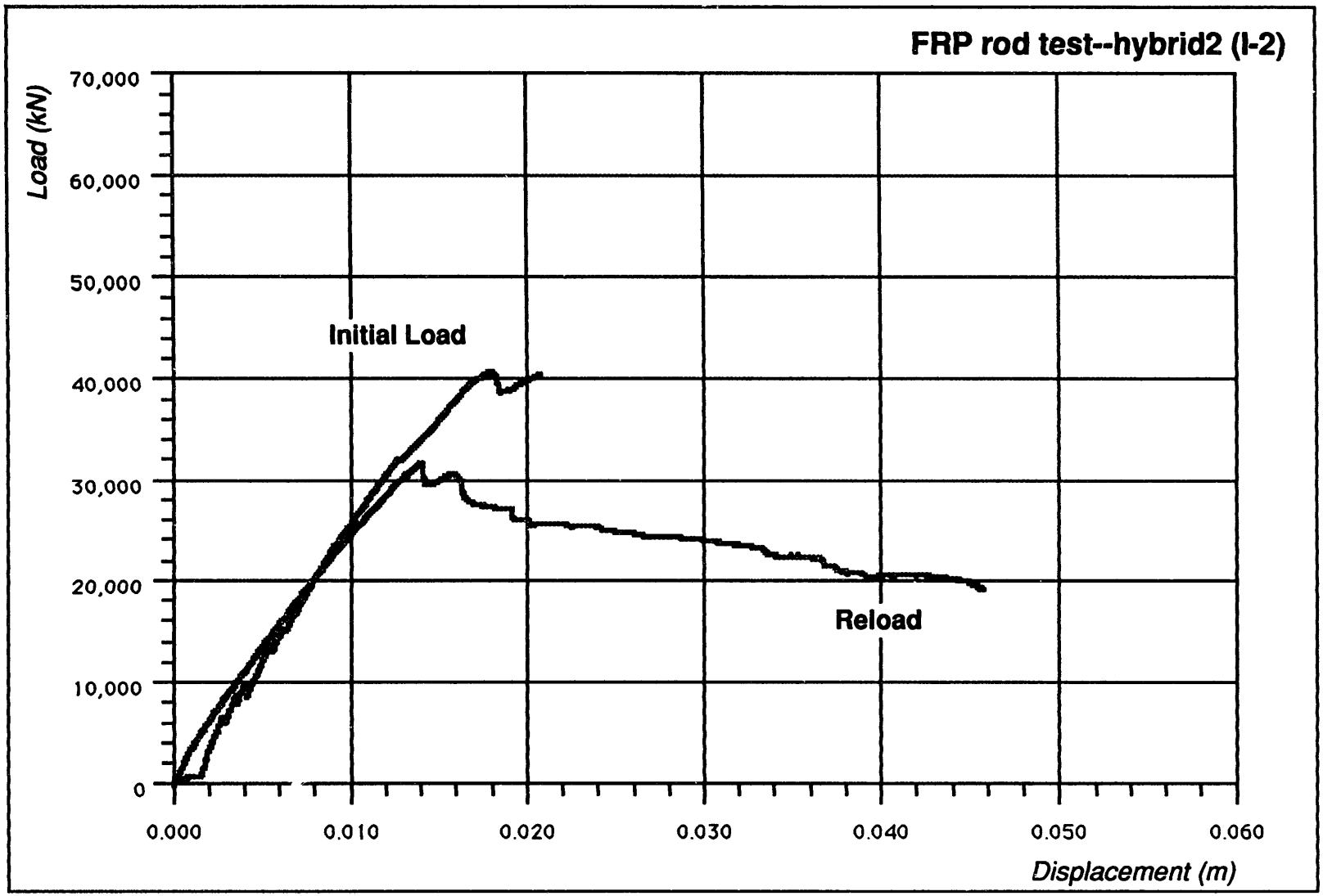

Figure B.2 Hybrid FRP Reinforced Concrete T-Beam Phase I, Test 2 (hybrid2)

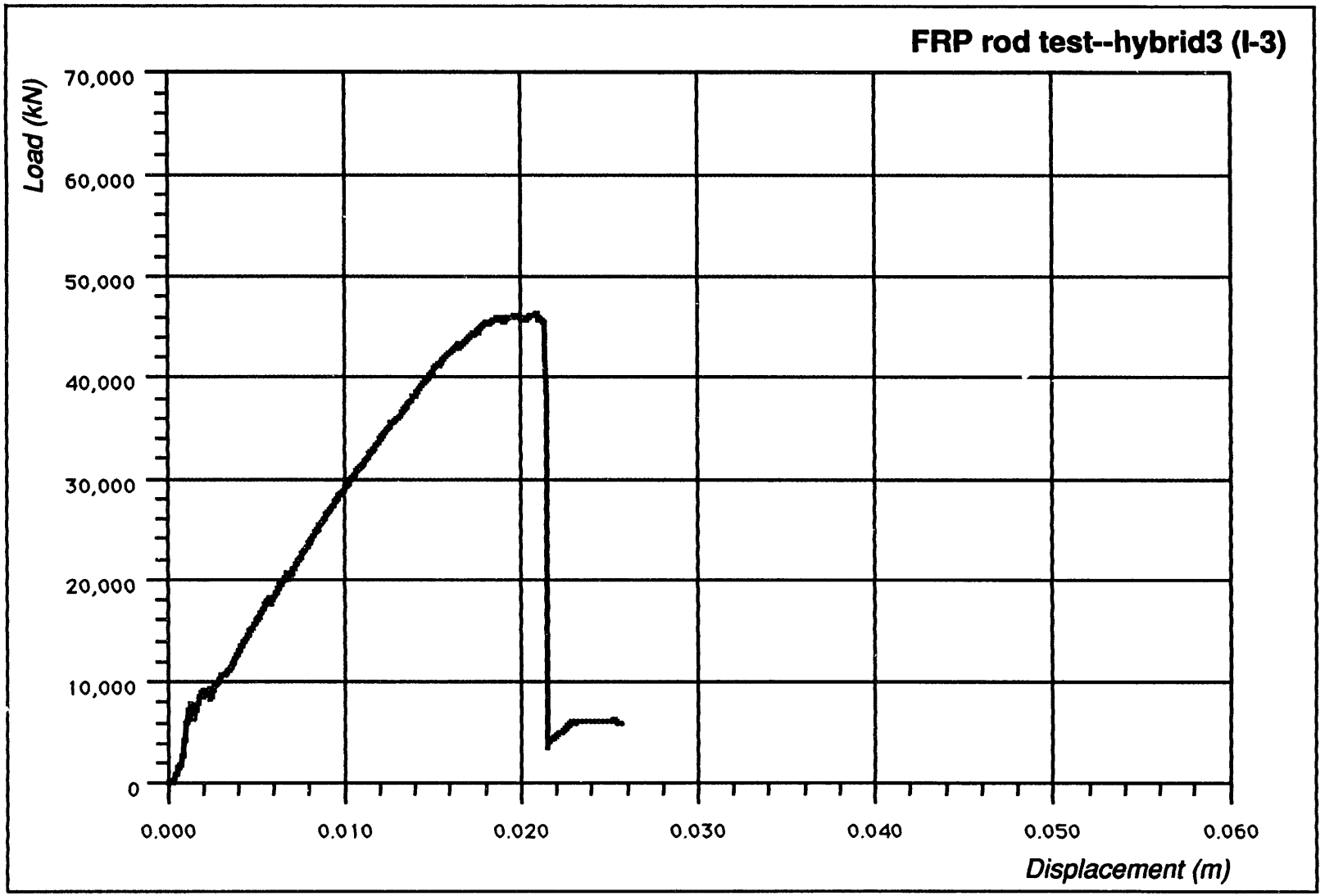

Figure B.3 Hybrid FRP Reinforced Concrete T-Beam Phase I, Test 3 (hybrid3)

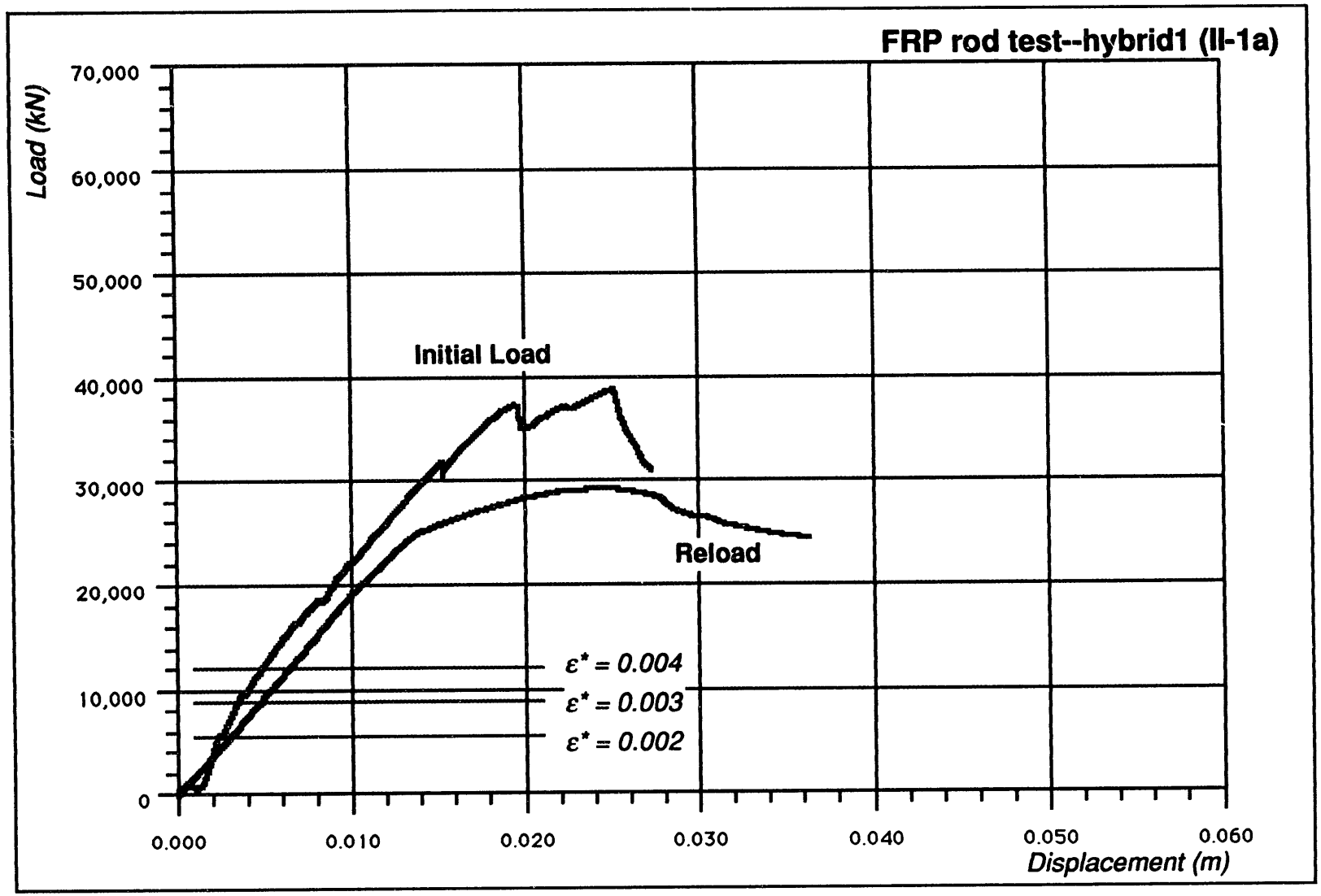

Figure B.4 Hybrid FRP Reinforced Concrete T-Beam Phase II, Test 1a (hybrid1)

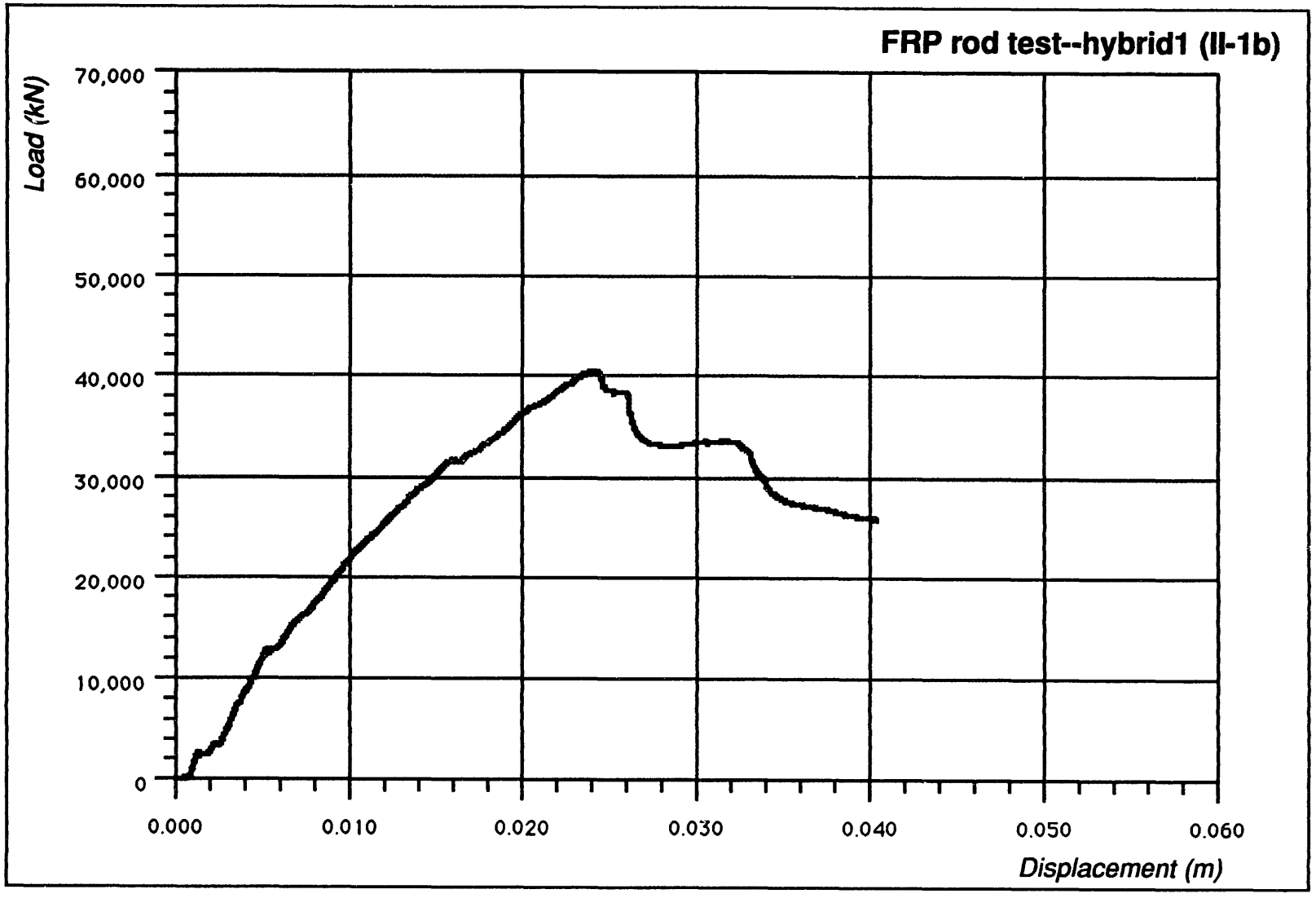

Figure B.5 Hybrid FRP Reinforced Concrete T-Beam Phase II, Test 1b (hybrid1)

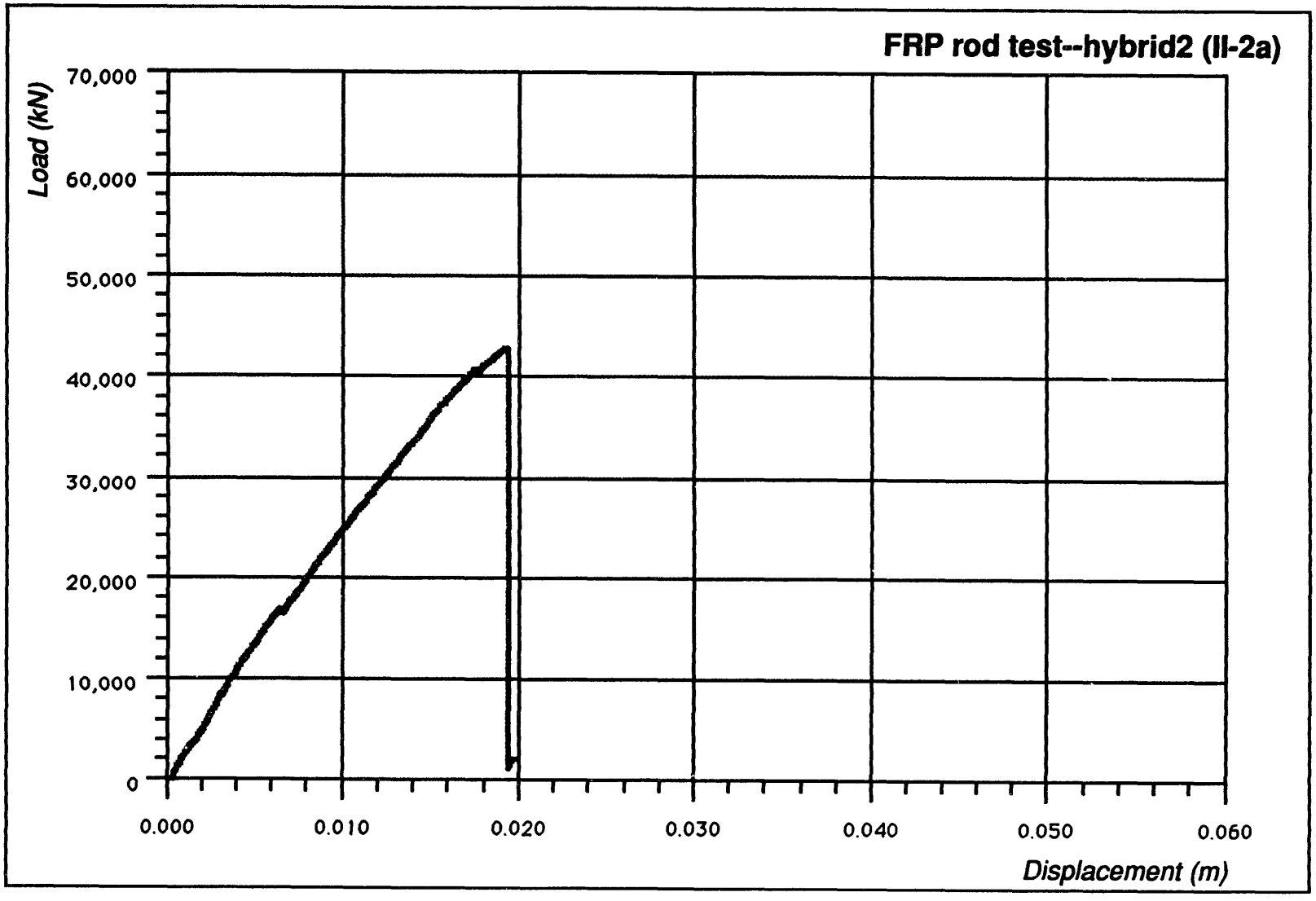

Figure B.6 Hybrid FRP Reinforced Concrete T-Beam Phase II, Test 2a (hybrid2)

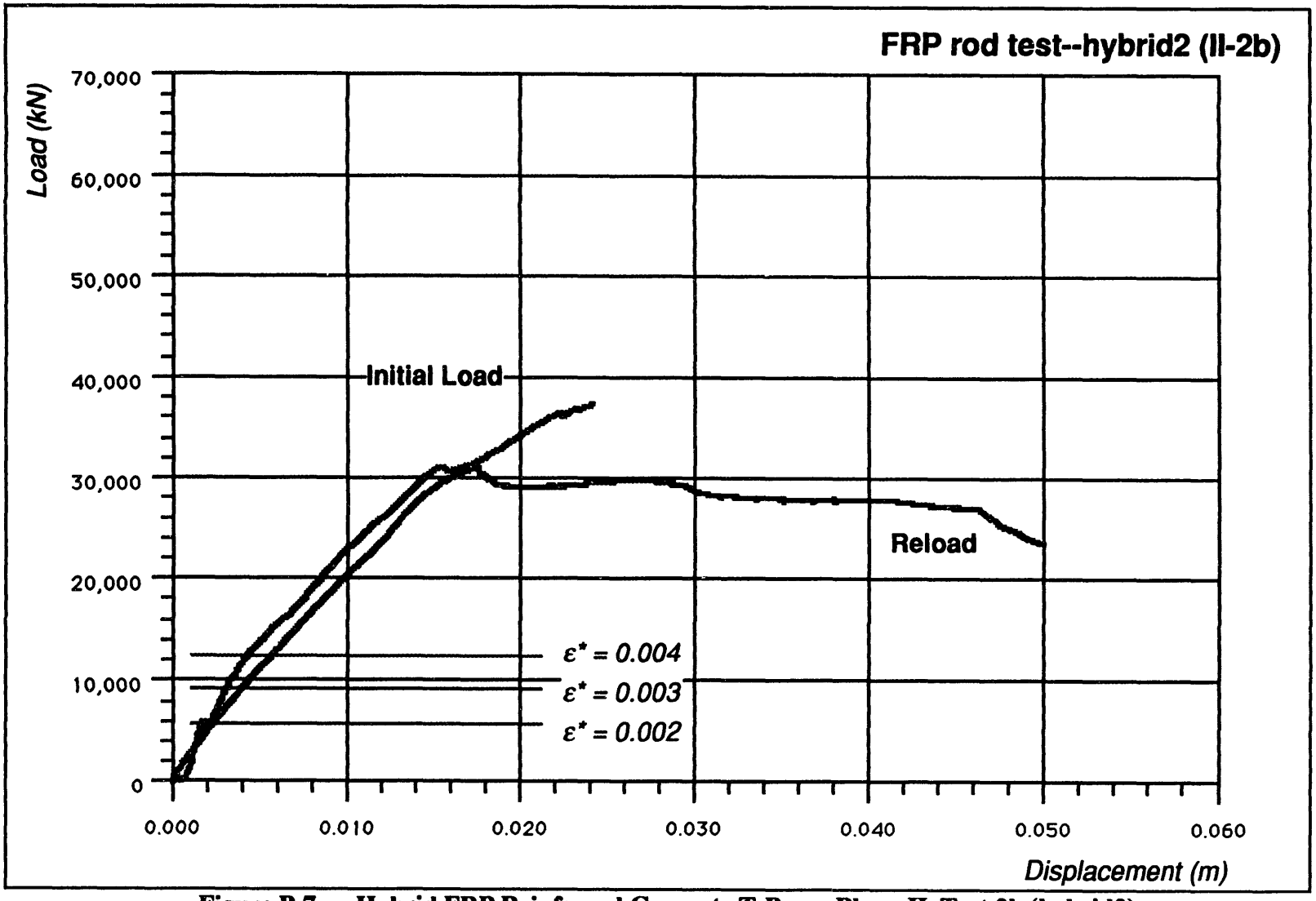

Figure B.7 Hybrid FRP Reinforced Concrete T-Beam Phase II, Test 2b (hybrid2)

Appendix C *BoxCost* Spreadsheet Analysis Program

	A	B	C	D	E	F	G
1	User Input:			okay!			page 1
2	material data			okay!			
3	Er =	200,000	(MPa)	okay!			
4	fconc =	41.50	(MPa)	okay!			
5	fr =	414.00	(MPa)	okay!			
6	rho.conc =	23.00	(kN/m^3)	okay!			
7	rho.rein =	77.00	(kN/m^3)				
8	$.conc =	$90.00	($/m^3)	okay!			
9	$.rein =	$0.55	($/kg)	okay!			
10	$.ps =	$2.25	($/kg)				
11	F.lp =	0.20		okay!			
12	frp data			okay!			
13	F.frp =	5.50		okay!			
14	b.frp =	0.20	(m)	okay!			
15	h.frp =	0.40	(m)		negative reinforcement fractions		
16	section data			okay!	F.nr.v =	0.25	
17	b =	1.40	(m)		F.nr.h =	1.00	
18	h =	2.10	(m)	okay!	bar and clearance dimensions		
19	t.min =	0.15	(m)	okay!	D.stir =	0.012700	(m)
20	L =	25.00	(m)		D.b =	0.015875	(m)
21	loadings			okay!	C.c =	0.038100	(m)
22	w.v =	2.00	(tonne/m)	okay!	concrete stress constraints		
23	P.v =	0.00	(tonne)	okay!	F.c.t* =	500	(f'c^.5) [Pa]
24	w.h =	1.50	(tonne/m)		F.c.c* =	0.45	(*f'c)
25	P.h =	0.00	(tonne)	okay!	permissible strains		
26	e.h =	3.00	(m)		eps.conc* =	0.0030	
27	w.m =	0.10	(tonne/m)		eps.r' =	0.0020	
28	deflection constraints				alpha.r =	0.6000	
29	kΔ.v.min =	1000			material reduction factors		
30	kΔ.h.min =	1000			phi =	0.90	
31	load factors				phi' =	0.85	
32	F.d =	1.40			max. shear zone check		
33	F.v =	1.40			?.av =	0.50	(*h)
34	F.h =	1.70			?.ah =	0.50	(*b)

1	2
3	4
5	6
7	8
9	10

Figure C.1a ***BoxCost*** **Spreadsheet Analysis Program (page 1 of 10)**

	H	I	J	K	L	M	N	O
1	Results:							page 2
2	total cost w/ frp				concrete modulus			
3	C.total =	$306.87	(per m)		E.conc =	28,300	(MPa)	
4	total cost w/o frp				section thickness			
5	C =	$242.74	(per m)		t =	0.15	(m)	
6	mild reinforcement costs				prestressing results			
7	C.r.v =	$28.71	(per m)		P =	3,153	(kN)	
8	C.r.h =	$42.16	(per m)		e =	0.74	(m)	
9	C.t.t =	$22.63	(per m)		beam dead weight			
10	C.t.l =	$13.99	(per m)		w.d =	2.442	(tonne/m)	
11	C.r =	$107.50	(per m)		fundamental frequency			
12	frp costs				f1 =	6.539	(Hz)	
13	C.r.v.frp =	$43.32	(per m)		deflection results			
14	C.r.h.frp =	$68.52	(per m)		kΔ.v =	4141		
15	C.t.t.frp =	$36.95	(per m)		kΔ.h =	2871		
16	C.t.l.frp =	$22.85	(per m)		Δ.v =	0.0060	(m)	
17	summary of costs				Δ.h =	0.0087	(m)	
18	C.r.frp =	$171.64	(per m)		resulting stiffness			
19	C.ps =	$51.07	(per m)		EI.v =	1.69E+09	(kg•m^2)	
20	C.c =	$84.16	(per m)		EI.h =	8.76E+08	(kg•m^2)	
21					percentage of reinforcement (w/o frp)			
22					%rho.r =	2.59	%	
23					percentage of frp cost to total mild rein. cost			
24					%rho.frp.r =	59.66	%	
25					percentage of frp cost to overall total cost			
26					%rho.frp.tot =	26.42	%	
27								
28								
29								
30								
31								
32								
33								
34								

1	2
3	4
5	6
7	8
9	10

Figure C.1b *BoxCost* Spreadsheet Analysis Program (page 2 of 10)

	A	B	C	D	E	F	G
35							*page 3*
36							
37							
38							
39							
40							
41				*(Note: 1 tonne/meter = .67196897514 kips/ft)*			
42		(MPa)	(psi)		(MPa)	(psi)	
43	fconc =	41.5	6,019	Econc =	28,300	4,103,306	
44	fr =	414	60,046	Er =	200,000	29,007,548	
45		(kN/m^3)	(lb/ft^3)	$.conc =	$68.81	(per yd^3)	
46	rho.conc =	23	146		$90.00	(per m^3)	
47	rho.rein =	77	490	$.rein =	$0.25	(per lb)	
48	Concrete Beam Design				$0.55	(per kg)	
49	Span, L =	984.25	(inches)	82.02	(feet)	25.00	(m)
50	b =	55.12	(inches)	4.59	(feet)	1.4000	(m)
51	t =	5.91	(inches)	0.49	(feet)	0.1500	(m)
52	d.v =	79.72	(inches)	6.64	(feet)	2.0250	(m)
53	h =	82.68	(inches)	6.89	(feet)	2.1000	(m)
54	t.min =	5.91	(inches)			0.15	(m)
55	Dead load multiplying factor (vertical), F.d=			1.40			
56	Live load multiplying factor (vertical), F.v=			1.40			
57	Wind load multiplying factor (horizontal), F.h=			1.70			
58	Vert. Strength Required:				1758.02	(ft•kip)	
59	Mn.v=[F.v/phi]•[[w.l•L^2/8] + [P.l•L/4]] =				2.3836E+06	(N•m)	
60	c.v=eps.conc*•d.v/[(eps.conc*+eps.r°]=				56.95	(in)	
61				ßc =	42.71	(in)	
62	T.v=Mn.v/(d.v-ßc/2)=				361,426	(lbs)	
63	Ar.v=max[T.v/(Ert•eps.r), Ar.vmin] =			6.23	(in^2)	4.0193E-03	(m^2)
64	Arc.v=max[%A.rt.v, Ar.vmin]=			4.08	(in^2)	2.6298E-03	(m^2)
65	Vert. Strength Provided:			okay!	okay!	*okay!*	*okay!*
66	Mn.prov=T•Ats(d-ßc/2)/12,000 =				1,820	(ft•kip)	okay!
67	Ig.wo(w/o reinf) = [bh^3-(b-2t)(h-2t)^3]/12 =				1,311,410	(in^4)	*okay!*
68	Mcr.wo=[[7.5•f'c^.5]•Ig.wo•2/h]/12,000 =				1,538	(ft•kip)	

1	2
3	4
5	6
7	8
9	10

Figure C.1c ***BoxCost*** **Spreadsheet Analysis Program (page 3 of 10)**

	H	I	J	K	L	M	N	O
35								*page 4*
36								
37								
38								
39								
40								
41		% =	0.25	eps.r' = fy	0.002070		eps.r' =	0.0020
42		eps.conc* =	0.0030	n = Er/Ec	7.07		alpha.r =	0.6000
43		phi =	0.90	ß =	0.75		eps.r° =	0.001200
44		phi' =	0.85					
45	Loadings:							
46	Ag=bh-(b-2t)(h-2t)=		1488.00	(in^2)	9.6000E-01	(m^2)		
47	Dead Load (Beam Weight),w.d={[Ag*rho.con]+(A.cs+A.ts+A.csh+A.tsh)(rho.rein-rho.conc)]/144,000}+w.m=							(in N)
48				2.441909	(tonne/m)	1.64	(kip/ft)	2.3947E+04
49	Distributed (vehicle) Vertical Live Load, w.v =			2.00	(tonne/m)	1.34	(kip/ft)	1.9613E+04
50	Concentrated (vehicle) Vertical Live Load, P.v =			0.00	(tonne)	0.00	(kip)	0.0000E+00
51	Distributed (wind) Horizontal Live Load, w.h =			1.50	(tonne/m)	1.01	(kip/ft)	1.4710E+04
52	Concentrated (wind) Horizontal Live Load, P.h =			0.00	(tonne)	0.00	(kip)	0.0000E+00
53	Eccentricity (vehicle to beam), e.h =			3.00	(m)	9.84	(ft)	
54	Distributed Torsional moment, Tn.d = w.h•e.h =			4.50	(tonne)	9.92	(kip)	4.4130E+04
55	Concentrated Torsional Moment, Tn.c = P.h•e.h =			0.00	(tonne•m)	0.00	(kip•ft)	0.0000E+00
56	Magnetic motor winding load, w.m =			0.10	(tonne/m)	0.07	(kip/ft)	9.8067E+02
57	*Md (unfactored) = [(w.d)*(L^2)/8]=*				*1379.87*	*(ft•kip)*	1.8709E+06	(m^2)
58	Horiz. Strength Required:				d.h=b-t/2 =	52.17	(in)	
59	Mn.h=[F.h/phi]•{[w.w•L^2/8] + [P.w•L/4]} =				1601	(ft•kip)	2.1707E+06	(N•m)
60	c.h=eps.con*•d.h/[(eps.conc*+eps.r°]=				37.26	(in)		
61				ßc.h =	27.95	(in)		
62	T.h=Mnh/(d.h-ßc.h/2)=				503,049	(lbs)		
63	Art.h=max{T.h/Ert•eps.r'-(t/b)(Artv+Arcv),Ar.hmin}=			7.57	(in^2)	4.8818E-03	(m^2)	
64	Arc.h=%Art.h=			7.57	(in^2)	4.8818E-03	(m^2)	
65	Horiz. Strength Provided:			okay!	okay!			
66	Mnh.prov=T.h•Ats.h(d.h-ßc.h/2)/12,000 =				1,701	(ft•kip)	okay!	
67	Igh.wo(w/o reinf) = [hb^3-(h-2t)(b-2t)^3]/12 =				674,024	(in^4)		
68	Mcrh.wo={[7.5•f'c^.5]•Igh.wo•2/b}/12,000 =				1,186	(ft•kip)		

1	2
3	4
5	6
7	8
9	10

Figure C.1d *BoxCost* Spreadsheet Analysis Program (page 4 of 10)

	A	B	C	D	E	F	G
69	Vert. Stiffness Required:						*page 5*
70	kΔv =	1000	Δv.max = L/? =	0.9843	(in)	0.0250	(m)
71	*bgv ={[2t(b-2t)] + [(n-1)(Arc.v + Art.v)] +2th} =*				*1550.53*		
72	*cgv ={th(b-2t) + (n-1)[Art.v•d.v+Arc.v•(t/2)] + th^2} =*				*64598.33*		
73	yc.v = _cgv_/_bgv_ =		1.0582E+00	(m)	41.66	(in)	
74	Igv=(2t/3)[yc.v^3+(h-yc.v)^3]+(b-2t)t^3/6+(yc.v-t/2)^2[(b-2t)t+(n-1)Arc.v]+(d.v-yc.v)^2[(b-2t)t+(n-1)Art.v]=						
75	(m) *Mn.reqd•h/[.45f'c+6f'c^.5] =*			*549,508*	5.8413E-01	(m^4)	
76	1.0418E+00 yt.v=h-yc.v =		41.02	(in)	1,403,382	(in^4)	
77	1.0582E+00 yc.v		41.66	(in)	*EI(kg•m^2)=*	*1.69E+09*	
78	Mcr = {7.5(f'c^.5)Ig/yt}/12,000 =				1659.12	(ft•kip)	
79	Vert. Stiffness Provided:		*L/?=*	*4141*	Iv.min=	1.4100E-01	(m)
80	Δ=[5w.l•L^4 + 8P.l•L^3]/[384(Econc*Ig)]=			0.24	(in)	0.0060	(m)
81	Prestressing Calculations:			prestress loss, F.lp =	0.20	okay!	*okay!*
82	Pv.max = [Ag/(1-loss)]+[(?.c)f'c-Mn•yc/Ig]=			3873.08	(kips)	1.7228E+07	(N)
83	Pv.min'= Ag/(1-loss)]+[Mn•yt/Ig - (?.t)f'c^.5]=			277.86	(kips)	1.2360E+06	(N)
84	Pv.min=max{Pv.min',Md/[emax(1-loss)]}=			708.74	(kips)	3.1526E+06	(N)
85	fc.min (compression) = -(?.c)f'c =		0.45	-2708.58	(psi)	0.00	(Pa)
86	ft.max (tension) = (?.t)f'c^.5 =		6.02	467.17	(psi)	467.17	(Pa)
87	P=max{P.min,Ph.min}=			708.74	(kips)	3.1526E+06	(N)
88	fc={(1-loss)[(-P/Ag)} - {(Mn)y.c/Ig} =			-1007.33	(psi)	okay!	*okay!*
89	ft={(1-loss)[(-P/Ag)} + {(Mn)y.t/Ig} =			235.52	(psi)	okay!	*okay!*
90	e=M.d/[P(1-loss)] =			29.20	(in)	7.4178E-01	(m)
91	Total wt of tendons, P*L*(0.021521281824lb/ft•kip) =			1251	(lbs)	1.6814E+06	(kg)
92	Unit cost of prestress steel =			1.02	($/lb)	2.25	($/kg)
93	Strength	Ats	Acs	Stiffness	$/km	$/mile	okay!
94	okay!	okay!	okay!	okay!	$242,736	$390,646	
95	*okay!*	*okay!*	*okay!*	*okay!*	$306,868	$493,856	
96				fc	ft	ε	
97	b(m)	h(m)	L(m)	okay!	okay!	okay!	
98	1.40	2.10	25	*okay!*	*okay!*		
99			D.h.(m)	*okay!*			
100	Tension Zone Calculations:		0.015875	1	(in^2)	(m^2)	
101	Min.vert.rein req'd,Ar.vmin=.0068*(bt^2/2)/(145,037/Ert•eps.t")^3 =				4.08	2.6298E-03	
102	Max.vert.reinf allowable, Ar.vmax = .08bt =				26.04	1.6800E-02	

1	2
3	4
5	6
7	8
9	10

Figure C.1e *BoxCost* Spreadsheet Analysis Program (page 5 of 10)

	H	I	J	K	L	M	N	O
69	Horiz. Stiffness Required:							*page 6*
70	kΔh =	1000	Δh.max = L/kΔh =	0.9843	(in)	0.0250	(m)	
71	*bgh = {[2t(h-2t)] + [(n-1)(Arc.h + Art.h)] +2tb} =*				*1579.82*			
72	*cgh = {tb(h-2t) + (n-1)[Art.h•d.h+Arc.h•(t/2)] + tb^2} =*				*43538.35*			
73	yc.h = cgh / bgh =		7.0000E-01	(m)	27.56	(in)		
74	Igh=(2t/3)[yc.h^3+(b-yc.h)^3]+(h-2t)t^3/6+(yc.h-t/2)^2[(h-2t)t+(n-1)Arc.h]+(d.h-yc.h)^2[(h-2t)t+(n-1)Art.h]=							
75	(m)				729,617	(in^4)	3.0369E-01	(m^4)
76	7.0000E-01	yt.h=b-yc.h =	27.56	(in)	*EI.h =*	*8.76E+08*	*(kg•m^2)*	
77	7.0000E-01	yc.h =	27.56	(in)				
78	Mcrh = {7.5(f'c^.5)Igh/yth}/12,000 =				1283.73	(ft•kip)		
79	Horiz. Stiffness Provided:		*L/?=*	*2871*	Ih.min=	1.0575E-01	(m)	
80	Δh=[5w.w•L^4+8P.w•L^3]/[384(Econc*Igh)]=			0.34	(in)	0.0087	(m)	
81	Prestressing Calculations:					okay!		
82	Pi.max = [Ag/(1-loss)]+[(?.c)f'c-Mnh•ych/Igh]=			3,688	(kips)	1.6406E+07	(N)	
83	Pi.min = [Ag/(1-loss)]•[Mnh•yth/Igh-(7.t)f'c^.5]=			481	(kips)	2.1390E+06	(N)	
84								
85								
86								
87	fch={(1-loss)[(-P/Ag)} - {(Mnh)ych/Igh} =			-1,107	(psi)	okay!		
88	fth={(1-loss)[(-P/Ag)} + {(Mnh)yth/Igh} =			345	(psi)	okay!		
89					<< ------ without FRP ------ >>			<<w/ FRP>>
90	Material Cost of Beam:				(cost/beam)	(cost/mile)	(cost/km)	*(+frp/km)*
91	Total Cost of concrete = [AgL-(Vt.t/b+Vt.l/b)]*$.conc =				$2,104	$135,442	$84,160	
92	Cost of vert. rein = [{Acs+Ats}L]*rho.rein*$.rein =				$718	$46,211	$28,714	*$14,602*
93	Cost of horiz. rein = [{Acsh+Atsh}L]*rho.rein*$.rein =				$1,054	$67,856	$42,164	*$26,352*
94	Cost of stirrup rein = [Vol.stir]*rho.rein*$.rein =				$566	$36,422	$22,632	*$14,322*
95	Total long. torsional rein cost=[Al•L]*rho.rein*$.rein =				$350	$22,522	$13,994	*$8,856*
96	Total mild rein cost =				$2,688	$173,011	$107,504	*$64,132*
97	Total Prestessing rein cost =				$1,277	$82,193	$51,073	
98	Total beam material cost =				$6,068	$390,646	$242,736	
99								
100	*FRP cost factor =*	*5.50*			*Total beam mat. cost w/frp =*			*$306,868*
101	*b.frp = width of "magnetic-free" zone =*						*$493,856*	*($/mile)*
102	*0.200*	*(m)*	*7.87*	*(in)*	okay!			

1	2
3	4
5	6
7	8
9	10

Figure C.1f *BoxCost* Spreadsheet Analysis Program (page 6 of 10)

	A	B	C	D	E	F	G
103	Min.h.reinf.reqd.Ar.hmin = .3068*(h-2t)(t^2/2)/(145,037/Er•eps.r')^3=				5.24	3.3812E-03	*page 7*
104	Max.hor.reinf allowable, Ar.hmax = .08(h-2t) =				33.48	2.1600E-02	
105	6.23						
106	1.40	2.10	25.00		*6.54*	*(Hz)*	
107	0.15	6019	0.24		L/?=	*4141*	
108	**2.00**	**1.50**	**3.00**	$242,736	*2.37*	*(tonnes/m)*	
109	Factor Vert. Shear, Vn.v=[F.v/phi']•[w.v•L/2+P.v]+[F.d•w.d•L/2•phi']=				201.62	(kip)	(N)
110	Factored Horizontal Shear, Vn.h = [F.h/phi']•[w.h•L/2+P.h] =				82.67	(kip)	(N)
111	Factored Torsional Moment, Tn = [F.h/phi']•e.h•[w.h•L/2+P.h] =				813.71	(kip•ft)	(N•m)
112	Torsion and Shear Calculations:			-->	9,765	(kip•in)	
113	Bt=(4t/b)•(b^2•h)=		107,646	(in^3)	1.7640E+00	(m^3)	
114	bwd = 2t•d =		942	(in^2)	6.0750E-01	(m^2)	
115	Ct=bwd/Bt =		0.008747	(1/in)	3.4439E-01	(1/m)	
116	Check: phi'•gam•0.5•f'c^0.5•Bt =		4,750	(kip•in)	5.3673E+05	(N•m)	*okay!*
117	Tn.max (N•m) = 635•gam2•(b•f'c)^0.5•ht/{1+b[127•gam2•h•Vu/(332d•Tu)]^2}^.5 =						*okay!*
118				26,985	(kip•in)	1.7204E+06	(N•m)
119	Tc=Tco/{1+[(Tco•Vu)/(Vco•Tu)]^2}^.5 =			4,455	(kip•in)	5.0337E+05	(N•m)
120	Vc=Vco/{1+[(Vco•Tu)/(Tco•Vu)]^2}^.5 =			91.99	(kip)	4.0919E+05	(N)
121							
122	Ts=Tn-Tc =			5,309	(kip•in)	5.9988E+05	(N•m)
123		*X1=b-Dstir-2Cc)=*		*51.62*	*(in)*	1.3111E+00	(m)
124		*Y1=h-Dstir-2Cc)=*		*79.18*	*(in)*	2.0111E+00	(m)
125		*a = .66 + .33(Y1/X1) =*		*1.1662*	*okay!*		
126	At/s=Ts/(alpha•X1•Y1•Er•eps.r')=		4.8771E-04	(m^2/m)	1.92E-02	(in^2/in)	
127	Stirrup Diameter, Dstir =			0.50	(in)	1.2700E-02	(m)
128	Vs=Vn.max-Vc =		4.8764E+05	(N)	109.63	(kip)	
129	Av/s=Vs/d•Er•eps.r'=		6.0203E-04	(m^2/m)	2.37E-02	(in^2/in)	
130	At.t= max(At/s +.5Av/s,At.tmin) =		7.8873E-04	(m^2/m)	3.11E-02	(in^2/in)	
131		*Astir = Dstir^2/4•π =*		*0.1963*	*(in^2)*	1.2668E-04	(m^2)
132	*s.'=Astir/(At/s +.5Av/s)=*		1.6061E-01	(m)	*6.32*	*(in)*	
133	*s.1=12" =*		3.0000E-01	(m)	*11.81*	*(in)*	
134	*s.2=(X1+Y1)/4 =*		8.3055E-01	(m)	*32.70*	*(in)*	
135	*s.3=min(d.v/2, d.h/2) =*		6.6250E-01	(m)	*26.08*	*(in)*	
136	F.al=	579.84	7.2310E-04	(m^2/m)	*2.85E-02*	(in^2/in)	*At.tmin/s=190•F.*

1	2
3	4
5	6
7	8
9	10

Figure C.1g *BoxCost* Spreadsheet Analysis Program (page 7 of 10)

	H	I	J	K	L	M	N	O
103	*h.frp = depth of "magnetic-free" zone =*							*page 8*
104	*0.400*	*(m)*	*15.75*	*(in)*	okay!			
105	gam = (1+[10P/(Ag•f'c)])^.5 =			1.338403				
106	gam1 = 2.5gam -1.5 =			1.846007				
107	gam2 = (1-.833P/(Ag•f'c))•gam			1.250179				
108								
109	8.9683E+05		Vu = max{ Vn.v, Vn.h}•phi'		7.6230E+05 (N)		171.37 (kip)	
110	3.6775E+05							
111	1.1032E+06		Tu = Tn•phi' =		9.3776E+05 (N•m)		8299.88 (kip•in)	
112	(?.av)=	0.50	a.v=(?.av)h=		41.34 (in)		1.0500E+00 (m)	
113	e.a=w.d•a.v(L-a.v)/[2P(1-F.lp)]=				4.70 (in)		1.1939E-01 (m)	
114	(?.ah)=	0.50	a.h=(?.ah)b=		27.56 (in)		7.0000E-01 (m)	
115								
116	d.pv= max{ (h/2 + e.a) , 0.8h } =				66.14 (in)		1.6800E+00 (m)	
117	d.ph= 0.8b =				44.09 (in)		1.1200E+00 (m)	
118	Vp= 2eP(1-F.lp)/L =				33.65 (kip)		1.4967E+05 (N)	
119	Vd = w.d(L/2-a.v) =				61.64 (kip)		2.7419E+05 (N)	
120								
121	Vi.v= 0.5•{ Fv[w.v(L-2a.v) + P.v]+Fd•w.d(L-2a.v) } =				156.98 (kip)		6.9827E+05 (N)	
122	Vi.h= 0.5•Fh[w.h(L-2a.h) + P.h] =				66.34 (kip)		2.9508E+05 (N)	
123	Mmax.v= 0.5•a.v•{ Fv[w.v(L-a.v) + P.v] +Fd•w.d(L-a.v) }=				6,787 (kip•in)		7.6680E+05 (N•m)	
124	Mmax.h= 0.5•a.h•Fh[w.h(L-a.h) + P.h] =				1,882 (kip•in)		2.1268E+05 (N•m)	
125	Mcr.v={[500•f'c^.5+P(1-Flp)/Ag]•Igv/ytv} =				29,023 (kip•in)		3.2791E+06 (N•m)	
126	Mcr.h={[500•f'c^.5+P(1-Flp)/Ag]•Igh/yth}=				22,456 (kip•in)		2.5372E+06 (N•m)	
127								
128	Vcw.v= [300•f'c^.5+(0.3P[1-F.lp]/Ag)]2t•d.pv + Vp =				341.92 (kip)		1.5209E+06 (N)	
129	Vcw.h= [300•f'c^.5+(0.3P[1-F.lp]/Ag)]2t•d.ph =				205.52 (kip)		9.1418E+05 (N)	
130	Vci.v= 50•f'c^.5•2t•d.pv+(Vi.v•Mcr.v/Mmax.v) + Vd =				769.43 (kip)		3.4226E+06 (N)	
131	Vci.h= 50•f'c^.5•2t•d.ph+(Vi.h•Mcr.h/Mmax.h) =				815.69 (kip)		3.6284E+06 (N)	
132	*Vci.vmin=1000/7•f'c^.5•2t•d.pv =*				*104.27 (kip)*		*4.6383E+05 (N)*	
133	*Vci.hmin=1000/7•f'c^.5•2t•d.ph =*				*69.52 (kip)*		*3.0922E+05 (N)*	
134	Vco= min{Vcw.v,Vcw.h, Vci.v, Vci.h} =				205.52 (kip)		9.1418E+05 (N)	
135	Tco=127(b•f'c)^.5•th•gam1 =				4,982 (kip•in)		5.6291E+05 (N•m)	
136	•[12P/(Ag•f'c) + 1]=							

Figure C.1h ***BoxCost*** **Spreadsheet Analysis Program (page 8 of 10)**

	A	B	C	D	E	F	G
137	s= min{s',s1,s2,s3}=		1.6061E-01	(m)	6.32	(in)	page 9
138	At.l°=(At/s)•[2•(X1+Y1)] =				5.02	(in^2)	(m^2)
139	At.lmin={[4F.t•s][Tu/{Tu+(Vu/3Ct)}]-2At.t•s}•{(X1+Y1/s)}=				-8.10	(in^2)	(m^2)
140	At.l = max{At.l°,At.lmin} or 0.0 if phi'•gam•f'c^.5•Bt > Tn =				5.02	(in^2)	(m^2)
141	*Volume of torsional rein./beam = A.l/144•L =*				*2.86*	*(ft^3)*	(m^3)
142	#stirrups reqd/beam, n.stir = L/s =				155.66		
143	Length of each stirrup, L.stir =2(X1+Y1)=				262	(in)	(m)
144	Vol.t=Volume of stirrup rein./beam = π/4•D.stir^2•n.stir/144•L.stir/12 =				4.63	(ft^3)	(m^3)
145							
146	*Vol.l=Volume of long. rein./beam = (At.l+Ats+Acs+Atsh+Acsh)•L =*				*17.35*	*(ft^3)*	(m^3)
147	*Vol.c=Volume of conc/beam = Ag/144•L - Vol.t - Vol.l =*				*825.57*	*(ft^3)*	(m^3)
148	*Wd=Weight of beam = (Vol.t+Vol.l)•rho.steel +Vol.c•rho.conc + P.d =*				*132,901*	*(lbs)*	(N)
149					*1.62*	*(kips/ft)*	
150					*2.37*	*(tonnes/m)*	
151	**Beam Dynamics:**				*2.3273E+04*	*(N/m)*	
152	g =	9.80665	(m/s^2)				
153	E = Econc =	28,300,000,000	(N/m^2)				
154	I = Ig =	0.584132	(m^4)				
155	m = w.d =	2,441.91	(kg/m)				
156	L =	25.00	(m)				
157							
158	*w1 = π^2•[EI/(m•L^4)]^.5 =*			*41.087*	*(rad/s)*		
159		*f1 = w1/2π =*		*6.539*	*(Hz)*		
160		*T1 = 1/f1 =*		*0.153*	*(s)*		
161	*w2 = 4π^2•[EI/(m•L^4)]^.5 =*			*164.348*	*(rad/s)*		
162		*f2 = w2/2π =*		*26.157*	*(Hz)*		
163		*T2 = 1/f2 =*		*0.038*	*(s)*		
164							
165	*w3 = 9π^2•[EI/(m•L^4)]^.5 =*			*369.782*	*(rad/s)*		
166		*f3 = w3/2π =*		*58.853*	*(Hz)*		
167		*T3 = 1/f3 =*		*0.017*	*(s)*		

Figure C.1i ***BoxCost*** **Spreadsheet Analysis Program (page 9 of 10)**

	H	I	J	K	L	M	N	O
137	F.t=ht(b•f'c)^.5/(alpha.t•X1•Y1•Er•eps.r')=				1.9521E-06			*page 10*
138	3.2406E-03							
139	-5.2261E-03							
140	3.2406E-03							
141	8.1014E-02							
142								
143	6.6444E+00							
144	1.3102E-01							
145								
146	4.9133E-01							
147	2.3378E+01							
148	5.9117E+05							
149								
150	Clear cover =		1.50	(in)	3.81E-02	(m)		
151	c.al=4t/b•400=	171.43						
152	c.al'=2•[1.5*2.4*(f'c/b)^.5/1.2•(b/X1)•(h/Y1)]=							
153		69.91						
154								
155								
156								
157								
158								
159								
160								
161								
162								
163								
164								
165								
166								
167								

1	2
3	4
5	6
7	8
9	10

Figure C.1j ***BoxCost*** **Spreadsheet Analysis Program (page 10 of 10)**

Appendix D *mode3* Spreadsheet Analysis Program

with test case examples

	A	B	C	D	E	F	G	H	I	J	K	L
1	**Dynamic Analysis:**			*g (m/s^2)*	*9.80665*	*π=*	*3.141592654*	L/v=	0.2	(s)	*/A/=*	*-1.49E-04*
2	velocity, v=		125.00	(m/s)	*6.666666667*	w1=π^2•√(EI/mL^4) =		41.8879	(rad/s)	*0.0239*	*/B/=*	*-4.15E-06*
3	beam unit mass, m=		2835.58	(kg/m)		w2=4w1=		167.5516	(rad/s)	*0.0060*	*/C/=*	*5.63E-20*
4	beam unit weight, w.b=		289.15	(N/m)		w3=9w1=		376.9911	(rad/s)	*0.0027*		
5	E=		2.00E+10	(Pa)					*T1-T3=*	*0.0212*		
6	I=		0.697968983	(m^4)	0.005	Δ=πx/L=		1.570796327			*/•A/=*	*-3.60E-03*
7	L=		28.00	(m)		∂=-2P/mL=		0.691685947	(m)		*/•B/=*	*1.20E-03*
8	EI=		1.9952E+10	(N•m^2)		ß=πv/L=		15.70796327	(1/s)		*/•C/=*	*-4.66E-04*
9	P=		-24,517	(N)		μ1=(πv/L)^2-w1^2=		-1507.86	(1/s^2)	7876.607747		
10	x=		0.5	(L)		μ2=(2πv/L)^2-w2^2=		-27086.58	(1/s^2)	*1*		
11	x= (fraction of L)		12.5	(m)		μ3=(3πv/L)^2-w3^2=		-139901.64	(1/s^2)	*6.666667*	*/:A/=*	*2.61E-01*
12	Vc=2πv/Lw1=		0.7500			*1*	*(if "1", use input v)*		*125*	*v (m/s)*	*/:B/=*	*1.16E-01*
13			*okay*			*1*	*(if "1", use input m)*		*2835.578769*	*m (kg/m)*	*/:C/=*	*-7.75E-15*
14						*0*	*(if "1", use input Vc)*		*0.75*	*Vc*		
15	A(t)=(∂/μ1) {ß/w1)sin_w1t - sin_ßt}				/A/ = A(L/v)		L/v <= t	T=t-L/v	0 <= T		m.veh (kg)=	60000
16	B(t)=(∂/μ2) {(2ß/w2)sin_w2t - sin_2ßt}				/B/ = B(L/v)		u(x,T) = [/A/cos_w1T + (/•A//w1)sin_w1T]sinΔ				#pads=	3
17	C(t)=(∂/μ3) {(3ß/w3)sin_w3t - sin_3ßt}				/C/ = C(L/v)		+ [/B/cos_w2T + (/•B//w2)sin_w2T]sin2Δ				Lp=	5.00
18							+ [/C/cos_w3T + (/•C//w3)sin_w3T]sin3Δ				Lg=	7.50
19	•A(t)=(∂/μ1) {ßcos_w1t - ßcos_ßt}				/•A/ = •A(L/v)						Sp=	12.5
20	•B(t)=(∂/μ2) {2ßcos_w2t - 2ßcos_2ßt}				/•B/ = •B(L/v)		•u(x,T) = [-/A/w1sin_w1T + /•A/cos_w1T]sinΔ				Np=	8
21	•C(t)=(∂/μ3) {3ßcos_w3t - 3ßcos_3ßt}				/•C/ = •C(L/v)		+ [-/B/w2sin_w2T + /•B/cos_w2T]sin2Δ				Ng=	12
22							+ [-/C/w3sin_w3T + /•C/cos_w3T]sin3Δ				max=	48
23	:A(t)=(∂/μ) {-ßw1sin_w1t + ß^2sin_ßt}				/:A/ = :A(L/v)						max #loads	100
24	:B(t)=(∂/μ2) {-2ßw2sin_w2t + (2ß)^2sin_2ßt}				/:B/ = :B(L/v)		:u(x,T) = [-/A/w1^2cos_w1T - /•A/w1sin_w1T]sinΔ				tot points	100
25	:C(t)=(∂/μ3) {-3ßw3sin_w3t + (3ß)^2sin_3ßt}				/:C/ = :C(L/v)		+ [-/B/w2^2cos_w2T - /•B/w2sin_w2T]sin2Δ				L.veh=	30
26							+ [-/C/w3^2cos_w3T - /•C/w3sin_w3T]sin3Δ				0	30.00
27	0 <= t <= L/v								*Static Displacement (uniform distribution)*			
28	u(x,t) = AsinΔ + Bsin2Δ + Csin3Δ								*5wL^4/384EI*	*w (kg/m) =*	2000	
29	•u(x,t) = •AsinΔ + •Bsin2Δ + •Csin3Δ								*Δs (m)=*	*-5.000E-03*	*-5.000E-03*	
30	:u(x,t) = :AsinΔ + :Bsin2Δ + :Csin3Δ								*Static Moment (uniform distribution)*			
31									*wL^2/8*			
32	Displacement:	Umax-pos (m)	tmax-pos (s)	Umax-pos/Δs	Umax-neg (m)	tmax-neg (s)	Umax-neg/Δs		*Ms (kg•m)=*	*1.5625E+05*		
33	center, force	4.869E-03	0.305	0.9738	*-4.700E-06*	*0.430*	-0.0009					
34	*center, free*	4.359E-06	0.455	0.0009	*-4.359E-06*	*0.530*	-0.0009					
35	Velocity:	•Umax-pos (m/s)	•tmax-pos (s)		•Umax-neg (m/s)	•tmax-neg (s)						
36	center, force	7.830E-02	0.085		*-7.745E-02*	*0.355*	DAF=	0.9738				
37	*center, free*	1.563E-03	0.585		*-1.563E-03*	*0.810*	NDAF =	0.0009				
38	Acceleration:	:Umax-pos(m/s^2)	:tmax-pos (s)		:Umax-neg(m/s^2)	:tmax-neg (s)	RDAF=	0.0009				
39	center, force	1.911E+00	0.390		*-2.550E+00*	*0.120*						
40	*center, free*	6.195E-01	0.705		*-6.195E-01*	*0.780*						
41	92											
42	93											
43					0.44	-0.009	0.13	4.5				
44					0.44	0.014	-0.13	-4.5				

1	5	9	13
2	6	10	14
3	7	11	15
4	8	12	16

Figure D.1a ***mode3*** **Spreadsheet Analysis Program (page 1 of 16)**

	A	B	C	D	E	F	G	H	I	J	K	L
45	0.75	4.869E-03	0.305	-4.700E-06	0.430	3	5	7.5	100	0.005	2500	24

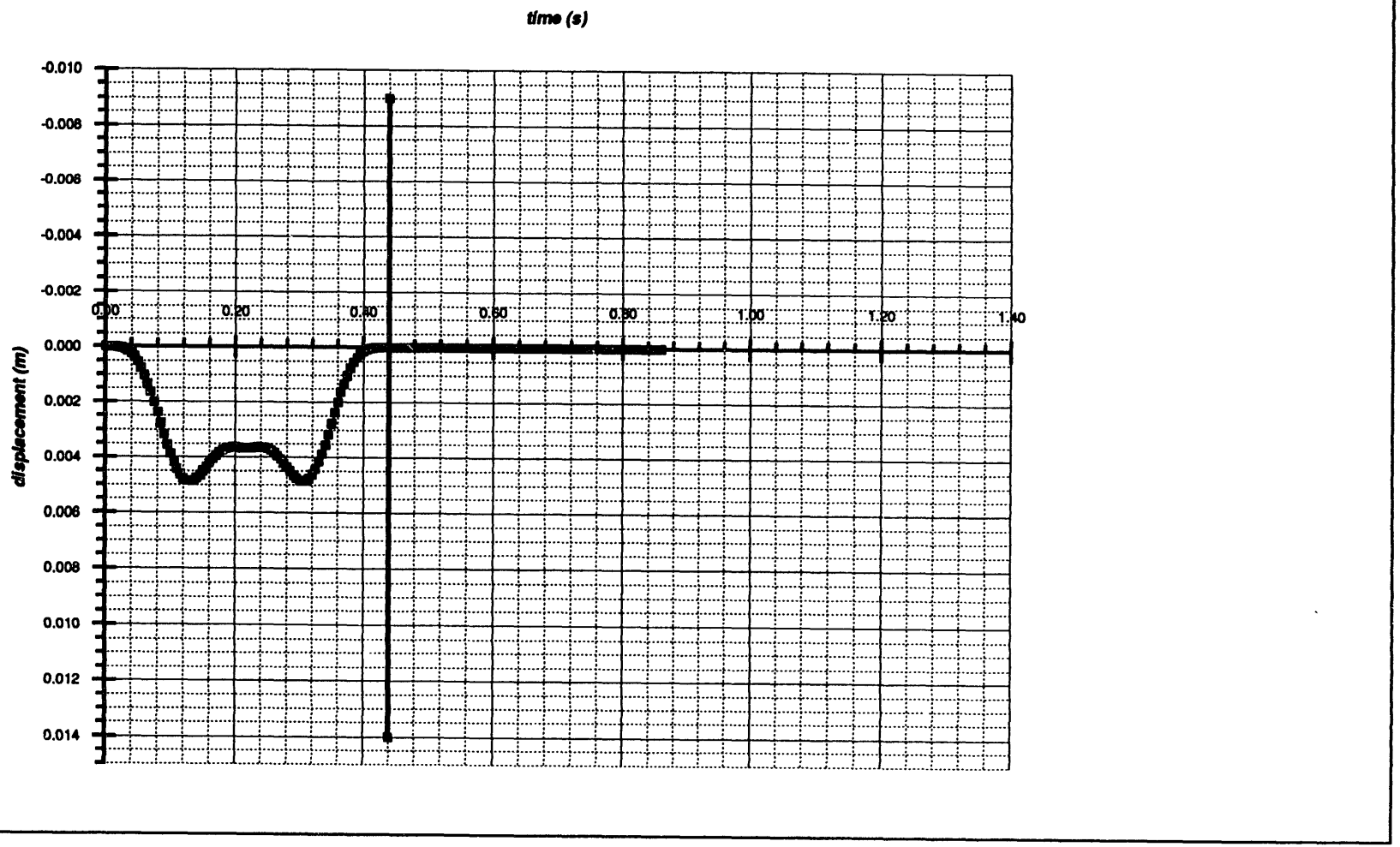

Figure D.1b ***mode3*** **Spreadsheet Analysis Program (page 2 of 16)**

	A	B	C	D	E	F	G	H	I	J	K	L
89	0.75	7.830E-02	0.085	-7.745E-02	0.355	3	5	7.5	100	0.005	2500	24

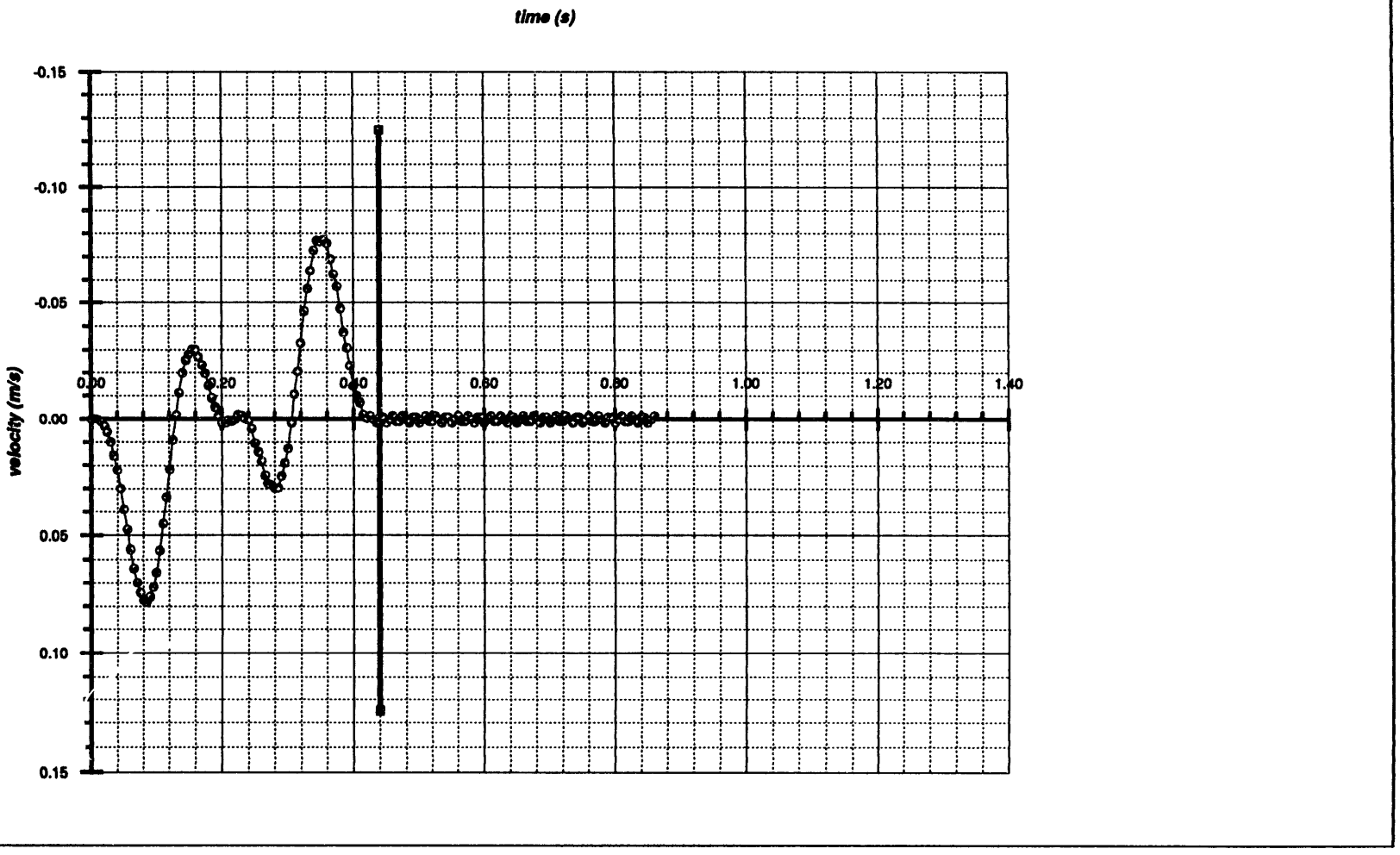

Figure D.1c ***mode3*** **Spreadsheet Analysis Program (page 3 of 16)**

	A	B	C	D	E	F	G	H	I	J	K	L
133	0.75	1.911E+00	0.390	-2.550E+00	0.120	3	5	7.5	100	0.005	2500	24

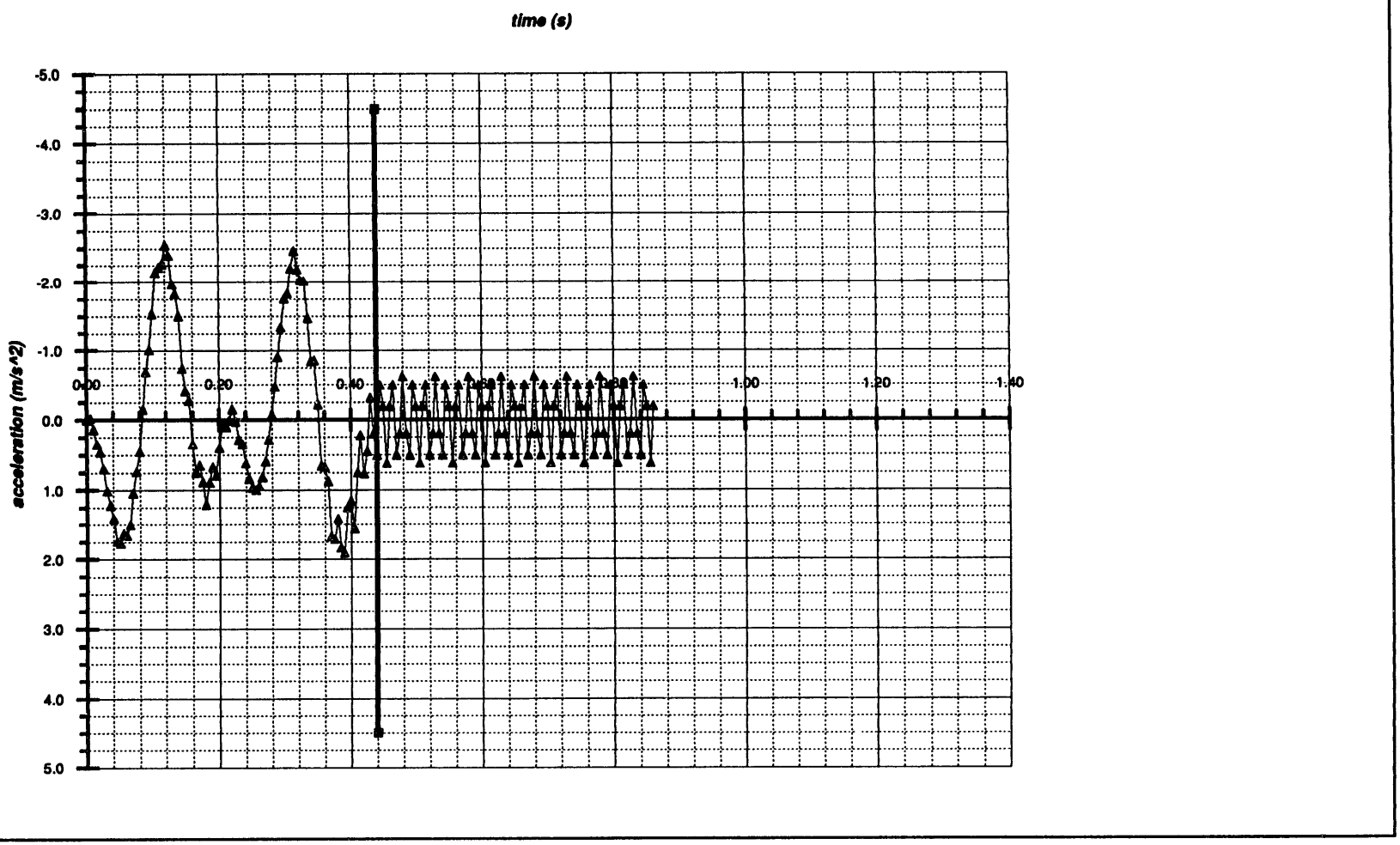

Figure D.1d *mode3* **Spreadsheet Analysis Program (page 4 of 16)**

	M	N	O	P	Q	R	S	T	U	V	W	X	Y
1		tstart	0										
2	*40*	t_inc	0.005	Total						(One point)			
3	*0*	*120*	t	U	•U	:U	*•U*	*t*	t	u	•u	:u	
4	P=	2,500	0.00000	0.000	0.00	0.0	*no*	*0.1700*	0.0000	0.0000E+00	0.0000E+00	0.0000E+00	
5	1	1	0.00500	0.000	0.00	0.0	*no*	*0.3950*	0.0050	-3.4062E-07	-1.6330E-04	-2.7098E-02	
6	2	1	0.01000	0.000	0.00	0.1	*no*	*0.6050*	0.0100	-8.1504E-07	1.3816E-04	1.6167E-01	
7	3	1	0.01500	0.000	0.00	0.3	*no*	*0.0000*	0.0150	2.4011E-06	1.1884E-03	2.0974E-01	
8	4	1	0.02000	0.000	0.00	0.5	*no*	*0.0050*	0.0200	1.0504E-05	1.9665E-03	1.1467E-01	
9	5	1	0.02500	0.000	0.01	0.7	*no*	*0.0100*	0.0250	2.2003E-05	2.7322E-03	2.2822E-01	
10	6	1	0.03000	0.000	0.01	1.0	*zero*	*0.0150*	0.0300	3.9183E-05	4.2291E-03	3.3005E-01	
11	7	1	0.03500	0.000	0.02	1.2	*no*	*0.0200*	0.0350	6.4038E-05	5.5973E-03	2.0035E-01	
12	8	1	0.04000	0.000	0.02	1.4	*no*	*0.0250*	0.0400	9.4213E-05	6.4661E-03	1.9246E-01	
13	9	0	0.04500	0.000	0.03	1.7	*no*	*0.0300*	0.0450	1.2951E-04	7.7555E-03	3.0644E-01	
14	10	0	0.05000	0.001	0.04	1.8	*no*	*0.0350*	0.0500	1.7189E-04	9.0956E-03	1.8912E-01	
15	11	0	0.05500	0.001	0.05	1.6	*no*	*0.0400*	0.0550	2.1898E-04	9.6278E-03	6.0437E-02	
16	12	0	0.06000	0.001	0.06	1.6	*no*	*0.0450*	0.0600	2.6811E-04	1.0098E-02	1.4086E-01	
17	13	0	0.06500	0.001	0.06	1.5	*no*	*0.0500*	0.0650	3.2041E-04	1.0768E-02	7.8746E-02	
18	14	0	0.07000	0.002	0.07	1.0	*no*	*0.0550*	0.0700	3.7432E-04	1.0621E-02	-1.2335E-01	
19	15	0	0.07500	0.002	0.07	0.7	*no*	*0.0600*	0.0750	4.2570E-04	9.9453E-03	-1.0877E-01	
20	16	0	0.08000	0.002	0.08	0.5	*no*	*0.0650*	0.0800	4.7435E-04	9.5353E-03	-9.3318E-02	
21	17	0	0.08500	0.003	0.08	-0.1	*no*	*0.0700*	0.0850	5.2014E-04	8.6045E-03	-2.9280E-01	
22	18	0	0.09000	0.003	0.08	-0.7	*no*	*0.0750*	0.0900	5.5895E-04	6.8739E-03	-3.5061E-01	
23	19	0	0.09500	0.004	0.07	-1.0	*no*	*0.0800*	0.0950	5.8936E-04	5.3692E-03	-2.6428E-01	
24	20	0	0.10000	0.004	0.07	-1.5	*no*	*0.0850*	0.1000	6.1264E-04	3.8358E-03	-3.8555E-01	
25	21	1	0.10500	0.004	0.06	-2.1	*no*	*0.0900*	0.1050	6.2630E-04	1.5349E-03	-4.9410E-01	
26	22	1	0.11000	0.004	0.05	-2.2	*no*	*0.0950*	0.1100	6.2819E-04	-6.6827E-04	-3.7012E-01	
27	23	1	0.11500	0.005	0.03	-2.3	*no*	*0.1000*	0.1150	6.2052E-04	-2.3981E-03	-3.6695E-01	
28	24	1	0.12000	0.005	0.02	-2.6	*no*	*0.1050*	0.1200	6.0337E-04	-4.5698E-03	-4.8469E-01	
29	25	1	0.12500	0.005	0.01	-2.4	*no*	*0.1100*	0.1250	5.7467E-04	-6.8085E-03	-3.7016E-01	
30	26	1	0.13000	0.005	0.00	-2.0	*no*	*0.1150*	0.1300	5.3675E-04	-8.2509E-03	-2.4333E-01	
31	27	1	0.13500	0.005	-0.01	-1.8	*no*	*0.1200*	0.1350	4.9221E-04	-9.6381E-03	-3.2468E-01	
32	28	1	0.14000	0.005	-0.02	-1.5	*no*	*0.1250*	0.1400	4.3992E-04	-1.1228E-02	-2.6257E-01	
33	29	0	0.14500	0.005	-0.03	-0.7	*no*	*0.1300*	0.1450	3.8141E-04	-1.1998E-02	-5.9549E-02	
34	30	0	0.15000	0.005	-0.03	-0.4	*no*	*0.1350*	0.1500	3.2087E-04	-1.2232E-02	-7.2270E-02	
35	31	0	0.15500	0.004	-0.03	-0.3	*no*	*0.1400*	0.1550	2.5852E-04	-1.2721E-02	-8.4928E-02	
36	32	0	0.16000	0.004	-0.03	0.3	*no*	*0.1450*	0.1600	1.9460E-04	-1.2673E-02	1.1830E-01	
37	33	0	0.16500	0.004	-0.03	0.8	*no*	*0.1500*	0.1650	1.3328E-04	-1.1803E-02	1.8084E-01	
38	34	0	0.17000	0.004	-0.02	0.6	*no*	*0.1550*	0.1700	7.6124E-05	-1.1133E-02	1.0023E-01	
39	35	0	0.17500	0.004	-0.02	0.9	*no*	*0.1600*	0.1750	2.2003E-05	-1.0404E-02	2.2822E-01	
40	36	0	0.18000	0.004	-0.01	1.2	*no*	*0.1650*	0.1800	-2.6436E-05	-8.8706E-03	3.4449E-01	
41	37	0	0.18500	0.004	-0.01	0.9	*no*	*0.1750*	0.1850	-6.6839E-05	-7.3940E-03	2.2925E-01	
42	38	0	0.19000	0.004	-0.01	0.7	*no*	*0.1800*	0.1900	-1.0120E-04	-6.3446E-03	2.3582E-01	
43	39	0	0.19500	0.004	0.00	0.8	*no*	*0.1850*	0.1950	-1.2935E-04	-4.8022E-03	3.6427E-01	
44	40	0	0.20000	0.004	0.00	0.4	*no*	*0.1900*	0.2000	-1.4897E-04	-3.1368E-03	2.6139E-01	

Figure D.1e ***mode3*** **Spreadsheet Analysis Program (page 5 of 16)**

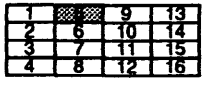

	M	N	O	P	Q	R	S	T	U	V	W	X	Y
45	41	1	0.20500	0.004	0.00	0.1	*no*	*0.1950*	0.2050	-1.6243E-04	-2.3706E-03	4.5412E-01	
46	42	1	0.21000	0.004	0.00	0.1	*zero*	*0.2000*	0.2100	-1.7180E-04	-1.1302E-03	1.9692E-01	
47	43	1	0.21500	0.004	0.00	0.0	*no*	*0.2050*	0.2150	-1.7180E-04	1.1302E-03	1.9692E-01	
48	44	1	0.22000	0.004	0.00	-0.2	*no*	*0.2100*	0.2200	-1.6243E-04	2.3706E-03	4.5412E-01	
49	45	1	0.22500	0.004	0.00	0.0	*no*	*0.2150*	0.2250	-1.4897E-04	3.1368E-03	2.6139E-01	
50	46	1	0.23000	0.004	0.00	0.3	*no*	*0.2200*	0.2300	-1.2901E-04	4.9655E-03	5.7232E-02	
51	47	1	0.23500	0.004	0.00	0.3	*no*	*0.2250*	0.2350	-1.0038E-04	6.2064E-03	2.8066E-01	
52	48	1	0.24000	0.004	0.00	0.6	*no*	*0.2300*	0.2400	-6.9241E-05	6.2056E-03	2.2602E-01	
53	49	0	0.24500	0.004	0.00	0.8	*no*	*0.2350*	0.2450	-3.6941E-05	6.9041E-03	-1.0432E-01	
54	50	0	0.25000	0.004	0.01	1.0	*zero*	*0.2400*	0.2500	-6.3058E-19	7.6715E-03	1.2023E-14	
55	51	0	0.25500	0.004	0.01	1.0	*no*	*0.2450*	0.2550	3.6941E-05	6.9041E-03	1.0432E-01	
56	52	0	0.26000	0.004	0.02	0.9	*no*	*0.2500*	0.2600	6.9241E-05	6.2056E-03	-2.2602E-01	
57	53	0	0.26500	0.004	0.02	0.8	*no*	*0.2550*	0.2650	1.0038E-04	6.2064E-03	-2.8066E-01	
58	54	0	0.27000	0.004	0.03	0.6	*no*	*0.2600*	0.2700	1.2901E-04	4.9655E-03	-5.7232E-02	
59	55	0	0.27500	0.004	0.03	0.3	*no*	*0.2650*	0.2750	1.4897E-04	3.1368E-03	-2.6139E-01	
60	56	0	0.28000	0.004	0.03	-0.1	*no*	*0.2700*	0.2800	1.6243E-04	2.3706E-03	-4.5412E-01	
61	57	0	0.28500	0.005	0.03	-0.5	*no*	*0.2750*	0.2850	1.7180E-04	1.1302E-03	-1.9692E-01	
62	58	0	0.29000	0.005	0.02	-0.9	*no*	*0.2800*	0.2900	1.7180E-04	-1.1302E-03	-1.9692E-01	
63	59	0	0.29500	0.005	0.02	-1.3	*no*	*0.2850*	0.2950	1.6243E-04	-2.3706E-03	-4.5412E-01	
64	60	0	0.30000	0.005	0.01	-1.8	*no*	*0.2900*	0.3000	1.4897E-04	-3.1368E-03	-2.6139E-01	
65	61	0	0.30500	0.005	0.00	-1.8	*no*	*0.2950*	0.3050	1.2901E-04	-4.9655E-03	-5.7232E-02	
66	62	0	0.31000	0.005	-0.01	-2.2	*no*	*0.3000*	0.3100	1.0038E-04	-6.2064E-03	-2.8066E-01	
67	63	0	0.31500	0.005	-0.02	-2.5	*no*	*0.3050*	0.3150	6.9241E-05	-6.2056E-03	-2.2602E-01	
68	64	0	0.32000	0.005	-0.03	-2.2	*no*	*0.3100*	0.3200	3.6941E-05	-6.9041E-03	1.0432E-01	
69	65	0	0.32500	0.004	-0.05	-2.0	*no*	*0.3150*	0.3250	7.3762E-19	-7.6715E-03	-1.0805E-14	
70	66	0	0.33000	0.004	-0.06	-2.0	*no*	*0.3200*	0.3300	-3.6941E-05	-6.9041E-03	-1.0432E-01	
71	67	0	0.33500	0.004	-0.06	-1.5	*no*	*0.3250*	0.3350	-6.9241E-05	-6.2056E-03	2.2602E-01	
72	68	0	0.34000	0.004	-0.07	-0.8	*no*	*0.3300*	0.3400	-1.0038E-04	-6.2064E-03	2.8066E-01	
73	69	0	0.34500	0.003	-0.08	-0.9	*no*	*0.3350*	0.3450	-1.2901E-04	-4.9655E-03	5.7232E-02	
74	70	0	0.35000	0.003	-0.08	-0.2	*no*	*0.3400*	0.3500	-1.4897E-04	-3.1368E-03	2.6139E-01	
75	71	0	0.35500	0.002	-0.08	0.7	*no*	*0.3450*	0.3550	-1.6243E-04	-2.3706E-03	4.5412E-01	
76	72	0	0.36000	0.002	-0.08	0.7	*no*	*0.3500*	0.3600	-1.7180E-04	-1.1302E-03	1.9692E-01	
77	73	0	0.36500	0.002	-0.07	0.9	*no*	*0.3550*	0.3650	-1.7180E-04	1.1302E-03	1.9692E-01	
78	74	0	0.37000	0.001	-0.06	1.7	*no*	*0.3600*	0.3700	-1.6243E-04	2.3706E-03	4.5412E-01	
79	75	0	0.37500	0.001	-0.06	1.7	*no*	*0.3650*	0.3750	-1.4897E-04	3.1368E-03	2.6139E-01	
80	76	0	0.38000	0.001	-0.05	1.4	*no*	*0.3700*	0.3800	-1.2901E-04	4.9655E-03	5.7232E-02	
81	77	0	0.38500	0.001	-0.04	1.8	*no*	*0.3750*	0.3850	-1.0038E-04	6.2064E-03	2.8066E-01	
82	78	0	0.39000	0.000	-0.03	1.9	*no*	*0.3800*	0.3900	-6.9241E-05	6.2056E-03	2.2602E-01	
83	79	0	0.39500	0.000	-0.02	1.2	*no*	*0.3850*	0.3950	-3.6941E-05	6.9041E-03	-1.0432E-01	
84	80	0	0.40000	0.000	-0.01	1.2	*no*	*0.3900*	0.4000	-1.0889E-18	7.6715E-03	9.2369E-15	
85	81	0	0.40500	0.000	-0.01	1.6	*no*	*0.4000*	0.4050	3.6941E-05	6.9041E-03	1.0432E-01	
86	82	0	0.41000	0.000	-0.01	0.8	*no*	*0.4050*	0.4100	6.9241E-05	6.2056E-03	-2.2602E-01	
87	83	0	0.41500	0.000	0.00	0.2	*no*	*0.4100*	0.4150	1.0038E-04	6.2064E-03	-2.8066E-01	
88	84	0	0.42000	0.000	0.00	0.8	*no*	*0.4150*	0.4200	1.2901E-04	4.9655E-03	-5.7232E-02	

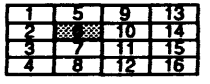

Figure D.1f ***mode3*** **Spreadsheet Analysis Program (page 6 of 16)**

	M	N	O	P	Q	R	S	T	U	V	W	X	Y
89	85	0	0.42500	0.000	0.00	0.5	no	0.4200	0.4250	1.4897E-04	3.1368E-03	-2.6139E-01	
90	86	0	0.43000	0.000	0.00	-0.3	no	0.4250	0.4300	1.6243E-04	2.3706E-03	-4.5412E-01	
91	87	0	0.43500	0.000	0.00	0.2	zero	0.4300	0.4350	1.7180E-04	1.1302E-03	-1.9692E-01	
92	88	0	0.44000	0.000	0.00	0.5	no	0.4350	0.4400	1.7180E-04	-1.1302E-03	-1.9692E-01	
93	89	0	0.44500	0.000	0.00	-0.5	no	0.4400	0.4450	1.6243E-04	-2.3706E-03	-4.5412E-01	
94	90	0	0.45000	0.000	0.00	-0.2	no	0.4450	0.4500	1.4897E-04	-3.1368E-03	-2.6139E-01	
95	91	0	0.45500	0.000	0.00	0.6	zero	0.4500	0.4550	1.2901E-04	-4.9655E-03	-5.7232E-02	
96	92	0	0.46000	0.000	0.00	-0.2	no	0.4550	0.4600	1.0038E-04	-6.2064E-03	-2.8066E-01	
97	93	0	0.46500	0.000	0.00	-0.5	no	0.4600	0.4650	6.9241E-05	-6.2056E-03	-2.2602E-01	
98	94	0	0.47000	0.000	0.00	0.5	zero	0.4650	0.4700	3.6941E-05	-6.9041E-03	1.0432E-01	
99	95	0	0.47500	0.000	0.00	0.2	no	0.4700	0.4750	1.1191E-18	-7.6715E-03	-7.2558E-15	
100	96	0	0.48000	0.000	0.00	-0.6	no	0.4750	0.4800	-3.6941E-05	-6.9041E-03	-1.0432E-01	
101	97	0	0.48500	0.000	0.00	0.2	no	0.4800	0.4850	-6.9241E-05	-6.2056E-03	2.2602E-01	
102	98	0	0.49000	0.000	0.00	0.5	zero	0.4850	0.4900	-1.0038E-04	-6.2064E-03	2.8066E-01	
103	99	0	0.49500	0.000	0.00	-0.5	no	0.4900	0.4950	-1.2901E-04	-4.9655E-03	5.7232E-02	
104	100	0	0.50000	0.000	0.00	-0.2	no	0.4950	0.5000	-1.4897E-04	-3.1368E-03	2.6139E-01	
105		24	0.50500	0.000	0.00	0.6	zero	0.5000	0.5050	-1.6243E-04	-2.3706E-03	4.5412E-01	
106			0.51000	0.000	0.00	-0.2	no	0.5050	0.5100	-1.7180E-04	-1.1302E-03	1.9692E-01	
107			0.51500	0.000	0.00	-0.5	no	0.5100	0.5150	-1.7180E-04	1.1302E-03	1.9692E-01	
108			0.52000	0.000	0.00	0.5	zero	0.5150	0.5200	-1.6243E-04	2.3706E-03	4.5412E-01	
109			0.52500	0.000	0.00	0.2	no	0.5200	0.5250	-1.4897E-04	3.1368E-03	2.6139E-01	
110			0.53000	0.000	0.00	-0.6	no	0.5250	0.5300	-1.2901E-04	4.9655E-03	5.7232E-02	
111			0.53500	0.000	0.00	0.2	no	0.5300	0.5350	-1.0038E-04	6.2064E-03	2.8066E-01	
112			0.54000	0.000	0.00	0.5	zero	0.5350	0.5400	-6.9241E-05	6.2056E-03	2.2602E-01	
113			0.54500	0.000	0.00	-0.5	no	0.5400	0.5450	-3.6941E-05	6.9041E-03	-1.0432E-01	
114			0.55000	0.000	0.00	-0.2	no	0.5450	0.5500	-1.1587E-18	7.6715E-03	5.1884E-15	
115			0.55500	0.000	0.00	0.6	zero	0.5500	0.5550	3.6941E-05	6.9041E-03	1.0432E-01	
116			0.56000	0.000	0.00	-0.2	no	0.5550	0.5600	6.9241E-05	6.2056E-03	-2.2602E-01	
117			0.56500	0.000	0.00	-0.5	no	0.5600	0.5650	1.0038E-04	6.2064E-03	-2.8066E-01	
118			0.57000	0.000	0.00	0.5	zero	0.5650	0.5700	1.2901E-04	4.9655E-03	-5.7232E-02	
119			0.57500	0.000	0.00	0.2	no	0.5700	0.5750	1.4897E-04	3.1368E-03	-2.6139E-01	
120			0.58000	0.000	0.00	-0.6	no	0.5750	0.5800	1.6243E-04	2.3706E-03	-4.5412E-01	
121			0.58500	0.000	0.00	0.2	zero	0.5800	0.5850	1.7180E-04	1.1302E-03	-1.9692E-01	
122			0.59000	0.000	0.00	0.5	no	0.5850	0.5900	1.7180E-04	-1.1302E-03	-1.9692E-01	
123			0.59500	0.000	0.00	-0.5	no	0.5900	0.5950	1.6243E-04	-2.3706E-03	-4.5412E-01	
124			0.60000	0.000	0.00	-0.2	no	0.5950	0.6000	1.4897E-04	-3.1368E-03	-2.6139E-01	
125			0.60500	0.000	0.00	0.6	zero	0.6000	0.6050	1.2901E-04	-4.9655E-03	-5.7232E-02	
126			0.61000	0.000	0.00	-0.2	no	0.6100	0.6100	1.0038E-04	-6.2064E-03	-2.8066E-01	
127			0.61500	0.000	0.00	-0.5	zero	0.6150	0.6150	6.9241E-05	-6.2056E-03	-2.2602E-01	
128			0.62000	0.000	0.00	0.5	no	0.6200	0.6200	3.6941E-05	-6.9041E-03	1.0432E-01	
129			0.62500	0.000	0.00	0.2	no	0.6250	0.6250	1.4869E-18	-7.6715E-03	-3.7624E-15	
130			0.63000	0.000	0.00	-0.6	no	0.6300	0.6300	-3.6941E-05	-6.9041E-03	-1.0432E-01	
131			0.63500	0.000	0.00	0.2	zero	0.6350	0.6350	-6.9241E-05	-6.2056E-03	2.2602E-01	
132			0.64000	0.000	0.00	0.5	no	0.6400	0.6400	-1.0038E-04	-6.2064E-03	2.8066E-01	

Figure D.1g *mode3* **Spreadsheet Analysis Program (page 7 of 16)**

	M	N	O	P	Q	R	S	T	U	V	W	X	Y
133			0.64500	0.000	0.00	-0.5	no	0.6450	0.6450	-1.2901E-04	-4.9655E-03	5.7232E-02	
134			0.65000	0.000	0.00	-0.2	zero	0.6500	0.6500	-1.4897E-04	-3.1368E-03	2.6139E-01	
135			0.65500	0.000	0.00	0.6	no	0.6550	0.6550	-1.6243E-04	-2.3706E-03	4.5412E-01	
136			0.66000	0.000	0.00	-0.2	no	0.6600	0.6600	-1.7180E-04	-1.1302E-03	1.9692E-01	
137			0.66500	0.000	0.00	-0.5	zero	0.6650	0.6650	-1.7180E-04	1.1302E-03	1.9692E-01	
138			0.67000	0.000	0.00	0.5	no	0.6700	0.6700	-1.6243E-04	2.3706E-03	4.5412E-01	
139			0.67500	0.000	0.00	0.2	no	0.6750	0.6750	-1.4897E-04	3.1368E-03	2.6139E-01	
140			0.68000	0.000	0.00	-0.6	no	0.6800	0.6800	-1.2901E-04	4.9655E-03	5.7232E-02	
141			0.68500	0.000	0.00	0.2	zero	0.6850	0.6850	-1.0038E-04	6.2064E-03	2.8066E-01	
142			0.69000	0.000	0.00	0.5	no	0.6900	0.6900	-6.9241E-05	6.2056E-03	2.2602E-01	
143			0.69500	0.000	0.00	-0.5	no	0.6950	0.6950	-3.6941E-05	6.9041E-03	-1.0432E-01	
144			0.70000	0.000	0.00	-0.2	zero	0.7000	0.7000	-2.1364E-18	7.6715E-03	2.7498E-15	
145			0.70500	0.000	0.00	0.6	zero	0.7000	0.7050	3.6941E-05	6.9041E-03	1.0432E-01	
146			0.71000	0.000	0.00	-0.2	zero	0.7000	0.7100	6.9241E-05	6.2056E-03	-2.2602E-01	
147			0.71500	0.000	0.00	-0.5	zero	0.7000	0.7150	1.0038E-04	6.2064E-03	-2.8066E-01	
148			0.72000	0.000	0.00	0.5	zero	0.7000	0.7200	1.2901E-04	4.9655E-03	-5.7232E-02	
149			0.72500	0.000	0.00	0.2	zero	0.7000	0.7250	1.4897E-04	3.1368E-03	-2.6139E-01	
150			0.73000	0.000	0.00	-0.6	zero	0.7000	0.7300	1.6243E-04	2.3706E-03	-4.5412E-01	
151			0.73500	0.000	0.00	0.2	zero	0.7000	0.7350	1.7180E-04	1.1302E-03	-1.9692E-01	
152			0.74000	0.000	0.00	0.5	zero	0.7000	0.7400	1.7180E-04	-1.1302E-03	-1.9692E-01	
153			0.74500	0.000	0.00	-0.5	zero	0.7000	0.7450	1.6243E-04	-2.3706E-03	-4.5412E-01	
154			0.75000	0.000	0.00	-0.2	zero	0.7000	0.7500	1.4897E-04	-3.1368E-03	-2.6139E-01	
155			0.75500	0.000	0.00	0.6	zero	0.7000	0.7550	1.2901E-04	-4.9655E-03	-5.7232E-02	
156			0.76000	0.000	0.00	-0.2	zero	0.7000	0.7600	1.0038E-04	-6.2064E-03	-2.8066E-01	
157			0.76500	0.000	0.00	-0.5	zero	0.7000	0.7650	6.9241E-05	-6.2056E-03	-2.2602E-01	
158			0.77000	0.000	0.00	0.5	zero	0.7000	0.7700	3.6941E-05	-6.9041E-03	1.0432E-01	
159			0.77500	0.000	0.00	0.2	zero	0.7000	0.7750	1.5351E-18	-7.6715E-03	-4.6789E-15	
160			0.78000	0.000	0.00	-0.6	zero	0.7000	0.7800	-3.6941E-05	-6.9041E-03	-1.0432E-01	
161			0.78500	0.000	0.00	0.2	zero	0.7000	0.7850	-6.9241E-05	-6.2056E-03	2.2602E-01	
162			0.79000	0.000	0.00	0.5	zero	0.7000	0.7900	-1.0038E-04	-6.2064E-03	2.8066E-01	
163			0.79500	0.000	0.00	-0.5	zero	0.7000	0.7950	-1.2901E-04	-4.9655E-03	5.7232E-02	
164			0.80000	0.000	0.00	-0.2	zero	0.7000	0.8000	-1.4897E-04	-3.1368E-03	2.6139E-01	
165			0.80500	0.000	0.00	0.6	zero	0.7000	0.8050	-1.6243E-04	-2.3706E-03	4.5412E-01	
166			0.81000	0.000	0.00	-0.2	zero	0.7000	0.8100	-1.7180E-04	-1.1302E-03	1.9692E-01	
167			0.81500	0.000	0.00	-0.5	zero	0.7000	0.8150	-1.7180E-04	1.1302E-03	1.9692E-01	
168			0.82000	0.000	0.00	0.5	zero	0.7000	0.8200	-1.6243E-04	2.3706E-03	4.5412E-01	
169			0.82500	0.000	0.00	0.2	zero	0.7000	0.8250	-1.4897E-04	3.1368E-03	2.6139E-01	
170			0.83000	0.000	0.00	-0.6	zero	0.7000	0.8300	-1.2901E-04	4.9655E-03	5.7232E-02	
171			0.83500	0.000	0.00	0.2	zero	0.7000	0.8350	-1.0038E-04	6.2064E-03	2.8066E-01	
172			0.84000	0.000	0.00	0.5	zero	0.7000	0.8400	-6.9241E-05	6.2056E-03	2.2602E-01	
173			0.84500	0.000	0.00	-0.5	zero	0.7000	0.8450	-3.6941E-05	6.9041E-03	-1.0432E-01	
174			0.85000	0.000	0.00	-0.2	zero	0.7000	0.8500	-2.2197E-18	7.6715E-03	-1.2987E-15	
175			0.85500	0.000	0.00	0.6	zero	0.7000	0.8550	3.6941E-05	6.9041E-03	1.0432E-01	
176			0.86000	0.000	0.00	-0.2	zero	0.7000	0.8600	6.9241E-05	6.2056E-03	-2.2602E-01	

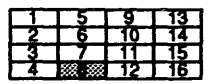

Figure D.1h ***mode3*** **Spreadsheet Analysis Program (page 8 of 16)**

	Z	AA	AB	AC	AD	AE	AF	AG	AH	AI	AJ	AK	AL	AM	AN	AO
1							2.8356E+03		0.005	6.6667	25.00	27.50	48	2	20.00	7.50
2							2.90E+10	0.6880				37.50				
3	T (t-L/v)		t	A(t)	B(t)	C(t)	u(t)	•A(t)	•B(t)	•C(t)	•u(t)	A(t)	B(t)	C(t)	:u(t)	0
4		1	0.0000	0.00E+00	0.00E+00	0.00E+00	0.0000E+00	0.00E+00	0.00E+00	0.00E+00	0.0000E+00	0.00E+00	0.00E+00	0.00E+00	0.0000E+00	150
5		2	0.0050	2.26E-07	4.37E-07	5.66E-07	-3.4062E-07	1.35E-04	2.56E-04	2.99E-04	-1.6330E-04	5.39E-02	9.59E-02	8.10E-02	-2.7098E-02	60
6		3	0.0100	1.79E-06	3.13E-06	2.61E-06	-8.1504E-07	5.34E-04	8.47E-04	3.96E-04	1.3816E-04	1.05E-01	1.26E-01	5.66E-02	1.6167E-01	2.5
7		4	0.0150	5.98E-06	8.78E-06	3.57E-06	2.4011E-06	1.18E-03	1.36E-03	-1.13E-05	1.1884E-03	1.51E-01	6.76E-02	5.88E-02	2.0974E-01	
8		5	0.0200	1.39E-05	1.60E-05	3.41E-06	1.0504E-05	2.03E-03	1.43E-03	6.49E-05	1.9665E-03	1.89E-01	4.28E-02	7.47E-02	1.1467E-01	13.33333333
9		6	0.0250	2.66E-05	2.22E-05	4.57E-06	2.2003E-05	3.05E-03	9.68E-04	3.22E-04	2.7322E-03	2.18E-01	-1.34E-01	-1.01E-02	2.2822E-01	14.49275362
10		7	0.0300	4.47E-05	2.52E-05	5.47E-06	3.9183E-05	4.19E-03	2.34E-04	-3.55E-05	4.2291E-03	2.36E-01	-1.48E-01	-9.44E-02	3.3005E-01	15.87301587
11		8	0.0350	6.86E-05	2.47E-05	4.57E-06	6.4038E-05	5.39E-03	-3.69E-04	-2.07E-04	5.5973E-03	2.41E-01	-7.71E-02	4.07E-02	2.0035E-01	20.83333333
12		9	0.0400	9.86E-05	2.23E-05	4.34E-06	9.4213E-05	6.58E-03	-4.85E-04	1.16E-04	6.4661E-03	2.34E-01	3.07E-02	4.12E-02	1.9246E-01	17.54385965
13		10	0.0450	1.34E-04	2.07E-05	4.80E-06	1.2951E-04	7.71E-03	-1.22E-04	-4.97E-05	7.7555E-03	2.14E-01	1.03E-01	-9.29E-02	3.0644E-01	22.72727273
14		11	0.0500	1.75E-04	2.14E-05	3.50E-06	1.7189E-04	8.70E-03	4.01E-04	-3.98E-04	9.0956E-03	1.81E-01	9.12E-02	-7.76E-03	1.8912E-01	19.60784314
15		12	0.0550	2.21E-04	2.42E-05	2.00E-06	2.1898E-04	9.50E-03	6.59E-04	-1.27E-04	9.6278E-03	1.38E-01	3.05E-03	7.78E-02	6.0437E-02	25.00000000
16		13	0.0600	2.70E-04	2.71E-05	1.89E-06	2.6811E-04	1.01E-02	4.01E-04	-3.31E-05	1.0098E-02	8.58E-02	-1.03E-01	-5.50E-02	1.4086E-01	22.22222222
17		14	0.0650	3.21E-04	2.75E-05	7.51E-07	3.2041E-04	1.03E-02	-2.80E-04	-4.21E-04	1.0768E-02	2.63E-02	-1.56E-01	-5.25E-02	7.8746E-02	27.77777778
18		15	0.0700	3.73E-04	2.42E-05	-1.36E-06	3.7432E-04	1.03E-02	-1.01E-03	-3.02E-04	1.0621E-02	-3.81E-02	-1.20E-01	8.53E-02	-1.2335E-01	25.64102564
19		16	0.0750	4.24E-04	1.81E-05	-1.89E-06	4.2570E-04	9.96E-03	-1.37E-03	1.77E-05	9.9453E-03	-1.05E-01	-1.78E-02	4.20E-03	-1.0877E-01	31.25000000
20		17	0.0800	4.72E-04	1.15E-05	-2.32E-06	4.7435E-04	9.27E-03	-1.19E-03	-2.60E-04	9.5353E-03	-1.70E-01	8.51E-02	-7.71E-02	-9.3318E-02	35.71428571
21		18	0.0850	5.16E-04	6.83E-06	-4.12E-06	5.2014E-04	8.26E-03	-6.31E-04	-3.40E-04	8.6045E-03	-2.33E-01	1.22E-01	6.00E-02	-2.9280E-01	30.30303030
22		19	0.0900	5.54E-04	5.08E-06	-4.77E-06	5.5895E-04	6.96E-03	-1.14E-04	8.27E-05	6.8739E-03	-2.89E-01	7.12E-02	6.14E-02	-3.5061E-01	41.66666667
23		20	0.0950	5.85E-04	4.99E-06	-4.22E-06	5.8936E-04	5.39E-03	-7.65E-06	1.76E-05	5.3692E-03	-3.37E-01	-3.19E-02	-7.29E-02	-2.6428E-01	37.03703704
24		21	0.1000	6.08E-04	4.15E-06	-4.94E-06	6.1264E-04	3.60E-03	-4.01E-04	-2.31E-04	3.8358E-03	-3.75E-01	-1.16E-01	1.10E-02	-3.8555E-01	50.00000000
25		22	0.1050	6.21E-04	5.59E-07	-5.40E-06	6.2630E-04	1.66E-03	-1.04E-03	1.26E-04	1.5349E-03	-4.00E-01	-1.24E-01	9.42E-02	-4.9410E-01	47.61904762
26		23	0.1100	6.24E-04	-5.94E-06	-4.04E-06	6.2819E-04	-3.74E-04	-1.50E-03	2.94E-04	-6.6827E-04	-4.12E-01	-4.69E-02	-4.18E-02	-3.7012E-01	62.50000000
27		24	0.1150	6.17E-04	-1.35E-05	-3.40E-06	6.2052E-04	-2.44E-03	-1.45E-03	-3.72E-05	-2.3981E-03	-4.10E-01	6.61E-02	-4.33E-02	-3.6695E-01	66.66666667
28		25	0.1200	6.00E-04	-1.96E-05	-3.49E-06	6.0337E-04	-4.45E-03	-8.97E-04	1.16E-04	-4.5698E-03	-3.95E-01	1.43E-01	9.00E-02	-4.8469E-01	83.33333333
29		26	0.1250	5.73E-04	-2.22E-05	-1.89E-06	5.7467E-04	-6.36E-03	-1.66E-04	4.48E-04	-6.8085E-03	-3.66E-01	1.34E-01	4.20E-03	-3.7016E-01	125.00000000
30		27	0.1300	5.37E-04	-2.17E-05	-1.86E-07	5.3675E-04	-8.09E-03	3.13E-04	1.58E-04	-8.2509E-03	-3.25E-01	4.83E-02	-8.18E-02	-2.4333E-01	111.11111111
31		28	0.1350	4.92E-04	-1.99E-05	2.47E-08	4.9221E-04	-9.59E-03	2.85E-04	4.38E-05	-9.6381E-03	-2.74E-01	-5.66E-02	5.08E-02	-3.2468E-01	250.00000000
32		29	0.1400	4.41E-04	-1.95E-05	1.16E-06	4.3992E-04	-1.08E-02	-1.64E-04	4.10E-04	-1.1228E-02	-2.14E-01	-1.10E-01	4.82E-02	-2.6257E-01	
33		30	0.1450	3.85E-04	-2.17E-05	3.17E-06	3.8141E-04	-1.17E-02	-6.62E-04	2.71E-04	-1.1998E-02	-1.49E-01	-7.50E-02	-8.93E-02	-5.9549E-02	
34		31	0.1500	3.24E-04	-2.55E-05	3.50E-06	3.2087E-04	-1.23E-02	-8.02E-04	-6.82E-05	-1.2232E-02	-8.00E-02	2.52E-02	-7.76E-03	-7.2270E-02	
35		32	0.1550	2.62E-04	-2.88E-05	3.63E-06	2.5852E-04	-1.25E-02	-4.11E-04	1.94E-04	-1.2721E-02	-1.08E-02	1.25E-01	7.42E-02	-8.4928E-02	
36		33	0.1600	2.00E-04	-2.90E-05	5.07E-06	1.9460E-04	-1.24E-02	3.32E-04	2.60E-04	-1.2673E-02	5.62E-02	1.58E-01	-6.21E-02	1.1830E-01	
37		34	0.1650	1.39E-04	-2.56E-05	5.29E-06	1.3328E-04	-1.20E-02	1.01E-03	-1.70E-04	-1.1803E-02	1.18E-01	1.01E-01	-6.26E-02	1.8084E-01	
38		35	0.1700	8.04E-05	-1.97E-05	4.30E-06	7.6124E-05	-1.12E-02	1.26E-03	-1.08E-04	-1.1133E-02	1.73E-01	-7.56E-03	7.27E-02	1.0023E-01	
39		36	0.1750	2.66E-05	-1.39E-05	4.57E-06	2.2003E-05	-1.03E-02	9.68E-04	1.44E-04	-1.0404E-02	2.18E-01	-9.86E-02	-1.01E-02	2.2822E-01	
40		37	0.1800	-2.18E-05	-1.05E-05	4.59E-06	-2.6436E-05	-9.08E-03	4.01E-04	-2.09E-04	-8.8706E-03	2.52E-01	-1.13E-01	-9.24E-02	3.4449E-01	
41		38	0.1850	-6.40E-05	-9.65E-06	2.85E-06	-6.6839E-05	-7.76E-03	-1.81E-05	-3.66E-04	-7.3940E-03	2.74E-01	-4.32E-02	4.45E-02	2.2925E-01	
42		39	0.1900	-9.93E-05	-9.84E-06	1.88E-06	-1.0120E-04	-6.36E-03	3.01E-05	-1.91E-05	-6.3446E-03	2.82E-01	6.25E-02	4.66E-02	2.3582E-01	
43		40	0.1950	-1.28E-04	-8.55E-06	1.74E-06	-1.2935E-04	-4.96E-03	5.44E-04	-1.55E-04	-4.8022E-03	2.78E-01	1.32E-01	-8.61E-02	3.6427E-01	
44	0.0000	41	0.2000	-1.49E-04	-4.15E-06	1.75E-20	-1.4897E-04	-3.60E-03	1.20E-03	-4.66E-04	-3.1368E-03	2.61E-01	1.16E-01	-1.35E-14	2.6139E-01	

1	5		13
2	6	10	14
3	7	11	15
4	8	12	16

Figure D.1i *mode3* **Spreadsheet Analysis Program (page 9 of 16)**

	Z	AA	AB	AC	AD	AE	AF	AG	AH	AI	AJ	AK	AL	AM	AN	AO
45	0.0050	42	0.2050	-1.64E-04	2.56E-06	-1.18E-06	-1.6243E-04	-2.23E-03	1.32E-03	1.44E-04	-2.3706E-03	2.87E-01	-7.19E-02	-1.67E-01	4.5412E-01	
46	0.0100	43	0.2100	-1.71E-04	7.58E-06	7.27E-07	-1.7180E-04	-7.53E-04	5.65E-04	3.77E-04	-1.1302E-03	3.00E-01	-2.13E-01	1.03E-01	1.9692E-01	
47	0.0150	44	0.2150	-1.71E-04	7.58E-06	7.27E-07	-1.7180E-04	7.53E-04	-5.65E-04	-3.77E-04	1.1302E-03	3.00E-01	-2.13E-01	1.03E-01	1.9692E-01	
48	0.0200	45	0.2200	-1.64E-04	2.56E-06	-1.18E-06	-1.6243E-04	2.23E-03	-1.32E-03	-1.44E-04	2.3706E-03	2.87E-01	-7.19E-02	-1.67E-01	4.5412E-01	
49	0.0250	46	0.2250	-1.49E-04	-4.15E-06	-2.17E-20	-1.4897E-04	3.60E-03	-1.20E-03	4.66E-04	3.1368E-03	2.61E-01	1.16E-01	1.29E-14	2.6139E-01	
50	0.0300	47	0.2300	-1.28E-04	-8.11E-06	1.18E-06	-1.2901E-04	4.82E-03	-2.89E-04	-1.44E-04	4.9655E-03	2.34E-01	2.28E-01	1.67E-01	5.7232E-02	
51	0.0350	48	0.2350	-1.01E-04	-6.71E-06	-7.27E-07	-1.0038E-04	5.83E-03	8.17E-04	-3.77E-04	6.2064E-03	1.77E-01	1.88E-01	-1.03E-01	2.8066E-01	
52	0.0400	49	0.2400	-7.00E-05	-8.67E-07	-7.27E-07	-6.9241E-05	6.58E-03	1.38E-03	3.77E-04	6.2056E-03	1.23E-01	2.43E-02	-1.03E-01	2.2602E-01	
53	0.0450	50	0.2450	-3.58E-05	5.55E-06	1.18E-06	-3.6941E-05	7.05E-03	1.03E-03	1.44E-04	6.9041E-03	6.28E-02	-1.56E-01	1.67E-01	-1.0432E-01	
54	0.0500	51	0.2500	-5.96E-19	8.29E-06	3.53E-20	-6.3058E-19	7.21E-03	1.96E-17	-4.66E-04	7.6715E-03	1.05E-15	-2.33E-01	-1.10E-14	1.2023E-14	
55	0.0550	52	0.2550	3.58E-05	5.55E-06	-1.18E-06	3.6941E-05	7.25E-03	-1.03E-03	1.44E-04	6.9041E-03	-6.28E-02	-1.56E-01	-1.67E-01	1.0432E-01	
56	0.0600	53	0.2600	7.00E-05	-8.67E-07	7.27E-07	6.9241E-05	6.58E-03	-1.38E-03	3.77E-04	6.2056E-03	-1.23E-01	2.43E-02	1.03E-01	-2.2602E-01	
57	0.0650	54	0.2650	1.01E-04	-6.71E-06	7.27E-07	1.0038E-04	5.83E-03	-8.17E-04	-3.77E-04	6.2064E-03	-1.77E-01	1.88E-01	1.03E-01	-2.8066E-01	
58	0.0700	55	0.2700	1.28E-04	-8.11E-06	-1.18E-06	1.2901E-04	4.82E-03	2.89E-04	-1.44E-04	4.9655E-03	-2.34E-01	2.28E-01	-1.67E-01	-5.7232E-02	
59	0.0750	56	0.2750	1.49E-03	-4.15E-06	-4.01E-20	1.4897E-04	3.60E-03	1.20E-03	4.66E-04	3.1368E-03	-2.61E-01	1.16E-01	1.03E-14	-2.6139E-01	
60	0.0800	57	0.2800	1.64E-04	2.56E-06	1.18E-06	1.6243E-04	2.23E-03	1.32E-03	-1.44E-04	2.3706E-03	-2.87E-01	-7.19E-02	1.67E-01	-4.5412E-01	
61	0.0850	58	0.2850	1.71E-04	7.58E-06	-7.27E-07	1.7180E-04	7.53E-04	5.65E-04	-3.77E-04	1.1302E-03	-3.00E-01	-2.13E-01	-1.03E-01	-1.9692E-01	
62	0.0900	59	0.2900	1.71E-04	7.58E-06	-7.27E-07	1.7180E-04	-7.53E-04	-5.65E-04	3.77E-04	-1.1302E-03	-3.00E-01	-2.13E-01	-1.03E-01	-1.9692E-01	
63	0.0950	60	0.2950	1.64E-04	2.56E-06	1.18E-06	1.6243E-04	-2.23E-03	-1.32E-03	1.44E-04	-2.3706E-03	-2.87E-01	-7.19E-02	1.67E-01	-4.5412E-01	
64	0.1000	61	0.3000	1.49E-04	-4.15E-06	4.06E-20	1.4897E-04	-3.60E-03	-1.20E-03	4.66E-04	-3.1368E-03	-2.61E-01	1.16E-01	-1.02E-14	-2.6139E-01	37.03703704
65	0.1050	62	0.3050	1.28E-04	-8.11E-06	-1.18E-06	1.2901E-04	-4.82E-03	-2.89E-04	1.44E-04	-4.9655E-03	-2.34E-01	2.28E-01	-1.67E-01	-5.7232E-02	41.66666667
66	0.1100	63	0.3100	1.01E-04	-6.71E-06	7.27E-07	1.0038E-04	-5.83E-03	8.17E-04	3.77E-04	-6.2064E-03	-1.77E-01	1.88E-01	1.03E-01	-2.8066E-01	47.61904762
67	0.1150	64	0.3150	7.00E-05	-8.67E-07	7.27E-07	6.9241E-05	-6.58E-03	1.38E-03	-3.77E-04	-6.2056E-03	-1.23E-01	2.43E-02	1.03E-01	-2.2602E-01	55.55555556
68	0.1200	65	0.3200	3.58E-05	5.55E-06	-1.18E-06	3.6941E-05	-7.05E-03	1.03E-03	-1.44E-04	-6.9041E-03	-6.28E-02	-1.56E-01	-1.67E-01	1.0432E-01	66.66666667
69	0.1250	66	0.3250	6.91E-19	8.29E-06	-4.54E-20	7.3762E-19	-7.21E-03	2.27E-17	4.66E-04	-7.6715E-03	-1.22E-15	-2.33E-01	9.55E-15	-1.0805E-14	83.33333333
70	0.1300	67	0.3300	-3.58E-05	5.55E-06	1.18E-06	-3.6941E-05	-7.05E-03	-1.03E-03	-1.44E-04	-6.9041E-03	6.28E-02	-1.56E-01	1.67E-01	-1.0432E-01	111.11111111
71	0.1350	68	0.3350	-7.00E-05	-8.67E-07	-7.27E-07	-6.9241E-05	-6.58E-03	-1.38E-03	-3.77E-04	-6.2056E-03	1.23E-01	2.43E-02	-1.03E-01	2.2602E-01	166.66666667
72	0.1400	69	0.3400	-1.01E-04	-6.71E-06	-7.27E-07	-1.0038E-04	-5.83E-03	-8.17E-04	3.77E-04	-6.2064E-03	1.77E-01	1.88E-01	-1.03E-01	2.8066E-01	
73	0.1450	70	0.3450	-1.28E-04	-8.11E-06	1.18E-06	-1.2901E-04	-4.82E-03	2.89E-04	1.44E-04	-4.9655E-03	2.34E-01	2.28E-01	1.67E-01	5.7232E-02	
74	0.1500	71	0.3500	-1.49E-04	-4.15E-06	5.03E-20	-1.4897E-04	-3.60E-03	1.20E-03	-4.66E-04	-3.1368E-03	2.61E-01	1.16E-01	-8.87E-15	2.6139E-01	
75	0.1550	72	0.3550	-1.64E-04	2.56E-06	-1.18E-06	-1.6243E-04	-2.23E-03	1.32E-03	1.44E-04	-2.3706E-03	2.87E-01	-7.19E-02	-1.67E-01	4.5412E-01	
76	0.1600	73	0.3600	-1.71E-04	7.58E-06	7.27E-07	-1.7180E-04	-7.53E-04	5.65E-04	3.77E-04	-1.1302E-03	3.00E-01	-2.13E-01	1.03E-01	1.9692E-01	
77	0.1650	74	0.3650	-1.71E-04	7.58E-06	7.27E-07	-1.7180E-04	7.53E-04	-5.65E-04	-3.77E-04	1.1302E-03	3.00E-01	-2.13E-01	1.03E-01	1.9692E-01	
78	0.1700	75	0.3700	-1.64E-04	2.56E-06	-1.18E-06	-1.6243E-04	2.23E-03	-1.32E-03	-1.44E-04	2.3706E-03	2.87E-01	-7.19E-02	-1.67E-01	4.5412E-01	
79	0.1750	76	0.3750	-1.49E-04	-4.15E-06	-5.51E-20	-1.4897E-04	3.60E-03	-1.20E-03	4.66E-04	3.1368E-03	2.61E-01	1.16E-01	8.18E-15	2.6139E-01	
80	0.1800	77	0.3800	-1.28E-04	-8.11E-06	1.18E-06	-1.2901E-04	4.82E-03	-2.89E-04	-1.44E-04	4.9655E-03	2.34E-01	2.28E-01	1.67E-01	5.7232E-02	
81	0.1850	78	0.3850	-1.01E-04	-6.71E-06	-7.27E-07	-1.0038E-04	5.83E-03	8.17E-04	-3.77E-04	6.2064E-03	1.77E-01	1.88E-01	-1.03E-01	2.8066E-01	
82	0.1900	79	0.3900	-7.00E-05	-8.67E-07	-7.27E-07	-6.9241E-05	6.58E-03	1.38E-03	3.77E-04	6.2056E-03	1.23E-01	2.43E-02	-1.03E-01	2.2602E-01	
83	0.1950	80	0.3950	-3.58E-05	5.55E-06	1.18E-06	-3.6941E-05	7.05E-03	1.03E-03	1.44E-04	6.9041E-03	6.28E-02	-1.56E-01	1.67E-01	-1.0432E-01	
84	0.2000	81	0.4000	-1.03E-18	8.29E-06	6.00E-20	-1.0839E-18	7.21E-03	3.32E-17	-4.66E-04	7.6715E-03	1.78E-15	-2.33E-01	-7.49E-15	9.2369E-15	
85	0.2050	82	0.4050	3.58E-05	5.55E-06	-1.18E-06	3.6941E-05	7.05E-03	-1.03E-03	1.44E-04	6.9041E-03	-6.28E-02	-1.56E-01	-1.67E-01	1.0432E-01	
86	0.2100	83	0.4100	7.00E-05	-8.67E-07	7.27E-07	6.9241E-05	6.58E-03	-1.38E-03	3.77E-04	6.2056E-03	-1.23E-01	2.43E-02	1.03E-01	-2.2602E-01	
87	0.2150	84	0.4150	1.01E-04	-6.71E-06	7.27E-07	1.0038E-04	5.83E-03	-8.17E-04	-3.77E-04	6.2064E-03	-1.77E-01	1.88E-01	1.03E-01	-2.8066E-01	
88	0.2200	85	0.4200	1.28E-04	-8.11E-06	-1.18E-06	1.2901E-04	4.82E-03	2.89E-04	-1.44E-04	4.9655E-03	-2.34E-01	2.28E-01	-1.67E-01	-5.7232E-02	

1	5	9	13
2	6	10	14
3	7	11	15
4	8	12	16

Figure D.1j *mode3* **Spreadsheet Analysis Program (page 10 of 16)**

	Z	AA	AB	AC	AD	AE	AF	AG	AH	AI	AJ	AK	AL	AM	AN	AO
89	0.2250	86	0.4250	1.49E-04	-4.15E-06	-6.48E-20	1.4897E-04	3.60E-03	1.20E-03	4.66E-04	3.1368E-03	-2.61E-01	1.16E-01	6.80E-15	-2.6139E-01	
90	0.2300	87	0.4300	1.64E-04	2.56E-06	1.18E-06	1.6243E-04	2.23E-03	1.32E-03	-1.44E-04	2.3706E-03	-2.87E-01	-7.19E-02	1.67E-01	-4.5412E-01	
91	0.2350	88	0.4350	1.71E-04	7.58E-06	-7.27E-07	1.7180E-04	7.53E-04	5.65E-04	-3.77E-04	1.1302E-03	-3.00E-01	-2.13E-01	-1.03E-01	-1.9692E-01	
92	0.2400	89	0.4400	1.71E-04	7.58E-06	-7.27E-07	1.7180E-04	-7.53E-04	-5.65E-04	3.77E-04	-1.1302E-03	-3.00E-01	-2.13E-01	-1.03E-01	-1.9692E-01	
93	0.2450	90	0.4450	1.64E-04	2.56E-06	1.18E-06	1.6243E-04	-2.23E-03	-1.32E-03	1.44E-04	-2.3706E-03	-2.87E-01	-7.19E-02	1.67E-01	-4.5412E-01	
94	0.2500	91	0.4500	1.49E-04	-4.15E-06	6.97E-20	1.4897E-04	-3.60E-03	-1.20E-03	-4.66E-04	-3.1368E-03	-2.61E-01	1.16E-01	-6.11E-15	-2.6139E-01	
95	0.2550	92	0.4550	1.28E-04	-8.11E-06	-1.18E-06	1.2901E-04	-4.82E-03	-2.89E-04	1.44E-04	-4.9655E-03	-2.24E-01	2.28E-01	-1.67E-01	-5.7232E-02	
96	0.2600	93	0.4600	1.01E-04	-6.71E-06	7.27E-07	1.0038E-04	-5.83E-03	8.17E-04	3.77E-04	-6.2064E-03	-1.77E-01	1.88E-01	1.03E-01	-2.8066E-01	
97	0.2650	94	0.4650	7.00E-05	-8.67E-07	7.27E-07	6.9241E-05	-6.58E-03	1.38E-03	-3.77E-04	-6.2056E-03	-1.23E-01	2.43E-02	1.03E-01	-2.2602E-01	
98	0.2700	95	0.4700	3.58E-05	5.55E-06	-1.18E-06	3.6941E-05	-7.05E-03	1.03E-03	-1.44E-04	-6.9041E-03	-6.28E-02	-1.56E-01	-1.67E-01	1.0432E-01	
99	0.2750	96	0.4750	1.04E-18	8.29E-06	-7.45E-20	1.1191E-18	-7.21E-03	3.39E-17	4.66E-04	-7.6715E-03	-1.80E-15	-2.33E-01	5.42E-15	-7.2558E-15	
100	0.2800	97	0.4800	-3.58E-05	5.55E-06	1.18E-06	-3.6941E-05	-7.05E-03	-1.03E-03	-1.44E-04	-6.9041E-03	6.28E-02	-1.56E-01	1.67E-01	-1.0432E-01	
101	0.2850	98	0.4850	-7.00E-05	-8.67E-07	-7.27E-07	-6.9241E-05	-6.58E-03	-1.38E-03	-3.77E-04	-6.2056E-03	1.23E-01	2.43E-02	-1.03E-01	2.2602E-01	
102	0.2900	99	0.4900	-1.01E-04	-6.71E-06	-7.27E-07	-1.0038E-04	-5.83E-03	-8.17E-04	3.77E-04	-6.2064E-03	1.77E-01	1.88E-01	-1.03E-01	2.8066E-01	
103	0.2950	100	0.4950	-1.28E-04	-8.11E-06	1.18E-06	-1.2901E-04	-4.82E-03	2.89E-04	1.44E-04	-4.9655E-03	2.24E-01	2.28E-01	1.67E-01	5.7232E-02	
104	0.3000	101	0.5000	-1.49E-04	-4.15E-06	6.18E-20	-1.4897E-04	-3.60E-03	1.20E-03	-4.66E-04	-3.1368E-03	2.61E-01	1.16E-01	-7.23E-15	2.6139E-01	
105	0.3050	102	0.5050	-1.64E-04	2.56E-06	-1.18E-06	-1.6243E-04	-2.23E-03	1.32E-03	1.44E-04	-2.3706E-03	2.87E-01	-7.19E-02	-1.67E-01	4.5412E-01	
106	0.3100	103	0.5100	-1.71E-04	7.58E-06	7.27E-07	-1.7180E-04	-7.53E-04	5.65E-04	3.77E-04	-1.1302E-03	3.00E-01	-2.13E-01	1.03E-01	1.9692E-01	
107	0.3150	104	0.5150	-1.71E-04	7.58E-06	7.27E-07	-1.7180E-04	7.53E-04	-5.65E-04	-3.77E-04	1.1302E-03	3.00E-01	-2.13E-01	1.03E-01	1.9692E-01	
108	0.3200	105	0.5200	-1.64E-04	2.56E-06	-1.18E-06	-1.6243E-04	2.23E-03	-1.32E-03	-1.44E-04	2.3706E-03	2.87E-01	-7.19E-02	-1.67E-01	4.5412E-01	
109	0.3250	106	0.5250	-1.49E-04	-4.15E-06	-6.66E-20	-1.4897E-04	3.60E-03	-1.20E-03	4.66E-04	3.1368E-03	2.61E-01	1.16E-01	6.54E-15	2.6139E-01	
110	0.3300	107	0.5300	-1.28E-04	-8.11E-06	1.18E-06	-1.2901E-04	4.82E-03	-2.89E-04	-1.44E-04	4.9655E-03	2.24E-01	2.28E-01	1.67E-01	5.7232E-02	
111	0.3350	108	0.5350	-1.01E-04	-6.71E-06	-7.27E-07	-1.0038E-04	5.83E-03	8.17E-04	-3.77E-04	6.2064E-03	1.77E-01	1.88E-01	-1.03E-01	2.8066E-01	
112	0.3400	109	0.5400	-7.00E-05	-8.67E-07	-7.27E-07	-6.9241E-05	6.58E-03	1.38E-03	3.77E-04	6.2056E-03	1.23E-01	2.43E-02	-1.03E-01	2.2602E-01	
113	0.3450	110	0.5450	-3.58E-05	5.55E-06	1.18E-06	-3.6941E-05	7.05E-03	1.03E-03	1.44E-04	6.9041E-03	6.28E-02	-1.56E-01	1.67E-01	-1.0432E-01	
114	0.3500	111	0.5500	-1.07E-18	8.29E-06	8.90E-20	-1.1587E-18	7.21E-03	3.46E-17	-4.66E-04	7.6715E-03	1.86E-15	-2.33E-01	-3.36E-15	5.1884E-15	
115	0.3550	112	0.5550	3.58E-05	5.55E-06	-1.18E-06	3.6941E-05	7.05E-03	-1.03E-03	1.44E-04	6.9041E-03	-6.28E-02	-1.56E-01	-1.67E-01	1.0432E-01	
116	0.3600	113	0.5600	7.00E-05	-8.67E-07	7.27E-07	6.9241E-05	6.58E-03	-1.38E-03	3.77E-04	6.2056E-03	-1.23E-01	2.43E-02	1.03E-01	-2.2602E-01	
117	0.3650	114	0.5650	1.01E-04	-6.71E-06	7.27E-07	1.0038E-04	5.83E-03	-8.17E-04	-3.77E-04	6.2064E-03	-1.77E-01	1.88E-01	1.03E-01	-2.8066E-01	
118	0.3700	115	0.5700	1.28E-04	-8.11E-06	-1.18E-06	1.2901E-04	4.82E-03	2.89E-04	-1.44E-04	4.9655E-03	-2.24E-01	2.28E-01	-1.67E-01	-5.7232E-02	
119	0.3750	116	0.5750	1.49E-04	-4.15E-06	-9.39E-20	1.4897E-04	3.60E-03	1.20E-03	4.66E-04	3.1368E-03	-2.61E-01	1.16E-01	2.67E-15	-2.6139E-01	
120	0.3800	117	0.5800	1.64E-04	2.56E-06	1.18E-06	1.6243E-04	2.23E-03	1.32E-03	-1.44E-04	2.3706E-03	-2.87E-01	-7.19E-02	1.67E-01	-4.5412E-01	
121	0.3850	118	0.5850	1.71E-04	7.58E-06	-7.27E-07	1.7180E-04	7.53E-04	5.65E-04	-3.77E-04	1.1302E-03	-3.00E-01	-2.13E-01	-1.03E-01	-1.9692E-01	
122	0.3900	119	0.5900	1.71E-04	7.58E-06	-7.27E-07	1.7180E-04	-7.53E-04	-5.65E-04	3.77E-04	-1.1302E-03	-3.00E-01	-2.13E-01	-1.03E-01	-1.9692E-01	
123	0.3950	120	0.5950	1.64E-04	2.56E-06	1.18E-06	1.6243E-04	-2.23E-03	-1.32E-03	1.44E-04	-2.3706E-03	-2.87E-01	-7.19E-02	1.67E-01	-4.5412E-01	
124	0.4000	121	0.6000	1.49E-04	-4.15E-06	9.87E-20	1.4897E-04	-3.60E-03	-1.20E-03	-4.66E-04	-3.1368E-03	-2.61E-01	1.16E-01	-1.90E-15	-2.6139E-01	
125	0.4050	122	0.6050	1.28E-04	-8.11E-06	-1.18E-06	1.2901E-04	4.82E-03	-2.89E-04	1.44E-04	-4.9655E-03	-2.24E-01	2.28E-01	-1.67E-01	-5.7232E-02	
126	0.4100	123	0.6100	1.01E-04	-6.71E-06	7.27E-07	1.0038E-04	-5.83E-03	8.17E-04	3.77E-04	-6.2064E-03	-1.77E-01	1.88E-01	1.03E-01	-2.8066E-01	
127	0.4150	124	0.6150	7.00E-05	-8.67E-07	7.27E-07	6.9241E-05	-6.58E-03	1.38E-03	-3.77E-04	-6.2056E-03	-1.23E-01	2.43E-02	1.03E-01	-2.2602E-01	
128	0.4200	125	0.6200	3.58E-05	5.55E-06	-1.18E-06	3.6941E-05	-7.05E-03	1.03E-03	-1.44E-04	-6.9041E-03	-6.28E-02	-1.56E-01	-1.67E-01	1.0432E-01	
129	0.4250	126	0.6250	1.38E-18	8.29E-06	-1.04E-19	1.4869E-18	-7.21E-03	4.52E-17	4.66E-04	-7.6715E-03	-2.44E-15	-2.33E-01	1.29E-15	-3.7624E-15	
130	0.4300	127	0.6300	-3.58E-05	5.55E-06	1.18E-06	-3.6941E-05	-7.05E-03	-1.03E-03	-1.44E-04	-6.9041E-03	6.28E-02	-1.56E-01	1.67E-01	-1.0432E-01	
131	0.4350	128	0.6350	-7.00E-05	-8.67E-07	-7.27E-07	-6.9241E-05	-6.58E-03	-1.38E-03	-3.77E-04	-6.2056E-03	1.23E-01	2.43E-02	-1.03E-01	2.2602E-01	
132	0.4400	129	0.6400	-1.01E-04	-6.71E-06	-7.27E-07	-1.0038E-04	-5.83E-03	-8.17E-04	3.77E-04	-6.2064E-03	1.77E-01	1.88E-01	-1.03E-01	2.8066E-01	

1	5	9	13
2	6	10	14
3	7	11	15
4	8	12	16

Figure D.1k *mode3* **Spreadsheet Analysis Program (page 11 of 16)**

	Z	AA	AB	AC	AD	AE	AF	AG	AH	AI	AJ	AK	AL	AM	AN	AO
133	0.4450	130	0.6450	-1.28E-04	-8.11E-06	1.18E-06	-1.2901E-04	-4.82E-03	2.89E-04	1.44E-04	-4.9655E-03	2.24E-01	2.28E-01	1.67E-01	5.7232E-02	
134	0.4500	131	0.6500	-1.49E-04	-4.15E-06	7.33E-20	-1.4897E-04	-3.60E-03	1.20E-03	-4.66E-04	-3.1368E-03	2.61E-01	1.16E-01	-5.60E-15	2.6139E-01	
135	0.4550	132	0.6550	-1.64E-04	2.56E-06	-1.18E-06	-1.6243E-04	-2.23E-03	1.32E-03	1.44E-04	-2.3706E-03	2.87E-01	-7.19E-02	-1.67E-01	4.5412E-01	
136	0.4600	133	0.6600	-1.71E-04	7.58E-06	7.27E-07	-1.7180E-04	-7.53E-04	5.65E-04	3.77E-04	-1.1302E-03	3.00E-01	-2.13E-01	1.03E-01	1.9692E-01	
137	0.4650	134	0.6650	-1.71E-04	7.58E-06	7.27E-07	-1.7180E-04	7.53E-04	-5.65E-04	-3.77E-04	1.1302E-03	3.00E-01	-2.13E-01	1.03E-01	1.9692E-01	
138	0.4700	135	0.6700	-1.64E-04	2.56E-06	-1.18E-06	-1.6243E-04	2.23E-03	-1.32E-03	-1.44E-04	2.3706E-03	2.87E-01	-7.19E-02	-1.67E-01	4.5412E-01	
139	0.4750	136	0.6750	-1.49E-04	4.15E-06	-7.81E-20	-1.4897E-04	3.60E-03	-1.20E-03	4.66E-04	3.1368E-03	2.61E-01	1.16E-01	4.91E-15	2.6139E-01	
140	0.4800	137	0.6800	-1.28E-04	-8.11E-06	1.18E-06	-1.2901E-04	4.82E-03	-2.89E-04	-1.44E-04	4.9655E-03	2.24E-01	2.28E-01	1.67E-01	5.7232E-02	
141	0.4850	138	0.6850	-1.01E-04	-4.71E-06	-7.27E-07	-1.0038E-04	5.83E-03	8.17E-04	-3.77E-04	6.2064E-03	1.77E-01	1.88E-01	-1.03E-01	2.8066E-01	
142	0.4900	139	0.6900	-7.00E-05	-8.67E-07	-7.27E-07	-6.9241E-05	6.58E-03	1.38E-03	3.77E-04	6.2056E-03	1.23E-01	2.43E-02	-1.03E-01	2.2602E-01	
143	0.4950	140	0.6950	-3.58E-05	5.55E-06	1.18E-06	-3.6941E-05	7.05E-03	1.03E-03	1.44E-04	6.9041E-03	6.28E-02	-1.56E-01	1.67E-01	-1.0432E-01	
144	0.5000	141	0.7000	-2.02E-18	8.29E-06	1.18E-19	-2.1364E-18	7.21E-03	6.56E-17	-4.66E-04	7.6715E-03	3.55E-15	-2.33E-01	7.74E-16	2.7498E-15	
145	0.5050	142	0.7050	3.58E-05	5.55E-06	-1.18E-06	3.6941E-05	7.05E-03	-1.03E-03	1.44E-04	6.9041E-03	-6.28E-02	-1.56E-01	-1.67E-01	1.0432E-01	
146	0.5100	143	0.7100	7.00E-05	-8.67E-07	7.27E-07	6.9241E-05	6.58E-03	-1.38E-03	3.77E-04	6.2056E-03	-1.23E-01	2.43E-02	1.03E-01	-2.2602E-01	
147	0.5150	144	0.7150	1.01E-04	4.71E-06	7.27E-07	1.0038E-04	5.83E-03	-8.17E-04	-3.77E-04	6.2064E-03	-1.77E-01	1.88E-01	1.03E-01	-2.8066E-01	
148	0.5200	145	0.7200	1.28E-04	-8.11E-06	-1.18E-06	1.2901E-04	4.82E-03	2.89E-04	-1.44E-04	4.9655E-03	-2.24E-01	2.28E-01	-1.67E-01	-5.7232E-02	
149	0.5250	146	0.7250	1.49E-04	-4.15E-06	-8.78E-20	1.4897E-04	3.60E-03	1.20E-03	4.66E-04	3.1368E-03	-2.61E-01	1.16E-01	3.53E-15	-2.6139E-01	
150	0.5300	147	0.7300	1.64E-04	2.56E-06	1.18E-06	1.6243E-04	2.23E-03	1.32E-03	-1.44E-04	2.3706E-03	-2.87E-01	-7.19E-02	1.67E-01	-4.5412E-01	
151	0.5350	148	0.7350	1.71E-04	7.58E-06	-7.27E-07	1.7180E-04	7.53E-04	5.65E-04	-3.77E-04	1.1302E-03	-3.00E-01	-2.13E-01	-1.03E-01	-1.9692E-01	
152	0.5400	149	0.7400	1.71E-04	7.58E-06	-7.27E-07	1.7180E-04	-7.53E-04	-5.65E-04	3.77E-04	-1.1302E-03	-3.00E-01	-2.13E-01	-1.03E-01	-1.9692E-01	
153	0.5450	150	0.7450	1.64E-04	2.56E-06	1.18E-06	1.6243E-04	-2.23E-03	-1.32E-03	1.44E-04	-2.3706E-03	-2.87E-01	-7.19E-02	1.67E-01	-4.5412E-01	
154	0.5500	151	0.7500	1.49E-04	-4.15E-06	1.28E-19	1.4897E-04	-3.60E-03	-1.20E-03	-4.66E-04	-3.1368E-03	-2.61E-01	1.16E-01	2.15E-15	-2.6139E-01	
155	0.5550	152	0.7550	1.28E-04	-8.11E-06	-1.18E-06	1.2901E-04	-4.82E-03	-2.89E-04	1.44E-04	-4.9655E-03	-2.24E-01	2.28E-01	-1.67E-01	-5.7232E-02	
156	0.5600	153	0.7600	1.01E-04	4.71E-06	7.27E-07	1.0038E-04	-5.83E-03	8.17E-04	3.77E-04	-6.2064E-03	-1.77E-01	1.88E-01	1.03E-01	-2.8066E-01	
157	0.5650	154	0.7650	7.00E-05	-8.67E-07	7.27E-07	6.9241E-05	-6.58E-03	1.38E-03	-3.77E-04	-6.2056E-03	-1.23E-01	2.43E-02	1.03E-01	-2.2602E-01	
158	0.5700	155	0.7700	3.58E-05	5.55E-06	-1.18E-06	3.6941E-05	-7.05E-03	1.03E-03	-1.44E-04	-6.9041E-03	-6.28E-02	-1.56E-01	-1.67E-01	1.0432E-01	
159	0.5750	156	0.7750	1.44E-18	8.29E-06	-9.75E-20	1.5351E-18	-7.21E-03	4.65E-17	4.66E-04	-7.6715E-03	-3.50E-15	-2.33E-01	2.15E-15	-4.6789E-15	
160	0.5800	157	0.7800	-3.58E-05	5.55E-06	1.18E-06	-3.6941E-05	-7.05E-03	-1.03E-03	-1.44E-04	-6.9041E-03	6.28E-02	-1.56E-01	1.67E-01	-1.0432E-01	
161	0.5850	158	0.7850	-7.00E-05	-8.67E-07	-7.27E-07	-6.9241E-05	-6.58E-03	-1.38E-03	-3.77E-04	-6.2056E-03	1.23E-01	2.43E-02	-1.03E-01	2.2602E-01	
162	0.5900	159	0.7900	-1.01E-04	-4.71E-06	-7.27E-07	-1.0038E-04	-5.83E-03	-8.17E-04	3.77E-04	-6.2064E-03	1.77E-01	1.88E-01	-1.03E-01	2.8066E-01	
163	0.5950	160	0.7950	-1.28E-04	-8.11E-06	1.18E-06	-1.2901E-04	-4.82E-03	2.89E-04	1.44E-04	-4.9655E-03	2.24E-01	2.28E-01	1.67E-01	5.7232E-02	
164	0.6000	161	0.8000	-1.49E-04	-4.15E-06	1.37E-19	-1.4897E-04	-3.60E-03	1.20E-03	-4.66E-04	-3.1368E-03	2.61E-01	1.16E-01	3.53E-15	2.6139E-01	
165	0.6050	162	0.8050	-1.64E-04	2.56E-06	-1.18E-06	-1.6243E-04	-2.23E-03	1.32E-03	1.44E-04	-2.3706E-03	2.87E-01	-7.19E-02	-1.67E-01	4.5412E-01	
166	0.6100	163	0.8100	-1.71E-04	7.58E-06	7.27E-07	-1.7180E-04	-7.53E-04	5.65E-04	3.77E-04	-1.1302E-03	3.00E-01	-2.13E-01	1.03E-01	1.9692E-01	
167	0.6150	164	0.8150	-1.71E-04	7.58E-06	7.27E-07	-1.7180E-04	7.53E-04	-5.65E-04	-3.77E-04	1.1302E-03	3.00E-01	-2.13E-01	1.03E-01	1.9692E-01	
168	0.6200	165	0.8200	-1.64E-04	2.56E-06	-1.18E-06	-1.6243E-04	2.23E-03	-1.32E-03	-1.44E-04	2.3706E-03	2.87E-01	-7.19E-02	-1.67E-01	4.5412E-01	
169	0.6250	166	0.8250	-1.49E-04	4.15E-06	-7.21E-20	-1.4897E-04	3.60E-03	-1.20E-03	4.66E-04	3.1368E-03	2.61E-01	1.16E-01	5.77E-15	2.6139E-01	
170	0.6300	167	0.8300	-1.28E-04	-8.11E-06	1.18E-06	-1.2901E-04	4.82E-03	-2.89E-04	-1.44E-04	4.9655E-03	2.24E-01	2.28E-01	1.67E-01	5.7232E-02	
171	0.6350	168	0.8350	-1.01E-04	-4.71E-06	-7.27E-07	-1.0038E-04	5.83E-03	8.17E-04	-3.77E-04	6.2064E-03	1.77E-01	1.88E-01	-1.03E-01	2.8066E-01	
172	0.6400	169	0.8400	-7.00E-05	-8.67E-07	-7.27E-07	-6.9241E-05	6.58E-03	1.38E-03	3.77E-04	6.2056E-03	1.23E-01	2.43E-02	-1.03E-01	2.2602E-01	
173	0.6450	170	0.8450	-3.58E-05	5.55E-06	1.18E-06	-3.6941E-05	7.05E-03	1.03E-03	1.44E-04	6.9041E-03	6.28E-02	-1.56E-01	1.67E-01	-1.0432E-01	
174	0.6500	171	0.8500	-2.07E-18	8.29E-06	1.47E-19	-2.2197E-18	7.21E-03	6.70E-17	-4.66E-04	7.6715E-03	3.64E-15	-2.33E-01	4.91E-15	-1.2987E-15	
175	0.6550	172	0.8550	3.58E-05	5.55E-06	-1.18E-06	3.6941E-05	7.05E-03	-1.03E-03	1.44E-04	6.9041E-03	-6.28E-02	-1.56E-01	-1.67E-01	1.0432E-01	
176	0.6600	173	0.8600	7.00E-05	-8.67E-07	7.27E-07	6.9241E-05	6.58E-03	-1.38E-03	3.77E-04	6.2056E-03	-1.23E-01	2.43E-02	1.03E-01	-2.2602E-01	

1	5	9	13
2	6	10	14
3	7	11	15
4	8		16

Figure D.11 *mode3* **Spreadsheet Analysis Program (page 12 of 16)**

	AP	AQ	AR	AS	AT	AU	AV	AW	AX	AY	AZ	BA	BB
1													
2	vel. (m/s)	max.Δ	maxΔ(neg)	res.vib.	Vc								
3		*0.9738*	*0.0009*	*0.0009*	*0.75*								
4	2.5	0.87	0.00	0.00	0.0150								
5	5.0	0.87	0.00	0.00	0.0300								
6	*5.6*	0.87	0.00	0.00	0.0333								
7	*6.7*	0.87	0.00	0.00	0.0400								
8	7.5	0.87	0.01	0.01	0.0450								
9	*8.3*	0.87	0.00	0.00	0.0500								
10	10.0	0.87	0.00	0.00	0.0600								
11	*11.1*	0.87	0.00	0.00	0.0667								
12	12.5	0.87	0.00	0.00	0.0750								
13	*13.3*	0.87	0.00	0.00	0.0800								
14	*14.5*	0.87	0.00	0.00	0.0870								
15	15.0	0.87	0.00	0.00	0.0900								
16	*15.9*	0.87	0.00	0.00	0.0952								
17	*16.7*	0.87	0.00	0.00	0.1000								
18	17.5	0.87	0.00	0.00	0.1050								
19	*17.5*	0.87	0.00	0.00	0.1053								
20	*19.6*	0.88	0.00	0.00	0.1176	*L (m) =*	25.00		npSp (m) =	37.50		*Lp (m) =*	5.00
21	20.0	0.89	0.01	0.01	0.1200	f1 (Hz) =	6.6667		f1 (Hz) =	6.6667		*f1 (Hz) =*	6.6667
22	*20.8*	*0.90*	*0.05*	*0.05*	*0.1250*		*m*			*n*			*n*
23	*22.2*	0.87	0.00	0.00	0.1333	*13.33333333*	*12.50*		20.83333333	*12.00*		*5.555556*	*6.00*
24	22.5	0.87	0.00	0.00	0.1350	*14.49275362*	*11.50*		22.72727273	*11.00*		*6.666667*	*5.00*
25	22.7	0.87	0.00	0.00	0.1364	*15.87301587*	*10.50*		25.00000000	*10.00*		*8.333333*	*4.00*
26	25.0	0.87	0.00	0.00	0.1500	*17.54385965*	*9.50*		27.77777778	*9.00*		*11.111111*	*3.00*
27	25.0	0.87	0.00	0.00	0.1500	*19.60784314*	*8.50*		31.25000000	*8.00*		*16.666667*	*2.00*
28	*25.6*	0.87	0.00	0.00	0.1538	*22.22222222*	*7.50*		35.71428571	*7.00*		*33.333333*	*1.00*
29	27.5	0.90	0.05	0.05	0.1650	*25.64102564*	*6.50*		41.66666667	*6.00*			
30	*27.8*	0.90	0.05	0.05	0.1667	*30.30303030*	*5.50*		50.00000000	*5.00*			
31	30.0	0.88	0.00	0.00	0.1800	*37.03703704*	*4.50*		62.50000000	*4.00*			
32	*30.3*	0.88	0.00	0.00	0.1818	*47.61904762*	*3.50*		83.33333333	*3.00*			
33	31.2	0.88	0.00	0.00	0.1875	*66.66666667*	*2.50*		125.00000000	*2.00*			
34	32.5	0.88	0.00	0.00	0.1950	*111.11111111*	*1.50*		250.00000000	*1.00*			
35	*33.3*	0.88	0.00	0.00	0.2000								
36	35.0	0.88	0.00	0.00	0.2100								
37	35.7	0.87	0.00	0.00	0.2143								
38	*37.0*	0.87	0.00	0.00	0.2222								
39	37.5	0.87	0.00	0.00	0.2250								
40	40.0	0.91	0.07	0.07	0.2400								
41	41.7	0.94	0.11	0.11	0.2500								
42	42.5	0.96	0.12	0.12	0.2550								
43	45.0	0.96	0.07	0.07	0.2700								
44	47.5	0.93	0.00	0.00	0.2850								

Figure D.1m *mode3* Spreadsheet Analysis Program (page 13 of 16)

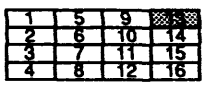

	AP	AQ	AR	AS	AT	AU	AV	AW	AX	AY	AZ	BA	BB
45	*47.6*	0.93	0.00	0.00	0.2857								
46	50.0	0.93	0.00	0.00	0.3000								
47	50.0	0.93	0.00	0.00	0.3000								
48	52.5	0.96	0.06	0.06	0.3150								
49	55.0	1.00	0.11	0.11	0.3300								
50	57.5	1.01	0.10	0.10	0.3450								
51	60.0	0.99	0.05	0.05	0.3600								
52	62.5	0.97	0.00	0.00	0.3750								
53	62.5	0.97	0.00	0.00	0.3750								
54	65.0	1.00	0.02	0.02	0.3900								
55	*66.7*	1.02	0.00	0.00	0.4000								
56	67.5	1.04	0.02	0.02	0.4050								
57	70.0	1.12	0.12	0.12	0.4200								
58	72.5	1.19	0.26	0.26	0.4350								
59	75.0	1.26	0.41	0.41	0.4500								
60	77.5	1.31	0.56	0.56	0.4650								
61	80.0	1.35	0.67	0.67	0.4800								
62	82.5	1.37	0.75	0.75	0.4950								
63	83.3	1.38	0.76	0.76	0.5000								
64	85.0	1.38	0.78	0.78	0.5100								
65	87.5	1.37	0.77	0.77	0.5250								
66	90.0	1.35	0.72	0.72	0.5400								
67	92.5	1.31	0.65	0.65	0.5550								
68	95.0	1.26	0.55	0.55	0.5700								
69	97.5	1.21	0.45	0.45	0.5850								
70	100.0	1.15	0.34	0.34	0.6000								
71	102.5	1.09	0.24	0.24	0.6150								
72	105.0	1.02	0.16	0.16	0.6300								
73	107.5	0.97	0.08	0.08	0.6450								
74	110.0	0.93	0.02	0.02	0.6600								
75	*111.1*	0.91	0.00	0.00	0.6667								
76	112.5	0.92	0.02	0.02	0.6750								
77	115.0	0.93	0.05	0.05	0.6900								
78	117.5	0.94	0.06	0.06	0.7050								
79	120.0	0.95	0.05	0.05	0.7200								
80	122.5	0.96	0.03	0.03	0.7350								
81	125.0	0.97	0.00	0.00	0.7500								
82	125.0	0.97	0.00	0.00	0.7500								
83	127.5	1.00	0.04	0.04	0.7650								
84	130.0	1.03	0.09	0.09	0.7800								
85	132.5	1.05	0.14	0.14	0.7950								
86	135.0	1.07	0.20	0.20	0.8100								
87	137.5	1.09	0.26	0.26	0.8250								
88	140.0	1.10	0.32	0.32	0.8400								

Figure D.1n *mode3* Spreadsheet Analysis Program (page 14 of 16)

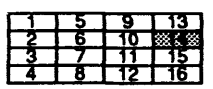

	AP	AQ	AR	AS	AT	AU	AV	AW	AX	AY	AZ	BA	BB
89	142.5	1.11	0.38	0.37	0.8550								
90	145.0	1.12	0.43	0.43	0.8700								
91	147.5	1.12	0.49	0.49	0.8850								
92	150.0	1.12	0.54	0.54	0.9000								
93	152.5	1.12	0.59	0.59	0.9150								
94	155.0	1.12	0.64	0.64	0.9300								
95	157.5	1.12	0.68	0.68	0.9450								
96	160.0	1.13	0.71	0.71	0.9600								
97	250.0	1.42	0.00	0.00	1.5000								
98													
99													
100													
101													
102													
103													
104													
105													
106													
107													
108													
109													
110													
111													
112													
113													
114													
115													
116													
117													
118													
119													
120													
121													
122													
123													
124													
125													
126													
127													
128													
129													
130													
131													
132													

Figure D.1o *mode3* Spreadsheet Analysis Program (page 15 of 16)

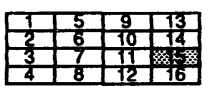

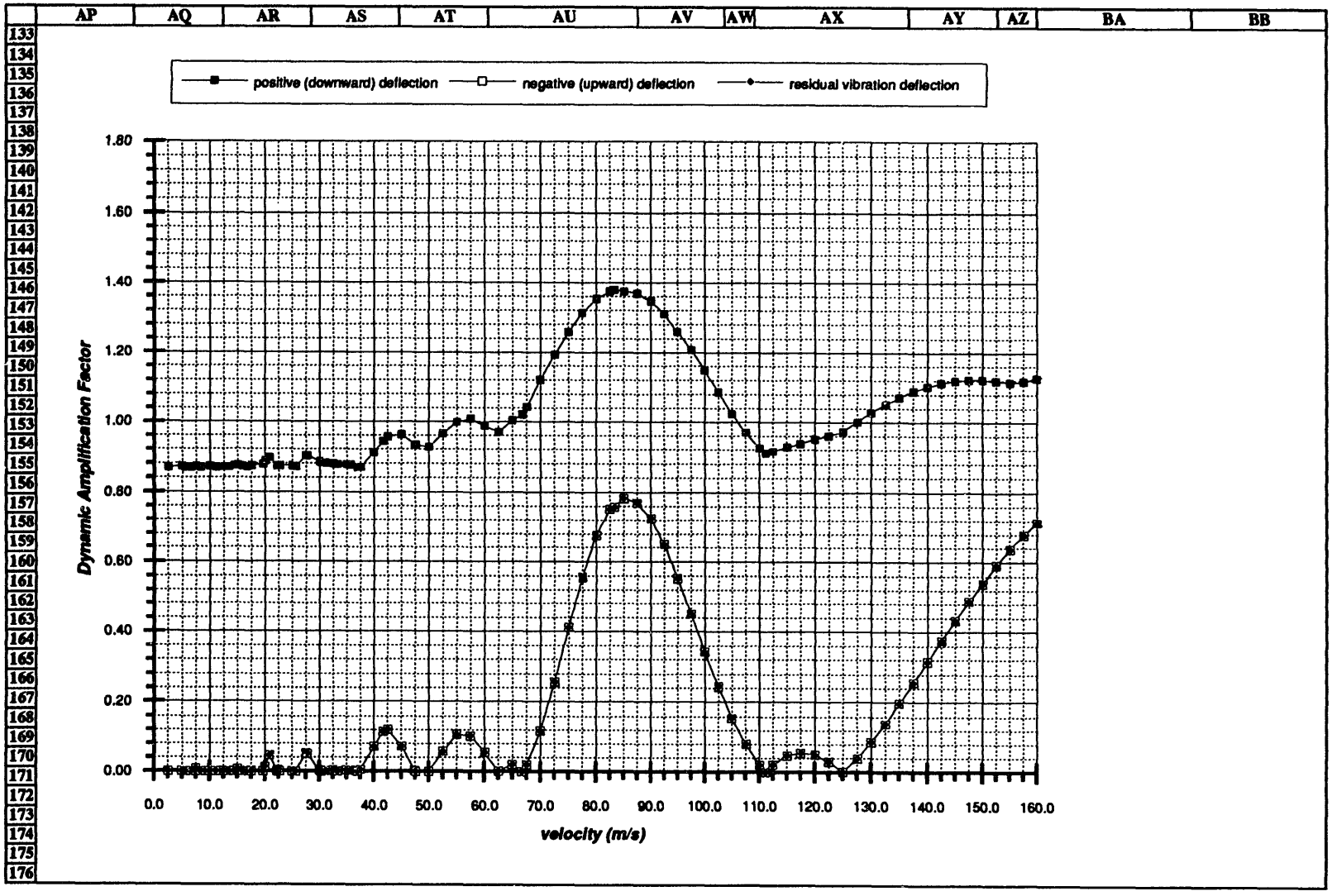

Figure D.1p *mode3* **Spreadsheet Analysis Program (page 16 of 16)**

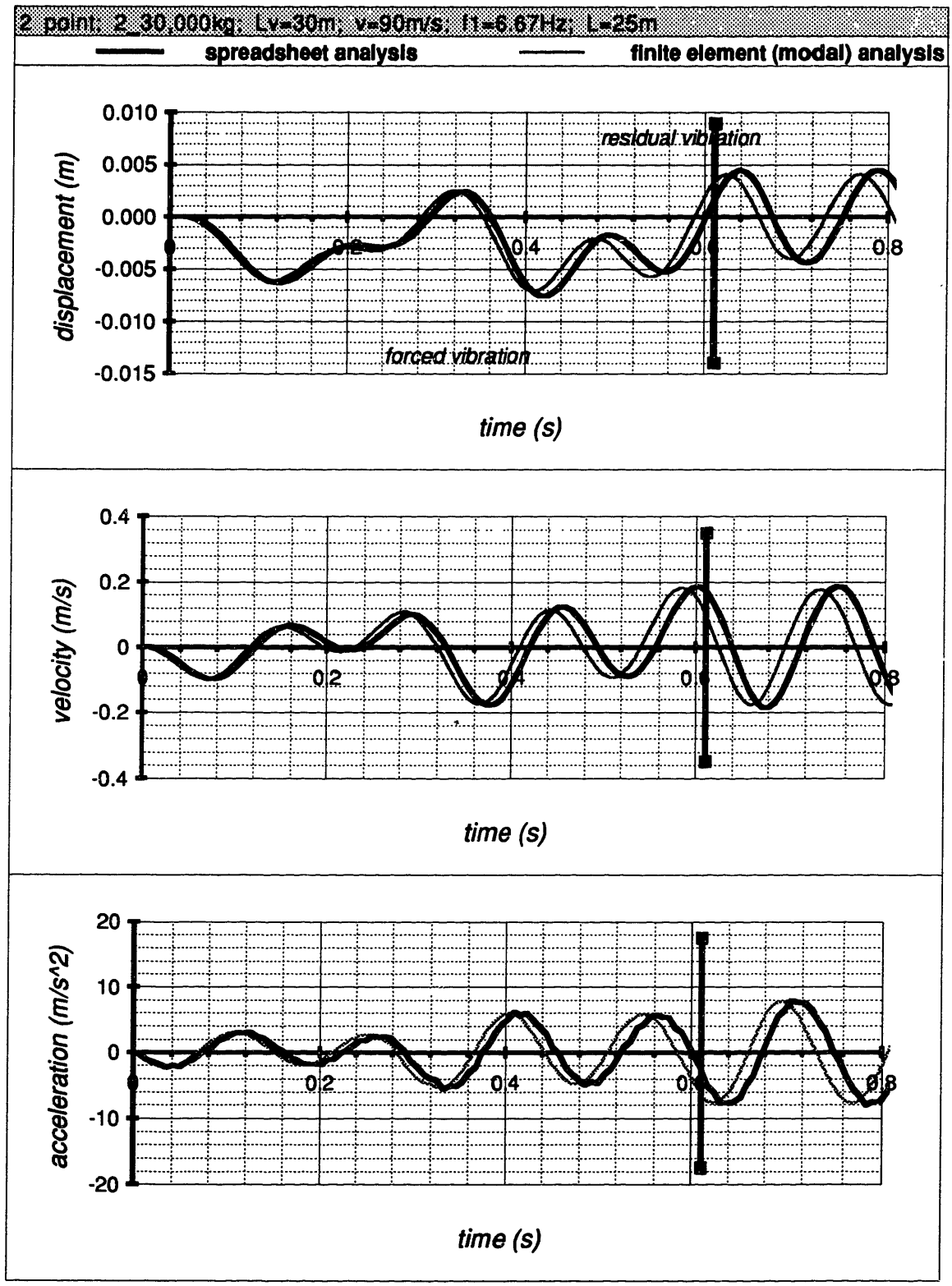

Figure D.2a Two Point Vehicle (v=90 m/s)

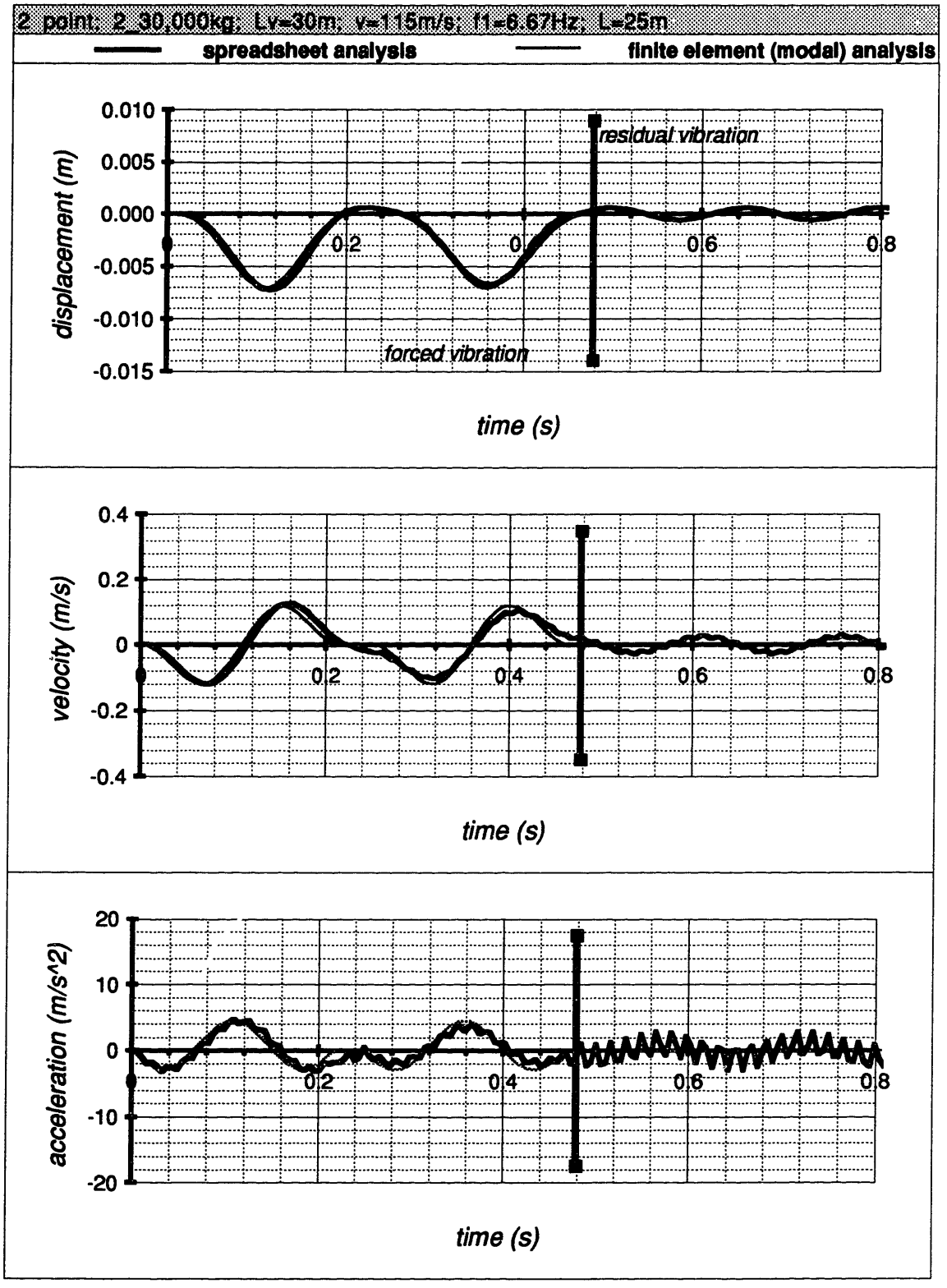

Figure D.2b Two Point Vehicle (v=115 m/s)

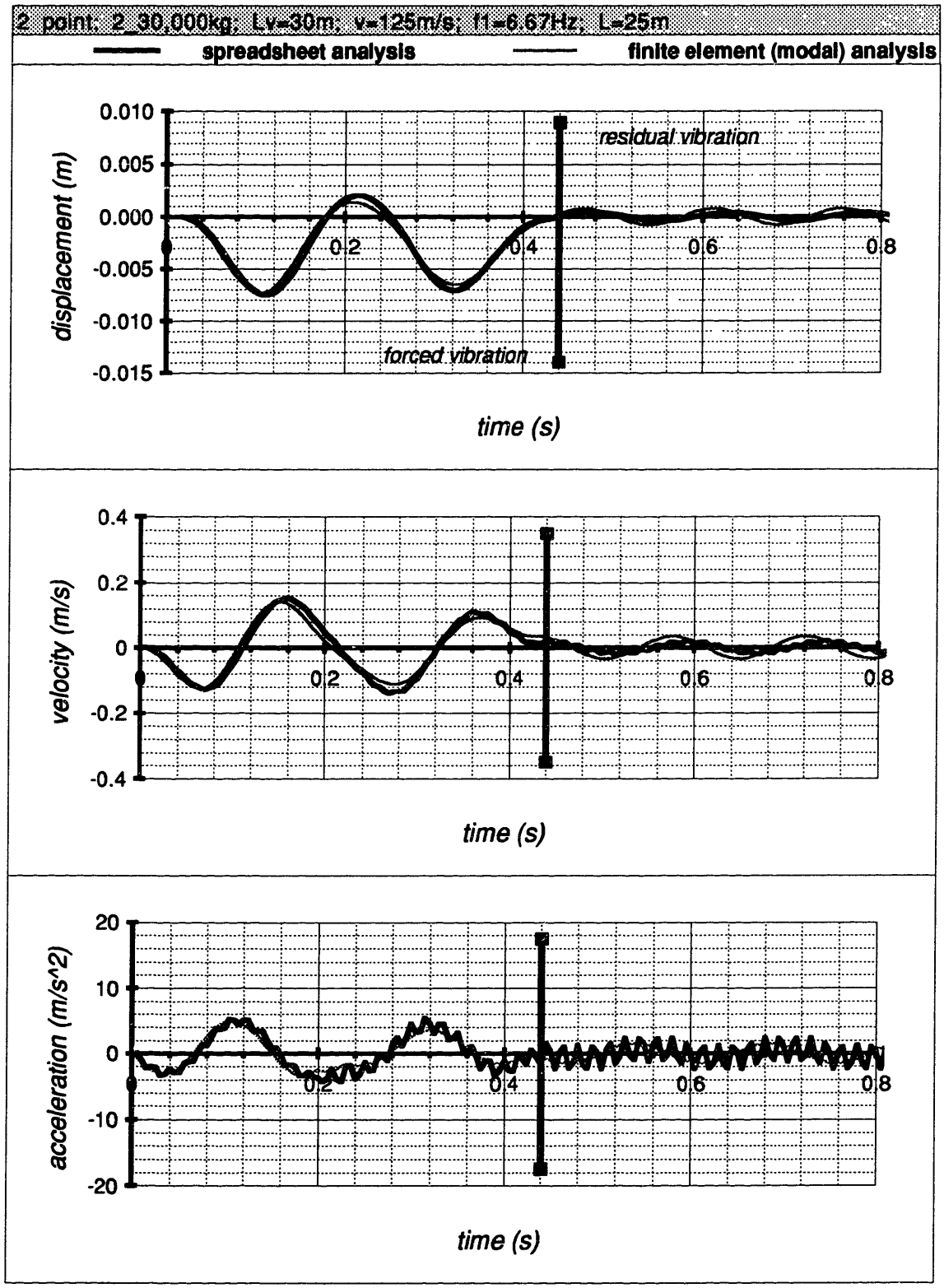

Figure D.2c Two Point Vehicle (v=125 m/s)

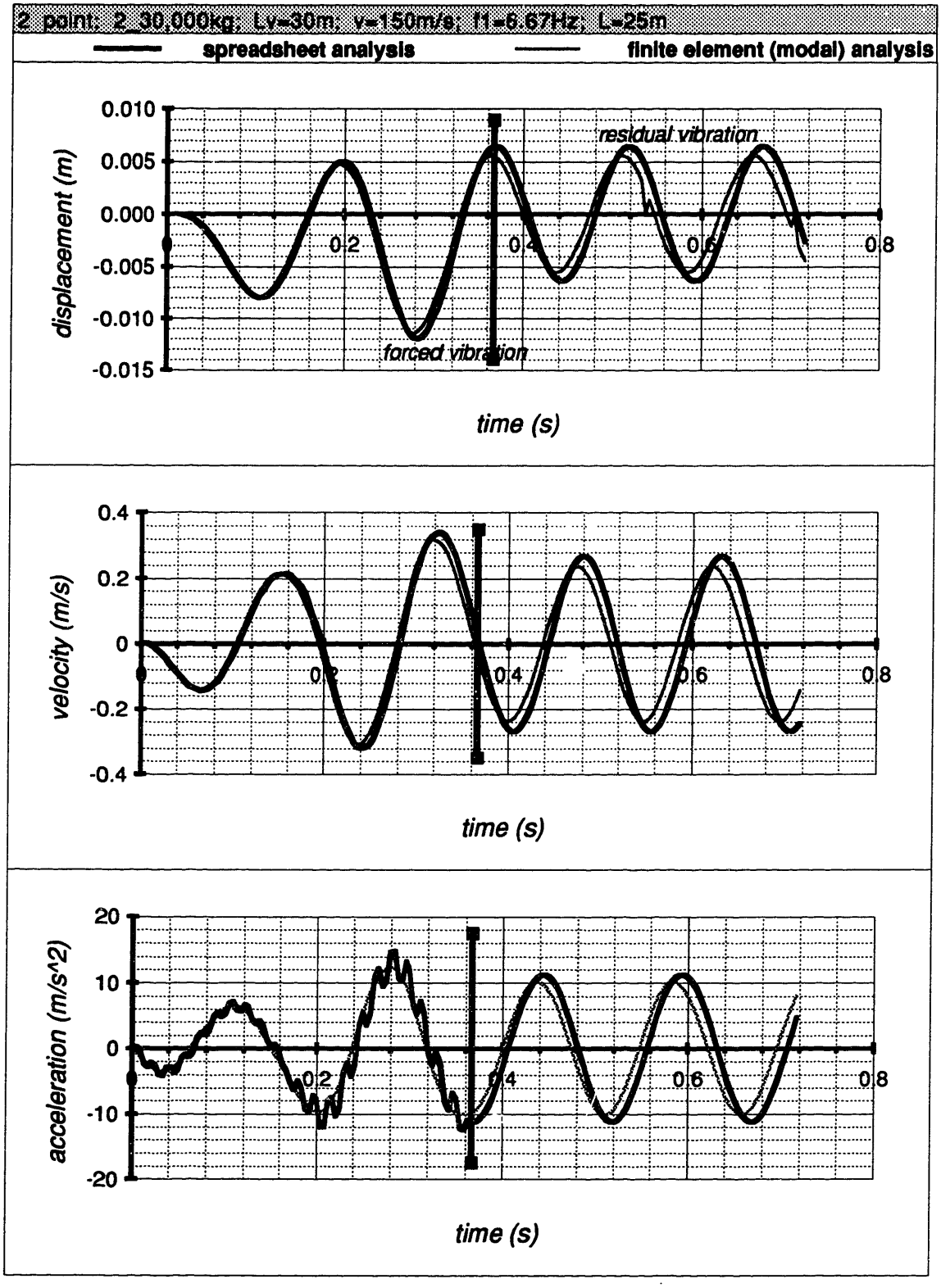

Figure D.2d Two Point Vehicle (v=150 m/s)

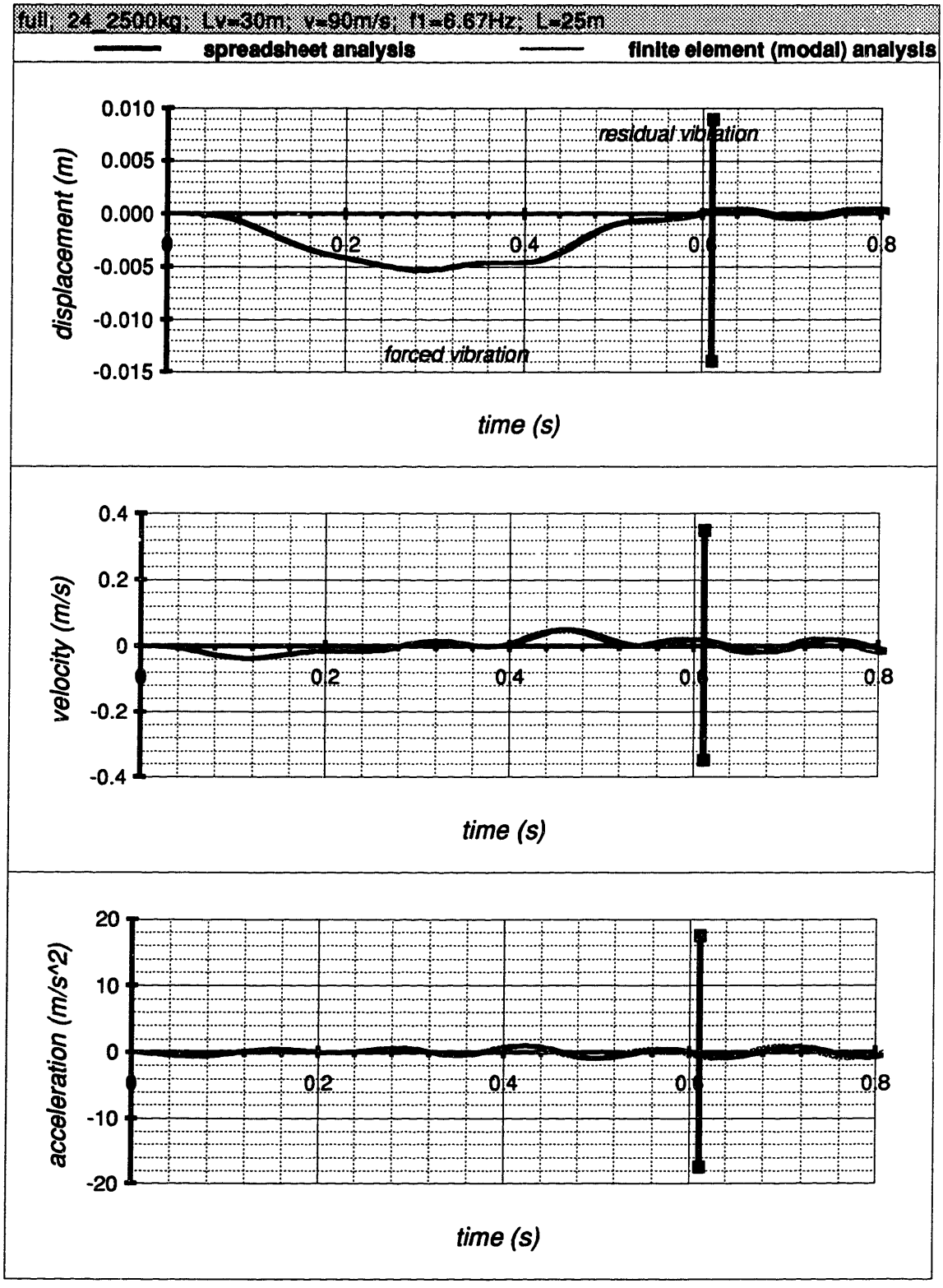

Figure D.3a Fully Distributed Vehicle (v=90 m/s)

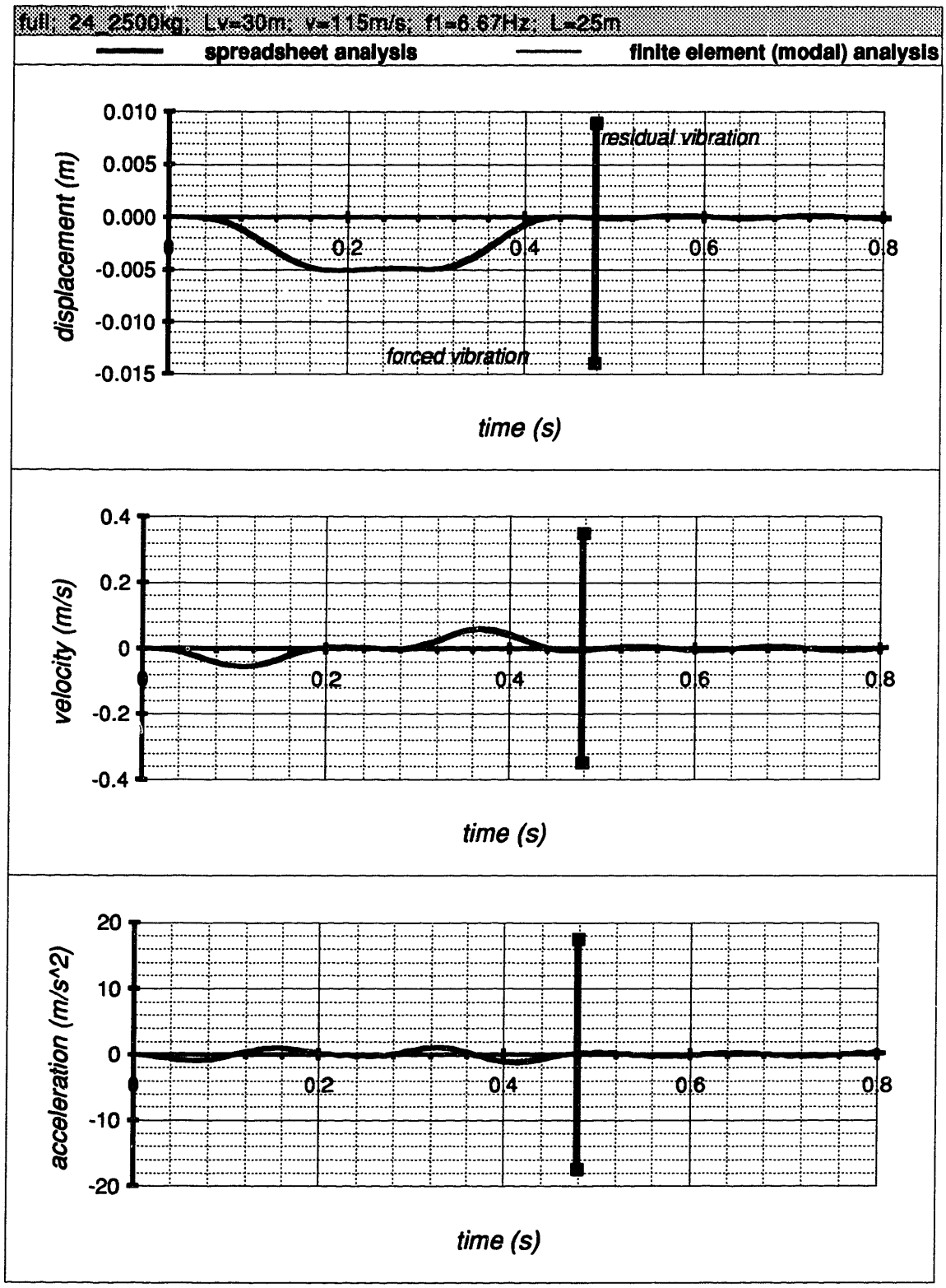

Figure D.3b Fully Distributed Vehicle (v=115 m/s)

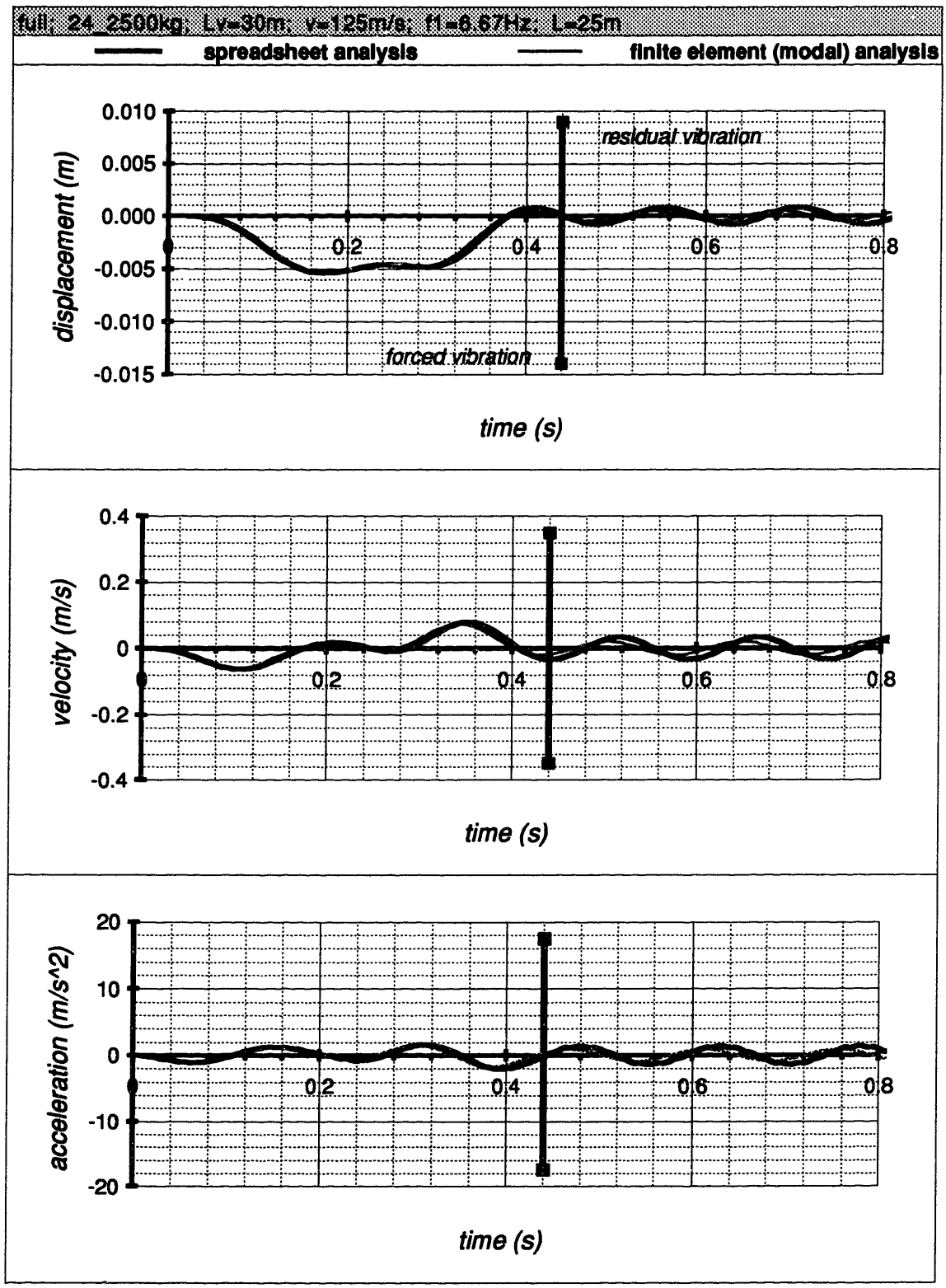

Figure D.3c Fully Distributed Vehicle (v=125 m/s)

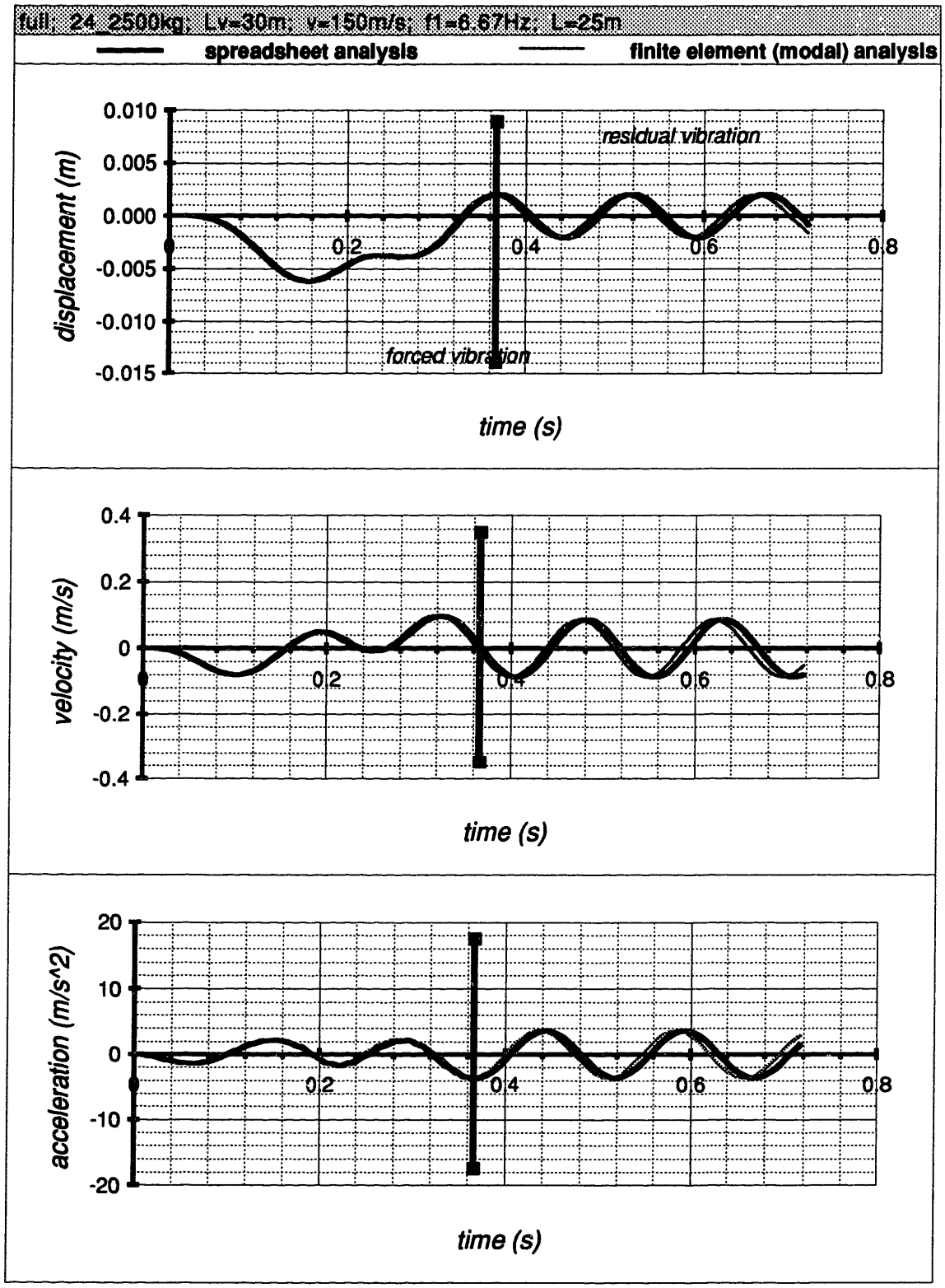

Figure D.3d Fully Distributed Vehicle (v=150 m/s)

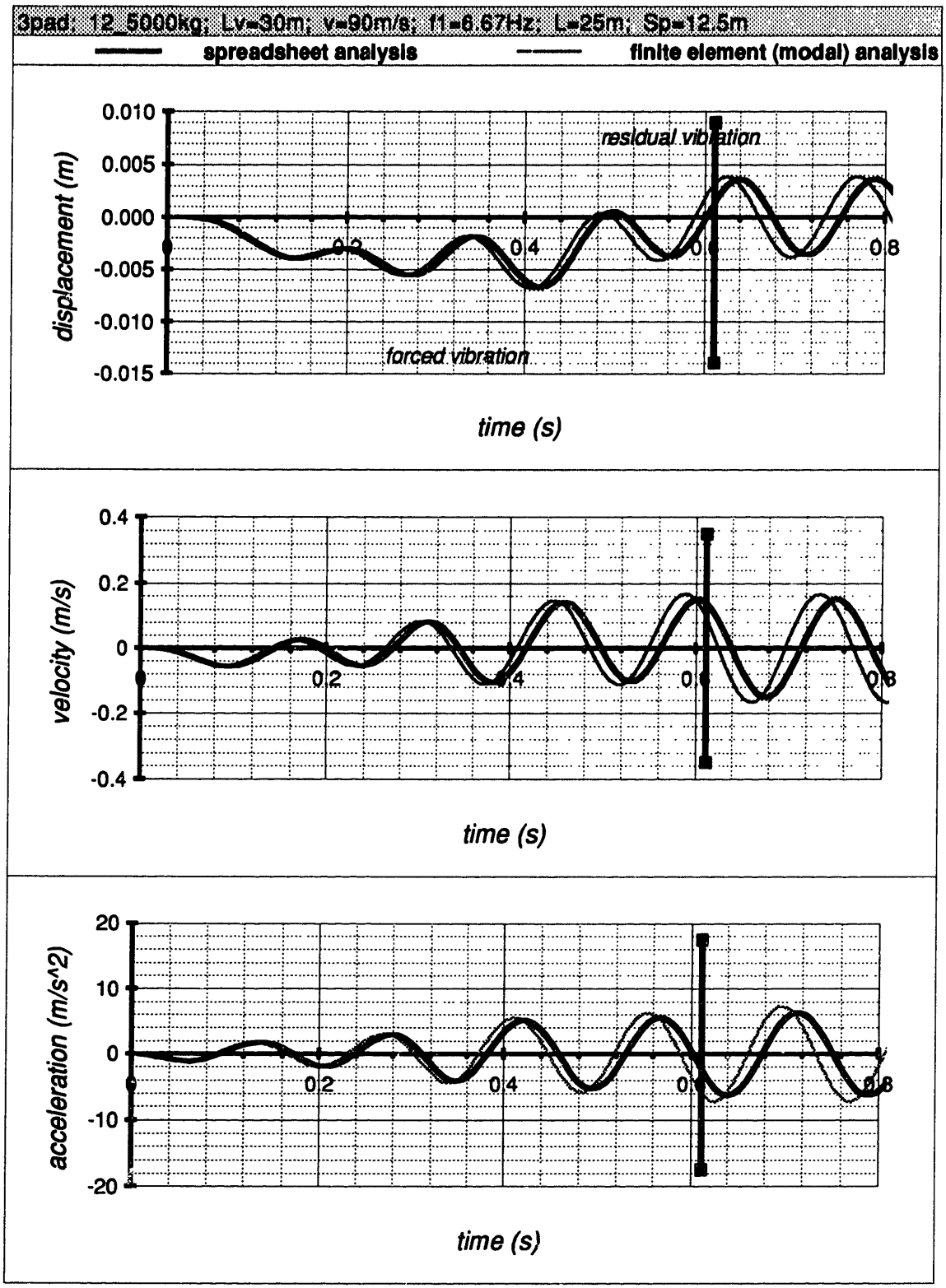

Figure D.4a Three Pad Vehicle (v=90 m/s)

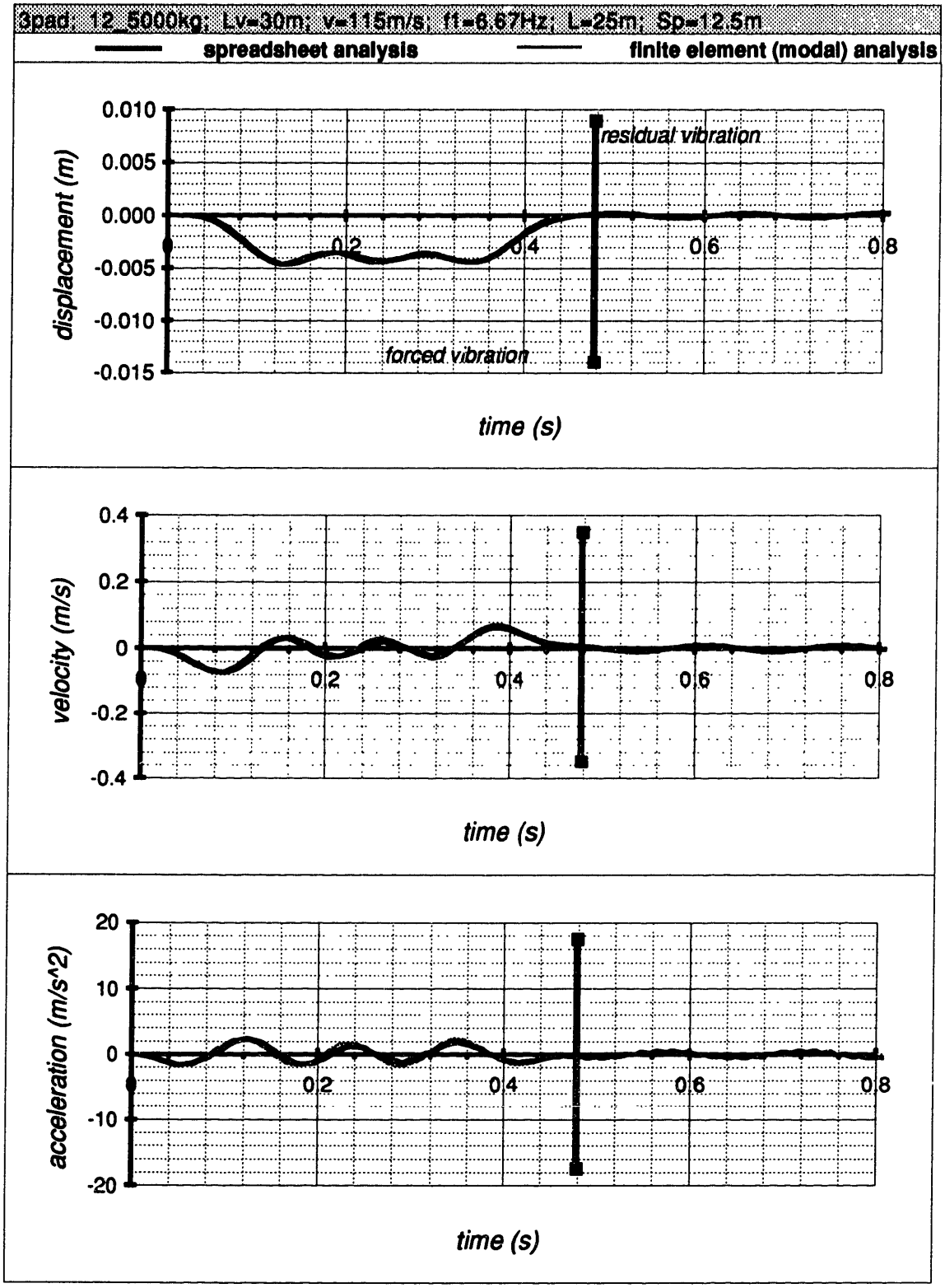

Figure D.4b Three Pad Vehicle (v=115 m/s)

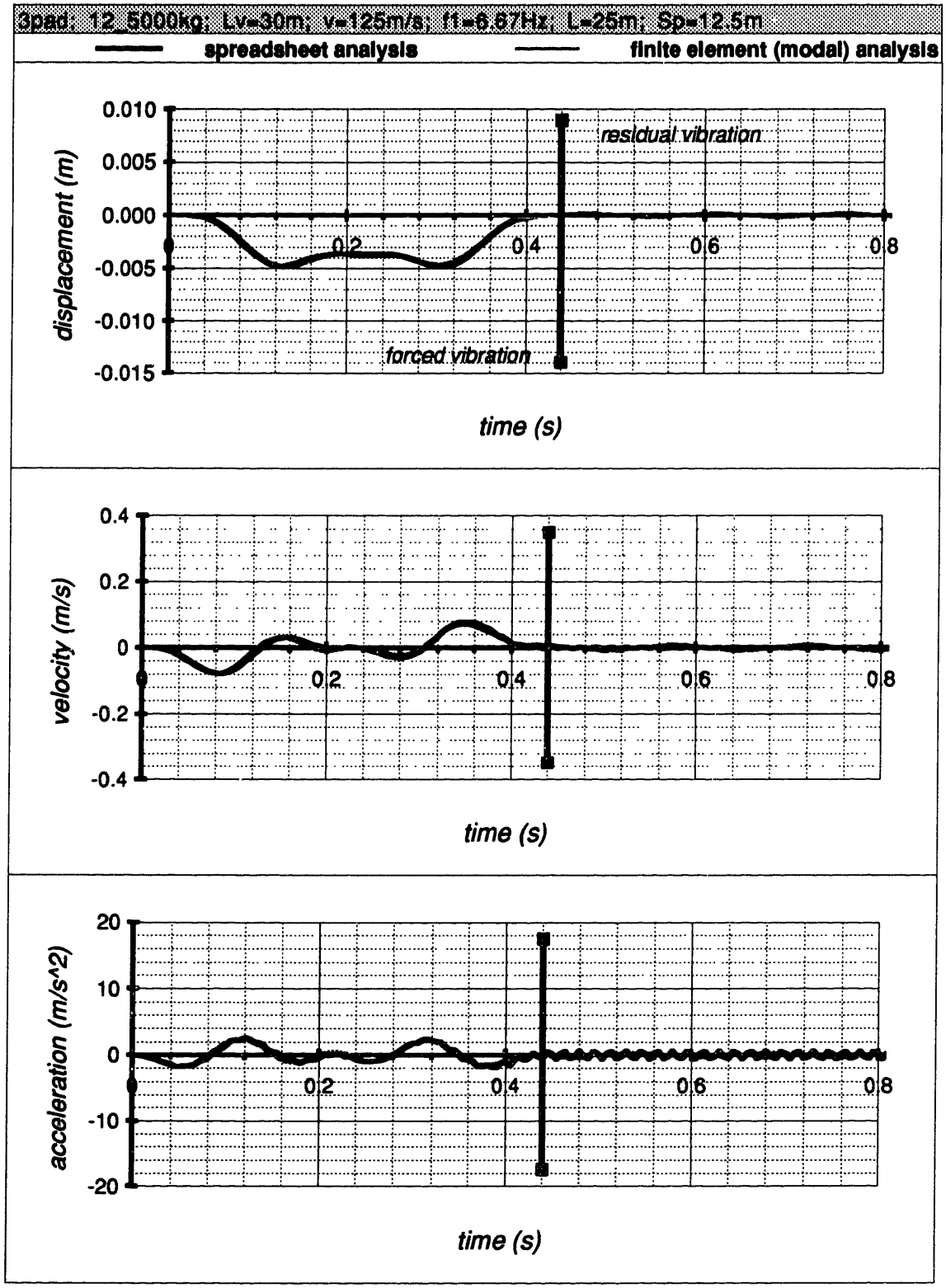

Figure D.4c Three Pad Vehicle (v=125 m/s)

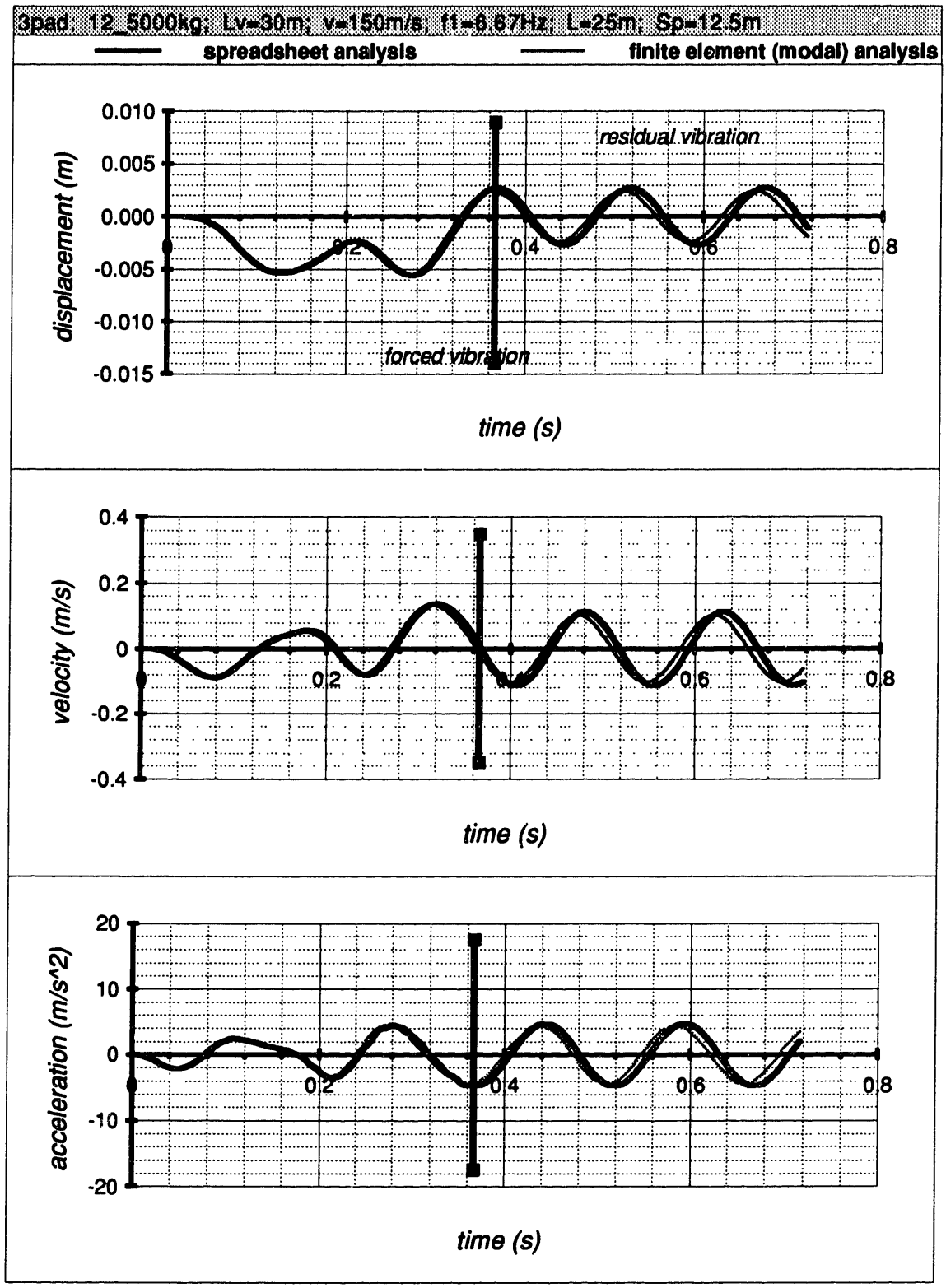

Figure D.4d Three Pad Vehicle (v=150 m/s)